TRANSACTIONS
AMERICAN GEOPHYSICAL UNION

Volume 31 OCTOBER 1950 Number 5 Part 1

ON THE EARTH TIDE OF THE COMPRESSIBLE EARTH OF VARIABLE DENSITY AND ELASTICITY

Hitoshi Takeuchi

Abstract--This paper presents a theoretical study of the phenomena of Earth tides. The differential equations of stress and motion are established to allow solution under various hypotheses as to elasticity, compressibility, and density in the interior of the Earth, and numerical integrations are made for several Earth models with internal constitutions inferred from recent studies of seismology combined with K. E. Bullen's studies of the density distribution within the Earth. The results are shown to be in satisfactory agreement with several observations of Earth tides.

Introduction--The deformation of the Earth by the tidal attractions of the Sun and Moon is called Earth tide. Kelvin was the first to point out that the Earth is deformed by the tidal forces. In his classical paper [KELVIN, 1863a], he discussed the elastic deformation of a homogeneous incompressible sphere by the tidal forces, and from this study he concluded that the Earth as a whole reacts as rigidly as steel to the tidal attractions of the Sun and Moon. The height of oceanic tides is reduced, as will be shown later, by the Earth tide. In fact, the mean rigidity of the Earth referred to above was determined from the result of oceanic tidal observations. Periodic deflections of the vertical line, periodic changes in gravity, and variation of latitude are closely connected with the Earth tide. The difference of the Chandler period and Euler period of latitude variation is also connected with the Earth tide. Since the time of Kelvin, many attempts were successfully made to study the Earth tide from these sources of data.

With these observational data in hand, theoretical studies of the elastic deformation of the Earth have been made by several authors. The theoretical study of Kelvin was made under the assumption that the Earth is an incompressible sphere of uniform density and elasticity. The known fact that the Earth is not homogeneous, but is of a mean density about twice that of superficial rocks, raised a problem. Would the estimation of the rigidity be much affected by the heterogeneity of the Earth? This question was discussed by DARWIN [1907a], HERGLOTZ [1905], and PRESCOTT [1911]. They discussed the problem by assuming that the Earth is an incompressible elastic sphere of homogeneous rigidity and density of Roche type. By Roche type is meant the density distribution of the type

$$\rho = \rho_0 (1 - \beta r_1^2)$$

where $r_1 = r/a$ is the distance from the center of the Earth measured by the radius (a) of the Earth as unity and ρ_0 and β are constants. HERGLOTZ [1905], SCHWEYDAR [1908], and JEFFREYS [1926] discussed the problem assuming that the Earth is an incompressible elastic sphere separated into two parts, in each part of which both the rigidity and the density are homogeneous. Furthermore, SCHWEYDAR [1908], HOSKINS [1920], and PREY [1929] assumed $\rho = \rho_0 (1 - \beta r_1^2)$, $\mu = \mu_0 (1 - \alpha r_1^2)$, and $\lambda = \infty$ (incompressible) (in which μ and λ are Lamé's elastic constants) and discussed the problem. PREY [1935] also used the distribution $\rho = \rho_0 (1 - \beta r_1^2)$, $\mu = \mu_0 r_1^2 (1 - \alpha r_1^2)$, and $\lambda = \infty$.

The investigations referred to above were based upon the supposition of incompressibility. The investigations under the assumption of compressibility were made by only two authors. LOVE [1909] made the discussion for the case ρ = constant, μ = constant, and λ = constant; HOSKINS [1920] investigated the problem for the case $\rho = \rho_0 (1 - \beta r_1^2)$, and $\lambda = \mu = \mu_0 (1 - \alpha r_1^2)$. The distribution of density and elastic constants assumed above is, however, very different from that inferred by the results of the investigations of modern seismology. For example, the rigidity is considered to become approximately zero at about 2900 km depth from the result of investigations of modern seismology, but this circumstance is not taken into account in almost all the investigations referred to above. Lamé's constant λ is not infinite in the actual Earth, but the model Earth is assumed to be incompressible in almost all these studies. For the purpose of inferring the internal constitution of the Earth by such an analysis, it is obviously desirable that the ideal sphere assumed in the computations should agree with the actual Earth as closely as possible in all the elements essential to the problem. But, as GUTENBERG [1939] remarks, there exist great mathematical difficulties in treating the problem for the actual Earth, and the problem has hitherto remained unsolved.

In this paper, an attempt is made to solve the problem. The Earth model with the internal constitution inferred from recent results of seismology combined with the studies of BULLEN [1936, 1940, 1942] about the density distribution within the Earth is adopted. The rigidity of the Earth's core is taken to vary parametrically. At the end of this paper, the following three problems are discussed.

(1) To find the most probable values of the characteristic numbers h, k and ℓ (the meaning of h, k and ℓ are given below).

(2) To study whether the dynamic elastic constants of the Earth determined by the study of seismic waves can be taken to be the same as the static elastic constants of the Earth determined by the Earth tide.

(3) To determine the largest value of the rigidity of the Earth's core that is compatible with the observations of the Earth tide.

CHAPTER I

Fundamental equations

Section 1--Fundamental differential equations of the Earth tide must be established taking into account the two circumstances that do not exist in the ordinary theory of elastic deformation. First, the Earth is in a state of initial stress. Second, the Earth is self-gravitational. In order to deal with these complications, the following four assumptions are made: (1) The initial stress in the Earth may be regarded as a hydrostatic pressure balancing the self-gravitation of the Earth in the initial state. (2) The stress in the Earth, when disturbed, may be regarded as consisting of the initial stress combined with an additional stress. (3) The additional stress may be taken to be connected with the strain, measured from the initial state as unstrained state, by Hooke's law of stress and strain. (4) The density and the elastic constants are considered as functions of the distance from the center of the Earth. (In the numerical calculations below, the Earth model referred to in the introduction is adopted.) This method of dealing with the complications is a kind of perturbation method. The additional stress and strain are considered to be small compared with the initial stress and strain, and their effects are taken into consideration in the form of perturbations.

Section 2--In this section, the fundamental differential equations will be established as described above. Let us now take the center of the Earth as the origin of the rectangular coordinates (x, y, z) and let ρ denote the density of the material point which is at the point (x, y, z) at time t, and V the potential at the same point and at the same time, of all the forces acting on the body, whether caused by the attraction of external bodies or to the attraction of the body itself. The external forces are assumed to be derivable from a potential. Let (u, v, w) denote the displacement of the material point from the initial state, so the material point which is at (x, y, z) at time t, would be at (x - u, y - v, z - w) in the initial state. The state of stress existing at the point (x, y, z) at time it may be specified by six components of stress X_x, X_y, ... Then the equations of motion are the three equations of the type

$$\rho\,\partial^2u/\partial t^2 = \rho\,\partial V/\partial x + \partial X_x/\partial x + \partial X_y/\partial y + \partial X_z/\partial z \quad \ldots\ldots\ldots\ldots\ldots\ldots (1)$$

Here X_x, X_y, ... denote the combined stresses of additional and intial stresses. As the initial stress contained in X_x, X_y, ... , we should take the initial stress at the point (x - u, y - v, z - w). This will be understood by considering the history of the material point which is at (x, y, z) at time t. The point is moved from (x - u, y - v, z - w) to (x, y, z) carrying its initial stress at (x - u, y - v, z - w) and acquiring the additional stress depending upon the displacement (v, v, w). The additional stress can be described by the space derivatives of (u, v, w), by the assumption (3) in the last section, as follows

$$X_x = \lambda\Delta + 2\mu\,\partial u/\partial x, \qquad X_y = \mu(\partial v/\partial x + \partial u/\partial y), \qquad X_z = \mu(\partial w/\partial x + \partial u/\partial z) \quad . (2)$$

Here λ and μ are the Lamé's elastic constants and Δ, as usual, is the volume divergence

$$\Delta = \partial u/\partial x + \partial v/\partial y + \partial w/\partial z \quad \ldots\ldots\ldots\ldots\ldots\ldots\ldots (3)$$

Let ρ_0, P_0, and V_0 denote the density, initial hydrostatic pressure, and the potential of the forces at (x, y, z) in the initial state. Then the initial stress at the point (x - u, y - v, z - w) is as follows by the assumption (1) referred to above.

$$X_x = Y_y = Z_z = -(P_0 - U\,dP_0/dr),\ X_y = X_z = \ldots\ldots = 0 \ldots\ldots\ldots\ldots (4)$$

where U denotes the radial displacement of the material point and can be written by the relation of projection,

$$rU = xu + yv + zw \ldots\ldots\ldots\ldots\ldots\ldots\ldots\ldots (5)$$

and r denotes the distance from the origin and can be written

$$r^2 = x^2 + y^2 + z^2 \ldots\ldots\ldots\ldots\ldots\ldots\ldots\ldots (6)$$

The stresses X_x, ... which appear in (1) are the combinations of X_x, ... which appear in (2) and (4)

$$\left.\begin{aligned} X_x &= -(P_0 - U\,dP_0/dr) + \lambda\Delta + 2\mu\,\partial u/\partial x \\ X_y = \mu(\partial v/\partial x + \partial u/\partial y),\ &\text{and}\ \ X_z = \mu(\partial w/\partial x + \partial u/\partial z) \end{aligned}\right\} \ldots\ldots\ldots (7)$$

The assumption that the initial stress balances the self-gravitation of the Earth in the initial state can be written in the form

$$\rho\,\partial V_0/\partial x = \partial P_0/\partial x \ldots\ldots\ldots\ldots\ldots\ldots\ldots\ldots (8)$$

The density ρ which appeared in (1) can be written as in (7)

$$\rho = \rho_0 - U\,d\rho_0/dr - \rho_0\Delta \ldots\ldots\ldots\ldots\ldots\ldots\ldots\ldots (9)$$

The potential V, which also appeared in (1), is the sum of V_0 and an additional potential K,

$$V = V_0 + K \ldots\ldots\ldots\ldots\ldots\ldots\ldots\ldots (10)$$

The additional potential K is the potential due to external disturbing bodies, together with that due to a volume distribution of additional density $-(U\,d\rho_0/dr + \rho_0\Delta)$, and that due to a surface distribution of density on several discontinuous surfaces of density. Inserting (9), (10), and (7) into (1), we can obtain the fundamental differential equations for our problem.

Section 3--We shall now regard (u, v, w) as small quantities of the second order and neglect their products and squares. U, Δ, and K are, also, small quantities of the same order. Taking these into account, we shall insert (9), (10), and (7) into (1). The left-hand side of equation (1) becomes

$$\rho\,\partial^2 u/\partial t^2 = \rho_0\,\partial^2 u/\partial t^2 \ldots\ldots\ldots\ldots\ldots\ldots\ldots\ldots (11)$$

The first term of the right-hand side of (1) becomes

$$\rho\,\partial V/\partial x = \rho_0\,\partial(V_0 + K)/\partial x - (U\,d\rho_0/dr + \rho_0\Delta)\,\partial V_0/\partial x \ldots\ldots\ldots (12)$$

Adding the relations

$$\partial X_x/\partial x = -\,\partial P_0/\partial x + \partial(U\,dP_0/dr)/\partial x + \Delta\,\partial\lambda/\partial x + \lambda\,\partial\Delta/\partial x + 2(\partial\mu/\partial x)(\partial u/\partial x) + 2\mu\,\partial^2 u/\partial x^2,$$

$$\partial X_y/\partial y = (\partial\mu/\partial y)(\partial v/\partial x + \partial u/\partial y) + \mu(\partial^2 v/\partial y\partial x + \partial^2 u/\partial y^2),\ \text{and}$$

$$\partial X_z/\partial z = (\partial\mu/\partial z)(\partial w/\partial x + \partial u/\partial z) + \mu(\partial^2 w/\partial z\partial x + \partial^2 u/\partial z^2),$$

we get the second term of the right-hand side of (1) as follows

$$-\partial P_0/\partial x + \partial(U\,dP_0/dr)/\partial x + (\lambda + \mu)\partial\Delta/\partial x + \mu\nabla^2 u + E_x \ldots\ldots\ldots (13)$$

where, as usual,

$$\nabla^2 u = (\partial^2/\partial x^2 + \partial^2/\partial y^2 + \partial^2/\partial z^2)u \ldots\ldots\ldots\ldots\ldots\ldots\ldots\ldots (14)$$

and E_x contains all the terms concerning the space derivatives of the elastic moduli, that is

$$E_x = \Delta\, \partial\lambda/\partial x + 2(\partial\mu/\partial x)(\partial u/\partial x) + (\partial\mu/\partial y)(\partial v/\partial x + \partial u/\partial y) + (\partial\mu/\partial z)(\partial w/\partial x + \partial u/\partial z)$$

Since P_o, ρ_o, λ, and μ are assumed to be the functions of the distance r from the origin only, there exist, for example, the relations

$$\partial\mu/\partial x = (x/r)\, d\mu/dr, \quad \partial\lambda/\partial x = (x/r)\, d\lambda/dr, \quad \partial\mu/\partial y = (y/r)\, d\mu/dr \quad \ldots\ldots\ldots\ldots (15)$$

so that

$$rE_x = x\Delta\, d\lambda/dr + (d\mu/dr)[2x\, \partial u/\partial x + y(\partial v/\partial x + \partial u/\partial y) + z(\partial w/\partial x + \partial u/\partial z)] \quad \ldots\ldots\ldots\ldots (16)$$

Adding (12) and (13), thereby canceling the first term of them by the relation (8), and equating it to (11), we get

$$\rho_o\, \partial^2 u/\partial t^2 = \rho_o\, \partial K/\partial x - (U\, d\rho_o/dr + \rho_o\Delta)(\partial V_o/\partial x) + \partial(U\, dP_o/dr)/\partial x$$
$$+ (\lambda + \mu)(\partial\Delta/\partial x) + \mu\nabla^2 u + E_x \quad \ldots\ldots\ldots\ldots (17)$$

From the other equations of (1), we get equations similar to (17). As stated in Section 2, K is the potential due to external disturbing bodies, together with that due to a volume distribution of the additional density $-(U\, d\rho_o/dr + \rho_o\Delta)$ and a surface distribution of density. Since the external bodies have no volume density distribution within the Earth, the so-called Poisson's formula gives one more relation

$$\nabla^2 K = -4\pi f[-(U\, d\rho_o/dr + \rho_o\Delta)] = 4\pi f(U\, d\rho_o/dr + \rho_o\Delta) \quad \ldots\ldots\ldots\ldots (18)$$

where f is Newton's gravitation constant. Eq. (17) and (18) are the fundamental differential equations required.

Section 4--We can obtain a typical solution of the system of equations (17) and (18), assuming that K is proportional to a spherical harmonic. We can afterwards, if we need, obtain a more general solution by adding the typical solutions containing different spherical harmonics. We assume, therefore, that K is of the form

$$K = K_n(r)\, W_n \quad \ldots\ldots\ldots\ldots (19)$$

where W_n is a solid spherical harmonic of degree n and $K_n(r)$ is a function of r only, and we assume also u, v, and w are given by the equations

$$\left.\begin{array}{l} u \\ v \\ w \end{array} = F_n(r) \begin{array}{l} \partial/\partial x \\ \partial/\partial y \\ \partial/\partial z \end{array} W_n + G_n(r) \begin{array}{l} x \\ y \\ z \end{array} W_n \right\} \quad \ldots\ldots\ldots\ldots (20)$$

where $F_n(r)$ and $G_n(r)$ are some functions of r only. We shall now calculate the quantities appearing in (17) for the assumed forms of K and (u, v, w). At first, since K_n is a function of r only,

$$\partial K/\partial x = K_n\, \partial W_n/\partial x + (x/r)(dK_n/dr)\, W_n \quad \ldots\ldots\ldots\ldots (21)$$

Next, for U, by (5) and (20)

$$rU = F_n(x\, \partial/\partial x + y\, \partial/\partial y + z\, \partial/\partial z)\, W_n + G_n\, r^2 W_n \quad \ldots\ldots\ldots\ldots (22)$$

Using the identity for a solid spherical harmonic

$$(x\, \partial/\partial x + y\, \partial/\partial y + z\, \partial/\partial z)\, W_n = nW_n \quad \ldots\ldots\ldots\ldots (23)$$

(22) can be written in the following form

$$rU = (nF_n + r^2 G_n)\, W_n \quad \ldots\ldots\ldots\ldots (24)$$

Next, for Δ, adding the equations

$$\left.\begin{aligned}
\partial u/\partial x &= (x/r)(dF_n/dr)(\partial W_n/\partial x) + F_n\,\partial^2 W_n/\partial x^2 + (x/r)(dG_n/dr)xW_n + G_nW_n + G_nx\,\partial W_n/\partial x\\
\partial v/\partial y &= (y/r)(dF_n/dr)(\partial W_n/\partial y) + F_n\,\partial^2 W_n/\partial y^2 + (y/r)(dG_n/dr)yW_n + G_nW_n + G_ny\,\partial W_n/\partial y\\
\partial w/\partial z &= (z/r)(dF_n/dr)(\partial W_n/\partial z) + F_n\,\partial^2 W_n/\partial z^2 + (z/r)(dG_n/dr)zW_n + G_nW_n + G_nz\,\partial W_n/\partial z
\end{aligned}\right\}(25)$$

and taking into account (6), (23), and

$$\nabla^2 W_n = 0 \;. \quad (26)$$

we get

$$\Delta = [(n/r)(dF_n/dr) + r\,dG_n/dr + (n+3)G_n]W_n \;.\;.\;.\;.\;.\;.\;.\;.\;.\;.\;. \quad (27)$$

We shall, for convenience, denote for it

$$\Delta = f_n W_n \;. (28)$$

where

$$f_n = (n/r)(dF_n/dr) + r\,dG_n/dr + (n+3)G_n \;.\;.\;.\;.\;.\;.\;.\;.\;.\;.\;.\;.\;. (29)$$

is a function of r only. Next, for $U\,dP_o/dr$ we have

$$U\,dP_o/dr = [(nF_n + r^2G_n)/r](dP_o/dr)\,W_n \;.\;.\;.\;.\;.\;.\;.\;.\;.\;.\;.\;.\;.\;. (30)$$

Remembering that $[(nF_n + r^2G_n/r)](dP_o/dr)$ and f_n are functions of r only, we get

$$\partial(U\,dP_o/dr)/\partial x = [(nF_n + r^2G_n)/r](dP_o/dr)(\partial W_n/\partial x) + W_n(x/r)d[(nF_n + r^2G_n)/r)(dP_o/dr)]/dr \;. \; (31)$$

and

$$\partial\Delta/\partial x = f_n\,\partial W_n/\partial x + (x/r)(df_n/dr)W_n \;.\;.\;.\;.\;.\;.\;.\;.\;.\;.\;.\;.\;.\;.\;.\;.\;. (32)$$

Though not in right order, we calculate $2x\,\partial u/\partial x + y(\partial v/\partial x + \partial u/\partial y) + z(\partial w/\partial x + \partial u/\partial z)$ in E_x next. Now

$$\left.\begin{aligned}
\partial u/\partial x &= (x/r)(dF_n/dr)(\partial W_n/\partial x) + F_n\,\partial^2 W_n/\partial x^2 + (x/r)(dG_n/dr)xW_n + G_nx\,\partial W_n/\partial x + G_nW_n\\
\partial u/\partial y &= (y/r)(dF_n/dr)(\partial W_n/\partial x) + F_n\,\partial^2 W_n/\partial y\partial x + (y/r)(dG_n/dr)xW_n + G_nx\,\partial W_n/\partial y\\
\partial u/\partial z &= (z/r)(dF_n/dr)(\partial W_n/\partial x) + F_n\,\partial^2 W_n/\partial z\partial x + (z/r)(dG_n/dr)xW_n + G_nx\,\partial W_n/\partial z\\
\partial v/\partial x &= (x/r)(dF_n/dr)(\partial W_n/\partial y) + F_n\,\partial^2 W_n/\partial x\partial y + (x/r)(dG_n/dr)yW_n + G_ny\,\partial W_n/\partial x\\
\partial w/\partial x &= (x/r)(dF_n/dr)(\partial W_n/\partial z) + F_n\,\partial^2 W_n/\partial x\partial z + (x/r)(dG_n/dr)zW_n + G_nz\,\partial W_n/\partial x
\end{aligned}\right\}(33)$$

We shall here introduce a subsidiary equation, that is

$$\begin{aligned}
(x\partial^2/\partial x^2 + y\partial^2/\partial x\partial y + z\partial^2/\partial x\partial z)W_n &= \partial(x\partial W_n/\partial x + y\partial W_n/\partial y + z\partial W_n/\partial z)/\partial x - \partial W_n/\partial x\\
&= (n-1)\partial W_n/\partial x \;. \quad (34)
\end{aligned}$$

Multiplying both sides of the equations in (33) by 2x, y, z, y, and z respectively, adding, and taking into account (6), (23), and (34), we obtain

$$\begin{aligned}
2x\partial u/\partial x + y(\partial v/\partial x + \partial u/\partial y) + z(\partial w/\partial x + \partial u/\partial z) &= [r\,dF_n/dr + 2(n-1)F_n + r^2G_n]\partial W_n/\partial x\\
&\quad + [(n/r)\,dF_n/dr + 2r\,dG_n/dr + (n+2)G_n]xW_n \;.\;.\;.\;.\;.\;.\;.\;.\;.\;.\;.\;.\;.\;. (35)
\end{aligned}$$

For $\nabla^2 u$, next, differentiating $\partial u/\partial x$, $\partial u/\partial y$, and $\partial u/\partial z$ in (33) with respect to x, y, and z respectively, we get

$$\partial^2 u/\partial x^2 = (1/r)(dF_n/dr)(\partial W_n/\partial x) + (x^2/r)(\partial W_n/\partial x)\,d\,[(1/r)\,dF_n/dr]/dr + (2x/r)(dF_n/dr)(\partial^2 W_n/\partial x^2)$$

$$\begin{aligned}&+ F_n\,\partial^3W_n/\partial x^3 + (x/r)W_n\,dG_n/dr + (x^3/r)W_n\,d[(1/r)\,dG_n/dr]/dr + (x/r)W_n\,dG_n/dr\\&+ (x^2/r)(dG_n/dr)(\partial W_n/\partial x) + (x/r)W_n\,dG_n/dr + G_n\,\partial W_n/\partial x + (x^2/r)(dG_n/dr)(\partial W_n/\partial x)\\&+ G_n\,\partial W_n/\partial x + G_n x\,\partial^2W_n/\partial x^2,\end{aligned}$$

$$\begin{aligned}\partial^2u/\partial y^2 = {}&(1/r)(dF_n/dr)(\partial W_n/\partial x) + (y^2/r)(\partial W_n/\partial x)\,d\,[(1/r)\,dF_n/dr]/dr\\&+ (2y/r)(dF_n/dr)(\partial^2W_n/\partial y\partial x) + F_n\,\partial^3W_n/\partial x\partial y^2 + (x/r)W_n\,dG_n/dr\\&+ (y^2x/r)W_n\,d[(1/r)\,dG_n/dr]/dr + 0 + (xy/r)(dG_n/dr)(\partial W_n/\partial y) + 0\\&+ 0 + (xy/r)(dG_n/dr)(\partial W_n/\partial y) + 0 + G_n x\,\partial^2W_n/\partial y^2,\text{ and}\end{aligned}$$

$$\begin{aligned}\partial^2u/\partial z^2 = {}&(1/r)(dF_n/dr)(\partial W_n/\partial x) + (z^2/r)(\partial W_n/\partial x)\,d\,[(1/r)\,dF_n/dr]/dr\\&+ (2z/r)(dF_n/dr)(\partial^2W_n/\partial z\partial x) + F_n\,\partial^3W_n/\partial x\partial z^2 + (x/r)W_n\,dG_n/dr\\&+ (z^2x/r)W_n\,d\,[(1/r)\,dG_n/dr]/dr + 0 + (xz/r)(dG_n/dr)(\partial W_n/\partial z) + 0\\&+ 0 + (xz/r)(dG_n/dr)(\partial W_n/\partial z) + 0 + G_n x\,\partial^2W_n/\partial z^2\end{aligned}$$

Adding these and considering (6), (23), (26), and (34), we get

$$\begin{aligned}\nabla^2u = {}&(3/r)(dF_n/dr)(\partial W_n/\partial x) + r(\partial W_n/\partial x)\,d\,[(1/r)\,dF_n/dr]dr + (2/r)(n-1)(dF_n/dr)(\partial W_n/\partial x)\\&+ (3x/r)W_n\,dG_n/dr + rx\,W_n\,d[(1/r)\,dG_n/dr]/dr + (2x/r)W_n\,dG_n/dr\\&+ (2nx/r)W_n\,dG_n/dr + 2G_n\,\partial W_n/\partial x = [d^2F_n/dr^2 + (2n/r)\,dF_n/dr + 2G_n]\partial W_n/\partial x\\&+ [d^2G_n/dr^2 + (2/r)(n+2)\,dG_n/dr]xW_n \qquad (36)\end{aligned}$$

Assuming here u, v, and $w \propto e^{ipt}$, we get

$$\partial^2u/\partial t^2 = -p^2[F_n\,\partial W_n/\partial x + G_n xW_n] \qquad (37)$$

Inserting (21), (24), (27), (31), (32), (35), (36), and (37) into (17), we get

$$\begin{aligned}&\Big\{\rho_0K_n + (1/r)(nF_n + r^2G_n)\,dP_0/dr + (\lambda+\mu)\,f_n + \mu[d^2F_n/dr^2 + (2n/r)\,dF_n/dr + 2G_n]\\&\quad+ (d\mu/dr)[dF_n/dr + (2/r)(n-1)\,F_n + rG_n] + \rho_0\,p^2F_n\Big\}\,\partial W_n/\partial x + \Big\{\rho_0\,dK_n/dx\\&\quad- [(1/r)(nF_n + r^2G_n)\,d\rho_0/dr + \rho_0f_n]\,dV_0/dr + d[(1/r)(nF_n + r^2G_n)\,dP_0/dr]/dr\\&\quad+ (\lambda+\mu)\,df_n/dr + \mu[rd^2\,G_n/dr^2 + 2(n+2)\,dG_n/dr] + (d\lambda/dr)[(n/r)\,dF_n/dr\\&\quad+ r\,dG_n/dr + (n+3)G_n] + (d\mu/dr)[(n/r)\,dF_n/dr + 2r\,dG_n/dr + (n+2)G_n]\\&\quad+ \rho_0p^2\,rG_n\Big\}\,(x/r)\,W_n = 0 \qquad (38)\end{aligned}$$

We denote this, for convenience, as

$$R_1\,\partial W_n/\partial x + R_2(x/r)W_n = 0 \qquad (39)$$

where R_1 and R_2 are functions of r only. From the other equations in (17), we get

$$R_1\,\partial W_n/\partial y + R_2(y/r)W_n = 0,\quad\text{and}\quad R_1\,\partial W_n/\partial z + R_2(z/r)W_n = 0 \qquad (40)$$

So, for the coexistence of the equations of motion, it is necessary and sufficient that

$$R_1 = R_2 = 0 \quad \ldots\ldots\ldots\ldots\ldots\ldots\ldots\ldots \quad (41)$$

Inserting (29) into these, we get, after a little rearrangement,

$$\begin{aligned}&\mu d^2F_n/dr^2 + [d\mu/dr + (n/r)(\lambda + 3\mu)]\, dF_n/dr + [-(2/r)\, d\mu/dr + \rho_0 p^2 + (n/r)\, d(P_0 + 2\mu)/dr]F_n \\ &\quad + (\lambda + \mu)r\, dG_n/dr + [rd(P_0 + \mu)/dr + (3\lambda + 5\mu) + n(\lambda + \mu)]G_n + \rho_0 K_n = 0 \quad \ldots\ldots\ldots \quad (42)\end{aligned}$$

$$\begin{aligned}&n(\lambda + \mu)\, d^2F_n/dr^2 + n[-(1/r)(\lambda + \mu) + d(\lambda + \mu)/dr]\, dF_n/dr + n[-(1/r)\, dP_0/dr + \rho_0\, d^2V_0/dr^2]F_n \\ &+ r^2(\lambda + 2\mu)\, d^2G_n/dr^2 + [r(4\lambda + 8\mu) + r^2\, d(\lambda + 2\mu)/dr + nr(\lambda + 3\mu)]\, dG_n/dr + [r^2\rho_0\, d^2V_0/dr^2 \\ &+ rd(3\lambda + 2\mu - 2P_0)/dr + \rho_0\, p^2r^2 + nrd(\lambda + \mu - P_0)/dr]G_n + \rho_0 rdK_n/dr = 0 \quad \ldots\ldots\ldots \quad (43)\end{aligned}$$

In the course of the rearrangement of (43), the following subsidiary relations were used

$$dP_0/dr = \rho_0\, dV_0/dr\ , \quad \text{and} \quad d^2P_0/dr^2 = (d\rho_0/dr)\, dV_0/dr + \rho_0\, d^2V_0/dr^2 \quad \ldots\ldots\ldots \quad (44)$$

Eq. (42) and (43) are two relations among the three unknown functions F_n, G_n, and K_n. One more relation can be obtained from (18) as follows: Differentiating (21) with respect to x again, we get

$$\begin{aligned}\partial^2K/\partial x^2 &= (2x/r)(dK_n/dr)\, \partial W_n/\partial x + K_n \partial^2W_n/\partial x^2 + (1/r)(dK_n/dr)W_n \\ &\quad + (x^2/r)W_n d[(1/r)\, dK_n/dr]/dr\end{aligned}$$

Similarly,

$$\begin{aligned}\partial^2K/\partial y^2 &= (2y/r)(dK_n/dr)\, \partial W_n/\partial y + K_n\partial^2W_n/\partial y^2 + (1/r)(dK_n/dr)W_n \\ &\quad + (y^2/r)W_n d[(1/r)dK_n/dr]/dr\ , \quad \text{and} \quad \partial^2K/\partial z^2 = (2z/r)(dK_n/dr)\, \partial W_n/\partial z \\ &\quad + K_n\, \partial^2W_n/\partial z^2 + (1/r)(dK_n/dr)W_n + (z^2/r)W_n\, d[(1/r)dK_n/dr]/dr\end{aligned}$$

Adding these and considering (6), (23), and (26), we get

$$\nabla^2K = [d^2K_n/dr^2 + (2/r)(n + 1)\, dK_n/dr]W_n \quad \ldots\ldots\ldots\ldots\ldots \quad (45)$$

By (27) and (24)

$$\rho_0\Delta + U\, d\rho_0/dr = \left\{\rho_0[(n/r)\, dF_n/dr + r\, dG_n/dr + (n + 3)G_n] + (d\rho_0/dr)(nF_n + r^2G_n)/r\right\}W_n \quad \ldots (46)$$

Inserting (45) and (46) into (18), we get

$$\begin{aligned}&d^2K_n/dr^2 + (2/r)(n + 1)\, dK_n/dr - 4\pi f \rho_0(n/r)\, dF_n/dr - 4\pi f(d\rho_0/dr)(n/r)F_n \\ &\quad - 4\pi f \rho_0 r\, dG_n/dr - [4\pi fr\, d\rho_0/dr + 4\pi f(n + 3)\rho_0]G_n = 0 \quad \ldots\ldots\ldots \quad (47)\end{aligned}$$

Eq. (42), (43), and (47) are the relations required and they will be used in numerical calculations later.

Section 5--In this section, we shall calculate the quantities which appear in the boundary conditions. Since the displacement is given by (20), the boundary condition that the displacement is continuous at the surface r = b, say, will be satisfied by making F_n and G_n continuous there. Next, for the stress, it is sufficient, for our purpose, to calculate the additional stress only. Since it is assumed that the condition of stress continuity at r = b, say, was satisfied by the initial stress, we have only to make the additional stress continuous there. Now we shall calculate the x, y, z components of the additional stress at r = constant. At first, for the x component X_r, by the relation of projection,

$$rX_r = xX_x + yX_y + zX_z$$

Omitting the initial stress $-(P_0 - U\, dP_0/dr)$ in the expression X_x, we have by (7)

$$X_r = (x/r)(\lambda\Delta + 2\mu\partial u/\partial x) + (\mu/r)[y(\partial v/\partial x + \partial u/\partial y) + z(\partial w/\partial x + \partial u/\partial z)] \quad \ldots\ldots\ldots \quad (48)$$

Inserting (27) and (35) into (48), we get

$$X_r = \mu[dF_n/dr + (2/r)(n-1)\,F_n + rG_n]\,\partial W_n/\partial x + \Big\{\mu[(n/r)\,dF_n/dr + 2r dG_n/dr + (n+2)G_n] + \lambda[(n/r)\,dF_n/dr + r dG_n/dr + (n+3)G_n]\Big\}(x/r)W_n \;\ldots\ldots\ldots\ldots \quad (49)$$

For Y_r and Z_r, we get similar expressions by cyclic interchange of x, y, z. Thus the boundary condition that the (additional) stress is continuous at r = b, say, is satisfied by taking

$$a \times \text{Stress I} = \mu[dF_n/dr + (2/r)(n-1)\,F_n + rG_n]$$

where a is the radius of the Earth.

$$\text{Stress II} = \mu[(n/r)\,dF_n/dr + 2r dG_n/dr + (n+2)G_n] + \lambda[(n/r)(dF_n/dr + r dG_n/dr + (n+3)G_n].\,.\,(50)$$

to be continuous there.

Section 6--In this section, by transforming the relations obtained in Sections 4 and 5 using rectangular coordinates, we shall obtain them in spherical coordinates. Usually, to obtain the solution of equations of motion in spherical coordinates, the equations of motion are transformed into spherical coordinates and then solved. In this way, however, the symmetry among x, y, and z in the equations of motion, for example, is lost, and an awkwardness occurs. In order to avoid this, the method of transforming the rectangular coordinate solution into the spherical coordinate solution is followed in this paper.

Let us now introduce spherical coordinates related to our rectangular coordinates as follows

$$x = r\sin\theta\cos\phi,\quad y = r\sin\theta\sin\phi,\quad z = r\cos\theta \;\ldots\ldots\ldots\ldots \quad (51)$$

$$r^2 = x^2 + y^2 + z^2,\quad \tan\theta = \sqrt{x^2+y^2}/z,\quad \text{and } \tan\phi = y/x \;\ldots\ldots\ldots \quad (52)$$

At first, to express the radial displacement in spherical coordinates, inserting the following expression for W_n

$$W_n = r^n P_n^m(\cos\theta)\cos m\phi \;\ldots\ldots\ldots\ldots \quad (53)$$

into (24), we get

$$U_r = (nF_n + r^2G_n)\,r^{n-1}P_n^m(\cos\theta)\cos m\phi \;\ldots\ldots\ldots \quad (54)$$

Next, for calculating the θ and ϕ components of displacement, we introduce here the relations between the (x, y, z) components and the (r, θ, ϕ) components of a vector quantity U, say

$$\left.\begin{aligned} U_r &= \sin\theta\cos\phi\,U_x + \sin\theta\sin\phi\,U_y + \cos\theta\,U_z \\ U_\theta &= \cos\theta\cos\phi\,U_x + \cos\theta\sin\phi\,U_y - \sin\theta\,U_z \\ U_\phi &= -\sin\phi\,U_x + \cos\phi\,U_y \end{aligned}\right\}\;\ldots\ldots\ldots \quad (55)$$

or expressing the direction cosines by rectangular coordinates,

$$\left.\begin{aligned} rU_r &= xU_x + yU_y + zU_z \\ rU_\theta &= (zx/\sqrt{x^2+y^2})\,U_x + (zy/\sqrt{x^2+y^2})\,U_y - \sqrt{x^2+y^2}\,U_z \\ U_\phi &= -(y/\sqrt{x^2+y^2})\,U_x + (x/\sqrt{x^2+y^2})\,U_y \end{aligned}\right\}\;\ldots\ldots\ldots \quad (56)$$

In fact, we calculated U_r in (24) by the first relation of (56). We shall now calculate U_θ and U_ϕ by the second and the third relations of (56). Multiplying U_x, U_y, and U_z in (20) by $zx/\sqrt{x^2+y^2}$, $zy/\sqrt{x^2+y^2}$, and $-\sqrt{x^2+y^2}$ respectively and adding, we get

$$rU_\theta = F_n[(zx/\sqrt{x^2+y^2})\,\partial W_n/\partial x + (zy/\sqrt{x^2+y^2})\,\partial W_n/\partial y - \sqrt{x^2+y^2}\,\partial W_n/\partial z]\;\ldots\ldots \quad (57)$$

Similarly,

$$U_\phi = F_n[-(y/\sqrt{x^2+y^2})\,\partial W_n/\partial x + (x/\sqrt{x^2+y^2})\,\partial W_n/\partial y]\;\ldots\ldots\ldots \quad (58)$$

On the other hand, we shall now calculate $\partial W_n/\partial\theta$ and $\partial W_n/\partial\phi$. At first by (51)

$$\left.\begin{aligned}\partial x/\partial\theta &= r\cos\theta\cos\phi\,,\ \ \partial y/\partial\theta = r\cos\theta\sin\phi\,,\ \ \partial z/\partial\theta = -r\sin\theta\\ \partial x/\partial\phi &= -r\sin\theta\sin\phi\,,\ \ \partial y/\partial\phi = r\sin\theta\cos\phi\,,\ \text{and}\ \partial z/\partial\phi = 0\end{aligned}\right\}\ldots\ldots\ldots\ldots(59)$$

Inserting this into the relations

$$\left.\begin{aligned}\partial W_n/\partial\theta &= (\partial W_n/\partial x)\partial x/\partial\theta + (\partial W_n/\partial y)\partial y/\partial\theta + (\partial W_n/\partial z)\partial z/\partial\theta\\ \partial W_n/\partial\phi &= (\partial W_n/\partial x)\partial x/\partial\phi + (\partial W_n/\partial y)\partial y/\partial\phi + (\partial W_n/\partial z)\partial z/\partial\phi\end{aligned}\right\}\ldots\ldots\ldots\ldots(60)$$

we get

$$\left.\begin{aligned}\partial W_n/\partial\theta &= r\cos\theta\cos\phi\,\partial W_n/\partial x + r\cos\theta\sin\phi\,\partial W_n/\partial y - r\sin\theta\,\partial W_n/\partial z\\ \partial W_n/\partial\phi &= -r\sin\theta\,[\sin\phi\,\partial W_n/\partial x - \cos\phi\,\partial W_n/\partial y]\end{aligned}\right\}\ldots\ldots\ldots(61)$$

or expressed in rectangular coordinates,

$$\left.\begin{aligned}\partial W_n/\partial\theta &= (zx/\sqrt{x^2+y^2})\,\partial W_n/\partial x + (zy/\sqrt{x^2+y^2})\,\partial W_n/\partial y - \sqrt{x^2+y^2}\,\partial W_n/\partial z\\ \partial W_n/\partial\phi &= r\sin\theta\,[-(y/\sqrt{x^2+y^2})\,\partial W_n/\partial x + (x/\sqrt{x^2+y^2})\,\partial W_n/\partial y]\end{aligned}\right\}\ldots\ldots(62)$$

Comparing these with (57) and (58), we get

$$U_\theta = (1/r)F_n\,\partial W_n/\partial\theta\,,\qquad U_\phi = (1/r\sin\theta)F_n\,\partial W/\partial\phi\ \ldots\ldots\ldots\ldots\ldots(63)$$

Inserting into these the expression for W_n in (53), we get

$$U_\theta = F_n r^{n-1}(\partial P_n^m/\partial\theta)\cos m\phi\,,\qquad U_\phi = -m\,F_n r^{n-1}P_n^m\sin m\phi/\sin\theta\ \ldots\ldots\ldots(64)$$

Next, for the volume divergence Δ, by (27) and (53),

$$\Delta = [(n/r)d\,F_n/dr + r\,dG_n/dr + (n+3)G_n]\,r^n P_n^m\cos m\phi\ \ldots\ldots\ldots\ldots\ldots(65)$$

To calculate the rotation of the displacement vector, we shall first calculate its (x, y, z) components ($\tilde{w}_x$, $\tilde{w}_y$, $\tilde{w}_z$). Inserting (20) into

$$\tilde{w}_x = \partial w/\partial y - \partial v/\partial z\ \ldots\ldots\ldots\ldots\ldots\ldots\ldots\ldots(66)$$

we get

$$\tilde{w}_x = [(1/r)\,dF_n/dr - G_n][y\,\partial W_n/\partial z - z\,\partial W_n/\partial y]\ \ldots\ldots\ldots\ldots(67)$$

Similarly for $\tilde{w}_y$ and $\tilde{w}_z$,

$$\left.\begin{aligned}\tilde{w}_y &= [(1/r)\,dF_n/dr - G_n][z\,\partial W_n/\partial x - x\,\partial W_n/\partial z]\\ \tilde{w}_z &= [(1/r)\,dF_n/dr - G_n][x\,\partial W_n/\partial y - y\,\partial W_n/\partial x]\end{aligned}\right.\ \ldots\ldots\ldots\ldots(68)$$

Since the transformation (56) can be used for the rotation, too, we get for the r component $\tilde{w}_r$ of the rotation

$$r\,\tilde{w}_r = x\,\tilde{w}_x + y\,\tilde{w}_y + z\,\tilde{w}_z\ \ldots\ldots\ldots\ldots\ldots\ldots\ldots\ldots(69)$$

Inserting (67) and (68) into (69), we get

$$\tilde{w}_r = 0\ \ldots\ldots\ldots\ldots\ldots\ldots\ldots\ldots\ldots\ldots(70)$$

Thus the solution of the equations of motion we have found in Section 4 is the solution for which the radial component of the rotation of the displacement vector vanishes. We shall consider in the next section the solution for which it does not vanish. Adding this solution to that obtained in Section 4, we get the most general solution of the equations of motion (1).

Returning to our main subject, we shall next calculate the θ and ϕ components of rotation. By the relations similar to (56), we get

$$\left.\begin{aligned} r\,\tilde{w}_\theta &= (zx/\sqrt{x^2+y^2})\,\tilde{w}_x + (zy/\sqrt{x^2+y^2})\,\tilde{w}_y - \sqrt{x^2+y^2}\,\tilde{w}_z \\ \tilde{w}_\phi &= -(y/\sqrt{x^2+y^2})\,\tilde{w}_x + (x/\sqrt{x^2+y^2})\,\tilde{w}_y \end{aligned}\right\}\ldots\ldots\ldots(71)$$

Inserting (67) and (68) into (71), we get

$$\left.\begin{aligned} r\,\tilde{w}_\theta &= -[(1/r)\,dF_n/dr - G_n][(x^2+y^2+z^2)/\sqrt{x^2+y^2}][x\partial W_n/\partial y - y\partial W_n/\partial x] \\ \tilde{w}_\phi &= [(1/r)\,dF_n/dr - G_n][(zx/\sqrt{x^2+y^2})\partial W_n/\partial x + (zy/\sqrt{x^2+y^2})\partial W_n/\partial y - \sqrt{x^2+y^2}\,\partial W_n/\partial z] \end{aligned}\right\}.(72)$$

Comparing this with (62), we get

$$\tilde{w}_\theta = -(dF_n/dr - rG_n)(1/r\sin\theta)\partial W_n/\partial\phi\,, \quad \tilde{w}_\phi = (dF_n/dr - rG_n)(1/r)\partial W_n/\partial\theta\ \ldots\ldots\ldots(73)$$

Inserting (53) into (73), we get

$$\begin{aligned} \tilde{w}_\theta &= (dF_n/dr - rG_n)\,mr^{n-1}\,P_n^m \sin m\phi/\sin\theta\,, \\ \tilde{w}_\phi &= (dF_n/dr - rG_n)\,r^{n-1}\,(\partial P_n^m/\partial\theta)\cos m\phi\ \ldots\ldots\ldots\ldots\ldots\ldots(74) \end{aligned}$$

Lastly, we shall calculate the (r, θ, ϕ) components of the additional stress at the surface r = constant. Comparing (49) with (20), we see that the (x, y, z) components of the stress at r = constant are of the same form as the (x, y, z) components of the displacement, if only we substitute $\mu[dF_n/dr + (2/r)(n-1)\,F_n + rG_n]$ and $\mu/r\,[(n/r)\,dF_n/dr + 2r\,dG_n/dr + (n+2)G_n] + \lambda/r[(n/r)dF_n/dr + r\,dG_n/dr + (n+3)G_n]$ for F_n and G_n in (20) respectively. Let R_r, Θ_r, and Φ_r denote the (r, θ, ϕ) components of the additional stress at the surface r = constant. Since the transformation from (X_r, Y_r, Z_x) to (R_r, Θ_r, Φ_r) is of the same form as that from (u, v, w) to (u_r, u_θ, u_y), the expressions for (R_r, Θ_r, Φ_r) can be obtained by the substitutions mentioned above in the expressions for (u_r, u_θ, u_ϕ) in (54) and (64). Thus we get

$$\left.\begin{aligned} R_r &= \Big\{2\mu[n\,dF_n/dr + (n/r)(n-1)\,F_n + r^2dG_n/dr + (n+1)\,rG_n] + \lambda\,[n\,dF_n/dr + r^2dG_n/dr \\ &\qquad + (n+3)\,rG_n]\Big\}\,r^{n-1}\,P_n^m\cos m\phi \\ \Theta_r &= \mu\,[dF_n/dr + (2/r)(n-1)\,F_n + rG_n]\,r^{n-1}\,(\partial P_n^m/\partial\theta)\cos m\phi \\ \Phi_r &= -m\mu[dF_n/dr + (2/r)(n-1)\,F_n + rG_n]\,r^{n-1}\,P_n^m\sin m\phi/\sin \end{aligned}\right\}\ldots.(75)$$

The expressions for the quantities in spherical coordinates obtained in this section will be used in the boundary value problems later.

Section 7--In this section, the solution of the equations of motion (1), for which the radial component of rotation does not vanish, will be obtained. Since it is sufficient for our purpose to obtain a solution of this type, we restrict the solution by imposing additional conditions upon it. We shall assume that our solution of the equations of motion is of the type for which both the radial component of displacement and the volume divergence vanish. By the assumption, (17) and (18) become

$$\rho_0\partial^2u/\partial t^2 = \mu\nabla^2u + (1/r)(d\mu/dr)[2x\partial u/\partial x + y(\partial v/\partial x + \partial u/\partial y) + z(\partial w/\partial x + \partial u/\partial z)]\ \ldots..(76)$$

and

$$K = 0\ \ldots\ldots\ldots\ldots\ldots\ldots\ldots\ldots\ldots\ldots\ldots\ldots\ldots(77)$$

We shall now assume

$$\left.\begin{aligned} U &= L_n(r)(y\partial W_n/\partial z - z\partial W_n/\partial y) \\ V &= L_n(r)(z\partial W_n/\partial x - x\partial W_n/\partial z) \\ W &= L_n(r)(x\partial W_n/\partial y - y\partial W_n/\partial x) \end{aligned}\right\}\ldots\ldots\ldots\ldots\ldots\ldots(78)$$

where $L_n(r)$ is a function of r only. We see that the form above assumed for (u, v, w) is of the same type as $\tilde{w}_x$, $\tilde{w}_y$, and $\tilde{w}_z$ in (67) and (68). At first we must verify that the radial displacement and volume divergence vanish for the assumed form of (u, v, w) in (78). By the same procedure as in (70)

$$u_r = 0 \qquad (79)$$

is verified easily. By differentiating (78), we get

$$\left.\begin{aligned}
\partial u/\partial x &= (x/r)(dL_n/dr)(y\partial W_n/\partial z - z\partial W_n/\partial y) + L_n\,(y\partial^2 W_n/\partial x\partial z - z\partial^2 W_n/\partial x\partial y)\\
\partial v/\partial y &= (y/r)(dL_n/dr)(z\partial W_n/\partial x - x\partial W_n/\partial z) + L_n\,(z\partial^2 W_n/\partial y\partial x - x\partial^2 W_n/\partial y\partial z)\\
\partial w/\partial z &= (z/r)(dL_n/dr)(x\partial W_n/\partial y - y\,\partial W_n/\partial x) + L_n\,(x\partial^2 W_n/\partial z\partial y - y\partial^2 W_n/\partial z\partial x)
\end{aligned}\right\} \qquad (80)$$

Adding these, we get the required equation

$$\Delta = 0 \qquad (81)$$

In the same way as in (73) and (74), we get

$$U_\theta = -L_n(r)(1/\sin\theta)\partial W_n/\partial\phi\,, \quad U_\phi = L_n(r)\partial W_n/\partial\theta \qquad (82)$$

or

$$U_\theta = mL_n(r)\,r^n P_n^m \sin m\phi/\sin\theta, \qquad U_\phi = L_n(r)\,r^n\,(\partial P_n^m/\partial\theta)\cos m\phi \qquad (83)$$

We shall next calculate the x component of rotation $\tilde{w}_x$. Inserting (78) into

$$\tilde{w}_x = \partial w/\partial y - \partial v/\partial z \qquad (84)$$

we get

$$\begin{aligned}
\tilde{w}_x = {}& (1/r)(dL_n/dr)[xy\partial W_n/\partial y - y^2\partial W_n/\partial x - z^2\partial W_n/\partial x + xz\partial W_n/\partial z]\\
&+ L_n[x(\partial^2 W_n/\partial y^2 + \partial^2 W_n/\partial z^2) - y\partial^2 W_n/\partial x\partial y - z\partial^2 W_n/\partial x\partial z - 2\partial W_n/\partial x]
\end{aligned}$$

Considering (6) and (26), this can be written

$$\begin{aligned}
\tilde{w}_x = {}& (x/r)(dL_n/dr)[x\partial W_n/\partial x + y\partial W_n/\partial y + z\partial W_n/\partial z] - r(dL_n/dr)\partial W_n/\partial x\\
&- [x\partial^2 W_n/\partial x^2 + y\partial^2 W_n/\partial x\partial y + z\partial^2 W_n/\partial x\partial z + 2\partial W_n/\partial x]\,L_n
\end{aligned}$$

Inserting (23) and (34) into this, we get

$$\tilde{w}_x = -[r dL_n/dr + (n+1)\,L_n]\,\partial W_n/\partial x + (n/r)(dL_n/dr)xW_n \qquad (85)$$

Similarly

$$\left.\begin{aligned}
\tilde{w}_y &= -[r dL_n/dr + (n+1)\,L_n]\,\partial W_n/\partial y + (n/r)(dL_n/dr)yW_n\\
\tilde{w}_z &= -[r dL_n/dr + (n+1)\,L_n]\,\partial W_n/\partial z + (n/r)(dL_n/dr)zW_n
\end{aligned}\right\} \qquad (86)$$

We see that the form for $(\tilde{w}_x, \tilde{w}_y, \tilde{w}_z)$ above obtained is of the same type as (u, v, w) in (20). Thus in the same way as we get from (u, v, w) to (u_r, u_θ, u_ϕ) in the last section,

$$\left.\begin{aligned}
\tilde{w}_r &= -n(n+1)(L_n/r)W_n\\
\tilde{w}_\theta &= -[r dL_n/dr + (n+1)L_n](1/r)\,\partial W_n/\partial\theta\\
\tilde{w}_\phi &= -[r dL_n/dr + (n+1)L_n](1/r\sin\theta)\,\partial W_n/\partial\phi
\end{aligned}\right\} \qquad (87)$$

or

$$\left.\begin{aligned}\widetilde{w}_r &= -n(n+1)\,r^{n-1}\,L_n P_n^m \cos m\phi\\ \widetilde{w}_\theta &= -[r dL_n/dr + (n+1)L_n]\,r^{n-1}(\partial P_n^m/\partial\theta)\cos m\phi\\ \widetilde{w}_\phi &= m[r dL_n/dr + (n+1)L_n]\,r^{n-1}P_n^m \sin m\phi/\sin\theta\end{aligned}\right\}\quad\text{. . . . . (88)}$$

As we see in (87) or (88), the radial component of rotation does not vanish for non-vanishing L_n, so the solution above obtained is of the type required. In order to obtain the differential equation for L_n, we insert (78) into (76), first reducing by (5) and (79)

$$xu + yv + zw = 0 \quad\text{. . . . . (89)}$$

Differentiating this with respect to x, we get

$$u + x\partial u/\partial x + y\partial v/\partial x + z\partial w/\partial x = 0 \quad\text{. . . . . (90)}$$

so $2x\partial u/\partial x + y(\partial v/\partial x + \partial u/\partial y) + z(\partial w/\partial x + \partial u/\partial z)$ in (76) becomes $-u + x\partial u/\partial x + y\partial u/\partial y + z\partial u/\partial z$. Now by (78)

$$\left.\begin{aligned}\partial u/\partial x &= (x/r)(dL_n/dr)(y\partial W_n/\partial z - z\partial W_n/\partial y) + L_n(y\partial^2W_n/\partial x\partial z - z\partial^2W_n/\partial x\partial y)\\ \partial u/\partial y &= (y/r)(dL_n/dr)(y\partial W_n/\partial z - z\partial W_n/\partial y) + L_n(y\partial^2W_n/\partial y\partial z - z\partial^2W_n/\partial y^2 + \partial W_n/\partial z)\\ \partial u/\partial z &= (z/r)(dL_n/dr)(y\partial W_n/\partial z - z\partial W_n/\partial y) + L_n(y\partial^2W_n/\partial z^2 - z\partial^2W_n/\partial y\partial z - \partial W_n/\partial y)\\ u &= \qquad\qquad\qquad\qquad\qquad\qquad\qquad L_n(y\partial W_n/\partial z - z\partial W_n/\partial y)\end{aligned}\right\}\text{. . (91)}$$

Multiplying by x, y, z and -1 on both sides of these equations respectively and adding, we get

$$\begin{aligned}&x\partial u/\partial x + y\partial u/\partial y + z\partial u/\partial z - u = r(dL_n/dr)(y\partial W_n/\partial z - z\partial W_n/\partial y)\\ &+ L_n\left\{y(x\partial/\partial x + y\partial/\partial y + z\partial/\partial z)\,\partial W_n/\partial z - z(x\partial/\partial x + y\partial/\partial y + z\partial/\partial z)\,\partial W_n/\partial y\right\}\text{. . . . . (92)}\end{aligned}$$

Taking into account the following subsidiary equations

$$\left.\begin{aligned}(x\partial/\partial x + y\partial/\partial y + z\partial/\partial z)\,\partial W_n/\partial y &= (n-1)\,\partial W_n/\partial y\\ (x\partial/\partial x + y\partial/\partial y + z\partial/\partial z)\,\partial W_n/\partial z &= (n-1)\,\partial W_n/\partial z\end{aligned}\right\}\text{. . . . . (93)}$$

[these relations are verified as in (34)], we get

$$\begin{aligned}&2x\partial u/\partial x + y(\partial v/\partial x + \partial u/\partial y) + z(\partial w/\partial x + \partial u/\partial z)\\ &\quad = [r dL_n/dr + (n-1)L_n](y\partial W_n/\partial z - z\partial W_n/\partial y)\text{. . . . . (94)}\end{aligned}$$

Differentiating ∂u/∂x, ∂u/∂y, and ∂u/∂z in (91) with respect to x, y, z again, we obtain

$$\left.\begin{aligned}\partial^2u/\partial x^2 &= (1/r)(dL_n/dr)(y\partial W_n/\partial z - z\partial W_n/\partial y) + (x^2/r)(y\partial W_n/\partial z - z\partial W_n/\partial y)d[(1/r)dL_n/dr]/dr\\ &\quad + (2x/r)(dL_n/dr)(y\partial^2W_n/\partial x\partial z - z\partial^2W_n/\partial x\partial y) + L_n(y\partial^3W_n/\partial x^2\partial z - z\partial^3W_n/\partial x^2\partial y)\\ \partial^2u/\partial y^2 &= (1/r)(dL_n/dr)(y\partial W_n/\partial z - z\partial W_n/\partial y) + (y^2/r)(y\partial W_n/\partial z - z\partial W_n/\partial y)d[(1/r)dL_n/dr]/dr\\ &\quad + (2y/r)(dL_n/dr)(\partial W_n/\partial z + y\partial^2W_n/\partial y\partial z - z\partial^2W_n/\partial y^2) + L_n(2\partial^2W_n/\partial y\partial z\\ &\quad + y\partial^3W_n/\partial y^2\partial z - z\partial^3W_n/\partial y^3)\\ \partial^2u/\partial z^2 &= (1/r)(dL_n/dr)(y\partial W_n/\partial z - z\partial W_n/\partial y) + (z^2/r)(y\partial W_n/\partial z - z\partial W_n/\partial y)d[(1/r)dL_n/dr]/dr\\ &\quad + (2z/r)(dL_n/dr)(v\partial^2W_n/\partial z^2 - \partial W_n/\partial y - z\partial^2W_n/\partial z\partial y) + L_n(y\partial^3W_n/\partial z^3\\ &\quad - z\partial^3W_n/\partial y\partial z^2 - 2\partial^2W_n/\partial y\partial z)\end{aligned}\right\}(95)$$

Adding these, we get

$$\nabla^2 u = \left\{(3/r)dL_n/dr + rd[(1/r)dL_n/dr]/dr\right\}(y\partial W_n/\partial z - z\partial W_n/\partial y) + (2/r)(dL_n/dr)\left\{y(x\partial/\partial x + y\partial/\partial y + z\partial/\partial z)\,\partial W_n/\partial z - z(x\partial/\partial x + y\partial/\partial y + z\partial/\partial z)\,\partial W_n/\partial y + (y\partial W_n/\partial z - z\partial W_n/\partial y)\right\} \quad (96)$$

Inserting (93) into (96), we get

$$\nabla^2 u = [d^2L_n/dr^2 + (2/r)(n+1)dL_n/dr](y\partial W_n/\partial z - z\partial W_n/\partial y) \quad (97)$$

Assuming $u \propto e^{ipt}$, we get

$$\partial^2 u/\partial t^2 = -p^2 L_n(y\partial W_n/\partial z - z\partial W_n/\partial y) \quad (98)$$

Inserting (94), (97), and (98) into (76), we get

$$\left\{\rho_o p^2 L_n + \mu[d^2L_n/dr^2 + (2/r)(n+1)dL_n/dr] + (d\mu/dr)[dL_n/dr + (n-1)L_n]\right\}(y\partial W_n/\partial z - z\partial W_n/\partial y) = 0 \quad (99)$$

We shall denote for this

$$R_3(y\partial W_n/\partial z - z\partial W_n/\partial y) = 0 \quad (100)$$

where R_3 is a function of r only. From the equations similar to (76), we get

$$R_3(z\partial W_n/\partial x - x\partial W_n/\partial z) = 0\,, \qquad R_3(x\partial W_n/\partial y - y\partial W_n/\partial x) = 0 \quad (101)$$

Thus for the coexistence of the equations of motion, it is necessary and sufficient that

$$R_3 = \mu[d^2L_n/dr^2 + (2/r)(n+1)dL_n/dr] + (d\mu/dr)[dL_n/dr + (n-1)L_n] + \rho_o p^2 L_n = 0 \quad (102)$$

This is the required differential equation for L_n. At last we shall calculate the additional stress at the surface r = constant. From (48), (81), and (94), we get

$$X_r = \mu[dL_n/dr + (1/r)(n-1)L_n](y\partial W_n/\partial z - z\partial W_n\partial y) \quad (103)$$

and the similar expressions for Y_r and Z_r. We see that the expressions for X_r, Y_r, and Z_r are of the same type as (u, v, w) in (78). Thus the expressions for R_r, Θ_r, and Φ_r can be obtained easily as in (79), (82), and (83).

$$\left.\begin{aligned} R_r &= 0 \\ \Theta_r &= -\mu[dL_n/dr + (1/r)(n-1)L_n](1/\sin\theta)\partial W_n/\partial\phi \\ \Phi_r &= \mu[dL_n/dr + (1/r)(n-1)L_n]\partial W_n/\partial\theta \end{aligned}\right\} \quad (104)$$

or

$$\left.\begin{aligned} R_r &= 0 \\ \Theta_r &= m\mu r^n[dL_n/dr + (1/r)(n-1)L_n]\,P_n^m \sin m\phi/\sin\theta \\ \Phi_r &= [dL_n/dr + (1/r)(n-1)L_n]\,r^n(\partial P_n^m/\partial\theta)\cos m\phi \end{aligned}\right\} \quad (105)$$

Adding the solution in this section to that in Section 4, we get the most general solution of the equations of motion.

Section 8--In this section, the fundamental differential equations of motion for an incompressible sphere will be obtained. These equations have been obtained by PREY [1929], but we shall introduce them here by considering their relation to those for the compressible sphere obtained in the preceding sections. By the assumption of incompressibility, we mean that the volume elastic modulus λ becomes infinite, and the volume divergence Δ becomes zero, keeping their product $\lambda\Delta$ finite and equal to δp, say. Under these circumstances, the fundamental equations (17) and (18) become

$$\rho_o\partial^2 u/\partial t^2 = \rho_o\partial K/\partial x - U(d\rho_o/dr)\partial V_o/\partial x + \partial(UdP_o/dr + \delta p)/\partial x + \mu\nabla^2 u + E_x = 0 \quad (106)$$

where

$$E_x = (1/r)(d\mu/dr)[2x\partial u/\partial x + y(\partial v/\partial x + \partial u/\partial y) + z(\partial w/\partial x + \partial u/\partial z)] \ldots\ldots \quad (107)$$

and

$$\nabla^2 K = 4\pi f\, U\, d\rho_o/dr \ldots\ldots \quad (108)$$

We shall put

$$U\, dP_o/dr + \delta p = -p$$

and assume for u, v, w, K, and p

$$\left.\begin{array}{l} \begin{matrix} u \\ v \\ w \end{matrix} = F_n(r) \begin{matrix} \partial/\partial x \\ \partial/\partial y \\ \partial/\partial z \end{matrix}\, W_n + G_n(r) \begin{matrix} x \\ y \\ z \end{matrix}\, W_n \\ K = K_n(r)\, W_n\,, \quad \text{and} \quad p = p_n(r)\, W_n \end{array}\right\} \ldots\ldots \quad (109)$$

where $F_n(r)$, $G_n(r)$, $K_n(r)$, and $p_n(r)$ are functions of r only. By the same procedure as before, we get from (106)

$$\rho_o p^2 F_n + \rho_o K_n - p_n + \mu[d^2F_n/dr^2 + (2n/r)\, dF_n/dr + 2G_n]$$
$$+ (d\mu/dr)[dF_n/dr + (2/r)(n-1)F_n + rG_n] = 0 \ldots\ldots \quad (110)$$

and

$$\rho_o p^2 rG_n + \rho_o dK_n/dr - [(nF_n + r^2G_n)/r](d\rho_o/dr)dV_o/dr - dp_n/dr + \mu[rd^2G_n/dr^2 + 2(n+2)dG_n/dr]$$
$$+ (d\mu/dr)[(n/r)dF_n/dr + 2rdG_n/dr + (n+2)G_n] = 0 \ldots\ldots \quad (111)$$

and from (108)

$$d^2K_n/dr^2 + (2/r)(n+1)dK_n/dr = 4\pi f(d\rho_o/dr)[(1/r)(nF_n + r^2G_n)] \ldots\ldots \quad (112)$$

These are three equations among the four unknown functions F_n, G_n, K_n, and p_n. The last equation is given by the assumption that the volume divergence vanishes, that is

$$f_n = (n/r)dF_n/dr + rdG_n/dr + (n+3)G_n = 0 \ldots\ldots \quad (113)$$

In order to eliminate p_n, differentiating (110) with respect to r, and subtracting this from (111), we get

$$p^2[\rho_o rG_n - d(\rho_o F_n)/dr] - (d\rho_o/dr)K_n - (1/r)(nF_n + r^2G_n)(d\rho_o/dr)dV_o/dr + \mu[rd^2G_n/dr^2$$
$$+ 2(n+1)dG_n/dr - d^3F_n/dr^3 - (2n/r)d^2F_n/dr^2 + (2n/r^2)dF_n/dr] + (d\mu/dr)[rdG_n/dr$$
$$+ (n-1)G_n - 2d^2F_n/dr^2 + (1/r)(2-3n)dF_n/dr + (2/r^2)(n-1)F_n] - (d^2\mu/dr^2)[dF_n/dr$$
$$+ (2/r)(n-1)F_n + rG_n] = 0 \ldots\ldots \quad (114)$$

Eq. (112), (113), and (114) are the three relations among the three unknown functions F_n, G_n, and K_n. Now we shall introduce a new function q_n, defined by

$$q_n = nF_n + r^2G_n \ldots\ldots \quad (115)$$

Differentiating this with respect to r, we get

$$dq_n/dr = ndF_n/dr + 2rG_n + r^2dG_n/dr \ldots\ldots \quad (116)$$

From (113) and (116), we get

$$G_n = -[1/r(n+1)]\, dq_n/dr \quad \ldots\ldots \quad (117)$$

From (117) and (115), we get

$$F_n = (1/n)\left\{q_n + [r/(n+1)]dq_n/dr\right\} \quad \ldots\ldots \quad (118)$$

Thus we can express the two functions F_n and G_n by a function q_n and its derivative, and reduce the number of unknown functions by one. For this purpose, differentiating (117) and (118) again and again, we get

$$\left.\begin{aligned} dG_n/dr &= [1/(n+1)][(1/r^2)\, dq_n/dr - (1/r)\, d^2q_n/dr^2] \\ d^2G_n/dr^2 &= [1/(n+1)][-(2/r^3)\, dq_n/dr + (2/r^2)\, d^2q_n/dr^2 - (1/r)\, d^3q_n/dr^3] \\ ndF_n/dr &= [1/(n+1)][(n+2)\, dq_n/dr + rd^2q_n/dr^2] \\ nd^2F_n/dr^2 &= [1/(n+1)][(n+3)\, d^2q_n/dr^2 + rd^3q_n/dr^3] \\ nd^3F_n/dr^3 &= [1/(n+1)][(n+4)\, d^3q_n/dr^3 + rd^4q_n/dr^4] \end{aligned}\right\} \ldots (119)$$

Inserting (117), (118), and (119) into (114), we get, after a little rearrangement,

$$\begin{aligned} &\mu d^4q_n/dr^4 + [2d\mu/dr + (4/r)(n+1)\mu]\, d^3q_n/dr^3 + [d^2\mu/dr^2 + (1/r)(6n+4)\, d\mu/dr \\ &+ (4n/r^2)(n+1)\mu]\, d^2q_n/dr^2 + [(2n/r)\, d^2\mu/dr^2 + (1/r^2)(4n^2-2)\, d\mu/dr - (4n/r^3)(n+1)\mu]dq_n/dr \\ &+ (n/r)(n+1)[(2/n)(1/r)(n-1)\, d^2\mu/dr^2 - (2/n)(1/r^2)(n-1)\, d\mu/dr + (1/r)(d\rho_0/dr)(dV_0/dr)]q_n \\ &+ (n/r)(n+1)(d\rho_0/dr)K_n + \rho_0 p^2\left\{d^2q_n/dr^2 + [(1/\rho_0)\, d\rho_0/dr + (2/r)(n+1)]\, dq_n/dr\right. \\ &\qquad\qquad \left.+ [(n+1)/r](1/\rho_0)(d\rho_0/dr)q_n\right\} = 0 \quad \ldots\ldots \quad (120) \end{aligned}$$

Inserting (115) into (112), we get

$$d^2K_n/dr^2 + (2/r)(n+1)\, dK_n/dr = (1/r)\, 4\pi f\, (d\rho_0/dr)q_n \quad \ldots\ldots \quad (121)$$

Eq. (120) and (121) can be written as follows

$$\begin{aligned} &D[\mu D(q_n)] - (2/r)(d\mu/dr)\, Dq_n - \left\{2d[(1/r)\, d\mu/dr]/dr\right\} r^{n^2-1}d[r^{1-n^2}q_n]/dr \\ &+ (1/r)(d\rho_0/dr)(dV_0/dr)q_n + (n/r)(n+1)(d\rho_0/dr)K_n + \rho_0 p^2\left\{d^2q_n/dr^2\right. \\ &\left.+ [(1/\rho_0)\, d\rho_0/dr + (2/r)(n+1)]\, dq_n/dr + [(n+1)/r](1/\rho_0)(d\rho_0/dr)q_n\right\} = 0 \quad \ldots\ldots \quad (122) \end{aligned}$$

and

$$DK_n = (1/r)\, 4\pi f\, (d\rho_0/dr)\, q_n \quad \ldots\ldots \quad (123)$$

where D is a differential operator defined by

$$D = d^2/dr^2 + (2/r)(n+1)d/dr \quad \ldots\ldots \quad (124)$$

Eq. (122) and (123) are the two relations between two unknown functions q_n and K_n, and these are nothing but the differential equations obtained by Prey.

Section 9--The deformation of the Earth by the tidal attraction of the Sun and Moon was discussed first by KELVIN [1863a] under the assumption that the Earth is an incompressible elastic sphere of uniform density and elasticity and the results of his study are referred to frequently, but Kelvin's method is rather clumsy. It is here discussed by the method which is used in our study. Assuming that the Earth tide can be treated by the equilibrium tidal theory, equations of equilibrium and the relation of incompressibility are written as follows

$$\rho\partial V/\partial x + \partial X_x/\partial x + \partial X_y/\partial y + \partial X_z/\partial z = 0 \quad \ldots\ldots \quad (125)$$

and

$$\Delta = \partial u/\partial x + \partial v/\partial y + \partial w/\partial z = 0 \quad \ldots\ldots\ldots\ldots \quad (126)$$

where

$$\left.\begin{aligned} \rho = \rho_0 - U\, d\rho_0/dr - \rho_0\Delta\,, \quad V = V_0 + K\,, \\ X_x = -(P_0 - U\, dP_0/dr) + \delta p + 2\mu\partial u/\partial x\,, \\ X_y = \mu(\partial u/\partial y + \partial v/\partial x)\,, \text{ and } X_z = \mu(\partial u/\partial z + \partial w/\partial x) \end{aligned}\right\} \ldots\ldots\ldots \quad (127)$$

By the assumption of homogeneity and incompressibility, ρ becomes equal to ρ_0, λ to infinity, and Δ to zero. The product of $\lambda\Delta$ takes a finite value δp, say. Denoting

$$U\, dP_0/dr + \delta p = -p \quad \ldots\ldots\ldots\ldots \quad (128)$$

and inserting (127) into (125), we get

$$\rho_0\partial(V_0 + K)/\partial x - \partial(P_0 + p)/\partial x + \mu(\nabla^2 u + \partial\Delta/\partial x) = 0$$

The first and the third terms in this equation cancel out by the relation

$$\rho_0\partial V_0/\partial x = \partial P_0/\partial x$$

and the last term vanishes by (126), so the above equation becomes

$$\rho_0\partial K/\partial x - \partial p/\partial x + \mu\nabla^2 u = 0$$

Similarly we get

$$\rho_0\partial K/\partial y - \partial p/\partial y + \mu\nabla^2 v = 0 \quad \ldots\ldots\ldots\ldots \quad (129)$$

and

$$\rho_0\partial K/\partial z - \partial p/\partial z + \mu\nabla^2 w = 0$$

Operating $\partial/\partial x$, $\partial/\partial y$, and $\partial/\partial z$ on the first, second, and the third equations in (129) and adding, we get

$$\nabla^2(\rho_0 K - p) = 0 \quad \ldots\ldots\ldots\ldots \quad (130)$$

Multiplying by x, y, and z respectively in the first, second, and third equations of (129) and adding, we get

$$(x\partial/\partial x + y\partial/\partial y + z\partial/\partial z)(\rho_0 K - p) + \mu\nabla^2(xu + yv + zw) = 0 \quad \ldots\ldots\ldots \quad (131)$$

Denoting

$$rU = xu + yv + zw = q \quad \ldots\ldots\ldots\ldots \quad (132)$$

Eq. (131) becomes

$$(x\partial/\partial x + y\partial/\partial y + z\partial/\partial z)(\rho_0 K - p) + \mu\nabla^2 q = 0 \quad \ldots\ldots\ldots \quad (133)$$

Considering $d\rho_0/dr = \Delta = 0$, Poisson's equation (18) becomes

$$\nabla^2 K = 0 \quad \ldots\ldots\ldots\ldots \quad (134)$$

Relations (130), (133), and (134) are the three differential equations among the three unknown functions K, p, and q. Putting

$$K = K_n(r)W_n\,, \quad p = p_n(r)W_n\,, \quad \text{and} \quad q = q_n(r)W_n \quad \ldots\ldots\ldots \quad (135)$$

(130), (133), and (134) become, as in Section 4,

$$[d^2/dr^2 + (2/r)(n + 1)](\rho_0 K_n - p_n) = 0 \quad \ldots\ldots\ldots \quad (136)$$

$$[d^2/dr^2 + (2/r)(n+1)]q_n = -(n/\mu)(\rho_0 K_n - p_n) \tag{137}$$

and

$$[d^2/dr^2 + (2/r)(n+1)]K_n = 0 \tag{138}$$

The relevant solutions of (138) and (136) are

$$K_n = \text{constant} = A \tag{139}$$

and

$$\rho_0 K_n - p_n = \text{constant} = B \tag{140}$$

and Eq. (137) becomes

$$[d^2/dr^2 + (2/r)(n+1)]q_n = -(n/\mu)B \tag{141}$$

the solution of which is

$$q_n = C - nBr^2/[2(2n+3)\mu] \tag{142}$$

Putting

$$\left.\begin{matrix} u \\ v \\ w \end{matrix} \begin{matrix} \\ = F_n(r) \\ \\ \end{matrix} \begin{matrix} \partial/\partial x \\ \partial/\partial y \\ \partial/\partial z \end{matrix} \begin{matrix} \\ W_n + G_n(r) \\ \\ \end{matrix} \begin{matrix} x \\ y \\ z \end{matrix} \begin{matrix} \\ W_n \\ \\ \end{matrix}\right\} \tag{143}$$

where $F_n(r)$ and $G_n(r)$ are functions of r only and can be expressed in terms of q_n and dq_n/dr as in (117) and (118)

$$\left.\begin{aligned} F_n &= (1/n)\{q_n + [r/(n+1)]dq_n/dr\} \\ G_n &= -(1/r)[1/(n+1)]dq_n/dr \end{aligned}\right\} \tag{144}$$

We shall now calculate the x-component of the additional stress at the surface r = constant. By (48)

$$X_r = (x/r)(\delta p + 2\mu\partial u/\partial x) + (\mu/r)[y(\partial v/\partial x + \partial u/\partial y) + z(\partial w/\partial x + \partial u/\partial z)] \tag{145}$$

Inserting (128) and (143) into (145), we get as in (49)

$$\begin{aligned} X_r = \mu[dF_n/dr + (2/r)(n-1)F_n + rG_n]\,\partial W_n/\partial x + \{\mu[(n/r)\,dF_n/dr \\ + 2rdG_n/dr + (n+2)G_n] - p_n + (\rho_0/r)q_n g\}(x/r)W_n \end{aligned} \tag{146}$$

The boundary conditions at the surface of the Earth are the vanishing of the additional stress there and a condition on the potential. The first boundary condition is satisfied by putting

$$dF_n/dr + (2/r)(n-1)F_n + rG_n = 0 \tag{147}$$

and

$$\mu[(n/r)\,dF_n/dr + 2rdG_n/dr + (n+2)G_n] - p_n + (\rho_0/r)q_n g = 0 \tag{148}$$

at r = a. The other boundary condition is obtained as follows: As is stated in Section 3, K is the potential due to external bodies together with that due to an additional density distribution caused by the deformation of the Earth. We shall now separate these two parts and denote the part due to external bodies as W_n, as is done in the theory of tidal attraction. The potential due to the deformation of the Earth is, therefore, expressed by $[K_n(r) - 1]W_n$. The potential outside the Earth caused by the additional density will be $[K_n(a) - 1](a/r)^{2n+1}W_n$. The potential gradients outside and inside of the surface of the Earth are $[K_n(a) - 1]\partial[(a/r)^{2n+1}W_n]/\partial r$ and $\partial\{[K_n(r) - 1]W_n\}/\partial r$ respectively. Equating their difference to $-4\pi f$ times the surface density $\rho_0(a)\,U(a)$, we get, after a little rearrangement,

$$rdK_n/dr + (2n+1)[K_n(r) - 1] = 4\pi f\,\rho_0 q_n \tag{149}$$

at $r = a$. Eq. (147), (148), and (149) are used to determine the three constants A, B, and C. Putting $n = 2$ and inserting (139), (140), (142), and (144) into (147), (148), and (149), and also taking into consideration (117), (118), and (119), we get

$$\left.\begin{aligned} &C - (8/21)\,Ba^2/\mu = 0\ , \quad \rho_o A - (19/21)B = (\rho_o g/a)(C - Ba^2/7\mu) \\ \text{and} \quad &5(A - 1) = (3g/a)(C - Ba^2/7\mu) \end{aligned}\right\} \ldots\ldots \quad (150)$$

where

$$g = (4/3)\pi f a \rho_o \ldots\ldots \quad (151)$$

From (150), we get

$$A = 1 + 3/(2m)\ , \quad B = (21/2)[\mu/(gam)]\ , \text{ and } C = 4a/(gm) \ldots\ldots \quad (152)$$

where

$$m = 1 + (19/2)[\mu/(\rho_o ga)] \ldots\ldots \quad (153)$$

Inserting this into (24), (63), and the expression for the potential caused by the deformation of the Earth $[K_2(a) - 1]W_2$, we get

$$\left.\begin{aligned} &u_r = [5/(2gm)]W_2\ , \quad u_\theta = [3/(4gm)]\,\partial W_2/\partial\theta\ , \\ &u_\phi = [3/(4gm)](1/\sin\theta)\,\partial W_2/\partial\phi\ , \text{ and } \quad [K_2(a) - 1]W_2 = [3/(2m)]W_2 \end{aligned}\right\} \ldots\ldots \quad (154)$$

at $r = a$. These are the relations frequently referred to.

Section 10--In this section, the differential equations (42), (43), and (47) are transformed to a convenient form for the numerical integrations to be carried out later. At first, the independent variable is changed from r to ξ by the relation

$$\xi = r/a \ldots\ldots \quad (155)$$

where a is the radius of the Earth. We shall also change the dependent variables from $F_n(r)$, $G_n(r)$, and $K_n(r)$ to $F_n(\xi)$, $G_n(\xi)$, and $K_n(\xi)$ by the relations

$$F_n(\xi) = F_n(r)/a^2\ , \quad G_n(\xi) = G_n(r)\ , \text{ and } K_n(\xi) = [1/(4\pi f a^2)]K_n(r) \ldots\ldots \quad (156)$$

We shall denote $F_n(\xi)$, $G_n(\xi)$, and $K_n(\xi)$ simply by F_n, G_n, and K_n. Inserting (155) and (156) into (42), (43), and (47), we get

$$\begin{aligned} &\mu d^2F_n/d\xi^2 + [d\mu/d\xi + (n/\xi)(\lambda + 3\mu)]dF_n/d\xi + [-(2/\xi)d\mu/d\xi + (n/\xi)d(P_o + 2\mu)/d\xi + \rho_o p^2 a^2]F_n \\ &\quad + (\lambda + \mu)\,\xi dG_n/d\xi + [3\lambda + 5\mu + \xi d(P_o + \mu)/d\xi + n(\lambda + \mu)]G_n + 4\pi f a^2 \rho_o K_n = 0 \ldots\ldots \quad (157) \end{aligned}$$

$$\begin{aligned} &n(\lambda + \mu)d^2F_n/d\xi^2 + n[-(\lambda + \mu)/\xi + d(\lambda + \mu)/d\xi]dF_n/d\xi + n[-(1/\xi)dP_o/d\xi + \rho_o d^2V_o/d\xi^2]F_n \\ &\quad + (\lambda + 2\mu)\xi^2 d^2G_n/d\xi^2 + [4(\lambda + 2\mu)\xi + \xi^2 d(\lambda + 2\mu)/d\xi + n(\lambda + 3\mu)\xi]dG_n/d\xi \\ &\quad + [\xi^2 \rho_o d^2V_o/d\xi^2 + \xi d(3\lambda + 2\mu - 2P_o)/d\xi + n\xi d(\lambda + \mu - P_o)/d\xi \\ &\quad + \rho_o p^2 a^2 \xi^2]G_n + 4\pi f a^2 \rho_o \xi dK_n/d\xi = 0 \ldots\ldots \quad (158) \end{aligned}$$

and

$$\begin{aligned} &d^2K_n/d\xi^2 + (2/\xi)(n + 1)dK_n/d\xi - (n\rho_o/\xi)dF_n/d\xi - (n/\xi)(d\rho_o/d\xi)F_n - \rho_o \xi dG_n/d \\ &\quad - [(n + 3)\rho_o + \xi d\rho_o/d\xi]G_n = 0 \ldots\ldots \quad (159) \end{aligned}$$

The differential equations (157), (158), and (159) are to be integrated numerically.

CHAPTER II

Numerical integration

Section 11--The elastic deformation of the Earth by the tidal attraction of the Sun and Moon is called the Earth tide. In this chapter, a theory of Earth tides for the model Earth with its internal constitution inferred from the study of seismic waves is established. From the mathematical point of view, this is done by solving the simultaneous differential equations (157), (158), and (159) in Chapter I under some boundary conditions. The potential for the tidal attraction of the Sun and Moon is given by

$$W_2 = fMD^{-3} r^2 P_2(\cos \theta) \quad \ldots\ldots\ldots\ldots\ldots\ldots (160)$$

where f is Newton's gravitation constant, M the mass of the Sun or the Moon, D the mean distance between the center of the Earth and that of the Sun or the Moon, and r and θ are polar coordinates of a point referred to the center of the Earth as origin and the line connecting the centers of the Earth and the Sun or the Moon as polar axis. On the other hand, in Chapter I, we assumed that the potential due to external bodies is of the form W_n and obtained the differential equations (157), (158), and (159). Thus we can obtain the theory of Earth tides by putting n = 2 in these equations. We may be fairly confident that an equilibrium theory of the Earth tide would be correct, whatever the rigidity of the Earth might be, because the period of free oscillation of tidal type of a fluid sphere of the size and mass of the Earth would be about one hour and 34 min [KELVIN, 1863b]. If the substance is as rigid as steel, instead of being fluid, and if it is homogeneous and incompressible, the period is about one hour and six minutes [LAMB, 1882]. These periods are very short compared with any tidal periods, and it is unlikely that they would be lengthened very much by assuming any admissible constitution of the Earth. Taking these circumstances into consideration, we get the fundamental differential equations of the Earth tide by putting n = 2 and p = 0 in the equations (157), (158), and (159). The differential equations thus obtained are

$$\begin{aligned} &\mu d^2F_2/d\xi^2 + [d\mu/d\xi + (2\lambda + 6\mu)/\xi]dF_2/d\xi + (2/\xi)[d(P_0 + \mu)/d\xi]F_2 \\ &+ (\lambda + \mu)\xi dG_2/d\xi + [\xi d(P_0 + \mu)/d\xi + 5\lambda + 7\mu]G_2 + 4\pi fa^2 \rho_0 K_2 = 0 \quad \ldots\ldots\ldots (161) \end{aligned}$$

$$\begin{aligned} &2(\lambda + \mu)d^2F_2/d\xi^2 + 2[d(\lambda + \mu)/d\xi - (\lambda + \mu)/\xi]dF_2/d\xi + 2[-(1/\xi)dP_0/d\xi + \rho_0 d^2V_0/d\xi^2]F_2 \\ &+ (\lambda + 2\mu)\xi^2 d^2G_n/d\xi^2 + [\xi^2 d(\lambda + 2\mu)/d\xi + (6\lambda + 14\mu)\xi]dG_2/d\xi \\ &+ [\xi^2 \rho_0 d^2V_0/d\xi^2 + \xi d(5\lambda + 4\mu - 4P_0)/d\xi]G_2 + 4\pi fa^2 \rho_0 \xi dK_2/d\xi = 0 \quad \ldots\ldots\ldots (162) \end{aligned}$$

and

$$\begin{aligned} &d^2K_2/d\xi^2 + (6/\xi)dK_2/d\xi - (2\rho_0/\xi)dF_2/d\xi - (2/\xi)(d\rho_0/d\xi)F_2 \\ &- \rho_0 \xi dG_n/d\xi - (\xi d\rho_0/d\xi + 5\rho_0)G_2 = 0 \quad \ldots\ldots\ldots\ldots\ldots\ldots (163) \end{aligned}$$

where

$$\xi = r/a\,, \quad F_2(\xi) = (1/a^2)F_2(r)\,, \quad G_2(\xi) = G_2(r)\,, \quad \text{and} \quad K_2(\xi) = [1/(4\pi fa^2)]K_2(r) \quad \ldots\ldots (164)$$

Section 12--Eq. (161), (162), and (163) will be solved by the method of numerical integration. In order to solve the equations numerically, it is necessary that the coefficients of F_2'', F_2', F_2, G_2'', G_2' . . . . in these equations are calculated numerically. Adopting the Earth model with the internal constitution inferred from the study of seismic waves passing through the Earth, the values of ρ_0, λ, and μ for depths from zero to 2900 km are calculated for the Earth Models 1 and 2. In the Earth Model 1, the value of ρ_0 obtained by BULLEN [1940] is used. The values of λ and μ are calculated by the formulas

$$V_P = \sqrt{(\lambda + 2\mu)/\rho_0}\,, \quad \text{and} \quad V_S = \sqrt{\mu/\rho_0} \quad \ldots\ldots\ldots\ldots\ldots (165)$$

where V_P and V_S are the velocities of P and S seismic waves, using the mean values of V_P and V_S obtained by GUTENBERG and RICHTER [1935] and WADATI [1933] and the value of ρ_0 referred to above. In the Earth Model 2, the value of ρ_0 obtained by BULLEN [1936] (the values of ρ_0 obtained by Bullen in 1940 and 1936 differ but little from each other) is used, and the values of λ and μ are calculated by the formula (165) using the value of ρ_0 referred to above and the values of V_P

and V_S obtained by JEFFREYS [1939] for the depths from zero to 500 km, and those obtained by Gutenberg and Wadati referred to above for the depths from 500 to 2900 km. The values of V_P and V_S obtained by Jeffreys, Gutenberg, and Wadati differ but little from each other for the depth from 500 to 2900 km. The so-called Jeffreys' discontinuity is assumed to be at the depth of 500 km in the Earth Model 2. The distributions of ρ_0, λ, and μ thus obtained are shown in Figures 1, 2, and 3.

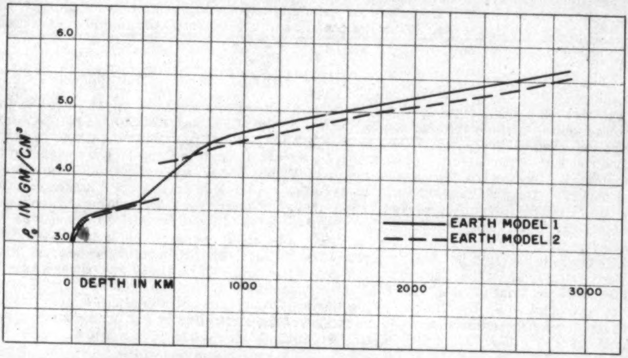

Fig. 1--The density distribution for the depth from 0 to 2900 km

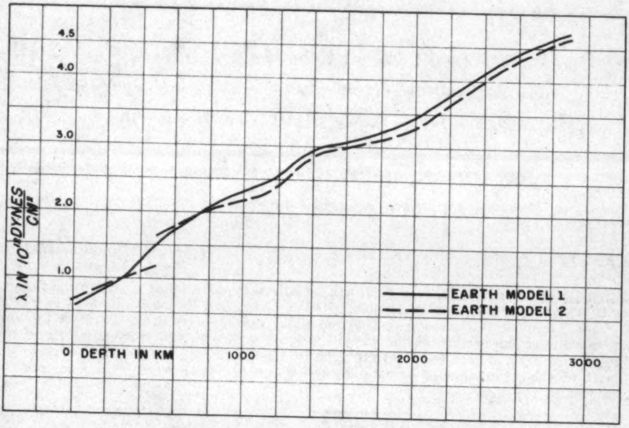

Fig. 2--The λ distribution for the depth from 0 to 2900 km

The values of ρ_0, λ, and μ that will be used in the boundary conditions later are shown in Table 1. In Table 1, the suffix "above" or "under" means the values above or under the discontinuous surfaces. The value of $dV_0/d\xi = -ag$, where g is the gravity at each depth and a is the radius of the Earth, is calculated by the formula

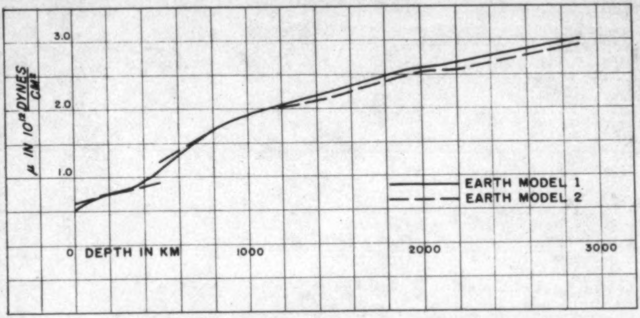

Fig. 3--The rigidity distribution for the depth from 0 to 2900 km

Table 1--Assumed boundary conditions (in CGS units)

Depth	Earth Model 1			Earth Model 2		
	ρ_0	λ	μ	ρ_0	λ	μ
km						
0	3.0	0.6 $\times 10^{12}$	0.5 $\times 10^{12}$	3.0	0.68 $\times 10^{12}$	0.6 $\times 10^{12}$
500 above	3.89	1.520	1.120	3.69	1.197	0.9262
500 under				4.22	1.644	1.217
2900 above	5.68	4.734	3.010	5.53	4.608	2.931

$$g = fM/r^2 \quad \ldots\ldots\ldots\ldots\ldots\ldots\ldots\ldots\ldots \quad (166)$$

where f is Newton's gravitation constant and M is the mass enclosed by a sphere of radius r. The value of M may be calculated from the value of the density shown above. The value of the initial hydrostatic pressure P_0 is calculated by the formula

$$dP_0/dr = -\rho_0 g \quad \ldots\ldots\ldots\ldots\ldots\ldots\ldots\ldots \quad (167)$$

using the value of ρ_0 and g above obtained. The values of g and P_0 thus calculated for the Earth Models 1 and 2 differ but little from each other and the distributions of g and P_0 are shown in Figures 4 and 5. The values of $d\rho_0/d\xi$, $d\lambda/d\xi$, ... are calculated numerically using the smoothed curves for ρ_0, λ, ...

Section 13--Substituting the values of ρ_0, $d\rho_0/d\xi$, λ, $d\lambda/d\xi$, ... calculated in the last section in (161), and (163) and solving them with respect to F_2'', G_2'', and K_2'', we get the equations

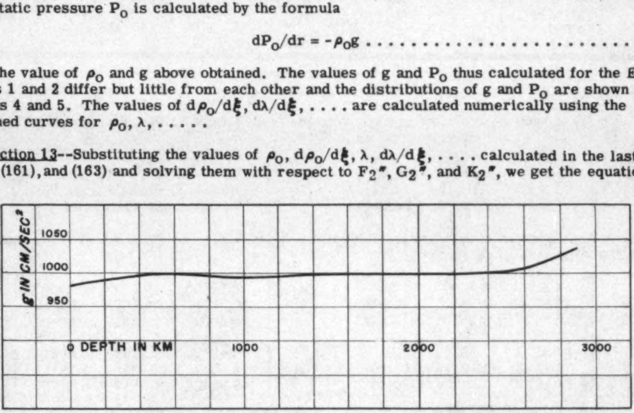

Fig. 4--The gravity distribution for the depth from 0 to 2900 km

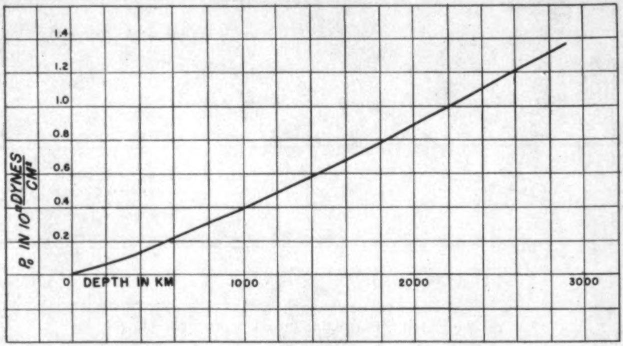

Fig. 5--The pressure distribution for the depth from 0 to 2900 km

of the following type for each ξ (actual figures appearing in the following equations are those for the depth of 2900 km or $\xi = 0.54474$ of the Earth Model 1).

$$\left.\begin{aligned} F'' &= -15.5983\,F' - 1.40149\,G' + 8.94718\,F - 13.5363\,G - 0.641792\,K \\ G'' &= 87.6187\,F' - 4.46119\,G' - 0.329764\,K' - 49.2933\,F + 67.1108\,G + 3.11489\,K \\ K'' &= 20.8540\,F' + 3.09412\,G' - 11.0144\,K' - 11.1090\,F + 26.7518\,G \end{aligned}\right\} \ldots\ldots (168)$$

In the above equations, the subscript 2 is omitted and $d^2F_2(\xi)/d\xi^2$, for example, is written simply as F''. Putting

$$\begin{bmatrix} F \\ G \\ K \end{bmatrix} = [y] \ldots\ldots (169)$$

Eq. (168) can be written in the form

$$[y''] = [P(\xi)]\,[y'] + [Q(\xi)]\,[y] \ldots\ldots (170)$$

where $[P(\xi)]$ and $(Q(\xi)]$ are some matrix functions of ξ of rank 3. For $\xi = 0.54474$ of the Earth Model 1, [P] and [Q] are given by (168) as follows

$$[P] = \begin{bmatrix} -15.5983 & -1.40149 & 0.0 \\ 87.6187 & -4.46119 & -0.329764 \\ 20.8540 & 3.09412 & -11.0144 \end{bmatrix}, \quad [Q] = \begin{bmatrix} 8.94718 & -13.5363 & -0.641792 \\ -49.2933 & 67.1108 & 3.11489 \\ -11.1090 & 26.7518 & 0.0 \end{bmatrix} \ldots (171)$$

Similarly for the depth of 2700 km and 2500 km or $\xi = 0.57614$ and $\xi = 0.60754$ of the Earth Model 1, [P] and [Q] are given by

$$\left.\begin{aligned} [P] &= \begin{bmatrix} -14.8010 & -1.48907 & 0.0 \\ 77.9546 & -3.58826 & -0.316831 \\ 19.3877 & 3.21774 & -10.4141 \end{bmatrix}, \quad [Q] = \begin{bmatrix} 8.19655 & -13.5625 & -0.654323 \\ -40.3310 & 65.1677 & 2.84261 \\ -10.5035 & 26.1817 & 0.0 \end{bmatrix} \\ [P] &= \begin{bmatrix} -13.8614 & -1.53259 & 0.0 \\ 69.1183 & -2.92119 & -0.310815 \\ 18.0729 & 3.33539 & -9.87588 \end{bmatrix} \quad [Q] = \begin{bmatrix} 7.49818 & -13.2293 & -0.665187 \\ -32.9646 & 62.4252 & 2.58113 \\ -9.96064 & 25.6117 & 0.0 \end{bmatrix} \end{aligned}\right\} \ldots (172)$$

As is seen from (171), and (172), $[P(\xi)]$ and $[Q(\xi)]$ are rather smooth functions of ξ.

Section 14--In this section, the method of numerical integration adopted in our study will briefly be explained. We tried to use other methods of numerical integration, for example, Runge-Kutta's method of integration, but the method here explained was the most effective. At first, expanding the matrix coefficients $[P(\xi)]$ and $[Q(\xi)]$ into power series of $\xi - \xi_o$, where ξ_o is an arbitrary value of ξ, we get

$$[P(\xi)] = \sum_{n=0}^{\infty} [P_n] (\xi - \xi_o)^n , \quad [Q(\xi)] = \sum_{n=0}^{\infty} [Q_n] (\xi - \xi_o)^n \quad \ldots\ldots\ldots\ldots (173)$$

where $[P_n]$ and $[Q_n]$ are some constant matrices. We shall now assume that $[y]$ is of the form

$$[y] = \sum_{n=0}^{\infty} [A_n] (\xi - \xi_o)^n \quad \ldots\ldots\ldots\ldots (174)$$

where $[A_n]$ is a constant matrix. Inserting (173) and (174) into (170), we get

$$\sum_n n(n-1)[A_n](\xi - \xi_o)^{n-2} - \sum_n \sum_m \Big\{[P_m] n [A_n](\xi - \xi_o)^{m+n-1} + [Q_m][A_n](\xi - \xi_o)^{m+n}\Big\} = 0 \quad \ldots\ldots\ldots\ldots (175)$$

Equating the matrix coefficient of $(\xi - \xi_o)^{n-2}$ in (175) to zero, we get the following recurrence formula for $[A_n]$.

$$n(n-1)[A_n] = \Big\{(n-1)[P_o][A_{n-1}] + (n-2)[P_1][A_{n-2}] + \ldots\Big\} + \Big\{[Q_o][A_{n-2}] + [Q_1][A_{n-3}] + \ldots\Big\} \quad \ldots\ldots\ldots\ldots (176)$$

Using (176), practical numerical calculation is made as follows. The values of $[y]$ and $[y']$ at $\xi = \xi_o + h$, where h is a sufficiently small interval, are obtained by (174) as follows.

$$[y(\xi_o + h)] = \sum_n [A_n h^n] , \quad [y'(\xi_o + h)] = (1/h) \sum_n n[A_n h^n] \quad \ldots\ldots\ldots\ldots (177)$$

Denoting

$$[A_n h^n] = [a_n] \quad \ldots\ldots\ldots\ldots (178)$$

(177) can be written in the form

$$[y(\xi_o + h)] = \sum_n [a_n] , \quad [y'(\xi_o + h)] = (1/h) \sum_n n[a_n] \quad \ldots\ldots\ldots\ldots (179)$$

On the other hand, multiplying by h^n on both sides of (176) and putting

$$[P_n h^{n+1}] = [p_n] , \quad [Q_n h^{n+2}] = [q_n] \quad \ldots\ldots\ldots\ldots (180)$$

(176) is written in the form

$$n(n-1)[a_n] = \Big\{(n-1)[p_o][a_{n-1}] + (n-2)[p_1][a_{n-2}] + \ldots\Big\} + \Big\{[q_o][a_{n-2}] + [q_1][a_{n-3}] + \ldots\Big\} \quad \ldots\ldots\ldots\ldots (181)$$

Thus, calculating the coefficients $[a_n]$ and $n[a_n]$ by the recurrence formula (181), we get the values of $[y]$ and $[y']$ at $\xi = \xi_o + h$ by the formula (179). Similarly, using the coefficients $[a_n]$ and $n[a_n]$, the values of $[y]$ and $[y']$ at $\xi = \xi_o - h$ are calculated by the formula

$$[y(\xi_o - h)] = \sum_n (-1)^n a_n , \quad [y'(\xi_o - h)] = (1/h) \sum_n n(-1)^n a_n \quad \ldots\ldots\ldots\ldots (182)$$

In order to calculate the values of $[a_n]$ in succession, the values of $[a_o]$ and $[a_1]$ must be given before the calculation. We shall calculate the values of $[a_n]$ for the following values of $[a_o]$ and $[a_1]$.

$$\left.\begin{array}{lll} [a_o] = 1 , & [a_1] = 0 , & \text{in Case 1} \\ [a_o] = 0 , & [a_1] = h , & \text{in Case 2} \end{array}\right\} \quad \ldots\ldots\ldots\ldots (183)$$

The values of $[y]$ and $[y']$ at $\xi = \xi_o$ are given by

$$[y(\xi_o)] = [A_o] = [a_o]\ , \quad [y'(\xi_o)] = [A_1] = [a_1]/h \qquad (184)$$

Comparing (183) and (184), we see that

$$\left.\begin{array}{l} [y(\xi_o)] = 1\ , \quad [y'(\xi_o)] = 0\ , \quad \text{for Case 1} \\ [y(\xi_o)] = 0\ , \quad [y'(\xi_o)] = 1\ , \quad \text{for Case 2} \end{array}\right\} \qquad (185)$$

Since (161), (162), and (163) are linear with respect to [y], the values of $[y(\xi_o + h)]$ and $[y'(\xi_o + h)]$ for arbitrary values of $[y(\xi_o)]$ and $[y'(\xi_o)]$ are given by

$$\begin{bmatrix} [y'(\xi_o + h)] \\ [y(\xi_o + h)] \end{bmatrix} = \begin{bmatrix} (1/h)\sum_n n[a_n] \text{ in Case 2}\ , & (1/h)\sum_n n[a_n] \text{ in Case 1} \\ \sum_n [a_n] \text{ in Case 2}\ , & \sum_n [a_n] \text{ in Case 1} \end{bmatrix} \begin{bmatrix} [y'(\xi_o)] \\ [y(\xi_o)] \end{bmatrix} \qquad (186)$$

Putting

$$\begin{bmatrix} [y'] \\ [y] \end{bmatrix} = [Y] \qquad (187)$$

and

$$\begin{bmatrix} (1/h)\sum_n n[a_n] \text{ in Case 2}\ , & (1/h)\sum_n n[a_n] \text{ in Case 1} \\ \sum_n [a_n] \text{ in Case 2}\ , & \sum_n [a_n] \text{ in Case 1} \end{bmatrix} = [f(\xi_o + h)] \qquad (188)$$

(186) may be written in the form

$$[Y(\xi_o + h)] = [f(\xi_o + h)]\ [Y(\xi_o)] \qquad (189)$$

Similarly, we get

$$[Y(\xi_o - h)] = [f(\xi_o - h)]\ [Y(\xi_o)] \qquad (190)$$

where

$$[f(\xi_o - h)] = \begin{bmatrix} -(1/h)\sum_n (-1)^n\ [a_n] \text{ in Case 2}\ , & -(1/h)\sum_n n(-1)^n\ [a_n] \text{ in Case 1} \\ \sum_n (-1)^n\ [a_n] \text{ in Case 2}\ , & \sum_n (-1)^n\ [a_n] \text{ in Case 1} \end{bmatrix} \qquad (191)$$

Operating with $[f(\xi_o - h)]^{-1}$, where $[f(\xi_o - h)]^{-1}$ is the reciprocal matrix of $[f(\xi_o - h)]$, on both sides of (190), we get

$$[Y(\xi_o)] = [f(\xi_o - h)]^{-1}\ [Y(\xi_o - h)] \qquad (192)$$

Inserting (192) into (189), we get

$$[Y(\xi_o + h)] = [f(\xi_o + h)]\ [f(\xi_o - h)]^{-1}\ [Y(\xi_o - h)] \qquad (193)$$

Thus the one step in our numerical integration from $\xi = \xi_o - h$ to $\xi = \xi_o + h$ is made.

Section 15--In this section, the computational procedures of the numerical integration explained in the last section will be shown by an example. The example is taken from the numerical calculation for the interval from $\xi = 0.54474$ to $\xi = 0.60754$ of the Earth Model 1. Taking $\xi_o = 0.57614$ and $h = 0.031397$, the matrix coefficients $[P(\xi)]$ and $[Q(\xi)]$ from $\xi = \xi_o - h = 0.54474$ to $\xi = \xi_o + h = 0.60754$ are expanded into power series of $\xi - \xi_o$. Since $[P(\xi)]$ and $[Q(\xi)]$ are rather smooth functions of ξ, as was shown in (171), and (172), it is sufficient for our purpose to expand the coefficients $[P(\xi)]$ and $[Q(\xi)]$ to the second power of $\xi - \xi_o$. The values of $[p_n]$ and $[q_n]$ thus calculated are

$$[p_o] = \begin{bmatrix} -0.464710 & -0.0467526 & 0.0 \\ 2.44755 & -0.112661 & -0.0994760 \\ 0.608719 & 0.101028 & -0.326975 \end{bmatrix},\ [q_o] = \begin{bmatrix} 0.0808002 & -0.0133697 & -0.0645020 \\ -0.0397576 & 0.0642412 & 0.0280220 \\ -0.0103542 & 0.0258095 & 0.0 \end{bmatrix}$$

$$[p_1] = \begin{bmatrix} 0.0272669 & -0.0205809 & 0.0 \\ -0.290430 & 0.0241758 & 0.0297473 \\ -0.0436593 & 0.0378760 & 0.0178738 \end{bmatrix}, \quad [q_1] = \begin{bmatrix} -0.0714200 & 0.0151318 & -0.0115302 \\ 0.0804828 & -0.0230949 & -0.0263086 \\ 0.0566007 & -0.0561946 & 0.0 \end{bmatrix}$$

$$[p_2] = \begin{bmatrix} 0.0223391 & 0.0691680 & 0.0 \\ 0.0129953 & -0.0323171 & -0.0108587 \\ 0.0237834 & -0.0937206 & -0.0973941 \end{bmatrix}, \quad [q_2] = \begin{bmatrix} 0.0257585 & 0.0177145 & 0.0820664 \\ -0.0786605 & -0.0394017 & 0.0532323 \\ -0.0308451 & 0.0492891 & 0.0 \end{bmatrix}$$

where $-0.\overset{2}{0}994760$, for example, means -0.00994760. Using these coefficients, the values of $[a_n]$ and $n[a_n]$ are calculated by (181). The values of $[a_n]$ thus calculated for the Case 1 in (183) are as follows.

$$[a_o] = [1.0], \quad [a_1] = [0.0],$$

$$[a_2] = \begin{bmatrix} 0.0404001 & -0.0668485 & -0.0322510 \\ -0.0198788 & 0.0321206 & 0.0140110 \\ -0.0517710 & 0.0129048 & 0.0 \end{bmatrix}, \quad [a_3] = \begin{bmatrix} -0.0435048 & 0.0560152 & 0.0262012 \\ 0.0540112 & -0.0708778 & -0.0359583 \\ 0.0808900 & -0.0177487 & -0.0182558 \end{bmatrix}$$

$$[a_4] = \begin{bmatrix} 0.0398847 & -0.0498511 & -0.0249716 \\ -0.0882808 & 0.0116472 & 0.0564747 \\ -0.0102092 & 0.0233532 & 0.0292057 \end{bmatrix}, \quad [a_5] = \begin{bmatrix} -0.0347560 & 0.0444595 & 0.0220730 \\ 0.0112241 & -0.0151201 & -0.0732005 \\ 0.0113003 & -0.0239369 & -0.0394658 \end{bmatrix}$$

$$[a_6] = \begin{bmatrix} 0.0387853 & -0.0433773 & -0.0239895 \\ -0.0125961 & 0.0164734 & 0.0806893 \\ -0.0111954 & 0.0218655 & 0.0390540 \end{bmatrix}, \qquad \cdots\cdots\cdots\cdots\cdots\cdots$$

Using the values of $[a_n]$ thus calculated, the coefficients $[f(\xi_o + h)]$ and $[f(\xi_o - h)]$ are calculated as follows.

$$[f(\xi_o + h)] = \begin{bmatrix} 0.59606 & -0.041584 & -0.076144 & 0.22038 & -0.37803 & -0.018328 \\ 1.73621 & 0.88503 & -0.069876 & -0.84692 & 1.49593 & 0.061056 \\ 0.48724 & 0.082750 & 0.72692 & -0.26391 & 0.67879 & -0.014286 \\ 0.024757 & -0.067834 & -0.082992 & 1.00364 & -0.061705 & -0.029861 \\ 0.030591 & 0.029594 & -0.012335 & -0.015260 & 1.02606 & 0.010914 \\ 0.082295 & 0.013866 & 0.026848 & -0.044601 & 0.011342 & 0.99998 \end{bmatrix}$$

$$[f(\xi_o - h)] = \begin{bmatrix} 1.54274 & 0.053279 & -0.010892 & -0.30463 & 0.48648 & 0.023405 \\ -3.54809 & 1.09801 & 0.014782 & 1.91540 & -2.89931 & -0.13214 \\ -0.78290 & -0.12703 & 1.39902 & 0.42208 & -1.02560 & -0.021877 \\ -0.039482 & -0.080018 & 0.010852 & 1.00452 & -0.072997 & -0.035145 \\ 0.049289 & -0.033035 & -0.020356 & -0.026289 & 1.04054 & 0.018254 \\ 0.011294 & 0.018458 & -0.037256 & -0.061005 & 0.014939 & 1.00002 \end{bmatrix}$$

Reciprocating $[f(\xi_o - h)]$, we get

$$[f(\xi_o - h)]^{-1} = \begin{bmatrix} 0.57651 & -0.039110 & -0.074936 & 0.23947 & -0.37664 & -0.017889 \\ 1.90380 & 0.86170 & -0.069680 & -1.02325 & 1.49593 & 0.066200 \\ 0.51293 & 0.077961 & 0.71406 & -0.27537 & 0.67932 & -0.014779 \\ 0.024424 & -0.063814 & -0.080275 & 1.00396 & -0.061505 & -0.029190 \\ 0.033835 & 0.029207 & -0.012500 & -0.018510 & 1.02633 & 0.011872 \\ 0.087280 & 0.013155 & 0.026618 & -0.046737 & 0.011431 & 0.99998 \end{bmatrix}$$

Operating with $[f(\xi_o + h)]$ upon $[f(\xi_o - h)]^{-1}$ from the left, we get

$$\begin{array}{c} [Y] = \\ \text{at} \\ \xi = \xi_o + h \\ = 0.60754 \end{array} \begin{bmatrix} 0.256858 & -0.0703563 & -0.0250060 & 0.413646 & -0.676307 & -0.0322565 \\ 2.71274 & 0.738498 & -0.0984766 & -1.36616 & 2.20649 & 0.0906183 \\ 0.827805 & 0.128914 & -0.0518330 & -0.445679 & 1.13235 & -0.0485825 \\ 0.0372824 & -0.0237390 & -0.0570393 & 1.01435 & -0.0228491 & -0.0108667 \\ 0.108268 & 0.0542742 & -0.0395776 & -0.0572408 & 1.08585 & 0.0372601 \\ 0.0301579 & 0.0461556 & 0.0457769 & -0.0162026 & 0.0403119 & 0.999884 \end{bmatrix} \begin{array}{c} [Y] \\ \text{at} \\ \xi = \xi_o - h \\ \xi = 0.54474 \end{array} \qquad \ldots\ldots (194)$$

Similarly for the depth from $\xi = 0.60754$ (2500 km) to $\xi = 0.67033$ (2100 km) of the Earth Model 1, we get

$$\begin{array}{c} [Y] = \\ \text{at} \\ \xi = 0.67033 \end{array} \begin{bmatrix} 0.331961 & -0.0781511 & -0.0279636 & 0.389358 & -0.666887 & -0.0343128 \\ 2.15424 & 0.778023 & -0.0103119 & -1.06919 & 1.96958 & 0.0804706 \\ 0.771229 & 0.150137 & 0.552703 & -0.444429 & 1.14949 & -0.0436961 \\ 0.0399547 & -0.0261779 & -0.0626237 & 1.01293 & -0.0224319 & -0.0114428 \\ 0.0856226 & 0.0559360 & -0.0402208 & -0.0419650 & 1.07756 & 0.0320956 \\ 0.0277219 & 0.0533735 & 0.0471652 & -0.0158594 & 0.0404408 & 0.999920 \end{bmatrix} \begin{array}{c} [Y] \\ \text{at} \\ \xi = 0.60754 \end{array} \quad \ldots\ldots (195)$$

Inserting (194) into (195), we get

$$\begin{array}{c} [Y] = \\ \text{at} \\ \xi = 0.67033 \end{array} \begin{bmatrix} 0.185689 & -0.118384 & -0.0767365 & 0.677880 & -1.13168 & -0.0550052 \\ 2.83115 & 0.531481 & -0.0106351 & -1.36579 & 2.41444 & 0.0900268 \\ 1.17066 & 0.191289 & 0.284159 & -0.648958 & 1.69369 & -0.0135603 \\ 0.0384574 & -0.0837245 & -0.0367392 & 1.04887 & -0.0803532 & -0.0385444 \\ 0.288597 & 0.0938307 & -0.0106004 & -0.145120 & 1.23622 & 0.0957868 \\ 0.0945857 & 0.0149192 & 0.0701450 & -0.0514483 & 0.131019 & 0.999332 \end{bmatrix} \begin{array}{c} [Y] \\ \text{at} \\ \xi = 0.54474 \end{array} \quad \ldots\ldots (196)$$

Proceeding in this way, we get finally for the Earth Model 1

$$\begin{array}{c} [Y] = \\ \text{at } \xi = 1.0 \end{array} \begin{bmatrix} -2.81673 & -0.713236 & -0.0223927 & 8.28626 & -6.51010 & -0.491453 \\ 5.27118 & 0.991182 & -0.0225260 & -5.08102 & 8.59320 & 0.175352 \\ 1.35137 & 0.261008 & 0.0988058 & -1.93372 & 2.32501 & -0.0727851 \\ -0.310584 & -0.101191 & -0.0186612 & 1.85222 & -0.943305 & -0.0569783 \\ 1.11466 & 0.236301 & -0.0419708 & -0.809362 & 2.23502 & 0.0395552 \\ 0.531405 & 0.0937663 & 0.100310 & -0.432304 & 0.841745 & 0.986826 \end{bmatrix} \begin{array}{c} [Y] \\ \text{at} \\ \xi = 0.54474 \\ \text{above} \end{array} \quad \ldots\ldots\ldots (197)$$

Similarly we get for the Earth Model 2

$$\begin{array}{c} [Y] = \\ \text{at} \\ \xi = 0.92151 \\ \text{under} \end{array} \begin{bmatrix} -1.42581 & -0.34764 & -0.073132 & 2.97600 & -3.23250 & -0.20161 \\ 2.17506 & 0.38263 & -0.066460 & -2.31952 & 3.06255 & 0.10242 \\ 1.47127 & 0.26559 & 0.029173 & -0.76006 & 2.42527 & -0.055988 \\ -0.15060 & -0.059612 & -0.071228 & 1.38128 & -0.56370 & -0.029864 \\ 0.82749 & 0.18072 & -0.031222 & -0.44236 & 1.76787 & 0.027194 \\ 0.42973 & 0.072887 & 0.098519 & -0.023256 & 0.65715 & 0.99102 \end{bmatrix} \begin{array}{c} [Y] \\ \text{at} \\ \xi = 0.54474 \\ \text{above} \end{array} \quad \ldots\ldots\ldots\ldots (198)$$

$$\begin{array}{c} [Y] = \\ \text{at } \xi = 1.0 \end{array} \begin{bmatrix} 0.72308 & -0.17780 & -0.016472 & 1.42662 & -0.50977 & -0.12724 \\ 1.16004 & 1.18941 & 0.029795 & -1.69263 & 1.92684 & 0.13779 \\ 0.50205 & 0.21993 & 0.60828 & -0.56340 & 0.90220 & -0.088502 \\ 0.066076 & -0.067085 & -0.038785 & 1.05120 & -0.020618 & -0.045721 \\ 0.047493 & 0.083983 & -0.011930 & -0.069376 & 1.07454 & 0.056917 \\ 0.021090 & 0.091179 & 0.061691 & -0.025523 & 0.037456 & 0.99977 \end{bmatrix} \begin{array}{c} [Y] \\ \text{at} \\ \xi = 0.92151 \\ \text{above} \end{array} \quad \ldots\ldots\ldots\ldots (199)$$

The values $\xi = 0.54474$, $\xi = 0.92151$, and $\xi = 1.0$ correspond to the depths of 2900 km, 500 km, and 0 km, and the suffix "above" or "under" means the values above or under the discontinuous surfaces.

Section 16--In this section, boundary conditions at the so-called Jeffreys' Discontinuity of the Earth Model 2 will be considered. The boundary conditions at the discontinuous surface are the continuity of additional potential, displacement, and additional stress there and a condition on the potential. As is seen from (19), (20), (50), (155), and (156), the first three conditions are satisfied by making the following functions continuous there.

$$\left.\begin{array}{l} F(\xi)\,, \quad G(\xi)\,, \quad K(\xi)\,, \\[1ex] \text{Stress I} = \mu[F' + (2/\xi)F + \xi G] \\[1ex] \text{Stress II} = \lambda[(2/\xi)F' + \xi G' + 5G] + \mu[(2/\xi)F' + 2\xi G' + 4G] \end{array}\right\} \quad \ldots\ldots (200)$$

In (200), F', for example, means $dF_2(\xi)/d\xi$. One more boundary condition is obtained as follows. By the deformation of the Earth, there arises a surface density $-\left\{(\rho_0 U)_{\text{above}} - (\rho_0 U)_{\text{under}}\right\}$ at the discontinuous surface. Since the radial displacement U is continuous there, this surface density can be written also $-U\left\{(\rho_0)_{\text{above}} - (\rho_0)_{\text{under}}\right\} = -\left\{(\rho_0)_{\text{above}} - (\rho_0)_{\text{under}}\right\}(1/r)[2F_2(r) + r^2G_2(r)]W_2$. Equating the difference of potential gradients above and under the discontinuous surface to $-4\pi f$ times the surface density obtained above, we get

$$(\partial K/\partial r)_{\text{above}} - (\partial K/\partial r)_{\text{under}} = (4\pi f/r)[2F_2(r) + r^2G_2(r)]\left\{(\rho_0)_{\text{above}} - (\rho_0)_{\text{under}}\right\}W_2 \;.\;.\;.\;. \; (201)$$

Inserting $K = K_2(r)W_2$ into (201) and considering that $\left\{K_2(r)\right\}_{\text{above}} = \left\{K_2(r)\right\}_{\text{under}}$ there, we get

$$[dK_2(r)/dr]_{\text{above}} - [dK_2(r)/dr]_{\text{under}} = (4\pi f/r)[2F_2(r) + r^2G_2(r)]\left\{(\rho_0)_{\text{above}} - (\rho_0)_{\text{under}}\right\} \;. \; (202)$$

Inserting (164) into (202), we get

$$(K')_{\text{above}} - (K')_{\text{under}} = (1/\xi)(2F + \xi^2G)\left\{(\rho_0)_{\text{above}} - (\rho_0)_{\text{under}}\right\} \;.\;.\;.\;.\;. \; (203)$$

In the above equation, K', for example, means $dK_2(\xi)/d\xi$. Eq. (200) and (203) are the boundary conditions to be satisfied at the Jeffreys' Discontinuity. Putting $\xi = 0.92151$ and inserting the values of ρ_0, λ, and μ in Table 1 into (200) and (203), we get

$$\left.\begin{aligned}
&F_{\text{above}} = F_{\text{under}}\,, \quad G_{\text{above}} = G_{\text{under}}\,, \quad K_{\text{above}} = K_{\text{under}} \\
&F'_{\text{above}} = 1.31397\,F'_{\text{under}} + 0.68142\,F_{\text{under}} + 0.28933\,G_{\text{under}} \\
&G'_{\text{above}} = 0.055408\,F'_{\text{under}} + 1.3375\,G'_{\text{under}} - 1.1173\,F_{\text{under}} + 0.73573\,G_{\text{under}} \\
&K'_{\text{above}} = K'_{\text{under}} - 1.15029\,F_{\text{under}} - 0.48840\,G_{\text{under}}
\end{aligned}\right\} \;.\;.\;.\;.\;. \; (204)$$

Substituting (198) into (204), we get

$$\begin{array}{c}[Y] = \\ \text{at} \\ \xi = 0.92151 \\ \text{above}\end{array}
\begin{bmatrix}
-1.73668 & -0.44512 & -0.010998 & 4.72362 & -4.12003 & -0.27739 \\
3.60722 & 0.69207 & -0.010795 & -4.80623 & 5.84755 & 0.17919 \\
1.24036 & 0.24590 & 0.031517 & -2.13288 & 2.21026 & -0.034917 \\
-0.15060 & -0.059612 & -0.071228 & 1.38128 & -0.56370 & -0.029864 \\
0.82749 & 0.18072 & -0.031222 & -0.44236 & 1.76787 & 0.027194 \\
0.42973 & 0.072857 & 0.098519 & -0.23256 & 0.65715 & 0.99102
\end{bmatrix}
\begin{array}{c}[Y] \\ \text{at} \\ \xi = 0.54474 \\ \text{above}\end{array}
\;.\;.\;.\;.\;.\;.\;.\;.\;. \; (205)$$

Inserting (199) into (205), we get

$$\begin{array}{c}[Y] = \\ \text{at } \xi = 1.0\end{array}
\begin{bmatrix}
-2.59052 & -0.63176 & -0.018045 & 6.49927 & -5.81145 & -0.41494 \\
4.14745 & 0.75863 & -0.017772 & -3.39584 & 6.56097 & 0.13189 \\
1.50353 & 0.27430 & 0.079880 & -1.15818 & 2.46879 & -0.088505 \\
-0.31632 & -0.10078 & -0.017902 & 1.80659 & -0.94353 & -0.056012 \\
1.12105 & 0.23543 & -0.042113 & -0.74924 & 2.23528 & 0.038850 \\
0.53725 & 0.093253 & 0.10001 & -0.36011 & 0.84038 & 0.98620
\end{bmatrix}
\begin{array}{c}[Y] \\ \text{at} \\ \xi = 0.54474 \\ \text{above}\end{array}
\;.\;.\;.\;.\;.\;.\;.\;.\;. \; (206)$$

Eq. (206) corresponds to (197) of the Earth Model 1.

Section 17--From the investigations of modern seismology, it is found that the S wave does not go through the Earth's central core enclosed by the 2900 km discontinuity. To signify this, it is called the "liquid" core of the Earth. We shall now adopt the liquid core model of the Earth and consider the fundamental differential equations of the elastic deformation of the liquid core at first. Putting

$$\mu = \text{constant} = 0\,, \quad p = 0 \;. \; (207)$$

and

$$U_n(r) = (1/r)[nF_n(r) + r^2G_n(r)] \;.\;.\;.\;.\;.\;.\;.\;.\;.\;.\;.\;.\;.\;.\;.\;.\;. \; (208)$$

in (38), we get

$$[\rho_o K_n(r) + (dP_o/dr)\,U_n(r) + \lambda f_n(r)]\,\partial W_n/\partial x + \Big\{\rho_o dK_n(r)/dr - [(d\rho_o/dr)U_n(r) + \rho_o f_n(r)]dV_o/dr + d[(dP_o/dr)U_n(r)]/dr + \lambda df_n(r)/dr + (d\lambda/dr)\,f_n(r)\Big\}(x/r)W_n = 0 \tag{209}$$

From this we get as in (41)

$$\rho_o K_n(r) + (dP_o/dr)\,U_n(r) + \lambda f_n(r) = 0 \tag{210}$$

and

$$\rho_o dK_n(r)/dr - [(d\rho_o/dr)\,U_n(r) + \rho_o f_n(r)]\,dV_o/dr + d[(dP_o/dr)\,U_n(r) + \lambda f_n(r)]/dr = 0 \tag{211}$$

Another relation, obtained from (45) and (46) is

$$d^2K_n(r)/dr^2 + (2/r)(n+1)\,dK_n(r)/dr = 4\pi f\,[\,\rho_o f_n(r) + (d\rho_o/dr)\,U_n(r)] \tag{212}$$

We now show that (210) and (211) are not independent of each other and that we have only two differential equations, say, (210) and (212) for the liquid core of the Earth. Differentiating (210) with respect to r and subtracting (211), we get

$$(d\rho_o/dr)\,K_n(r) + (d\rho_o/dr)(dV_o/dr)\,U_n(r) + (dP_o/dr)\,f_n(r) = 0 \tag{213}$$

Multiplying (210) and (213) by $d\rho_o/dr$ and $-\rho_o$ respectively and adding, we get

$$(\lambda d\rho_o/dr - \rho_o dP_o/dr)\,f_n(r) = 0$$

Since $\lambda = k = \rho_o\,dP_o/d\rho_o$ for a liquid, this is an identity. Thus the linear dependence between (210) and (211) is verified. Inserting (213) into (212), we get

$$d^2K_n(r)/dr^2 + (2/r)(n+1)\,dK_n(r)/dr + 4\pi f K_n(r)(d\rho_o/dr)/(dV_o/dr) = 0 \tag{214}$$

Thus we get a differential equation of $K_n(r)$ only for the liquid core of the Earth. Changing the independent variable from r to ξ as in (164) and introducing new dependent variables

$$U_n(\xi) = (1/\xi)[nF_n(\xi) + \xi^2 G_n(\xi)] = U_n(r)/a \tag{215}$$

and

$$f_n(\xi) = (n/\xi)\,dF_n(\xi)/d\xi + \xi dG_n(\xi)/d\xi + (n+3)\,G_n(\xi) \tag{216}$$

we get

$$d^2K_n(\xi)/d\xi^2 + (2/\xi)(n+1)\,dK_n(\xi)/d\xi + 4\pi f a^2 K_n(\xi)(d\rho_o/d\xi)/(dV_o/d\xi) = 0 \tag{217}$$

and

$$(dP_o/d\xi)\,U_n(\xi) + \lambda f_n(\xi) + 4\pi f a^2 \rho_o K_n(\xi) = 0 \tag{218}$$

The boundary conditions at the 2900 km discontinuity are the continuity of displacement, additional stress, additional potential, and $dK_n(\xi)/d\xi - \rho_o U_n(\xi) = dK_n(\xi)/d\xi - (\rho_o/\xi)[nF_n(\xi) + \xi^2 G_n(\xi)]$ there as in (210) and (213), but by the assumption of a liquid core, the lateral displacement U_θ and U_ϕ outside the discontinuity become quite independent of those inside the discontinuity. Since $U_\theta = (1/r)\,F_n(r)\,\partial W_n/\partial\theta$ and $U_\phi = [1/(r \sin\theta)]\,F_n(r)\,\partial W_n/\partial\phi$, this means that $F_n(\xi)$ outside the discontinuity is independent of $F_n(\xi)$ inside. Putting n = 2 and $\mu = 0$, these boundary conditions may be written in the following form

$$\left.\begin{aligned}
&F_{\text{above}} = \text{independent}\,, \quad U_{\text{above}} = U_{\text{under}} \\
&G_{\text{above}} = (\xi U_{\text{above}} - 2F_{\text{above}})/\xi^2 = (\xi U_{\text{under}} - 2F_{\text{above}})/\xi^2 \\
&K_{\text{above}} = K_{\text{under}}\,, \quad \text{Stress I}_{\text{above}} = [\mu(F' + 2F/\xi + \xi G)]_{\text{above}} = \text{Stress I}_{\text{under}} = 0 \\
&\text{Stress II}_{\text{above}} = [\lambda(2F'/\xi + \xi G' + 5G) + \mu(2F'/\xi + 2\xi G' + 4G)]_{\text{above}} \\
&\qquad\qquad = \text{Stress II}_{\text{above}} = (\lambda f)_{\text{under}} \\
&K'_{\text{above}} = K'_{\text{under}} + U_{\text{under}}\,[(\rho_o)_{\text{above}} - (\rho_o)_{\text{under}}]
\end{aligned}\right\} \tag{219}$$

In the above equation, U, f, F′, ... mean $U_2(\xi)$, $f_2(\xi)$, $dF_2(\xi)/d$, ... , and the suffixes "above" and "under" mean, as stated earlier, the values above and under the discontinuous surface. In order to express (219) numerically, we must first consider the distributions of ρ_0, and $dV_0/d\xi$ in the liquid core and solve (217) for $K_2(\xi)$. In Earth Model 1 of our study, the density distribution obtained by BULLEN [1940] was used for the depth from zero to 2900 km, whereas in Earth Model 2, the density distribution obtained by BULLEN [1936] was used for this depth. Since Bullen's study in 1942, which is the extension of his study in 1940 to the depth under the 2900 km discontinuity, does not arrive at a definite conclusion about the density distribution within the Earth's core, the density distribution within the Earth's core obtained by him in 1936 is used in Earth Models 1 and 2 of our study. In Earth Model 1, the density distribution thus adopted (see Fig. 6) will give a little too low a value for the density within the core. This density distribution can be expressed by

$$\rho_0 = 12.284(1 - 0.64014\ \xi^2) \qquad (220)$$

with a relative error of less than one per cent, so we shall use this for ρ_0 in (217). The distribution of $dV_0/d\xi = -ag$ in the Earth's core is expressed approximately by

$$dV_0/d\xi = -1.14831\,\xi \times 10^{12} \qquad (221)$$

which will be used as $dV_0/d\xi$ in (217). The value of g calculated by (221) is about g = 982 at the 2900 km depth. Inserting (220) and (221) into (217), we get

$$d^2K_2/d\xi^2 + (6/\xi)\,dK_2/d\xi + (2.15825)^2K_2 = 0 \qquad (222)$$

Complete primitives of (222) are not required in our study, because the relevant solution must satisfy a certain condition at $\xi = 0$. The potential $K_n(r)W_n$ is the potential due to external bodies together with that due to a volume density throughout the sphere r = a and that due to a surface density distribution at several discontinuous surfaces of density, and therefore $K_n(r)r^n$ must be finite at r = 0, that is, $K_n(\xi)\xi^n$ must be finite at $\xi = 0$. The solution satisfying this condition is obtained in the next form

$$K_2(\xi) = C\left\{1 - x^2/(2.7) + x^4/(2\cdot 4\cdot 7\cdot 9) - \ldots\right\} \qquad (223)$$

where $x = 2.15825\,\xi$ and C is a constant. From this we get

$$K_2'(\xi) = 2.15825\ dK_2(x)/dx \qquad (224)$$

Putting $\xi = 0.54474$ or $x = 1.17569$ in (223) and (224), we get

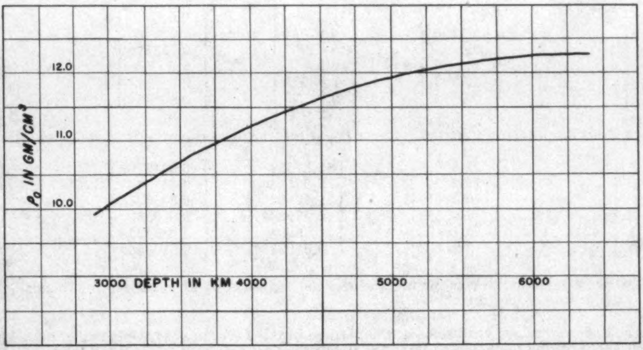

Fig. 6--The density distribution from 2900 km depth to the center of the Earth

$$K_2 = 0.904980\ C\ ,\quad \text{and}\quad K_2' = -0.335515\ C \quad \ldots\ldots (225)$$

The value of $(\lambda f)_{\text{under}}$ in (219) is obtained by (218) as follows

$$(\lambda f)_{\text{under}} = -\left\{dP_o/d\xi + 4\pi f a^2 \rho_o K\right\}_{\text{under}} = -\left\{\rho_o dV_o/d\xi + 4\pi f a^2 \rho_o K\right\}_{\text{under}} \quad \ldots\ldots (226)$$

The other numerical values of the quantities appearing in (219) are as follows

$$\left.\begin{array}{c}(\rho_o)_{\text{above}} = 5.53\ ,\quad \lambda_{\text{above}} = 4.608 \times 10^{12}\ ,\quad \mu_{\text{above}} = 2.931 \times 10^{12}\ \text{(Table 1)} \\ (\rho_o)_{\text{under}} = 9.95\ [\text{Eq. (220)}]\end{array}\right\} \ldots (227)$$

Putting

$$F_{\text{above}} = A\ ,\quad \text{and}\quad U_{\text{above}} = U_{\text{under}} = B \quad \ldots\ldots (228)$$

and inserting these values into (219), we get, after a little arrangement

$$\begin{bmatrix} F' \\ G' \\ K' \\ F \\ G \\ K \end{bmatrix}_{\substack{\text{at } \xi = \\ 0.54474 \\ \text{above}}} = \begin{bmatrix} 0.0 \\ 41.0815 \\ 0.0 \\ 1.0 \\ -6.73988 \\ 0.0 \end{bmatrix} A + \begin{bmatrix} -1.0 \\ -5.24498 \\ -4.42 \\ 0.0 \\ 1.83574 \\ 0.0 \end{bmatrix} B + \begin{bmatrix} 0.0 \\ -0.536963 \\ -0.335515 \\ 0.0 \\ 0.0 \\ 0.904980 \end{bmatrix} C \quad \ldots\ldots (229)$$

Inserting (206) into (229), we get the value of [Y] at the surface of the Earth Model 2 as follows

$$\begin{bmatrix} F' \\ G' \\ K' \\ F \\ G \\ K \end{bmatrix}_{\text{at } \xi = 1.0} = \begin{bmatrix} 19.7142 \\ -16.4502 \\ -6.52915 \\ 4.02551 \\ -6.14295 \\ -2.19322 \end{bmatrix} A + \begin{bmatrix} -4.68449 \\ 3.99632 \\ 1.55457 \\ -0.879231 \\ 1.76613 \\ 0.0743114 \end{bmatrix} B + \begin{bmatrix} -0.0302308 \\ -0.282044 \\ -0.230062 \\ 0.0402804 \\ -0.0898458 \\ 0.808865 \end{bmatrix} C \quad \ldots\ldots (230)$$

Similarly, for the Earth Model 1, using (220), (221), (225), (226), and

$$\left.\begin{array}{c}(\rho_o)_{\text{above}} = 5.68\ ,\quad \lambda_{\text{above}} = 4.734 \times 10^{12}\ ,\quad \mu_{\text{above}} = 3.010 \times 10^{12}\quad \text{(Table 1)} \\ (\rho_o)_{\text{under}} = 9.95\ [\text{Eq. (220)}]\end{array}\right\} \ldots (231)$$

we get

$$\begin{bmatrix} F' \\ G' \\ K' \\ F \\ G \\ K \end{bmatrix}_{\substack{\text{at} \\ \xi = 0.54474 \\ \text{above}}} = \begin{bmatrix} 0.0 \\ 41.0850 \\ 0.0 \\ 1.0 \\ -6.73988 \\ 0.0 \end{bmatrix} A + \begin{bmatrix} -1.0 \\ -5.27445 \\ -4.27 \\ 0.0 \\ 1.83574 \\ 0.0 \end{bmatrix} B + \begin{bmatrix} 0.0 \\ -0.522780 \\ -0.335515 \\ 0.0 \\ 0.0 \\ 0.904980 \end{bmatrix} C \quad \ldots\ldots (232)$$

Inserting (197) into (232), we get the value of [Y] at the surface of the Earth Model 1 as follows

$$\begin{bmatrix} F' \\ G' \\ K' \\ F \\ G \\ K \end{bmatrix}_{\text{at } \xi = 1.0} = \begin{bmatrix} 22.8603 \\ -22.2754 \\ -6.88049 \\ 4.05255 \\ -6.16470 \\ -2.25318 \end{bmatrix} A + \begin{bmatrix} -5.27658 \\ 5.37195 \\ 1.49788 \\ -0.879384 \\ 1.75982 \\ 0.0909306 \end{bmatrix} B + \begin{bmatrix} -0.0643765 \\ -0.351922 \\ -0.205634 \\ 0.0196252 \\ -0.0863286 \\ 0.810383 \end{bmatrix} C \quad \ldots\ldots (233)$$

Thus it remains for us to determine the constants A, B, and C so as to satisfy the boundary conditions at the surface of the Earth.

Section 18--Boundary conditions at the surface of the Earth are the vanishing of the additional stress and a condition on the potential. The first boundary condition is satisfied by putting

$$\text{Stress I} = \mu(F' + 2F'/\xi + \xi G) = 0 \ldots\ldots\ldots\ldots (234)$$

$$\text{Stress II} = \lambda(2F'/\xi + \xi G' + 5G) + \mu(2F'/\xi + 2\xi G' + 4G) = 0 \ldots\ldots\ldots\ldots (235)$$

there. The latter boundary condition is satisfied, as in (149), by putting

$$K' + 5K - \rho_0(\xi = 1.0)(2F + G) = 5/(4\pi fa^2) \ldots\ldots\ldots\ldots (236)$$

there. In (234), (235), and (236), F′ means $dF_2(\xi)/d\xi$. For the Earth Model 1 of our study, putting $\rho_0 = 3.0$, $\lambda = 0.6 \times 10^{12}$, and $\mu = 0.5 \times 10^{12}$ (Table 1) in (234), (235), and (236), we get

$$\left.\begin{aligned} &F' + 2F + G = 0\,, \quad 2.2\,F' + 1.6\,G' + 5.0\,G = 0 \\ &K' + 5K - 3.0(2F + G) = K' + 5K + 3.0\,F' = 5/(4\pi fa^2) \end{aligned}\right\} \ldots\ldots\ldots (237)$$

Inserting (233) into (237), we get the following three equations to determine A, B, and C.

$$\left.\begin{aligned} 24.8007\,A - 5.27553\,B - 0.146780\,C &= 0 \\ -16.1717\,A + 5.78574\,B - 1.13635\,C &= 0 \\ 50.4345\,A - 13.8772\,B + 3.65315\,C &= 5/(4\pi fa^2) \end{aligned}\right\} \ldots\ldots\ldots\ldots (238)$$

From this we get

$$A = 0.255997/4\pi fa^2\,, \quad B = 1.14291/4\pi fa^2\,, \text{ and } C = 2.17604/4\pi fa^2 \ldots\ldots\ldots (239)$$

Inserting these values into (233) again, we get the values of $F_2(\xi)$, $U_2(\xi) = [2F_2(\xi) + \xi^2 G_2(\xi)]/\xi$ and $K_2(\xi)$ at the surface of the Earth as follows

$$F_2(\xi) = 0.03665/(4\pi fa^2)\,, \quad U_2(\xi) = 0.3185/(4\pi fa^2)\,, \text{ and } K_2(\xi) = 1.290/(4\pi fa^2) \ldots\ldots (240)$$

Considering (24), (63), and (164), we get

$$\left.\begin{aligned} &K = 1.290\,W_2\,, \quad U_r = 0.3185\,W_2/(4\pi fa) \\ &U_\theta = [0.03665/(4\pi fa)]\,\partial W_2/\partial\theta, \text{ and } U_\phi = [0.03665/(4\pi fa)](1/\sin\theta)\,\partial W_2/\partial\phi \end{aligned}\right\} \ldots (241)$$

The potential K (deformed Earth) due to the additional density caused by the deformation of the Earth is obtained by subtracting W_2 from K obtained above.

$$K\ (\text{deformed Earth}) = 0.290\,W_2 \ldots\ldots\ldots\ldots (242)$$

Inserting $g = (4/3)\pi fa\rho_m$, where g is the gravity at the surface of the Earth and $\rho_m = 5.53$ is the mean density of the Earth, into (241), we get

$$U_r = (0.587/g)W_2\,, \quad U_\theta = (0.068/g)\,\partial W_2/\partial\theta\,, \text{ and } U_\phi = (0.068/g)(1/\sin\theta)\partial W_2/\partial\phi \ldots (243)$$

Similarly, we get for the Earth Model 2

$$\left.\begin{aligned} &F' + 2F + G = 0\,, \quad 2.56\,F' + 1.88\,G' + 5.8\,G = 0 \\ &K' + 5K - 3.0(2F + G) = K' + 5K + 3.0\,F' = 5/(4\pi fa^2) \end{aligned}\right\} \ldots\ldots\ldots\ldots (224)$$

$$\left.\begin{aligned} 21.6223\,A - 4.67682\,B - 0.112021\,C &= 0 \\ -16.0871\,A + 5.76434\,B - 1.12874\,C &= 0 \\ 41.6475\,A - 12.1273\,B + 3.72357\,C &= 5/(4\pi fa^2) \end{aligned}\right\} \ldots\ldots\ldots\ldots (245)$$

$$A = 0.262465/(4\pi fa^2)\,, \quad B = 1.16103/(4\pi fa^2)\,, \quad C = 2.18854/(4\pi fa^2) \ldots\ldots (246)$$

$$\left.\begin{aligned} &K\ (\text{deformed Earth}) = 0.281\,W_2\,, \quad U_r = (0.610/g)W_2 \\ &U_\theta = (0.082/g)\,\partial W_2/\partial\theta\,, \quad U_\phi = (0.082/g)(1/\sin\theta)\,\partial W_2/\partial\phi \end{aligned}\right\} \ldots\ldots (247)$$

Section 19--The results obtained in the last section may be put in the form

$$\left.\begin{array}{l} K\ (\text{deformed Earth}) = kW_2\ ,\quad U_r = (h/g)\,W_2 \\ U_\theta = (\ell/g)\partial W_2/\partial\theta\ ,\ \text{and}\ \ U_\phi = (\ell/g)(1/\sin\theta)\partial W_2/\partial\phi \end{array}\right\} \ldots\ldots (248)$$

where

$$k = \begin{cases} 0.290\ , \\ 0.281\ , \end{cases}\qquad h = \begin{cases} 0.587\ , \\ 0.610\ , \end{cases}\qquad \ell = \left\{\begin{array}{l} 0.068\ \text{ for the Earth Model 1} \\ 0.082\ \text{ for the Earth Model 2} \end{array}\right\} \ldots\ldots (249)$$

k and h are called Love's numbers in the theory of Earth tides and ℓ is called Lambert's number. The density distribution within the Earth's liquid core obtained by BULLEN [1936] was used for the Earth Models 1 and 2. This density distribution is considered to give a little too low a value for the density in the core in the Earth Model 1. Therefore, the values k, h, and ℓ obtained using the Earth Model 1 may be less reliable than those using the Earth Model 2.

CHAPTER III

Earth tide

(In this chapter, the three problems that were mentioned in the introduction of this paper are discussed, using the results obtained in Chapter 2)

Section 20--As was mentioned in the introduction, the height of oceanic tides is reduced by the Earth tide. This may be understood as follows. The potential at the deformed surface of the Earth is given by

$$\text{Total potential} = V_0 + U dV_0/dr + (1 + k)W_2 \quad \text{at } r = a \ldots\ldots\ldots (250)$$

where V_0 is the potential of the undeformed Earth, W_2 that of the tide generating force, and kW_2 is the potential due to the additional density caused by the deformation of the Earth. Since $V_0(a) = 0$ and $(dV_0/dr)_{r=a} = -g$, where g is the gravity at the surface of the Earth, (250) becomes

$$\text{Total potential} = (1 + k)W_2 - Ug \ldots\ldots\ldots\ldots\ldots\ldots\ldots\ldots (251)$$

Inserting

$$\left.\begin{array}{l} K\ (\text{deformed Earth}) = kW_2\ ,\quad U_r = U = (h/g)W_2 \\ U_\theta = (\ell/g)\partial W_2/\partial\theta\ ,\ \text{and}\ \ U_\phi = [\ell/(g\sin\theta)]\partial W_2/\partial\phi \end{array}\right\} \ldots\ldots\ldots (252)$$

into (251), we get

$$\text{Total potential} = (1 + k - h)W_2 \ldots\ldots\ldots\ldots\ldots\ldots\ldots\ldots (253)$$

If the Earth is perfectly rigid, k = h = 0, and we get W_2 as the total potential. Thus we get the result that the total potential or the equilibrium height of oceanic tides is reduced, when the Earth is deformed by the tidal attraction, in the ratio $D = (1 + k - h):1$ to that for a perfectly rigid Earth. Signifying this, the number

$$D = 1 + k - h \ldots\ldots\ldots\ldots\ldots\ldots\ldots\ldots\ldots (254)$$

is called the diminishing factor in the theory of Earth tides. The value of the diminishing factor is obtained also from the observations of periodic deflections of the vertical using water-pipe tiltmeters or horizontal pendulems.

The values of D obtained by DARWIN [1907a] and SCHWEYDAR [1908] from the observations of oceanic tides are

$$D = 0.68 \sim 0.65 \ldots\ldots\ldots\ldots\ldots\ldots\ldots\ldots\ldots (255)$$

For the values of D above obtained, a doubt may remain as to the applicability of an equilibrium theory to oceanic tides.

The value of D obtained by MICHELSON and GALE [1919] using water-pipe tiltmeters is

$$D = 0.69 \ldots\ldots\ldots\ldots\ldots\ldots\ldots\ldots\ldots (256)$$

For the value of D thus obtained, the question arises as to the secondary effects of oceanic tides. The secondary effects of oceanic tides on pure Earth tides are the following three: (1) The oceanic tides exert a gravitational attraction upon the mass of horizontal pendulums, for example, and disturb the pure Earth tide. (2) The oceanic tides produce a deformation of the Earth by the normal traction of their weight, and from this deformation of the Earth, there arises a secondary tilting of the Earth. (3) Because of the deformation of the Earth caused by the surface load, the gravitational field of the Earth itself changes a little. This produces a secondary effect upon the pure Earth tide. Since the observations by Michelson were made at about 1000 km from the nearest sea, the secondary effects of oceanic tides upon his results are considered to be small.

Since the time of Kelvin, many observations of the deflections of vertical lines have been made using horizontal pendulums. Observations using horizontal pendulums are disturbed by the secondary effects of oceanic tides and by the variations in meteorological elements, such as pressure and temperature. In order to eliminate the secondary effects of oceanic tides, the observations using horizontal pendulums must be made at points far from the sea, and, in order to eliminate the effects of the variations in meteorological elements, they must be made far below the Earth's surface. Observations that were made under such conditions are those made by HECKER [1911], SCHWEYDAR [1921], and NISHIMURA [1950]. The values of D obtained by them are about

$$D = 0.6 \sim 0.7 \qquad (257)$$

The value of D obtained by Nishimura may be most reliable. He made his observations at Barim (48° 18′ N, 122° 10′ E) in Manchuria. Barim is about 1000 km from the nearest sea, and the observation point was 44 m below the Earth's surface. The values of D obtained by him are

$$D = \begin{Bmatrix} 0.715 \\ 0.672 \end{Bmatrix} \text{ for the } \begin{Bmatrix} \text{NS component} \\ \text{EW component} \end{Bmatrix} \text{ of } M_2 \qquad (258)$$

The values of D for the Earth Model 1 and 2 are calculated by (249) in Chapter II as follows

$$D = \begin{cases} 0.703 & \text{for the Earth Model 1} \\ 0.671 & \text{for the Earth Model 2} \end{cases} \qquad (259)$$

The value of D for the Earth Model 2 may be more reliable than that for the Earth Model 1. Taking into account the values of D in (255) to (259), we may be fairly confident that the most reliable value of D is about

$$D = 0.66 \sim 0.70 \qquad (260)$$

Section 21--The value of k is obtained from the ratio of the Chandler period T and the Euler period T_0 of the latitude variation by the formula [LOVE, 1909]

$$k = [(2g\epsilon)/(a\omega) - 1](1 - T_0/T) \qquad (261)$$

where g is gravity at the surface of the Earth, ϵ the ellipticity of the meridian, a the radius of the Earth, and ω the angular velocity of rotation. Putting

$$T_0 = 303.8 \text{ days}, \quad T = 1.20 \text{ year} \qquad (262)$$

in (261), we get

$$k = 0.287 \qquad (263)$$

This value of k includes effects due to the oceans, which yield completely to disturbing forces. According to LARMOR [1915], the correction to k due to these effects is very small, probably less than -0.02. Our calculated value of k is

$$k = 0.281 \sim 0.290 \qquad (264)$$

Taking into account (263) and (264), we may say that the most reliable value for k is about

$$k = 0.27 \sim 0.29 \qquad (265)$$

Section 22--The value of 1 + h - 3k/2 is obtained from the observations of the periodic variations of gravity using gravimeters. This may be understood as follows. As was seen in Section 1, the variable part of the total potential outside the Earth's surface is given by

$$UdV_o/dr + W_2 + \overline{K} \qquad (266)$$

where $\overline{K}$ is the potential due to the deformation of the Earth. Differentiating (266) with respect to r, we get for the variation of gravity

$$\Delta g = -(Ud^2V_o/dr^2 + \partial W_2/\partial r + \partial\overline{K}/\partial r) \qquad (267)$$

Since V_o, W_2, and $\overline{K}$ behave as r^{-1}, r^2, and r^{-3} with respect to r in the outer part of the Earth, we get

$$d^2V_o/dr^2 = -(2/r)dV_o/dr = 2g/r\ , \quad \partial W_2/\partial r = 2W_2/r\ , \quad \partial\overline{K}/\partial r = -(3/r)\overline{K} \qquad (268)$$

Inserting (268) and (252) into (267), we get

$$\Delta g = -(1 + h - 3k/2)(\partial W_2/\partial r)_{r = a} \qquad (269)$$

If the Earth is perfectly rigid, h and k become zero and Δg becomes

$$\Delta g = -(\partial W_2/\partial r)_{r = a} \qquad (270)$$

Thus we get the result that, if the Earth is deformed by the tidal attraction of the Sun or the Moon, the amplitude of the tidal variation of gravity will be magnified in the ratio G = (1 + h - 3k/2):1 to that for a perfectly rigid Earth. The values of G obtained by SCHWEYDAR [1914], HARTLEY [1933], WYCKOFF [1941], and TOMASCHEK and SCHAFFERNICHT [1933] are

$$G \begin{array}{c} = \\ \gtreqless \\ = \end{array} \left\{ \begin{array}{ll} 1.20 & \text{(Schweydar)} \\ 1.0 & \text{(Hartley, Wyckoff)} \\ 0.5 \sim 0.6 & \text{(Tomaschek)} \end{array} \right\} \qquad (271)$$

The values of G for the Earth Model 1 and 2 are calculated by (249) as follows

$$G = 1.15 \sim 1.19 \qquad (272)$$

Taking into account the values of G in (271) and (272), we may say that the most reliable value of G is about

$$G = 1.15 \sim 1.20 \qquad (273)$$

Modern developments in making sensitive gravimeters and accurate clocks will throw new light upon the problem of the periodic variations of gravity.

Section 23--The value of $1 + k - \ell$ is obtained from observations of the periodic variations of latitude. This may be understood as follows. Let us take polar coordinates (r, θ) with the center of the Earth as origin and the line connecting the center of the Earth and that of the Moon (or the Sun) as polar axis. In Figure 7, AB is the equatorial plane of the Earth, and m is the Moon, the declination of which is assumed to be zero. In Figure 7, θ is measured counter-clockwise. Note that θ_1 is negative if $\partial\overline{W}_2/\partial\theta$ is positive whereas θ_2 is positive. The undisturbed latitude of a point P at the surface of the Earth is θ. The tidal attraction of the Moon in the θ direction along the meridian passing through P is given by $[(1 + k)/a]\partial W_2/\partial\theta$. Due to the tidal attraction of the Moon along the meridian, the vertical line at P is deflected by the angle

$$\alpha = [(1 + k)/(ag)]\partial W_2/\partial\theta \qquad (274)$$

Observing the deflection of vertical line with respect to the equatorial plane, we take $\theta + \delta\theta_1 = \theta - \alpha$ as the latitude of our observatory. There is another variation of latitude caused by the tidal attraction of the Moon. As was seen in Section 20, due to the tidal attraction of the Moon, the point P is moved in the θ direction along the meridian by $u_\theta = (\ell/g)\partial W_2/\partial\theta$. The latitude variation thus caused is $\delta\theta_2 = u_\theta/a$. Adding the latitude variation $\delta\theta_2$ to $\delta\theta_1$, we get the total latitude variation $\delta\theta$ with respect to the equatorial plane as

$$\delta\theta = -[(1 + k - \ell)/(ag)]\partial W_2/\partial\theta \qquad (275)$$

If the Earth is perfectly rigid, k and ℓ become zero and

$$\delta\theta = -(1/ag)\partial\overline{W}_2/\partial\theta \qquad (276)$$

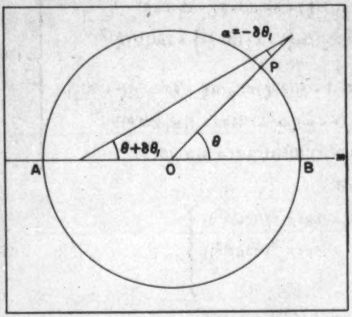

Fig. 7--Periodic deflections of latitude

Thus we get the result that, if the Earth is deformed by the tidal attraction of the Moon, the amplitude of the tidal variations of latitude will be magnified in the ratio $L = (1 + k - \ell):1$ to that for a perfectly rigid Earth. The values of L for the Earth Models 1 and 2 are

$$L = 1.22 \sim 1.20 \quad \ldots\ldots\ldots \quad (277)$$

The value of L obtained from the observations of the tidal variations of latitude [NISHIMURA, 1950]

$$L = 1.22 \quad \ldots\ldots\ldots \quad (278)$$

Taking these into account we may say that the most reliable value for L is about

$$L = 1.22 \sim 1.20 \quad \ldots\ldots\ldots \quad (279)$$

Section 24--Among the three problems mentioned in the introduction of this paper, the first two may be considered to be solved. Problem (1) is to find the most reliable values of the characteristic numbers k, h, and ℓ; we may say

$$k = 0.27 \sim 0.29\,, \quad h = 0.59 \sim 0.61\,, \text{ and } \ell = 0.07 \sim 0.08 \quad \ldots\ldots \quad (280)$$

Problem (2) is to determine whether the static elastic constants of the Earth determined by the study of Earth tide can be taken to be the same as the dynamic elastic constants of the Earth obtained by the study of seismic waves passing through the Earth; we may say "yes." We study the deformation of the Earth by the tidal attraction of the Sun or the Moon for the model Earth with an internal constitution inferred from the study of modern seismology, and compare the results thus obtained with the observations of Earth tides. The values of the characteristic numbers k, h, and ℓ calculated for the model Earth agree quite well with those obtained from the observations of Earth tides.

Section 25--Let us now study the last problem mentioned in the introduction, which is to determine the largest value of the rigidity of the Earth's core that is compatible with the observations of Earth tides. For this purpose, we shall now take up the Earth Models 3-6. In these Earth models, the internal constitution above the 2900 km discontinuity is assumed to be the same as that of the Earth Model 2, but under the discontinuity the density and elastic constants are assumed to be homogeneous. Because of these assumptions, the result of the calculation (206) for the Earth Model 2 can be used for the Earth Models 3-6, and the results of the study by Love [1911] for a homogeneous elastic sphere become available for our analysis. The results of this investigation are as follows

$$\left.\begin{aligned}
K_2(\xi) &= A\psi_2(\alpha a\xi)/(4\pi f a^2) + B\chi_2(\beta a\xi)/(4\pi f a^2) + C/(4\pi f a^2) \\
F_2(\xi) &= A'\psi_2(\alpha a\xi)/(\alpha^2 a^2) + [A'/(2\alpha^2 a^2) - A/(8\pi f \rho_0 a^2)]\psi_1(\alpha a\xi) \\
&\quad + B'\chi_2(\beta a\xi)/(\beta^2 a^2) - [B'/(2\beta^2 a^2) - B/(b\pi f \rho_0 a^2)]\chi_1(\beta a\xi) + 3C/(8\pi f \rho_0 a^2) \\
G_2(\xi) &= A'\psi_3(\alpha a\xi) + B'\chi_3(\beta a\xi) \\
dK_2(\xi)/d\xi &= [(Aa\alpha)/(4\pi f a^2)]\,d[\psi_2(\alpha a\xi)]/d(\alpha a\xi) + [(Ba\beta)/(4\pi f a^2)]\,d[\chi_2(\beta a\xi)]/d(\beta a\xi) \\
\text{Stress I} &= \mu[dF_2(\xi)/d\xi + (2/\xi)F_2(\xi) + \xi G_2(\xi)] \\
&= \mu[A'/(\xi\alpha^2 a^2)]\left\{(1/2)(\alpha a\xi)^2\psi_2(\alpha a\xi) - 8\psi_2(\alpha a\xi) - \psi_1(\alpha a\xi)\right\} \\
&\quad - \mu[A/(\xi 4\pi f \rho_0 a^2)]\left\{(1/2)(\alpha a\xi)^2\psi_2(\alpha a\xi) + \psi_1(\alpha a\xi)\right\} \qquad \text{(continued)}
\end{aligned}\right\}. \quad (281)$$

$$\left.\begin{aligned}
&-\mu[B'/(\xi\beta^2a^2)]\Big\{(1/2)(\beta a\xi)^2\chi_2(\beta a\xi) + 8\chi_2(\beta a\xi) - \chi_1(\beta a\xi)\\
&+\mu[B/(\xi 4\pi f\rho_0 a^2)]\Big\{(1/2)(\beta a\xi)^2\chi_2(\beta a\xi) + \chi_1(\beta a\xi)\Big\} + 2\mu C'/(\xi a^2)\\
\text{Stress II} &= \mu[(2/\xi)dF_2/d\xi + 2\xi dG/d\xi + 4G_2] + \lambda[(2/\xi)dF_2/d\xi + \xi dG_2/d\xi + 5G_2]\\
&= -\mu A'\Big\{8\psi_3(\alpha a\xi) + \psi_2(\alpha a\xi)\Big\} - (\lambda+\mu)[(\alpha^2 A)/(4\pi f\rho_0)]\psi_2(\alpha a\xi)\\
&\quad -\mu B'\Big\{8\chi_3(\beta a\xi) - \chi_2(\beta a\xi)\Big\} + (\lambda+\mu)[(\beta^2 B)/(4\pi f\rho_0)]\chi_2(\beta a\xi)
\end{aligned}\right\}. \quad (281)$$

where A, B, and C are undetermined constants and

$$\left.\begin{aligned}
A' &= [(A\alpha^2)/(4\pi f\rho_0)][1 + (8\pi f\rho_0{}^2)/(3\mu\alpha^2)]\\
B' &= [(B\beta^2)/(4\pi f\rho_0)][1 - (8\pi f\rho_0{}^2)/(3\mu\beta^2)]\\
C' &= C/[(8/3)\pi f\rho_0]
\end{aligned}\right\} \ldots\ldots\ldots\ldots\ldots\ldots (282)$$

The constants $-\alpha^2$ and β^2 are determined as the roots of the equation

$$\mu(\lambda + 2\mu)x^2 + (16/3)\pi f\rho_0{}^2\mu x - 6[(4/3)\pi f\rho_0{}^2]^2 = 0 \ldots\ldots\ldots\ldots (283)$$

and

$$\left.\begin{aligned}
\psi_n(x) &= [(-1)^n/1\cdot 3\cdot 5\cdot\cdots\cdot(2n+1)]\Big\{1 - x^2/[2(2n+3)]\\
&\qquad + x^4/[2\cdot 4\cdot(2n+3)(2n+5)] - \cdots\cdot\Big\}\\
\chi_n(x) &= [1/1\cdot 3\cdot 5\cdot\cdots\cdot(2n+1)]\Big\{1 + x^2/[2(2n+3] + x^4/[2\cdot 4\cdot(2n+3)(2n+5)] + \cdots\cdot\Big\}
\end{aligned}\right\} (284)$$

Recurrence formulas for $\psi_n(x)$ and $\chi_n(x)$ are

$$\left.\begin{aligned}
(1/x)d\psi_n(x)/dx &= \psi_{n+1}(x) = -[(2n+1)\psi_n(x) + \psi_{n-1}(x)]/x^2\\
(1/x)d\chi_n(x)/dx &= \chi_{n+1}(x) = -[(2n+1)\chi_n(x) - \chi_{n-1}(x)]/x^2
\end{aligned}\right\} \ldots\ldots\ldots (285)$$

The values of ρ_0, λ, and μ within the core are taken as follows. The distribution of gravity within the Earth's core is expressed approximately by a linear function (221). On the other hand, the gravity distribution within a sphere of uniform density ρ_0 is

$$g = g_0 r/b \ldots\ldots\ldots\ldots\ldots\ldots\ldots\ldots\ldots (286)$$

where b is the radius of the sphere and $g_0 = (4/3)\pi f\rho_0 b$ is the gravity at the surface of the sphere. Thus it may be natural to take the value of ρ_0 so as to make $g_0 = 982$ [see (221)] for b = 6370 - 2900 = 3470 km. The value of ρ_0 thus determined is

$$\rho_0 = 10.13 \ldots\ldots\ldots\ldots\ldots\ldots\ldots\ldots (287)$$

The value of λ within the Earth's core is about $\lambda = 6.0\times 10^{12}$ at 2900 km depth and $\lambda = 15\times 10^{12}$ at the center of the Earth, so we shall take tentatively

$$\lambda = 11\times 10^{12} \ldots\ldots\ldots\ldots\ldots\ldots\ldots\ldots (288)$$

For the value of μ within the core, we shall take

$$\mu = \left\{\begin{aligned}
&10^7 \text{ for the Earth Model 3}\\
&10^9 \text{ for the Earth Model 4}\\
&10^{11} \text{ for the Earth Model 5}\\
&10^{13} \text{ for the Earth Model 6}
\end{aligned}\right\} \ldots\ldots\ldots\ldots\ldots\ldots (289)$$

The process of calculation will be shown below for the Earth Model 3. At first, inserting (287), (288), and (289) into (283), we get

$$\alpha b = 28.404 \ , \text{ and } \beta b = 28.382 \ \ldots\ldots\ldots\ldots\ldots\ldots \ (290)$$

Inserting (282) - (290) into (281) and putting $\xi = 0.54474$, we get the value of $\left\{F, G, K, K', \text{Stress I}, \text{and Stress II}\right\}$ at $\xi = 0.54474$ under

$$\begin{bmatrix} F \\ G \\ K \\ K' \\ \text{Stress I} \\ \text{Stress II} \end{bmatrix} = \begin{bmatrix} -0.14939 \\ 0.98237 \\ 0.029970 \\ 0.063278 \\ 0.23966 \times 10^{8} \\ -0.88631 \times 10^{11} \end{bmatrix} A/10^{12} + \begin{bmatrix} 0.14749 \\ -0.88831 \\ 0.012237 \\ 0.057262 \\ 0.72284 \times 10^{8} \\ 0.36051 \times 10^{12} \end{bmatrix} B/10^{12} + \begin{bmatrix} 0.43538 \\ 0.0 \\ 2.94022 \\ 0.0 \\ 0.15985 \times 10^{8} \\ 0.0 \end{bmatrix} C/10^{12}$$

$$\text{at } \xi = 0.54474 \text{ under} \qquad \ldots\ldots \ (291)$$

Boundary conditions at the 2900 km discontinuity are the same as in (200) and (203). Putting $\rho_{0\,\text{above}} = 5.53$, $\lambda_{\text{above}} = 4.608 \times 10^{12}$, and $\mu_{\text{above}} = 2.931 \times 10^{12}$, and inserting (197), (198), and (199) into these equations, we get

$$\begin{bmatrix} F' \\ G' \\ K' \\ F \\ G \\ K \end{bmatrix} = \begin{bmatrix} 0.013358 \\ -6.06815 \\ 0.067705 \\ -0.14939 \\ 0.98237 \\ 0.029970 \end{bmatrix} A/10^{12} + \begin{bmatrix} -0.057587 \\ 5.75746 \\ -0.25926 \\ 0.14749 \\ -0.88831 \\ 0.012237 \end{bmatrix} B/10^{12} + \begin{bmatrix} -1.59845 \\ 7.75745 \\ -7.35292 \\ 0.43538 \\ 0.0022 \\ 2.94200 \end{bmatrix} C/10^{12} \ . \ (292)$$

$$\text{at } \xi = 0.54474 \text{ above}$$

Inserting (206) into (292) above, we get

$$\begin{bmatrix} F' \\ G' \\ K' \\ F \\ G \\ K \end{bmatrix} = \begin{bmatrix} -2.88214 \\ 2.40333 \\ 0.95441 \\ -0.58958 \\ 0.89387 \\ 0.32747 \end{bmatrix} A/10^{12} + \begin{bmatrix} 2.63742 \\ -2.19546 \\ -0.87324 \\ 0.54304 \\ -0.80411 \\ -0.31948 \end{bmatrix} B/10^{12} + \begin{bmatrix} 0.98226 \\ -1.70446 \\ -1.09865 \\ 0.35885 \\ -0.14661 \\ 1.87213 \end{bmatrix} C/10^{12} \ \ldots\ldots \ (293)$$

$$\text{at } \xi = 1.0$$

Boundary conditions at the surface of the Earth are the same as in (244). Inserting (293) into these equations, we get

$$\left.\begin{aligned} -3.16743\, A/10^{12} + 2.91939\, B/10^{12} + 1.55335\, C/10^{12} &= 0 \\ 2.32443\, A/10^{12} - 2.03951\, B/10^{12} - 1.54014\, C/10^{12} &= 0 \\ -6.05466\, A/10^{12} + 5.44162\, B/10^{12} + 11.2088\, C/10^{12} &= 5/(4\pi f a^2) \end{aligned}\right\} \ldots\ldots\ldots \ (294)$$

From this we get

$$A/10^{12} = 2.64654/(4\pi f a^2) \ , \quad B/10^{12} = 2.52586/(4\pi f a^2) \ , \text{ and } C/10^{12} = 0.649415/(4\pi f a^2) \ . \ . (295)$$

Inserting (295) into (293), we get, after a little rearrangement

$$\left.\begin{aligned} K \text{ (deformed Earth)} = 0.275 W_2 \ , \quad & U_r = (0.601/g) W_2 \\ U_\theta = (0.081/g)\, \partial W_2/\partial\theta \ , \quad & U_\phi = (0.081/g)(1/\sin\theta)\, \partial W_2/\partial\phi \end{aligned}\right\} \ldots\ldots \ (296)$$

or expressing the results in terms of k, h, and ℓ, we get

$$k = 0.275 \ , \quad h = 0.601 \ , \text{ and } \ell = 0.081 \ \ldots\ldots\ldots\ldots\ldots\ldots (297)$$

The results of the calculations for the Earth Model 4 - 6, together with those of Earth Model 2 and 3, are shown in Table 2. As we see in Table 2, the results of the calculations for the Earth models which have the rigidity $0 - 10^9$ in the core are practically the same, whereas those for the

P 348-9 Chap XIV Int Const. of Earth

Table 2--Values of k, h, and *ℓ* corresponding to various assumed values of μ

Item	Earth Model				
	2	3	4	5	6
μ in the core	0	10^7	10^9	10^{11}	10^{13}
k	0.281	0.275	0.275	0.243	0.055
h	0.606	0.601	0.600	0.530	0.109
ℓ	0.082	0.081	0.081	0.083	0.092

Earth models which have the rigidity 10^{11} - 10^{13} in the core are considerably different. Thus for the question (3) in the introduction of this paper, we may say that the largest value of μ is about 10^9 - 10^{10} in cgs units.

Summary--The results of our study are summed up as follows:

(1) The most reliable values of the characteristic numbers k, h, and *ℓ* are k = 0.27 - 0.29, h = 0.59 - 0.61, and *ℓ* = 0.07 - 0.08.

(2) The static elastic constant of the Earth determined by the study of Earth tide can be taken to be the same as the dynamic elastic constants of the Earth determined by the study of seismic waves passing through the Earth.

(3) The largest value of the rigidity of the core that is compatible with the observations of Earth tide is about 10^9 - 10^{10}.

Acknowledgments--The author wishes to express his sincere thanks to Chuji Tsuboi, of Tokyo University in Japan, under whom this study was made; to W. D. Lambert and F. Birch for their kindness in submitting this paper to the Transactions; and to T. Matsuzawa, B. Gutenberg, and R. Stonely for their kindness in reading the manuscript.

References

BULLEN, K. E., The variation of density and ellipticities of strata of equal density within the Earth, Mon. Not. R. Astr. Soc., Geophys. Supp., v. 3, pp. 395-401, 1936.

BULLEN, K. E., The problem of Earth's density variation, Bull. Seis. Soc. Amer., v. 30, pp. 235-250, 1940.

BULLEN, K. E., The density variation of the Earth's central core, Bull. Seis. Soc. Amer., v. 32, pp. 19-30, 1942.

DARWIN, G. H., Attempted evaluation of the rigidity of the Earth from the tides of long period, Sci. Papers, Cambridge, v. 1, pp. 340-346, 1907a.

GUTENBERG, B., and C. F. RICHTER, On seismic waves, Beitr. Geophysik, v. 45, pp. 280-360, 1935.

GUTENBERG, B., Internal constitution of the Earth, Chap. 14, pp. 345-360, New York, 1939.

HARTLEY, K., Direct measurement of the gravitational effect of the moon, Physics, v. 4, pp. 162-163, 1933.

HECKER, O., and O. MEISSNER, Beobachtungen an Horizontalpendeln über die Deformation des Erdkörpers, Veröff. Preuss. Geodät. Inst. no. 49, Potsdam, 1911.

HERGLOTZ, G., Über die Elastizität der Erde bei Berucksichtung jhrer variablen Dichte, Zs. Math. Physik, v. 52, pp. 275-299, 1905.

HOSKINS, L. M., The strain of a gravitating sphere of variable density and elasticity, Trans. Amer. Math. Soc., v. 21, pp. 1-43, 1920.

JEFFREYS, H., The rigidity of the Earth's central core, Mon. Not. R. Astr. Soc., Geophys. Suppl., v. 1, pp. 371-383, 1926.

JEFFREYS, H., The times of P, S, and Sks, and the values of P and S, Mon. Not. R. Astr. Soc., Geophys. Suppl., v. 4, pp. 498-533. 1939.

KELVIN, LORD, On the rigidity of the Earth, Phil. Trans. R. Soc. London, Series A, v. 153, pp. 573-582, 1863a.

KELVIN, LORD, Dynamical problems regarding elastic spheriodal shells and spheriods of incompressible liquid, Phil. Trans. R. Soc. London, Series A, v. 153, pp. 583-616, 1863b.

LAMB, H., The vibration of elastic sphere, Proc. London Math. Soc., v. 13, pp. 189-212, 1882.

LARMOR, J., On the influence of the oceanic waves on the law of variation of latitude, Proc. London Math. Soc., v. 14, pp. 440-449, 1915.

LOVE, A. E. H., The yielding of the Earth to disturbing forces, Proc. R. Soc. London, v. 82, pp. 73-82, 1909.

LOVE, A. E. H., Some problems of geodynamics, Cambridge, 1911.

MICHELSON, A. A., and H. G. GALE, The rigidity of the Earth, Astrophys. J., v. 50, pp. 330-345, 1919.

NISHIMURA, E., On Earth tides, Trans. Amer. Geophys. Union, v. 31, pp. 357-376, 1950.

PRESCOTT, J., On the rigidity of the Earth, Phil. Mag., v. 22, pp. 481-505, 1911.

PREY, A., Über die Elastizität der Erde, Beitr. Geophysik, v. 23, pp. 379-429, 1929, and v. 44, pp. 59-80, 1935.

SCHWEYDAR, W., Ein Beitrag zur Bestimmung des Starheitskoeffizienten der Erde, Beitr. Geophysik, v. 9, pp. 41-77, 1908.
SCHWEYDAR, W., Harmonische Analyse der Lotstörungen durch Sonne und Mond, SitzBer Preuss. Akad. Wiss., no. 59, 1914.
SCHWEYDAR, W., Lotschwankung und Deformation der Erde durch Flutkräfte, Zentralbureau der International Erdmessung, no. 38, Berlin, 1921.
TOMASCHEK, R., and W. SCHAFFERNICHT. Über die Messung der zeitlichen Schwankungen mit Gravimetern, Zs. Geophysik, v. 9, pp. 125-136, 1933.
WADATI, K., On the travel time of earthquake waves (part 4), Geophys. Mag., v. 7, pp. 149-160, 1933.
WYKOFF, R. D., The Gulf-gravimeter, Geophysics, v. 6, pp. 13-33, 1941.

Additional bibliography

DARWIN, G. H., Dynamical theory of tides of long period, Sci. Papers, Cambridge, v. 1, pp. 366-371, 1907b.
POLLACK, L., Das Periodogram der Polbewegung, Beitr. Geophysik, v. 16, pp. 108-194, 1927.
RAYLEIGH, LORD, On the dilatational stability of the Earth, Proc. R. Soc. London, v. 77, pp. 486-489, 1906.
SCHWEYDAR, W., Untersuchungen über die Gezeiten der festen Erde, Veröff. Preuss. Geodät. Inst. no. 54, Potsdam, 1912.
SEZAWA, K., Amplitude of P and S waves at different focal distances, Bull. Earthq. Res. Inst., v. 10, pp. 299-344, 1932.

Geophysical Institute,
Faculty of Science,
Tokyo University,
Tokyo, Japan

(Communicated manuscript received November 4, 1949;
open for formal discussion until March 1, 1951.)

Transactions, American Geophysical Union Volume 31, Number 5 October 1950

THE ABSOLUTE CALIBRATION OF A BRUSH ACCELEROMETER AND ITS RESPONSE TO SQUARE WAVES OF DISPLACEMENT AND VELOCITY

Pierre M. Honnell

Abstract--While it is not too difficult to determine the steady-state sinusoidal response of accelerometers and seismographs, the absolute calibration of these instruments is a more difficult matter. A new method for the absolute calibration of seismographs and accelerometers dynamically is based upon matching the peak sinusoidal acceleration of the instrument on test against the constant vertical acceleration of gravity. The method is described in its application to the calibration of a Brush accelerometer. The technique in its present simple form appears to enjoy a precision of five parts per 100.

The response of the same accelerometer to square waves of displacement and velocity, and to simple transient wave-forms, is also shown as a matter of interest.

Introduction--As is well known, the output response of seismographs and similar instruments may be obtained conveniently by use of a testing transducer or shaking table. Electromagnetic testing transducers driven by electronic amplifiers are highly desirable for this purpose due to their convenience, flexibility, and purity of waveform.

The electrical output voltage of the instrument on test, which is placed upon the moving platform of the testing transducer, is then measured for purely sinusoidal motions. Figure 1 is a typical response curve of this type. It shows the relative voltage output of a Brush type BL-301 crystal accelerometer for constant sinusoidal velocity, as a function of frequency. The ordinates of the data plotted represent the ratio (V_1/V_2), where V_1 is the root-mean-square voltage output of the accelerometer, and V_2 is the root-mean-square voltage output of the testing transducer velocity monitor. This voltage ratio is in effect a normalized calibration of the accelerometer.

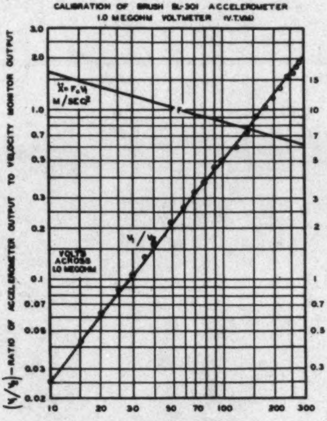

Fig. 1--Calibration curve of Brush BL-301 accelerometer

The absolute calibration of the instrument on test requires a determination of the actual amplitude of the sinusoidal displacement of the platform, or its equivalent. One usual solution to this problem is the direct optical observation of the platform motion, with or without levers, and also requires a static determination of the lever ratio if used. A more involved method requires the linear micrometric calibration of the testing transducer under static conditions, provided it utilizes a monitoring transducer (such as one of the variable capacitance type) which is presumed to behave alike for static and for dynamic conditions. Both of these methods are described in an excellent paper by LEE and IRLAND [1932]. Neither method is very convenient, and they are both open to questionable errors particularly at the higher frequencies. The remaining bibliographical references describe a reciprocity technique which is presently in vogue.

The principal purpose of this note is to describe a new and relatively simple technique for performing the absolute calibration. As a matter of collateral interest, the responses of the BL-301 accelerometer to square waves of displacement and velocity are also included.

The new absolute calibration technique--The new calibration technique makes advantageous use of presently available commercial electronic laboratory apparatus, and is easily applied. The fundamental concept of the method is extraordinarily simple: namely, the principle is to match the peak magnitude of the sinusoidal vertical acceleration of the moving platform of the testing electromechanical transducer against the vertical acceleration of gravity.

When equality of the two peak accelerations exists, the following relation obtains

$$\omega^2 x = g \quad \ldots\ldots\ldots\ldots\ldots\ldots \quad (1)$$

where $\omega = 2\pi f$ is the radian frequency of the driving oscillator and f is the frequency in hertz, or cycles per second; x = the peak amplitude of the sinusoidal motion of the platform of the testing transducer in meters; and g = the constant vertical acceleration due to gravity in meters per second per second. The corresponding peak displacement and velocity of the sinusoidal platform motion then are, respectively,

$$x = g/(2\pi f)^2 \doteq 0.249/f^2 \text{ meters} \quad \ldots\ldots\ldots\ldots \quad (2)$$

$$\dot{x} = dx/dt = \omega x = g/2\pi f \doteq 1.56/f \text{ meters per second} \quad \ldots\ldots\ldots \quad (3)$$

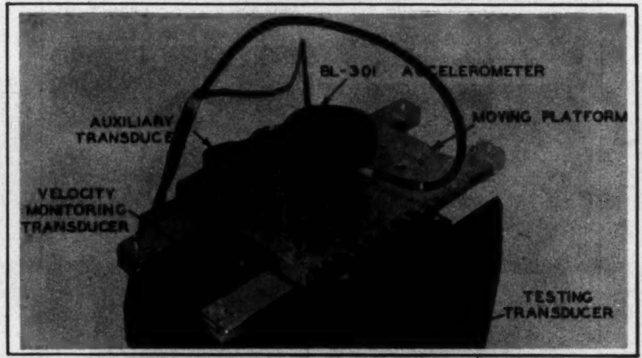
BL-301 ACCELEROMETER
AUXILIARY TRANSDUCER
MOVING PLATFORM
VELOCITY MONITORING TRANSDUCER
TESTING TRANSDUCER

Fig. 2--Physical arrangement for absolute calibration

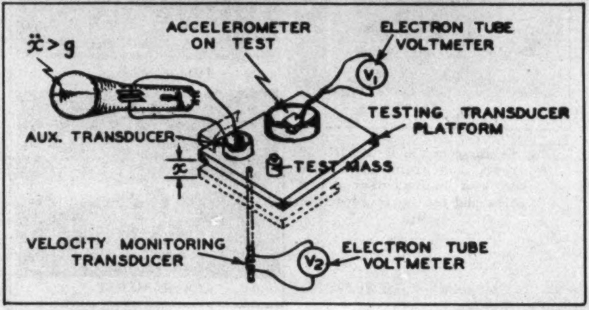
$\ddot{x} > g$
ACCELEROMETER ON TEST
ELECTRON TUBE VOLTMETER
V_1
TESTING TRANSDUCER PLATFORM
AUX. TRANSDUCER
x
TEST MASS
VELOCITY MONITORING TRANSDUCER
ELECTRON TUBE VOLTMETER
V_2

Fig. 3--Electrical connections for absolute calibration

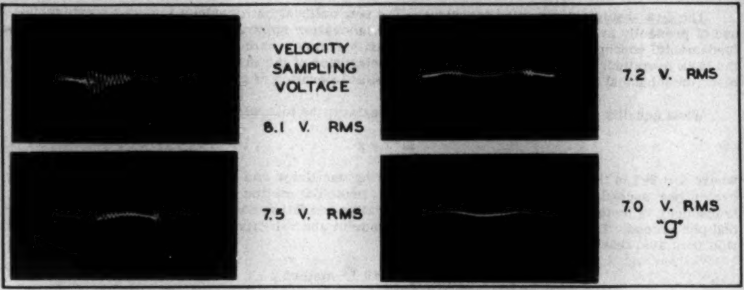

Fig. 4--Typical oscillograms of auxiliary transducer output during absolute calibration at 20 hertz sinusoidal motion of platform

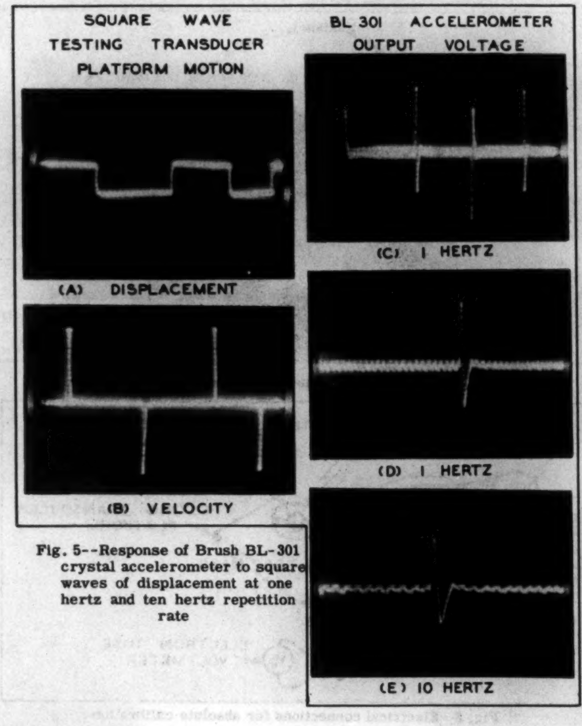

Fig. 5--Response of Brush BL-301 crystal accelerometer to square waves of displacement at one hertz and ten hertz repetition rate

It should be noted that the technique is useful for the calibration of testing transducers or shaking tables proper, as well as for the calibration of seismographs and similar instruments.

Instrumentation--The equality of the peak magnitudes of the two accelerations - one sinusoidal and the other constant - is indicated by the motion of a test mass placed upon the moving platform of the testing transducer. When the platform acceleration exceeds that of gravity, the test mass rattles against the moving platform. While this chattering is audible, it is best indicated visually by means of a cathode-ray oscillograph connected to an auxiliary transducer (a headphone with cover removed) clamped to the moving platform.

The physical arrangement is depicted in Figure 2, which shows the Brush BL-301 accelerometer under calibration, the test mass (100 gm), and the auxiliary transducer. The output of the auxiliary transducer is placed upon the y-axis of the cathode-ray oscillograph which has its linear x-axis time sweep synchronized with the driving test frequency. The electrical connections are shown symbolically in Figure 3. The testing transducer platform motion is monitored with an electron tube voltmeter V_2 and an oscillograph (not shown in Fig. 3). The output voltage of the instrument on test is measured with an electron tube voltmeter V_1.

The type of waveform observed from the auxiliary transducer during calibration is shown by the series of oscillograms in Figure 4. The minute, relatively high frequency, transient oscillations initiated by the test mass rattling against the moving platform are clearly discernible. Since the synchronization of the x-axis sweep of the cathode-ray trace is independent of the transient amplitude, the location of the transient wave on the time axis remains fixed. The procedure is to reduce the platform acceleration until the chattering transient just ceases to be visible on the oscillograph. The two accelerations of the mass are then equal, as given in (1). The precision of measurement obtained with the present crude arrangement is of the order of five parts in 100, as indicated from the typical data in Figure 4.

Calibration of the Brush BL-301 accelerometer--Typical results obtained on test are as follows: frequency, 25 hertz; BL-301 accelerometer voltage $V_1 = 0.61$ volts rms; velocity monitoring transducer voltage $V_2 = 6.55$ volts rms; and peak acceleration $\ddot{x} = g = 9.8$ m/sec. Since the

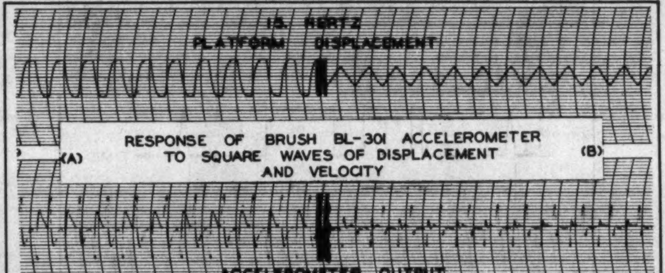

Fig. 6--Response of Brush BL-301 crystal accelerometer to square waves of displacement and velocity at 15 and 20 hertz

velocity monitoring transducer is the more reliable instrument, the data given above are preferably used to calibrate the testing transducer. Since

$$V_2 = K\dot{x} \quad \ldots\ldots\ldots\ldots\ldots\ldots\ldots\ldots\ldots\ldots \quad (4)$$

the data above gives

$$K = 6.55\sqrt{2}/6.24 \cdot 10^{-2} = 148$$

a constant factor. (Note that $\dot{x}$ is obtained from (3) at 25 hertz).

Now it is convenient to express the calibration of accelerometers as

$$\ddot{x} = F \cdot V_1 \quad \ldots\ldots\ldots\ldots\ldots\ldots\ldots\ldots\ldots\ldots \quad (5)$$

where $\ddot{x}$ is the acceleration and V_1 the corresponding voltage output of the acclerometer (peak or root-mean-square, depending upon V_1). The proportionality factor F is then given by

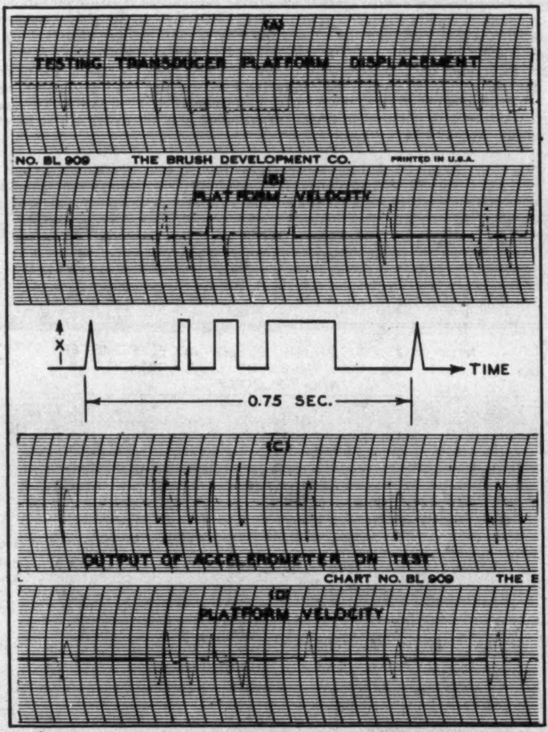

Fig. 7--Response of Brush BL-301 accelerometer to an arbitrary transient wave repeating at 0.75 sec intervals

$$F = \omega/K\,(V_1/V_2) \ldots\ldots\ldots\ldots\ldots\ldots\ldots\ldots (6)$$

where the ratio (V_1/V_2) is the normalized accelerometer response determined experimentally, such as is plotted in Figure 1. The curve labeled F in the same Figure is then obtained from (6).

From the curve F in Figure 1, it is evident that the output of the BL-301 accelerometer is not independent of frequency for a constant acceleration. This is due partly to the loading of the vacuum tube voltmeter V_1 which has an input resistance of 1.0 megohm. Furthermore, the instrument output voltage amplitude is a non-linear function of the amplitude of motion. This is indicated by the data tabulated above, which gives for g at 25 hertz

$$g = \ddot{x} = F \cdot V_1 \sqrt{2} = 12.5\ (0.61)\ 1.41 = 10.7\ \text{m/sec}^2$$

This is about ten per cent high, and is due to the non-linearity of amplitude response previously mentioned. The calibration curve (V_1/V_2) and the calibration factor F plotted in Figure 1 were determined with motions approximately 1/10 of that used in determining the acceleration equal to g. (The effects of temperature upon the accelerometer characteristics must also not be overlooked.)

Output of Brush accelerometer to non-sinusoidal motions--As a matter of interest, the response of the Brush BL-301 accelerometer to square waves of displacement is presented in Figure 5. The oscillograms shown are the testing transducer platform displacement, 5a; the velocity, 5b; and the Brush accelerometer response in 5c and 5d, the latter with an expanded time scale. Finally, Figure 5e is the BL-301 accelerometer response to ten hertz square waves of displacement, also with an expanded time sweep.

Oscillograms of the Brush BL-301 accelerometer output (as recorded on a Brush a-c pen-writing oscillograph) for square waves of displacement and velocity at 15 hertz are shown in Figure 6a and 6b, respectively; similarly, the response to 20 hertz square waves of velocity is shown in Figure 6c.

Finally, the response of the accelerometer to an arbitrary transient displacement is depicted in Figure 7, in which 7c is the accelerometer output; 7a is the testing transducer platform displacement, and 7b and 7d the testing transducer platform velocity. (Oscillograms 7a and 7b were not taken simultaneously with 7c and 7d and thus the records differ somewhat.)

Acknowledgments--The results indicated herein are phases of a research program on seismograph testing instrumentation under the direction of James B. Macelwane, whose guidance it is a pleasure to acknowledge. The critical and constructive review of the work by Florence Robertson is also appreciated.

References

HASKELL, N. A., A substitution method for the absolute calibration of vibration pick-ups, Geophys., v. 14, no. 4, pp. 558-561, October, 1949.

LONDON, A., The absolute calibration of vibration pickups, Nat. Bur. Stand. Tech. News Bull., v. 32, no. 1, pp. 8-10, January, 1948.

LEE, F. W., and G. A. IRLAND, Construction of master mechanical oscillator for testing seismic recorders and other allied apparatus, Tech. Pap. no. 518, Bur. Mines, Dept. Comm., Washington, D. C., 1932.

THOMPSON, S. P., Reciprocity calibration of primary vibration standards, J. Acoustical Soc. Amer., v. 20, no. 5, pp. 637-640, September, 1948.

TRENT, H. M., The absolute calibration of electromechanical pickups, J. Appl. Mech., v. 15, no. 1, pp. 49-52, March, 1948.

Department of Geophysics,
Saint Louis University,
St. Louis, Missouri

(Manuscript received May 2, 1950; presented at the Thirty-First Annual Meeting, Washington, D. C., May 2, 1950; open for formal discussion until March 1, 1951.)

Transactions, American Geophysical Union Volume 31, Number 5 October 1950

NEW STANDARDS FOR LANDSBERG'S GLASS ROD METHOD OF INTEGRATING ULTRAVIOLET RADIATION

J. Sherrod, H. Neuberger, and D. Yerg

Abstract--Landsberg's method of obtaining integrated values of ultraviolet radiation makes use of small glass rods that, under the influence of ultraviolet radiation, change their color from green to various shades of purple when longitudinally viewed. Investigations of the original standards consisting of a set of pre-exposed and calibrated rods revealed the instability of the glass color. Two new methods of standardization have been developed; one involves a complementary wedge filter by means of which the color of the rod is compensated to neutral, the other one employs a set of partly-covered rods, so that the rods themselves furnish the chromatic compensation. The stability and saturation characteristics are discussed and tentative calibration curves presented.

More than a decade ago, LANDSBERG and WEYL [1939] developed a phototropic glass containing small amounts of cerium and vanadium oxides. This glass changes in color from green to colorless to pink, and eventually to purplish-red when exposed to ultraviolet (UV) radiation in the spectral range between 3400 and 4000 Å, with a maximum response to a wave length of about 3600 Å. LANDSBERG [1940] utilized this glass to establish a method for integrating UV-radiation. This method consists of exposing a glass rod of the standard size of 50 mm length and one milimeter diameter and measuring the amount of color change. The color change was determined by viewing the rod longitudinally and comparing the exposed rod with a standard set of 11 similar rods, with color shades ranging from green to red, arbitrarily numbered from zero to ten. The integrated UV-radiation values pertaining to the various rods of the standard set were determined by calibration. Exposed rods can be used repeatedly, since the color changes produced by UV-radiation are reversible by heating to 300° C. The color changes were originally thought to be stable at ordinary temperatures. However, it soon became apparent that some of the exposed rods faded at ordinary temperatures for reasons as yet unknown. At any rate, that standard scale became useless, since it consisted of unstable colored rods.

YERG [1947] tested the spontaneous color reduction of rods that had been previously exposed to different UV-radiation doses and subsequently stored in the dark. He found that the fading in the rods was more rapid the greater the color change. Table 1 shows the results of the chromatic evaluation, at different intervals of time, of rods having various initial colors, ranging from one (colorless) to 19 (deep purplish-red). The scale used is shown in Table 2. According to Table 1, the evaluation of exposed rods must take place within one day if the influence of spontaneous fading is to be avoided. Nevertheless, in view of the simplicity and inexpensiveness of the rod-method, further investigation into the possibility of other standards for evaluating the UV-induced chromatic changes of the glass rods, seemed warranted.

A search for a suitable comparison standard in the form of other glasses or plastics of similar, but stable colors, proved fruitless. However, a chromatic compensation system similar to that employed in the well-known Frankenburger UV-dosimeter [LANDSBERG, 1937] was found to be quite expedient. In the dosimeter, UV-radiation produces a photochemical change in a colorless organic liquid which rapidly turns to various shades of red. Instantaneous UV-values are then determined by compensating the color of the liquid column to a neutral gray with a complementary green color wedge. Similarly, the reddish color of the exposed rods can be compensated by the various shades of blue-green obtained with a solution of ten grams of nickelous sulfate in 100 cc of water, enclosed in a wedge-shaped glass container of about 30° angle at the apex. An arbitrary standard scale of 20 divisions of 1/8 inch each, with the zero point at the apex of the wedge, was devised and calibrated

Table 1--Spontaneous color reduction of phototropic glass rods

Initial color scale	Color scale reading after		
	One day	Three days	17 days
1	1	1	1
2	2	2	1
4	4	4	3
6	6	6	5
9	9	8	6
11	11	10	7
19	19	15	12

Table 2--Calibration of green-wedge method

Scale number	UV radiation	
	μw-hr/cm^2	10^4ergs/cm^2
1	1	4
2	2	7
3	4	14
4	5	18
5	7	25
6	9	32
7	12	43
8	14	50
9	17	61
10	20	72
11	24	86
12	28	101
13	33	119
14	40	144
15	48	173
16	57	205
17	65	234
18	74	266
19	82	295
20	90	324

by means of the dosimeter. To facilitate viewing of the small cross section of the rod, the image of one end of an exposed rod was projected on a small screen by means of a microprojector, and the compensating wedge was inserted in the optical train. A recomputed calibration curve of this 20-step scale is given in Table 2. The nonlinearity of this scale is apparent, and presents a distinct disadvantage, for example, in computing climatological means, because the scale readings cannot be added or averaged, but must first be converted into UV-radiation units, such as μw-hr/cm^2 or ergs/cm^2. In addition, although the nickelous sulfate represents an easily reproducible standard, the handling of a glass-wedge filled with a liquid is a precarious proposition in routine work. Subsequent attempts at solidifying the solution by means of gelatin failed because of deterioration by mold.

It occurred to us, that the original green color of the unexposed rods might be used to compensate the reddish tints of the exposed rods, particularly since the green rods are stable. In order to test this possibility of autostandardization, sets of 50 rods were fastened side by side on small white plates and covered diagonally in such a manner that the rod on one end of the set was completely exposed, the rod at the other end completely covered. In this way, a progressive change is produced in the ratio of exposed to covered portion of the rods. On clear days, these sets of rods were exposed to solar and sky radiation and, at intervals, viewed longitudinally with a magnifying glass. That rod which appeared colorless, that is, the rod in which the amount of red of the exposed portion was compensated by the unchanged green of the unexposed portion of the same rod, then served as a relative measure of integrated UV intensity. Instantaneous measurements made by means of the UV-dosimeter at half-hour intervals during exposure of the rod sets, were used for the subsequent calibration of the rods. Figure 1 shows the average relationship between the covered portion in per cent of the total rod length, and the integrated UV intensities in μw-hr/cm^2. This curve, which is based on the averages of 58 individual measurements, indicates that the response of rods with more than 80 per cent cover is such, that a slight increase in the cover corresponds to a large increase in integrated UV-values, thus causing large errors in the UV determinations in this range. For this reason, only the steep branch of the curve between zero and 80 per cent rod cover was considered for the selection of a linear scale of ten steps corresponding to 3.5 μw-hr/cm^2 each. Table 3 shows the arbitrary scale

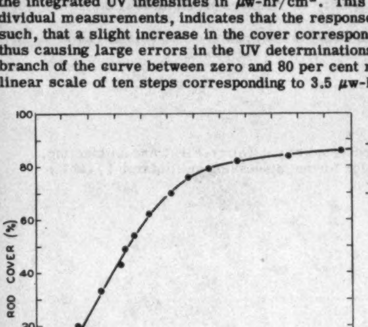

Fig. 1--Calibration curve for UV-sensitive glass rods

Table 3--Calibration of the autocompensation method

Scale number	Rod cover	Integrated UV intensities	
	pct	μw-hr/cm^2	10^4ergs/cm^2
1	0	3.5	12.6
2	14	7.0	25.2
3	28	10.5	37.8
4	40	14.0	50.4
5	52	17.5	63.0
6	60	21.0	75.6
7	68	24.5	88.2
8	74	28.0	100.8
9	78	31.5	113.4
10	80	35.0	126.0

divisions, and the pertinent relative covered portion of the rods, and integrated UV intensities. It is realized that the wave-length response of the dosimeter is not strictly the same as that of the glass rods; nevertheless, this procedure appeared acceptable for testing the suitability of the autocompensation method.

In practice, a set of 12 rods is mounted on a plate; the first and twelfth rods are completely covered and merely serve to facilitate the detection of a change in color of the second and eleventh rods, which represent number one and ten, respectively, of the scale shown in Table 3. The number of the colorless rod is easily established by selecting that rod which appears neither in a pinkish nor greenish hue. Any bright, colorless surface may serve as an illumination source. A sheet of white paper illuminated by sunlight is preferable to one illuminated by an incandescent light bulb. Colored light sources must be avoided in order to preserve the delicate color contrasts exhibited by the rods. The average accuracy obtainable with this method is well within 20 per cent. However, this method has, in its present design, a serious limitation with regard to the length of time for which the UV-radiation can be integrated. Under conditions of strong UV-radiation, scale number ten is reached after an exposure of approximately one hour, then, the last rod of the set will turn from colorless to pink, thus preventing further usefulness of that particular rod set. In order to obtain integrated UV-intensities for an entire day, a device similar to that designed by NEUBERGER [1944] for recording hourly precipitation traces, could be adopted. With such an arrangement a new set of rods can be automatically exposed every hour. In this connection, it may be mentioned that the orientation of the rods during exposure appears to have no effect on the measured intensities.

The reduction of the incident radiation intensity by means of suitable filters, which, at the same time would serve to absorb some of the longer UV-wave lengths which are biologically less important, represents a possibility for increasing the exposure time of a rod set. This possibility is now being investigated; work is also being conducted on the problem of improving the color contrast of the rod sets by increasing the length of the rods.

References

LANDSBERG, H., The ultraviolet dosimeter, Bull. Amer. Met. Soc., v. 18, pp. 161-167, April-May, 1937.

LANDSBERG, H., A method of measuring radiation of short wave length by means of a photochemical reaction in a special glass. Pennsylvania State College Studies No. 5, 1940.

LANDSBERG, H., and W. WEYL, Measurements of ultraviolet sums with photosensitive glass, Bull. Amer. Met. Soc., v. 20, pp. 254-256, June, 1939.

NEUBERGER, H., On the measurement and frequency of traces of precipitation, Bull. Amer. Met. Soc., v. 25, pp. 183-188, May, 1944.

YERG, D. G., Standardization of sensitive glass rods for integration of ultraviolet radiation, M. S. thesis, Pennsylvania State College, 1947.

Division of Meteorology,
The Pennsylvania State College,
State College, Pennsylvania

(Manuscript received April 24, 1950; presented at the Thirty-First Annual Meeting, Washington, D. C., May 1, 1950; open for formal discussion until March 1, 1951.)

Transactions, American Geophysical Union Volume 31, Number 5 October 1950

A NUMERICAL SOLUTION FOR IRROTATIONAL FLOW OVER A MOUNTAIN BARRIER

C. S. Gilman and L. L. Weiss

Abstract--The "relaxation method" is applied to Pockels' equation for a particular case of flow over a given mountain profile with boundary conditions specified to be that the isopleths of velocity potential be normal to the top and bottom boundaries. The values of vertical velocity thus found are then compared with those from Pockels' solution for the same profile and with the exponential rate of decrease assumed by BJERKNES [1940]. The different methods give quite different results, the principal difference being that at higher elevations (five to ten kilometers) the vertical velocities computed by the relaxation method are larger than those computed by Bjerknes' method and much smaller than those computed by Pockels' method. The large disagreement between these results shows the dangers involved in a purely theoretical approach to the problem. Evidently more observations of vertical velocities in regions of rough orography are needed before the various theories can be evaluated.

Introduction--The problem of computing precipitation rates in the flow of moist air over orographic barriers depends intrinsically on the variation of the vertical velocity with height. Investigations of this variation have been confined mostly to two idealized types of treatment, neither of which is entirely satisfactory. The first makes use of the ideal fluid of hydrodynamics, and the second makes use of the method of small perturbations. Both introduce unrealistic assumptions, and require much work with the equations of motion. POCKELS [1901] attacked the problem by use of the first method, and the later work of QUENEY [1947] is based on the second.

Pockels' analytical solution of the differential equation that he uses to describe the air flow over an orographic barrier was based on two additional assumptions. The first is that temperature can be considered independent of height, and the second essentially presupposes a very slight rate of decrease of vertical velocity with height. If these assumptions are not made, the conditions are more nearly those in nature but the analytic solution is much more difficult.

In this paper it is intended to summarize Pockels' solution and then present a more exact solution based on the "relaxation method" of SOUTHWELL [1946].

Solution by Pockels' method

Derivation of Pockels' differential equation--In deriving his differential equation to describe the flow of air over an orographic barrier, Pockels assumed the following conditions to hold: (a) The flow is steady with respect to time. (b) It is continuous and free from whirls (irrotational). (c) It is everywhere parallel to a definite vertical plane perpendicular to the mountain ridge and thus depends only on the vertical coordinate, z, and the horizontal coordinate, x. (d) Internal and external friction are negligible. (e) At some great height there must prevail a purely horizontal velocity, a. (f) $\partial\rho/\partial x = 0$, where ρ is the air density. (g) Flow at the surface follows the surface profile.

From (c), the wind velocity $\mathbf{V} = u\,\mathbf{i} + w\,\mathbf{k}$, where u is the horizontal wind speed and w, the vertical wind speed, and $\mathbf{i}$ and $\mathbf{k}$ are unit vectors along x- and z-axes, respectively. From (a) and (c), the equation of continuity becomes

$$\nabla\cdot(\rho\mathbf{V}) = \mathbf{V}\cdot\nabla\rho + \rho\nabla\cdot\mathbf{V} = 0 \qquad (\nabla = \mathbf{i}\,\partial/\partial x + \mathbf{k}\,\partial/\partial z)$$

From (b) if follows that there exists a velocity potential ϕ such that

$$\mathbf{V} = \nabla\phi$$

therefore

$$\nabla\phi\cdot\nabla\rho + \rho\nabla\cdot\nabla\phi = 0$$

and from (f) we get

$$\rho \nabla^2 \phi = -(\partial \rho/\partial z)\, \partial \phi/\partial z$$

This is Pockels' differential equation, which he rewrites as

$$\nabla^2 \phi = q\, \partial \phi/\partial z \quad \text{.........................} \quad (1)$$

where $q = (-1/\rho)\, \partial \rho/\partial z$.

Pockels' method of solving his differential equation--In order to solve his equation, Pockels makes two further assumptions. The first is that temperature is independent of height. This allows him to perform the integration in the hydrostatic equation

$$P = P_o \exp - (g/R) \int_o^z 1/T\, dz$$

and to set $\log_e \rho_o/\rho = \log_e P_o/P = gz/RT = qz$, where q is considered a constant, equal to 1.23×10^{-4} when z is expressed in meters and T (the air temperature) is 5° C.

A solution satisfying assumption (e) is

$$\phi = a(x - b e^{-Nz} \cos mx)$$

where a, b, and m are arbitrary constants and

$$N = q/2 + \sqrt{m^2 + q^2/4}$$

The horizontal and vertical velocities are then, respectively,

$$w = \partial \phi/\partial z = a\, b\, N\, e^{-Nz} \cos mx$$

$$u = \partial \phi/\partial x = a\,(1 + b\, m\, e^{-Nz} \sin mx)$$

If the profile of the mountain can be expressed in the form $\bar{z} = A \sin mx$, where $m = h\pi/L$, $(h = 1, 2, 3, \ldots)$, the slope will be $d\bar{z}/dx = Am \cos mx$.

When the lowest streamline coincides with the mountain profile,

$$d\bar{z}/dx = (\partial \phi/\partial z)/(\partial \phi/\partial x)\Big|_{z = \bar{z}} = w/u\Big|_{z = \bar{z}}$$

or

$$Am \cos mx = b\, N\, e^{-N\bar{z}} \cos mx/(1 + b\, m\, e^{-N\bar{z}} \sin mx)$$

and

$$Am = bN\, [e^{-N\bar{z}}/(1 + b\, m\, e^{-N\bar{z}} \sin mx)] \quad \text{.....................} \quad (2)$$

Since the differential equation is linear, the sum of solutions can be set equal to a solution and therefore both ϕ and $\bar{z}$ can be expressed to any degree of approximation by means of a Fourier series of a finite number of terms. Pockels made a second assumption, that the quantity in brackets in (2) is equal to unity and computed his Fourier coefficients from $A_h\, m_h = b_h\, N_h$.

Pockels' method of solution applied to a mountain profile--The mountain profile used in this example is a sine curve of one cycle with x-axis tangent to the curve at the minima, first minimum at the origin and second minimum at 100 km. The mountain height is three kilometers. The equation of this profile is

$$\bar{z} = f(x) = 1.5\, (1 - \cos 2\pi x/L)$$

where L = 100 km. The first half cycle of this curve is shown in the lower part of Figure 1, with the vertical scale six and two-thirds times the horizontal.

This profile can be expressed as a Fourier series

$$f(x) = b_1' \sin(\pi x/L) + b_2' \sin(2\pi x/L) + \ldots b_n' \sin(n\pi x/L) + \ldots$$

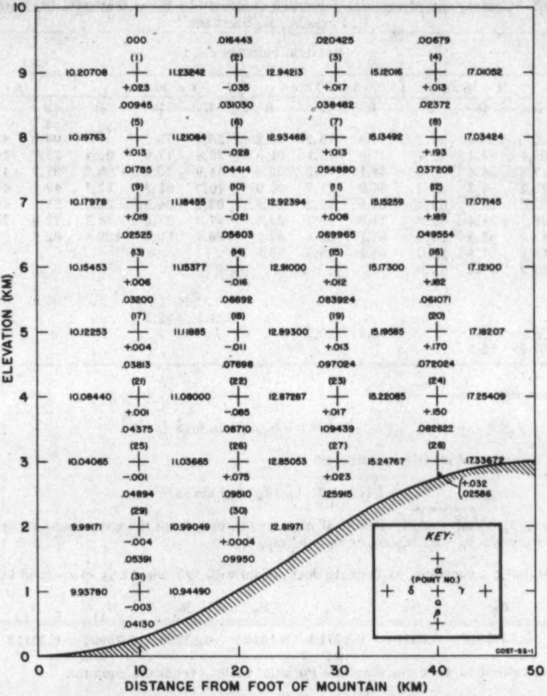

Fig. 1--Wind velocity field above mountain profile

The coefficients are then

$$b_n' = (2/L)\int_0^L f(x)\sin(n\pi x/L)\,dx$$

Integrating,

$$b_n' = (3.0/\pi)\,(-8)/n(n-2)(n+2) \quad \text{for n odd}$$

$$= 0 \qquad \text{for n even}$$

The values of b_n' are

n =	1	3	5	7	9	11	13
b_n' =	2.5464	-0.5092	-0.0728	-0.0242	-0.0110	-0.0059	-0.0036

The mountain profile is represented by a Fourier sine series as

$$f(x) = \sum_{n=1}^{13} b_n' \sin(n\pi/L)x$$

Table 1--Comparison of vertical velocities computed by three methods: (R, Relaxation; P, Pockels'; B, Bjerknes')

Elevation	Vertical velocity cm/sec											
	x = 10 km			x = 20 km			x = 30 km			x = 40 km		
km	R	P	B	R	P	B	R	P	B	R	P	B
9.5	00.0	54.6	00.2	16.4	75.3	00.8	20.4	75.2	01.7	06.8	43.7	01.3
8.5	09.4	54.4	00.4	31.0	75.1	01.5	38.5	77.6	03.4	23.7	44.8	02.6
7.5	17.8	54.4	00.8	44.1	76.2	03.0	54.9	79.9	06.8	37.2	45.8	05.2
6.5	25.2	54.3	01.7	56.0	77.7	06.0	70.0	81.2	13.7	49.6	47.1	10.3
5.5	32.0	54.3	03.4	66.9	79.2	11.9	83.9	84.5	27.4	61.1	48.5	20.6
4.5	38.1	54.4	06.8	77.0	80.7	23.8	97.0	87.0	54.7	72.0	49.8	41.3
3.5	43.8	54.5	13.5	87.1	82.1	47.6	109.4	89.7	109.4	82.6	51.2	82.6
2.5	48.9	54.9	27.0	95.1	83.8	95.1	..	..	..	..	..	..
1.5	53.9	55.4	53.9	..	..	..	..	..	..	..	..	..
2.8568	..	..	..	..	..	..	..	..	..	90.4	60.0	..
2.4817	..	..	..	..	..	..	121.5	89.1	..	..	..	..
1.4818	..	..	..	103.3	90.3	..	..	..	..	..	..	..
0.6433	57.9	56.8	..	..	..	..	..	..	..	..	..	..

Pockels' assumption that

$$e^{N_h \bar{z}} = 1 - b_h m_h \sin m_h x$$

allows him to write the profile equation as

$$f(x) = \sum_{h=1}^{n} b_h (N_h/m_h) \sin m_h x$$

where $N_h = (q/2) + \sqrt{m_h^2 + q^2/4}$. Hence, if $m_h = n\pi/L$, then from the uniqueness theorem of Fourier coefficients, $b_n' = b_h N_h/m_h$ or $b_h = b_n' m_h/N_h$.

Considering q a constant, as Pockels does, equal to 0.123 when z is expressed in kilometers

N_1	N_3	N_5	N_7	N_9	N_{11}	N_{13}
0.0075616	0.05104	0.10719	0.16685	0.22786	0.28951	0.35152

Vertical velocities were computed by Pockels' method from the equation

$$w = \partial\phi/\partial z = a \sum_{h=1}^{n} b_h N_h e^{-N_h z} \cos m_h x$$

using the constants determined above. These are shown in the column headed P in Table 1.

To illustrate how closely Pockels' second assumption holds in this example, we take the values of N_h, b_h, m_h, as given above and calculate the value of the summations at x = 25 km, $\bar{z}$ = 1.5 km, in the expression

$$\Sigma e^{N_h \bar{z}} = \Sigma (1 - b_h m_h \sin m_h x) \quad \ldots\ldots\ldots\ldots\ldots\ldots (3)$$

The left-hand member of (3) is found to be 9.18, and the right-hand, 6.59. The second assumption is thus seen to be only approximately satisfied.

Relaxation method solution

A solution of the differential equation with prescribed boundary conditions can be found, provided a solution exists, to any desired accuracy by applying the "method of relaxations" discussed by SOUTHWELL [1946] and by SHORTLY and WELLER [1938]. Using this procedure it is not necessary to make the assumption that temperature is independent of height, nor is it necessary to use Pockels' other assumption that $e^{N\bar{z}} = 1 - b\, m \sin mx$.

The relaxation procedure consists of a systematic trial-and-error method of finding at each point of a suitable network values of the velocity-potential such that the finite-difference equation corresponding to the differential equation is satisfied at each point. First, some trial set of values of ϕ is assumed for the various points, and the values of the finite-difference function or residual,

$$Q \equiv \Delta_x(\Delta_x\phi)/(\Delta x)^2 + \Delta_z(\Delta_z\phi)/(\Delta z)^2 - q\,\Delta_z\phi/\Delta z \ldots\ldots\ldots\ldots\ldots (4)$$

is computed at each point. The "relaxing" refers to changing the values of ϕ in such a manner that Q becomes smaller and smaller. The values of ϕ will constitute an approximate solution of the difference equation when Q approaches zero at every point of the network.

If we select the net of points shown in Figure 1, the residual at any point of the net where no border points are involved in its computation is

$$Q = \phi_1 + \phi_2 - 202\phi_0 + 100\phi_3 + 100\phi_4 - 5q\,(\phi_3 - \phi_4) \ldots\ldots\ldots\ldots\ldots (5)$$

where the points in the set are numbered as in Figure 2, Q is the residual at the point labeled 0 in units of ϕ per 100 km^2, and q is used in units of "per ten kilometers." Letting

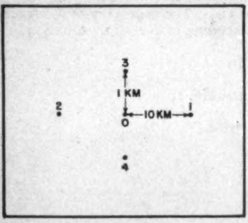

Fig. 2--Set of points used in relaxation method

$$\left.\begin{aligned} \gamma &= \phi_1 - \phi_0 \\ \delta &= \phi_0 - \phi_2 \\ \alpha &= \phi_3 - \phi_0 \\ \beta &= \phi_0 - \phi_4 \end{aligned}\right\} \ldots\ldots\ldots\ldots\ldots\ldots\ldots (6)$$

the residual formula can be written as

$$Q = (\gamma - \delta) + 100\,(\alpha - \beta) - 5q\,(\alpha + \beta)$$

and using it in this form makes the computation easier in the reduction of the residuals.

Computation of the residuals at points where the pattern involves boundary points will require special formulas which take into account the boundary conditions. When the distance from point zero to point four is different from that between zero and three (and this is the case for the lower boundary points) we can call this distance Δ km. Then the relaxation formula will be

$$Q = (\gamma - \delta) + 200\,(\alpha - \beta/\Delta)/(1 + \Delta) - 10q\,(\alpha + \beta)/(1 + \Delta) \ldots\ldots\ldots (7)$$

where q is in units per "ten kilometers."

The values of Δ for the boundary points of Figure 1 which are not regularly spaced are

Point no.	27	28	30	31
Δkm	1.0365	0.2865	0.9635	0.7135

Then the relaxation formulas for the boundary points become

$$Q_{27} = (\gamma - \delta) + 98.2077\alpha - 94.7494\beta - 5.0606\,(\alpha + \beta)$$

$$Q_{28} = (\gamma - \delta) + 155.4606\alpha - 542.6197\beta - 8.0109\,(\alpha + \beta)$$

$$Q_{30} = (\gamma - \delta) + 101.8589\alpha - 105.7176\beta - 5.1220\,(\alpha + \beta)$$

$$Q_{31} = (\gamma - \delta) + 116.7202\alpha - 163.5882\beta - 5.7350\,(\alpha + \beta)$$

In addition, the requirements that the streamline at the ten-kilometer level be horizontal and that the lowest streamline follow the mountain profile impose the restriction that the isopleths of velocity potential be perpendicular to the ten-kilometer level and to the mountain profile and be vertical above the crest of the mountain and in the undisturbed flow at the foot of the mountain and to windward. The mountain is symmetrical about a vertical at x = 50 km and the flow will be symmetrical also. Hence, the net covers the area between the mountain top and the ten-kilometer level, and between x = 0 and x = 50 km. For those residuals whose computation involves the top boundary points, these restrictions require that α approach zero. For those where the boundary points on the mountain profile are involved, the profile slope must be taken into account.

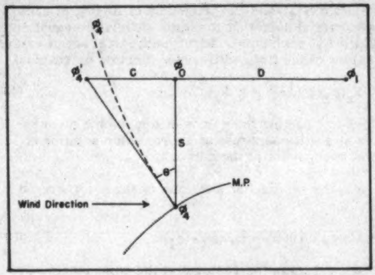

Fig. 3--Set of points used in computing residuals at points near mountain surface

In the vicinity of the mountain profile (M.P. in Figure 3), the isopleth of velocity potential through point four (ϕ_4) will be perpendicular to M.P. at that point. If we draw a straight line perpendicular to the M.P. curve from point four, it will intersect the horizontal line through point zero at ϕ_4'. We can consider ϕ_4' as an approximation to ϕ_4 and the approximation will be better, the shorter the distance s, but ϕ_4' will always be smaller than ϕ_4. The geometry of the figure then gives $\phi_0 = \phi_4' + (\phi_1 - \phi_4') C/(C + D)$ where $C = S \tan \theta$, or, according to our approximation,

$$\phi_0 - \phi_4 = (\phi_1 - \phi_4) C/(C + D)$$

Substituting from (6), $\beta = (\gamma + \beta) C/(C + D)$, and since D is ten kilometers,

$$\beta = (\gamma + \beta) S \tan \theta/(10 + S \tan \theta)$$

or

$$\beta = 0.1 (S \tan \theta)\gamma$$

From the equation of the mountain profile,

$$\tan \theta = d f(x)/dx = 0.03\pi \sin (2\pi x/L)$$

and the relations for points 27, 28, 30, and 31 are

$$\beta_{27} = 0.0092907\gamma$$

$$\beta_{28} = 0.0015872\gamma$$

$$\beta_{30} = 0.0086364\gamma$$

$$\beta_{31} = 0.0039572\gamma$$

Improved values of q--Lacking upper-air data, Pockels used a constant value for q. Data from a large number of upper-air soundings now enable us to use a value of q varying with height more nearly in accordance with the conditions obtaining in the atmosphere. Values of q for use in the residual formulas were based on the air density of the Standard Atmosphere at height intervals of one kilometer as taken from the SMITHSONIAN PHYSICAL TABLES [1934]. Since

$$q = -(1/\rho)\, \partial\rho/\partial z = -\partial \log_e \rho/\partial z$$

the difference of the natural logarithms of the densities given in the table gives directly the value of q at the elevation midway between the elevations of the two densities. These q values were plotted on a graph and a curve drawn for use in interpolating values at other elevations. The q values thus determined are in units of per kilometer and must be multiplied by ten (to give units per ten kilometer) for use in the residual formulas. The values of 5q used in computing the residuals are shown in Table 2.

Mass transport and first approximate solution--While it is possible to start with any numbers for the values of α, β, γ, and δ, any information that will serve to give a better estimate of their true magnitude will save an enormous amount of arithmetical work. These improved estimates can be made if we make use of the requirement that the mass inflow of air must equal the mass outflow for any region bounded by the mountain profile, the ten-kilometer level, and two verticals.

Table 2--Values of 5q

Elevation	5q
km	
0	4.8025
1	4.9134
2	5.0290
3	5.1530
4	5.2785
5	5.4134
6	5.5556
7	5.7015
8	5.8600
9	6.0290

Hence, the same mass of air must be transported per unit time past each vertical. Since the density varies with z, the total mass transported past each vertical is

$$\Sigma(\Delta p_i)\, u_i = \Sigma(\Delta p_i')\, u_i'$$

where the Δp_i are the pressure increments along the windward vertical across which the average horizontal velocity of inflow is u, and the $\Delta p_i'$ are those for the leeward vertical, with u′ the average horizontal velocity of outflow.

For the vertical five kilometers to the left of the edge of Figure 1 (x = -5 km) the velocity of inflow in the undisturbed current is assumed uniform with height and equal to ten meters per second; we take the Δp_i from the Standard Atmosphere pressure-height relationship and compute the mass transport across this vertical. For the next vertical to the right (x = 5 km) we compute the average u′ and plot it at the height where the average density along this vertical occurs, and so on for the other verticals. These values of u′ are kept approximately the same through the rest of the computation but above and below the point of average density in each vertical they are raised or lowered as the residuals are reduced, always keeping the summations of the products constant.

Internal consistency of solution--Assumption (b) requires that $\partial u/\partial z = \partial w/\partial x$. Using increments taken from a square net of points of Figure 1 (where Δz = 1 km, Δx = 10 km) the sum of the velocity potential difference along the bottom side of any square of points and the velocity potential difference along the right side must equal the sum of the velocity potential difference on the left side and the velocity potential difference along the top side, or (see Fig. 4) $0.1w + (u + \Delta u) = u + (0.1w + 0.1\Delta w)$. This is used to improve the horizontal velocities as we improve the vertical velocities in the reduction of the residuals.

Results--After reducing the residuals to less than 0.2, we get the solution given in Figure 1. Reduction of the residuals below these magnitudes would require changes in the α's and β's in the fifth or sixth decimal place. This means that further reduction of the residuals would change the vertical velocities at most by less than 0.1 cm sec^{-1}. The vertical velocities are shown in Table 1, column R. Those which result from BJERKNES'[1940] assumption are in column B. Since the horizontal velocity is ten meters per second when $\Delta_H\phi$ is 10

$$\Delta_H\phi/\Delta x = 10 \text{ mps}/10 \text{ km}$$

the numbers in the horizontal (see Fig. 1) multiplied by 100 and those in the vertical multiplied by 1000 give the velocities in centimeters per second.

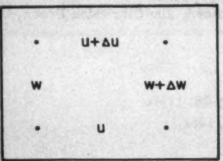

Fig. 4--Set used in adjusting horizontal velocities for changes in vertical velocities

Summary

The foregoing work gives an approximate solution of the differential equation given by Pockels but with two of his restrictive assumptions removed. The essential difference between Pockels' solution and the numerical one given here is that he made additional assumptions which enabled him to secure an analytic solution but which altered the character of the result, while the numerical solution avoids these assumptions. The example given uses a simple profile but the procedure can be used for any profile that can be expressed by a Fourier series. The solution is effected by the method of relaxations. It is for a particular case where the mountain profile is given by the equation

$$f(x) = 1.5\ [1 - \cos(2\pi x/L)]$$

together with the arbitrary restriction that above the ten-kilometer level the vertical velocity is everywhere zero and with boundary conditions as previously described. In Figure 1 the solution is given for the region windward from the crest of the mountain. But the velocity potential field is symmetrical with respect to the vertical through the crest so the vertical velocities to the lee of the crest are given by prefixing a minus sign to those given in Figure 1 and then plotting them at an equal distance to leeward of the crest.

This method can, of course, be applied to cases where the mountain profile is different from that in the example. Also the height above which it is assumed that there is no vertical velocity can be different. If it is higher than in the example, with the same undisturbed-flow velocity, the rate of decrease of vertical velocity with height will be smaller.

Concluding remarks

It is to be emphasized that the numerical solution given here is for the highly artificial case specified by the seven assumptions which Pockels used. It is a classical hydrodynamics solution for a case of irrotational flow. Some of the things not included in the seven basic assumptions and which would, in nature, influence the vertical velocity are: centrifugal force on the particle due to its curved trajectory; coriolis forces; convective forces; moisture content of the air; density variations in the horizontal; variation of the mountain profile in the y direction; surface friction; and eddies in the flow.

It would be desirable to have measurements of the velocity components in air streams flowing over mountains for use both as checks on existing theories and speculations and to provide a basis for further theoretical work. Very few such measurements have been attempted. Until they are available, estimates of orographic effects on air-stream flow will probably be based on such mathematical exercises with simplified models as the one presented here. An illustration of the errors introduced by different models is given by the divergent results obtained by Pockels' solution and the more detailed work of this paper.

Acknowledgments--L. P. Harrison and J. L. Paulhus reviewed the text and made several valuable suggestions.

References

BJERKNES, J., A method of approximate computation of orographic precipitation, (processed), 1940.
POCKELS, F., The theory of the formation of precipitation on mountain slopes, (Translation from Ann. d. Physik, ser. 4, v. 4(3), pp. 459-480, 1901) Mon. Wea. Rev., v. 29, pp. 152-159, 1901.
QUENEY, P., Theory of perturbations in stratified currents with applications to air flow over mountain barriers, Dept. Met., Univ. Chicago Misc. Rep. No. 23, 1947.
SHORTLY, G. H., and R. WELLER, Numerical solution of Laplace's equation, J. Appl. Phys., v. 9, pp. 334-348, 1938.
SMITHSONIAN PHYSICAL TABLES (8th rev. ed., 1st reprint), p. 559, 1934.
SOUTHWELL, R. V., Relaxation methods in theoretical physics, Oxford, The Clarendon Press, 1946.

U. S. Weather Bureau,
Washington 25, D. C.

(Communicated manuscript received February 28, 1950;
open for formal discussion until March 1, 1951.)

Transactions, American Geophysical Union Volume 31, Number 5 October 1950

PRELIMINARY INVESTIGATION OF CONDENSATION NUCLEI UNDER THE ELECTRON MICROSCOPE

C. L. Hosler

Abstract--Condensation nuclei have been examined and photographed in the electron microscope. The apparatus used and the technique employed to prepare specimens are described. Preliminary electron-photomicrographic investigations into the nature of condensation nuclei have demonstrated several important facts. Measurements of nuclei which were photographed and calculations of the mass of the nuclei, give figures in good agreement with those obtained by other authors by indirect means. However, the nuclei counts made using the electron microscope indicate that those taken with an Aitken counter do not even closely approximate the total number of nuclei. The majority of nuclei seem to be of such small size that the droplets formed on them are not visible in the Aitken counter. Using the electron microscope the nuclei can be examined for their structure and form. This enables study of different types of nuclei and the properties which determine the degree of supersaturation required for condensation on them.

Only since the advent of the electron microscope has the direct observation of condensation nuclei been possible. As a consequence, investigators in the past were forced to answer some of the questions regarding the nature of nuclei by deductive reasoning. Nuclei were counted by observing those visible droplets formed upon them. Numerous methods of measuring mass and size were devised, all of which required some basic initial assumptions, such as a definite relationship between the degree of supersaturation in a cloud chamber and the size of the nuclei around which droplets condense. Many investigations of this type have been undertaken. (LANDSBERG [1938] gives a list of 227 references.) Through these efforts, and many more recent ones, we are in possession of a great deal of material regarding the nature of condensation nuclei, without ever having seen them. As will be pointed out later, the mass and size of nuclei as found by previous investigators agrees well with the present measurements made by means of electron-photomicrography.

Examination of nuclei under the optical microscope is confined to the extremely large ones; and these are present in very small numbers, as shown by the measurements made over the sea by WOODCOCK and GIFFORD [1949]. The presence of smaller nuclei has been detected in the ultramicroscope, but no measurements of shape or size can be made. The limitations imposed on microscopy by the wave length of light have been overcome to a degree by the use of the electron microscope. This relatively new research tool extends our world of vision down to particles which are as small as 10^{-7} cm in diameter, theoretically the size of the smallest nuclei still active in natural condensation [LANDSBERG, 1938].

First use of the electron microscope to view condensation nuclei was made by LINKE [1943]. So far as is known, only one set of photographs was published before Linke's tragic death. These photographs proved that nuclei could be seen; however, no positive identification of the nuclei was made.

Linke collected nuclei by placing a film of some sort in the bottom of an Aitken counter and expanding the air a number of times permitting the fog droplets which formed to fall on the film. After evaporation of the droplets, only the nuclei remained on the film, which could then be examined. This same principle for collection was used by the author in a systematic study employing special techniques.

Ordinarily, samples to be examined in the electron microscope are mounted on a very fine (200 mesh) steel screen which is one-eighth inch in diameter. In order to suspend a sample over the screen's interstices, a thin transparent film is placed on the screen. This film is made by placing a drop of a solution containing collodion (other films are also used) on a surface of distilled water where it spreads out and hardens. Usually this film is placed on the screen wet side up and the water evaporates leaving a dry film. These films, however, were not satisfactory for catching nuclei because even distilled water leaves deposits of dissolved material which obscure any nuclei which might subsequently be deposited on the film. It was found that when the wet side of the film was placed in contact with the screen, the water flowed off to the screen and left the film clean and transparent.

The use of spider webs for suspension of nuclei in the electron beam also proved successful. This technique was used by DESSENS [1946] for observing the behavior of fog and haze particles under the optical microscope. Because of the small dimensions of the collecting surface of spider webs, they were found unsuitable for examination of large numbers of nuclei deposited by sedimentation, although they are very satisfactory when placed in an air stream carrying fog particles, because of the greater probability of deposition. Webs as fine as 10^{-6} cm have been obtained DESSENS [1949].

The field of the electron microscope is confined to an area of about 4×10^{-6} cm^2 under ordinary conditions. The most convenient area for counting nuclei is the area that makes up one open space in the screen which occupies about 64×10^{-6} cm^2. Nuclei examined in the microscope are placed in a vacuum and under continued exposure to the electron beam may reach a temperature of 100° C.

An apparatus was designed to hold 18 of the small screens used for collecting the nuclei; a wide range of expansion ratios could be employed for the deposition of various parts of the nuclei spectrum. Figure 1 shows the expansion apparatus and cloud chamber. The screens upon which the nuclei are deposited are placed inside the chamber A, on a platform which is supported by, and pivots on, the center of the chamber floor. The top of this platform contains six groups of three holes each into which the screens fit. A cover plate fits over the platform and rests on a ledge in the chamber leaving a clearance of less than one-half millimeter between cover and platform. An opening in the cover is large enough to expose one set of three screens at any one time. The platform can be revolved from the outside by means of a magnet placed on the turntable B, beneath the chamber. The effective air layer above the screens is one centimeter thick and the volume of the chamber is 38 cu cm. The air can be circulated through the chamber by manipulation of a stopcock. A source of moisture is provided by lining the chamber with wet blotting paper.

The remainder of the apparatus pictured in Figure 1 serves the following purposes: evacuation of the chamber to any desired degree by means of various buffer chambers C; filtering of air through glass wool and bubbling through a column of water D; admission of nuclei to the air in the system from a special container E. The vacuum gages F, show the vacuum in the line and in the chamber respectively.

At low expansion ratios or low nuclei concentrations, it is expedient to refill the chamber one or more times and produce one or more expansions over a given set of screens. This makes the nuclei on the screen more numerous and thus easier to find. Several sets of screens can be exposed at the same expansion ratio, or as many as six sets of screens can be exposed at different expansion ratios.

Figures 2 and 3 are representative photographs of nuclei which were formed by the atomization of a solution of sodium chloride into the nuclei container. After a minute or two the cloud chamber was filled with air from the container, and a series of screens was exposed. Figure 2 shows a nuclei deposit as a result of three expansions at an expansion ratio of 1.05. Only the larger nuclei are deposited at the small resulting supersaturation and the number observed represents a concentration of between 5000 and 10,000 per cu cm. If the concentration of nuclei on all parts of the screen had been as great as shown in the photograph, a much higher count would result; however, some parts of the screen were devoid of nuclei and the count was obtained by averaging the number deposited over a great number of similar areas on several different screens which were exposed simultaneously. The cubic form of the nuclei is easily recognized. Where doubt exists as to the structure of such particles, the screens can be shadowed by vaporizing a metal onto the film from an angle so that deposits will

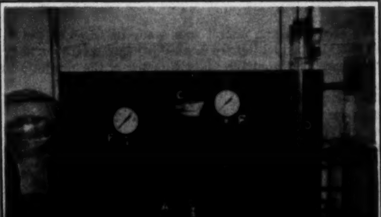

Fig. 1--Cloud chamber and expansion apparatus

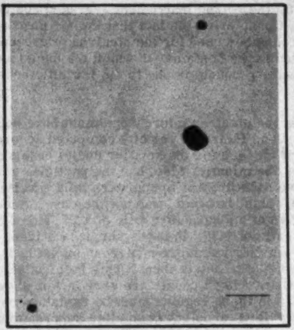

Fig. 2--Sodium chloride nuclei deposited at an expansion ratio of 1.05 (line represents one micron)

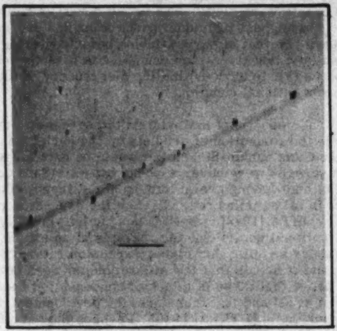

Fig. 3--Sodium chloride nuclei deposited at an expansion ratio of 1.15 (line represents one micron)

Table 1--Size, weight, and number of sodium chloride nuclei obtained at expansion ratio 1.15

Range of diameter ($\times 10^6$)	Weight per nucleus ($\times 10^{16}$)	Number ($\times 10^{-6}$)	Per cent of total number
cm	gm		
1.0 - 1.9	0.06	17	24
2.0 - 2.9	0.30	15	21
3.0 - 3.9	0.9	13	18
4.0 - 4.9	1.9	9	13
5.0 - 5.9	3.5	8	11
6.0 - 6.9	5.8	3	4
7.0 - 7.9	8.9	4	6
8.0 - 8.9	13.0	1	1
9.0 - 9.9	18.0	1	1
10 - 19	65.0	0.5	<1
20 - 29	320	0.01	<1
30 - 39	590	0.005	<1

cast shadows. This was not necessary with the sodium chloride since the shape was easily seen. The straight line in each photograph represents a length of one micron.

Figure 3 is a photograph of a section of a screen which was exposed three times at an expansion ratio of 1.15. The film moved during exposure and thus destroyed the cubic appearance of the nuclei in the photograph; however, the counting and measuring of the nuclei was thereby facilitated. The size range of the nuclei obtained at this expansion ratio extends to below the resolving power of the electron microscope used and it is probable that many nuclei did not show in the picture. The smallest streaks represent particles about 1×10^{-6} cm in diameter. The average nuclei count on this particular set of screen was $72 \times 10^6/\mathrm{cm}^3$. (An expansion ratio of 1.10 for this same group of nuclei gave a count of $6 \times 10^6/\mathrm{cm}^3$.) This count is broken down into size groups in Table 1. It can be readily seen that the number of nuclei increased as the size decreased and that the greatest percentage of the total was in the smallest size range. More than half of the total number of nuclei were smaller than 4×10^{-6} cm in diameter. Calculations of the mass of these nuclei assuming cubic form and a density of 2.16 yield the figures in the second column of Table 1. These are in agreement with those found by other investigators [LANDSBERG, 1938].

The very large nuclei count confirmed the suspicion that the conventional counts made by the Aitken apparatus fall far short of the actual number of nuclei present. In order to compare the two methods of counting nuclei, the Aitken counter was inserted in the nuclei container and operated from the outside. The same procedure was followed for producing nuclei as before, and numerous counts were made. The nuclei counts obtained with the Aitken instrument averaged 208,000/cm^3, the highest individual count being 255,000/cm^3. Considering the fact that the air must pass through two feet of narrow tubing before entering the chamber used for the electron microscope count, and that the Aitken counter was directly inserted in the container in which the nuclei were produced, it is obvious that the discrepancy in the resulting counts is due to the low efficiency of the conventional counter.

The deposits of material on the screens viewed in the electron microscope must have been due to the formation of droplets on the nuclei, inasmuch as their fall velocity computed according to the Cunningham-Stokes law would be only 1.6×10^{-5} cm/sec for the smaller nuclei observed. The screens were never exposed for a time exceeding one minute. Also, had the particles settled out without having grown into droplets, they would have been present in approximately equal numbers in all samples regardless of the expansion ratio. This, however, was not the case. According to OHTA [1949] most "Aitken nuclei" become active at an expansion ratio of 1.05, although the conventional nuclei counter operates at an expansion ratio of 1.20. In any event, it is evident from the above results, that higher expansion ratios cause smaller and more numerous nuclei to fall out; and it seems that the Aitken counter does not enable us to detect them. This fact has lead to the belief that there is a lack of condensation nuclei where Aitken counts are very low or show no nuclei at all and that therefore, the development of rain in these regions must be explained on another basis [BYERS, 1949]. Perhaps the nuclei which form droplets at smaller supersaturations than are produced in the Aitken counter but which are not counted in it, are the ones that are active in condensation processes in those regions where there is a lack of larger nuclei. Also, it may be that the critical height that must be reached by a cloud in order for precipitation to fall from it, is closely related to the size and number of these nuclei present and that the presence of the freezing level at this height may be merely a coincidence, since precipitation has been observed falling from clouds whose tops were below the freezing level.

The above studies are being continued, including other nucleogenic substances, in order to establish the prototypes of nuclei for the identification of unknown samples. Moreover, the problem of the type and size of nuclei that actually participate in natural condensation processes, will be attacked. The Aitken counter will be subjected to critical study in order to establish whether it actually counts all of those nuclei which take part in atmospheric condensation.

Acknowledgments--The author is indebted to Ethel Senkovits, electron microscopist, for aid in this investigation, and to H. Neuberger and T. F. Bates for their many helpful suggestions.

References

BYERS, H. R., Condensation nuclei and precipitation, J. Met., v. 6, p. 363, 1949.
DESSENS, H., La brume et le brouillard étudiés à l'aide des fils d'arignées, Annales de Geophysique, v. 2, pp. 276-278, 1946.
DESSENS, H., The use of spiders' threads in the study of condensation nuclei, Q. J. R. Met. Soc., v. 25, pp. 23-36, 1949.
LANDSBERG, H., Atmospheric condensation nuclei, Ergebnisse der Kosmischen Physik, v. 3, pp. 155-252, 1938.
LINKE, F., Kondensationskerne in Elektronmikroskop sichtbar gemacht, Die Naturwissenschaften, v. 31, pp. 230-231, 1943.
OHTA, S., Investigations of condensation nuclei, Bull. Amer. Met. Soc., v. 30, pp. 295-296, 1949.
WOODCOCK, A. H., and M. M. GIFFORD, Sampling atmospheric sea-salt nuclei over the ocean, J. Marine Res., v. 8, pp. 177-197, 1949.

Division of Meteorology,
The Pennsylvania State College,
State College, Pennsylvania

(Manuscript received April 24, 1950; presented at the Thirty-First Annual Meeting Washington, D. C., May 1, 1950; open for formal discussion until March 1, 1951.)

Transactions, American Geophysical Union Volume 31, Number 5 October 1950

THE THERMOPILE WAVE METER

J. D. Isaacs and R. L. Wiegel

Abstract--The thermopile or Mark V wave meter is designed to be a low cost, simple yet durable instrument which can be considered expendable upon its installation in the ocean. Its electrical characteristics are such that the cable requirements are not rigorous. Its construction is simple. A synthetic rubber bellows is mounted on a plastic base which is in turn mounted on a brass cable connection. A thermopile is mounted inside the bellows with one group of junctions in contact with the air chamber of the bellows, and the reference junctions, insulated from the air chamber, in thermal contact with the surrounding sea water. Thus when a wave passes over the unit, the crest and trough produce a compression and expansion of the bellows with the corresponding temperature change in the gas due to the polytropic cycle. The temperature difference between the air chamber and the sea water causes an emf from the thermopile, which is transmitted to shore by means of a two-conductor submarine cable, and recorded on a commercial null recorder.

Introduction

The problem of the measurement of ocean surface waves has manifold aspects. Statistical historical data are imperative in the proper design of engineering structures, the planning and construction of channels, the design of amphibious vehicles, and the planning of amphibious military operations. Records of ocean waves are a necessary complement to the full development of wave forecasting, permitting perfection of techniques and determination of significant wave generating areas not covered by existing meteorological data [FOLSOM, 1949].

Direct measurement of wave height is possible only in certain cases where a pier exists or photographic methods are feasible. In the general case, however, the indirect method of measuring subsurface pressure fluctuations is utilized [FOLSOM, 1947]. Of the shore recording instruments used, expensive and complex underwater heads have been employed in addition to specially designed recording apparatus and multi-conductor armored submarine cables of large sizes.

The principle intent of the development of the thermopile (Mark V, see Fig. 1) wave meter was to obtain a statistically correct record of waves with an instrument having an inexpensive, practically expendable, underwater head, with no rigorous cable requirements, readily installed, and utilizing a standard recorder. In order to avoid many of the complexities of existing wave recorders, it was decided to develop an instrument to record subsurface pressures which would be capable of utilizing the polytropic gas law. In consideration of heat capacity, response time, and sensitivity, a thermopile was selected. The general requirements were a thermopile which would: (1) produce an electrical signal capable of being transmitted through at least a half-mile of cable and of sufficient intensity to be picked up by some standard electrical recording instrument on the shore; (2) use the temperature variation caused by the pressure fluctuation in a gas-filled bellows of insulating material sufficient to prevent rapid heat flow; (3) have a good reference junction; (4) be light and yet capable of withstanding the rather rough treatment of being placed on the ocean floor for long periods of time; (5) be waterproof; and (6) be capable of indicating pressure fluctuations of periods of at least eight to 20 sec without great variation of response for the interval.

Design limits

In order to ascertain the approximate range in which the thermopile unit would operate, the assumption was made that the process would be polytropic and hence

$$T_1/T_o = (p_1/p_o)^{(n-1)/n}$$

$$\Delta T/T_o = (1 + \Delta p/p_o)^{(n-1)/n} - 1$$

where T_o is the water temperature, p_o the absolute pressure on the instrument (atmospheric plus depth of water), Δp is the pressure fluctuation at this depth due to a passing wave, ΔT is the

(a) The Mark V, disassembled

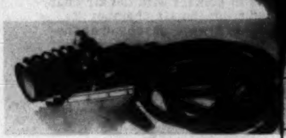

(b) The Mark V, assembled

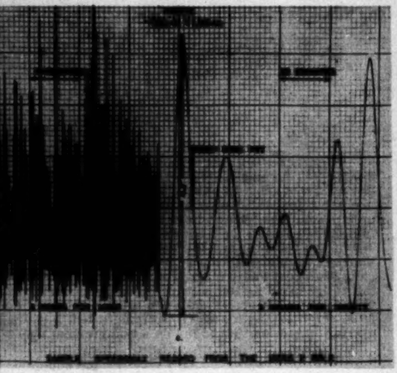

Fig. 1--Views of the Mark V recorder and a sample record

corresponding temperature change in the bellows, n is the polytropic exponent.

It was desired to install the instrument in about 50 ft of water with air as the gas in the bellows. Then, considering the bottom pressure fluctuation produced by the highest probable waves to be about 20 ft and the water temperature at the location to be 59° F (518.4° F absolute)

$$\Delta T/T_o = [(1 + 20/(50 + 33))]^{(1.4 - 1)/1.4} - 1 = (1.241)^{0.286} - 1 = 0.0659$$

$$\Delta T = 34.2° \text{ F}$$

This established the maximum limit.

To determine the minimum limit (it was assumed desirable to record a 0.1 ft difference of wave height in 50 ft of water) use had to be made of two wave theory relationships. Considering the unit to be placed on the bottom of the ocean, the pressure fluctuation at the bottom would be given by [FOLSOM, 1947]

$$\Delta p = \Delta p_o/\cosh (2\pi D/L)$$

where Δp is the fluctuation on the bottom, D is the depth of water, L is the wave length, and Δp_o is the wave height (in feet). L is a known function of the wave period (T) and depth.

$$L = gT^2 (\tanh 2\pi D/L)/2\pi$$

Thus, for a constant Δp_o and D, Δp will vary with the period of the wave. The periods of significant waves along the Pacific Coast normally vary between eight and 20 sec and so for the minimum limit (eight-second wave)

$$\Delta p = 0.1/1.762 = 0.0563$$

and

$$\Delta T = 518.4 (1 + 0.0563/83.1)^{0.286} - 1$$

$$\Delta T = 0.10° \text{ F}$$

Thus, an instrument with a least reading of 0.10° F with a total range of 34.2° F was required.

A thermopile made of silver-constantine has a constant of 0.02 mv/junction/° F. A Speedomax was available with a -1.25 to +1.25 mv range with a least reading of 0.01 mv. Hence the number of junctions needed would be

$$N = E_{min}/0.02\ \Delta T_{min} = 0.0125/0.02 \times 0.10 = 6.25 \cong 6$$

Using six junctions, the maximum would be

$$E_{max} = 0.02\ \Delta T_{max} \times 6 = 0.12\ \Delta T_{max} = 0.12 \times 34.2 = 4.1 \text{ mv}$$

while the total range of this Speedomax is only 2.5 mv. Hence either another range would have been needed or a half-way tap be taken off of the thermopile. However, it was found experimentally that because of heat loss through the walls, lag of the thermopile, and departure of air from a perfect gas, the actual measurements were only one-fifth to one-third of the ideal (see Fig. 2), and hence a thermopile with 32 junctions was built, and a voltage divider constructed for the upper ranges.

Long period tidal changes will not enter in the record as these temperature changes are dissipated through the walls.

Instrument

Preliminary work indicated that a 32-junction silver-constantine thermopile would give ample signal to operate a standard Speedomax recorder. It was thought that insulation requirements would be served by a rubber bellows attached to a plastic base mounting the thermopile. As the temperature of the ocean is relatively constant (in fact, the yearly variation, even at shallow depths, is only 10° C along the Pacific Coast), it was decided to use sea water temperatures as the reference junction. This was done by attaching the reference junctions to a copper block, insulated from the bellows chamber in which the measuring junctions operate, but in thermal contant with the surrounding water.

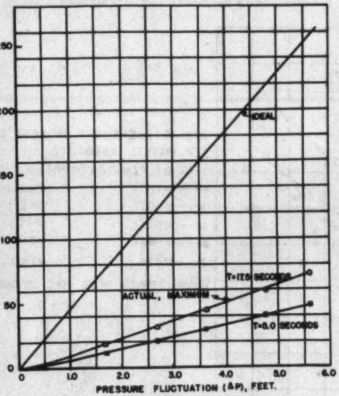

Fig. 2--Relationship between recorder readings and pressure fluctuations; comparison of ideal with actual case (water depth of 81.1 ft of sea water, absolute); a 32-junction silver-constantine thermopile was used

The instrument was constructed with low conductance material in contact with the gas wherever possible; the bellows was of synthetic rubber mounted on a plexiglass base. This involved a difficulty in obtaining thermal contact of the reference junctions of the thermopile with the surrounding water. Such a contact was secured by wrapping the junctions a about bakelite frame with the measuring junctions above, exposed to the air in the bellows, and the reference junctions underneath the frame. The bottom of the frame was then attached to the copper block (in thermal contact with the water) by means of a commercial electrical varnish. This assembly, except the measuring junctions, was thermally insulated from the air in the bellows by casting in paraffin or filling with commercial silicone grease.

The instrument was waterproofed by employing fused glass connectors for the cable leads. All assembly joints were given an application of vaseline or silicone grease to help prevent leaking. More important in preventing leakage was the absence of differential pressure across any part of the instrument.

Calibration

The thermopile recorder was dynamically calibrated in the following manner: The instrument was immersed horizontally in a water-

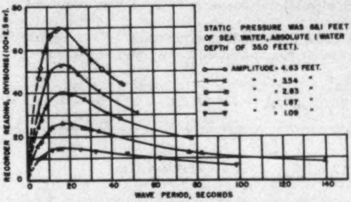

Fig. 3--Relationship between recorder readings and wave periods

filled pressure vessel with the leads connected to a Speedomax (Leeds and Northrup millivolt recorder). The standard pressure was recorded on a modified Esterline-Angus recorder in conjunction with the Mark IV pressure head, a mechanical pressure recorder [FOLSOM, 1949]. The static head was developed by pumping air into the pressure head and a fluctuating pressure was imposed by means of a power-driven series of sylphon bellows.

The instrument was calibrated with static heads from ten to 86 ft of water (absolute). At each of the static heads a series of fluctuating heads was used, and at each of these, the range of periods was covered from five to over 80 sec. From these data, curves of period versus recorder readings were plotted for each static depth, using the fluctuating head as a parameter (see Fig. 3). From these, new graphs were made showing curves of equal period for recorder readings versus actual pressure fluctuations (Fig. 3). Ideally this should be a single straight line in the region covered; the data, however, show a series of lines, one for each static head. In addition, a graph was constructed of recorder reading versus Δp/p for a constant period (see Fig. 4).

Summary of field installations

Point Cabrillo, California--On May 8, 1948, the first Mark V instrument was taken to Point Cabrillo and installed 46 ft below MLLW. A rubber-covered cable was used to test the feasibility of light installation. Excellent recordings were obtained for a few days. The cable parted about a week after installation. Evidently it was too light for this rugged location. The instrument was recovered on June 3, 1948 and was in perfect condition. Obviously, failure of the cable would have no effect on the adequacy of the test of the transmitting unit.

Point Arguello, California--Installation was made on July 25, 1948. Two leads of a ten-conductor armored submarine cable were used for the unit; the remaining leads operated a Mark III

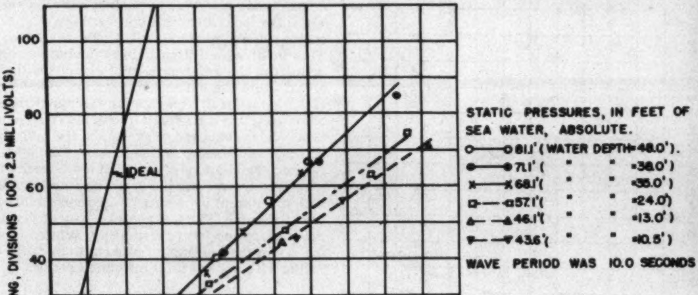

Fig. 4--Relationship between recorder reading and pressure change wave recorder and a Mark II direction recorder (using 110 v AC). The Mark V operated successfully for at least three months. It finally failed after a fire had burned through the insulation of an onshore section of the cable. It is believed that the elements were damaged by the 100 v of the direction recorder shorting across the Mark V leads.

Quillayute, Washington-- Installation was made on October 27, 1948. A bight of cable was inadvertently dropped in the surf during installation. A storm developed on November 3, 1948 with breakers as high as 25 ft. This storm occurred before the cable had become sanded down and a large log in the surf became tangled with the bight tearing out the cable when the log was thrown about by the breakers.

Camp Pendleton, Oceanside, California--Installation was made on March 7, 1949. A light two-conductor demolition cable was used. The instrument failed on March 22, 1949 as a result of a cable break in the surf. When the instrument was recovered it was found that one of the wires of the thermopile had corroded. All subsequent instruments have incorporated a bag of silica gel to absorb any moisture inside the air chamber.

Camp Pendleton, Oceanside, California--Installation was made on May 4, 1949. An armored submarine cable was used through the surf with a demolition cable spliced to it seaward and running to the site of pressure head installation. On September 19, 1949 the cable broke at a splice. The instrument and the demolition cable were recovered. The instrument was found to be in good condition.

Camp Pendleton, Oceanside, California--Installation was made on September 21, 1949. An armored cable was used through the surf zone with two conductor demolition cable spliced to the end. All splices were doubled over twice and bound in such a manner so as to take all tension off the splices. It was still operating satisfactorily on August 1, 1950.

Miscellaneous installations--A portable mount was made at Camp Pendleton, Oceanside, California to be used for speedy installations at temporary sites [PATRICK and WIEGEL, 1950]. This has operated successfully on four different occasions. On three of the installations it was installed for only a one-day period. On the major installation (Operation MIKI, Pokai Bay, Oahu, T. H.) it operated continuously from October 20 through October 27, 1949.

La Jolla, California--A thermopile unit was manufactured by the Scripps Institution of Oceanography and used intermittently for wave measurement. Its performance has been excellent.

Discussion and conclusions

If there were no heat loss and no thermopile lag, the curve of recorder displacement versus period should be a horizontal line, that is, for any particular depth a certain fluctuation at the bottom should produce the same reading for all periods. However, heat loss through the walls exists and there is a definite lag in the thermopile. It can be seen that the effect of lag predominates to about 14 sec. The region of 14 to 21 sec is one of almost equal effect (with the maximum reading between 16 and 17 sec). The effect of heat loss predominates for all periods greater than 21 sec for the instrument tested. The curve (to 14 sec) is the same type as that calculated from the equation of BAILEY [1931] for the measurement of periodic temperatures. The heat loss curve is quite typical.

The instrument is light and relatively inexpensive in itself. In addition, as no electrical current flows with the null recorder, a very light cable will satisfy the electrical requirements, and the main consideration is its mechanical strength.

The instrument is as accurate as the Mark III wave recorder, a slide-wire transmitter, and is readily calibrated [FOLSOM, 1949]. It has no moving parts, except the bellows, and is practically free of mechanical difficulties and breakdowns.

The principal cost of the installation is the recorder; however, this is ashore and thus relatively safe. The relative inexpensiveness of the thermopile pressure unit makes it unnecessary to recover it as the recovery operation would usually cost more than a new instrument. The nonlinearity of response of the Mark V is advantageous in many ways. It is sensitive to small waves, yet has a large range. The variation of response to period is, of course, not unique among the records of measuring instruments, for the subsurface pressure variation itself is always a function of period. This additional influence of period is merely incorporated in the analysis overlays and has no further effect.

Acknowledgments

This instrument was developed as part of an extensive investigation of surface ocean waves conducted for the Office of Naval Research and the Bureau of Ships, United States Navy by the University of California, Department of Engineering. The portable wave recorder was developed and used in an investigation of the amphibious factors influencing landing craft operation performed by the University of California, Department of Engineering, and the United States Marine Corps for the Office of Naval Research. The design and manufacturing of the special thermopile was performed by J. T, Gier, Lecturer in Electrical Engineering, and R. V. Dunkel, Assistant Professor of Mechanical Engineering, Department of Engineering, University of California.

References

BAILEY, N. P., Response of thermocouples, Mech. Eng., pp. 797-804, November, 1931.
FOLSOM, R. G., Subsurface pressures due to oscillatory waves, Trans. Amer. Geophys. Union, v. 28, pp. 375-381, 1947.
FOLSOM, R. G., Measurement of ocean waves, Trans. Amer. Geophys. Union, v. 30, pp. 691-699, 1949.
PATRICK, D. A., and R. L. WIEGEL, Portable Mark V wave recorder, Inst. Eng. Res., Dept. Eng. University of California, ser. 29, issue 17, January, 1950 (unpublished).

University of California,
Berkeley, California

(Manuscript received March 27, 1950; presented by title at the Thirty-First Annual Meeting, Washington, D. C., May 3, 1950; open for formal discussion until March 1, 1951.)

Transactions, American Geophysical Union Volume 31, Number 5 October 1950

SOUTHERN SWELL OBSERVED AT OCEANSIDE, CALIFORNIA

R. L. Wiegel and H. L. Kimberley

__Abstract__--A wave recorder has been in operation at Camp Pendleton, Oceanside, California, since May 4, 1949. Owing to its fortunate location in relation to the Western Hemisphere's hydrography, it has recorded southerly swell almost continuously throughout the summer, the origins of which appear to lie in the area between 40° and 65° S and 120° and 160° W.

Swell from the south through southwest was found to run almost continuously from May through September, and to dominate the surf zone for that period. Twenty- to thirty-minute averages (taken three times daily) of the "significant" breaker heights ranged from two to six feet, with most breakers being between two and four feet. The "maximum" breakers occurring during the 20- to 30-min periods were usually between four and eight feet, with heights of 10 to 12 ft observed on occasions. The average wave period of the southern swell ranged from 12 to 18 sec, with short-time averages of predominant groups as great as 22 sec.

__Introduction__--One of the requirements for a study, being conducted by the University of California in cooperation with the U. S. Marine Corps and the Office of Naval Research, was the installation of a wave recorder at Camp Pendleton, Oceanside, California. This instrument, a thermopile wave meter [see Fig. 1, ISAACS and WIEGEL, 1950, p. 712], was placed approximately 4200 ft offshore in 43 ft of water (below MLLW).

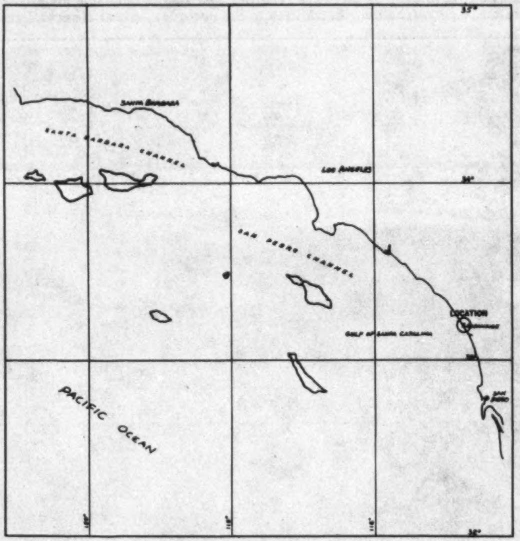

Fig. 1--Location of wave recorder (traced from U. S. C. and G. S. 5020, San Diego to San Francisco Bay)

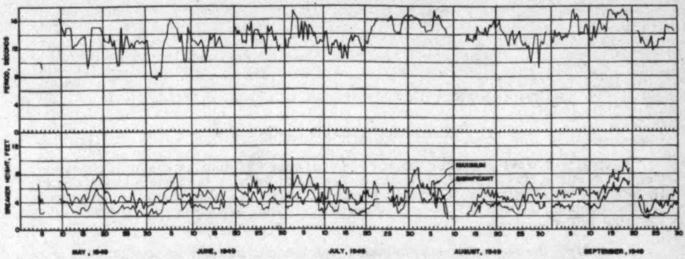

Fig. 2--Breaker records at Camp Del Mar, Oceanside, California, from May 1 through September, 1949; wave records were obtained by thermopile wave meter

Figure 1 shows the location of the recorder and the sector of the shore between San Clemente Island and Point Loma, through which the swell from the south enters the Gulf of Santa Catalina. Refraction studies had been made for the locality in which this instrument was placed and the refraction coefficients for the southern sector were found to be between 0.9 and 1.2 (that is, considering only the refraction effect, the swell would be from 90 to 120 per cent as high as if there had been no refraction) [PATRICK, 1949].

Thus, the swell registered by the wave recorder had almost the same amplitude as it would have had, were there no refraction. In addition to the recorder, visual observations were made

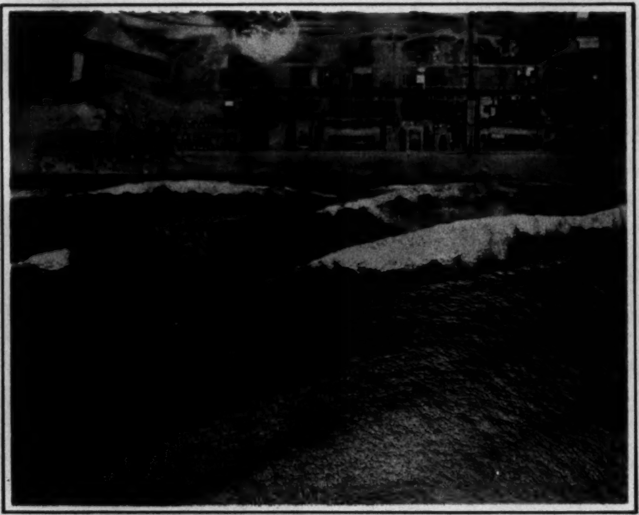

Fig. 3--Vertical aerial photograph of beach at Camp Pendleton, showing swell from southwest almost daily beginning March 28, 1949. These included the breaker heights, direction from which the swell approached the beach, type of breakers, angle of breaking, and magnitude and direction of the littoral current.

Wave recorder--A thermopile wave meter was used as the underwater pick-up unit [FOLSOM, 1949 and ISAACS and WIEGEL, 1950]. Its recorder was operated with a chart speed of six inches per hour except at regular intervals when it was operated at three inches per minute for 20 to 30 min.

The records were analyzed with the use of calibration charts obtained by the dynamic testing of the unit for the same static and dynamic pressures to which it was subjected in its installed location. The pressure readings were then corrected to surface wave heights by use of hydrodynamic theory [FOLSOM, 1947].

Results--The wave records were transformed into breaker heights by means of published curves [HYDROGRAPHIC OFFICE, 1944] as presented in Figure 2. Visual observations, taken almost every day, produced the fact that the swell came, almost continuously, from a south through southwest direction. Occasionally aerial photographs verified this observation (see Fig. 3). Of course, at times, there was secondary swell coming from the west through northwest, but it was usually a foot or less in height with periods of four and five seconds. There was, at times, swell of 8- to 10-sec periods from the west-northwest (the origin of which appears to have been near Pt. Arguello, California). This happened to be present on the few occasions when there was no noticeable swell from a southerly direction.

The "significant" breaker height (the average of the highest one-third of the breakers) has been used as it has been found to be the height noticed by the average observer as well as being more of an indication to danger to craft and structures than an overall average wave height which is somewhat lower in value [SVERDRUP and MUNK, 1947]. Figure 2 shows the "average" significant breaker height. These are the averages over the 20- to 30-min periods for which the charts were analyzed at approximately eight hours intervals. The significant breaker heights were between two and six feet, with most breakers being between two and four feet. Table 1 shows the percentage of time that the significant breakers were in certain height groups for each two-week period from May through September.

The "maximum" breakers as shown in Figure 2 are the highest occurring during the 20- to 30-min periods for which the charts were analyzed. These "maximum" breakers ranged from four to eight feet in height. However, there were some from 10 to 12 ft in height recorded at the peak of very large storm arrivals. It was found that the "maximum" breakers were from one and a quarter to two times as high as the significant breakers, with the average about 1.5.

The average wave periods (the average for the 20- to 30-min runs for which the records were analyzed) of the southern swell ranged from 12 to 18 sec. However, within these runs there were certain distinct groups of five or six waves in succession that had periods as great as 22 sec. The manner in which the periods fluctuated with time indicated that often there was swell from two or more storms present at the same time.

Table 1--Data on the time that the average of the significant breakers was in certain height groups during the summer of 1949

Date	Limits			
	0-2.0 ft	2.1-4.0 ft	4.1-6.0 ft	6.1-8.0 ft
	pct	pct	pct	pct
May 1-15	0	75	25	0
May 16-31	0	84	16	0
June 1-15	0	75	22	3
June 16-30	0	66	34	0
July 1-15	0	62	38	0
July 16-31	0	65	35	0
Aug. 1-15	16	56	25	3
Aug. 16-31	0	84	16	0
Sep. 1-15	0	73	25	2
Sep. 16-30	0	66	13	21

Daily measurements were made of the littoral current. It was found that the current ran almost continuously from south to north with velocities of from one-tenth to one knot with an average of approximately a quarter knot.

Meteorology--Data obtained by use of published decay curves [HYDROGRAPHIC OFFICE, 1944] indicated that the fetch areas for the southern swell would be located in the area of 5° S to 15°N and 120° to 140° W. This lies in the doldrums, the equatorial belt of calms or light winds. Upon using the storm tracking method of MUNK [1947] it was found that the observed swell probably would have been generated in an area 4500 to 7000 mi from Camp Pendleton. Using the observed directions, ranging from

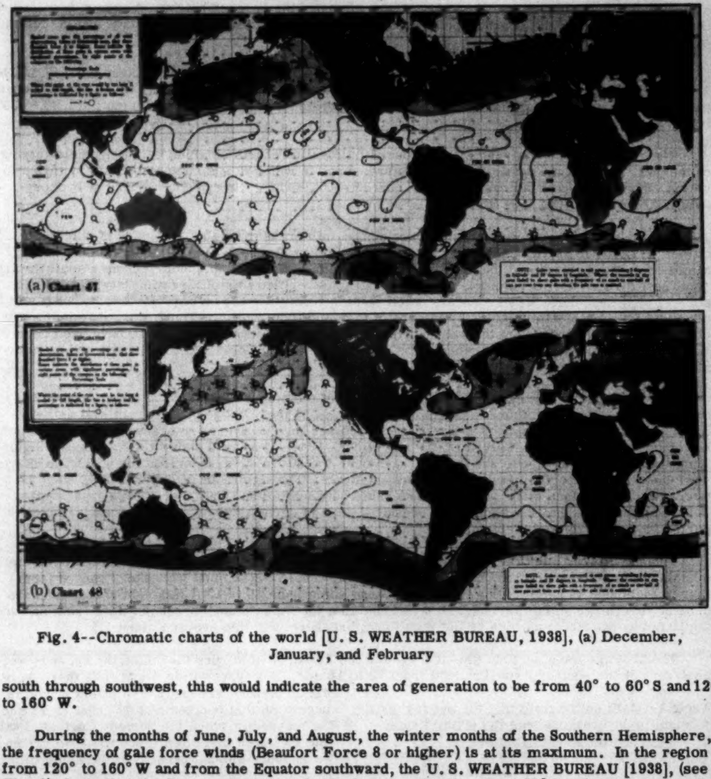

Fig. 4--Chromatic charts of the world [U. S. WEATHER BUREAU, 1938], (a) December, January, and February

south through southwest, this would indicate the area of generation to be from 40° to 60° S and 120° to 160° W.

During the months of June, July, and August, the winter months of the Southern Hemisphere, the frequency of gale force winds (Beaufort Force 8 or higher) is at its maximum. In the region from 120° to 160° W and from the Equator southward, the U. S. WEATHER BUREAU [1938], (see Fig. 4) shows that the five per cent line of gale force winds runs along 30° S. The ten per cent line approaches the 35° S and the 15 per cent line 40° S. Although observations south of 50° S are scarce, it is probable that the percentage of gale force winds between 50° and 60° S would be between 20 and 25 per cent. The prevailing directions for these gale force winds are shown as predominately from the southwest to south.

Discussions and conclusions--It has been found that throughout the months of May through September swell from the Southern Hemisphere dominates the surf at Oceanside, California, almost continuously. Visual observations indicate that this is true for most of that section of the California coastline extending from the Mexican border north to Long Beach, except at certain protected locations. This fact indicates that although statistical wave data obtained from a study of the Northern Hemisphere weather maps may be quite reliable for many locations, it is inadequate for others during certain seasons of the year.

It appears that the present decay curves do not hold when the wave distances are great. The storm tracking method, however, appears to give reasonable decay distances, considering the conceivable fetch areas that could produce this southern swell.

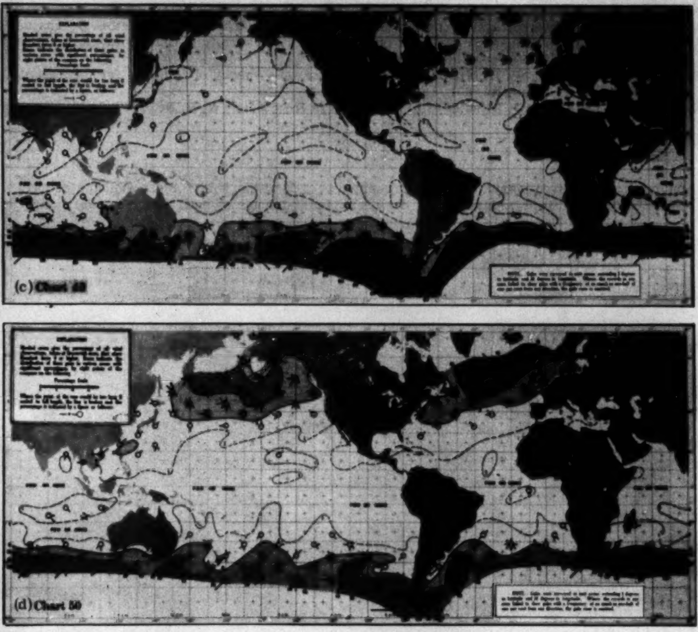

(b) March, April, and May; (c) June, July, and August; (d) September, October, and November

The littoral currents, and probably the sand transport, are from south to north in this area during the summer. This fact, together with the continuous nature of relatively high waves, should be of prime consideration for harbor development in this area.

The presence of the southern swell also points to one of the hazards of wave forecasting by use of weather maps; that is, owing to the lack of weather data in the Southern Hemisphere, swell may well appear which has not been forecasted. Hence, until weather maps of the Southern Hemisphere are available, local observations should be made of areas of interest to either military or civilian organizations.

References

FOLSOM, R. G., Sub-surface pressures due to oscillatory waves, Trans. Amer. Geophys. Union, v. 28, pp. 875-881, 1947.

FOLSOM, R. G., Measurement of ocean waves, Trans. Amer. Geophys. Union, v. 30, pp. 691-699, 1949.

HYDROGRAPHIC OFFICE, U. S. NAVY, Breakers and surf, principles in forecasting, H. O. Pub. No. 234, 1944.

ISAACS, J. D., and R. L. WIEGEL, The thermopile wave meter, Trans. Amer. Geophys. Union, v. 31, pp. 711-716, 1950.

MUNK, WALTER H., and MELVIN A. TRAYLOR. Refraction of ocean waves, J. Geol., v. 55, pp. 1-26, 1947.

MUNK, WALTER H., Tracking storms by forerunners of swell, J. Met., v. 4, pp. 45-57, 1947.
PATRICK, D. A., Wave refraction at Santa Margarita River Beach, Camp Pendleton, Oceanside, California, Report 155-4, Department of Engineering, University of California, Berkeley, California, July 1949 (unpublished).
SVERDRUP, H. U., and W. H. MUNK, Wind, sea, and swell: theory of relations for forecasting, U. S. Navy, H. O. Pub. No. 601, 1947.
U. S. WEATHER BUREAU, Atlas of climatic charts of the oceans, W. B. No. 1247, 1938.

University of California,
Berkeley, California

(Manuscript received March 13, 1950; presented by title at the Thirty-First Annual Meeing, Washington, D. C., May 3, 1950; open for formal discussion until March 1, 1951.)

Transactions, American Geophysical Union Volume 31, Number 5 October 1950

STABILITY AND MEANDERING OF THE GULF STREAM

B. Haurwitz and H. A. Panofsky

(Contribution from the Woods Hole Oceanographic Institution, No. 513)

Abstract--It is suggested that the meandering of the Gulf Stream can be produced by the instability of the velocity profile across the current. Various theoretical models are considered which resemble the Gulf Stream inasmuch as they have a sharp shear zone on the left side (facing downstream) where the current increases very rapidly to its maximum velocity and a much broader transition zone where the velocity decreases again. It is found that instability exists under certain conditions when the shear zone is not too close to the continental shelf. The type of observations required for a check of this hypothesis is discussed.

Introduction--Recent improvements in navigation and in oceanographic instrumentation have contributed greatly to our knowledge of the surface current distribution in the Gulf Stream. These new observations have confirmed a deduction first made by CHURCH [1937] from surface temperature data, namely that the position of the Gulf Stream is quite variable. In numerous later expeditions of the *Atlantis* equipped with the bathythermograph (BT) large changes were found in the position of the Gulf Stream in general and of the "shear zone" between the waters over the continental slope and the Gulf Stream in particular. By rapidly moving along the strongest current, the 1948 expedition produced evidence that east of Cape Hatteras the shear zone often forms a pattern which seems to have a wave-like appearance.

The term "meandering" has been given by ISELIN and FUGLISTER [1948] to this behavior of the Gulf Stream. No sign of meandering has been observed, at least until now, south of Cape Hatteras where the shear zone is adjacent to the continental slope, except for eddies formed by bays and tides. It is also pertinent to add here that UDA [1949] has noted a similar structure of the Kuroshio as well as similar changes of pattern.

While the existence of these meanders is well established, little is known about their formation, motion, and life history because of the absence of a network of oceanographic observations. Oceanographic surveys are, as a rule, carried out by a single ship for a large area so that, unlike those of meteorology, simultaneous observations at different places are generally not available. Under these conditions it is highly desirable to have some preliminary guiding ideas concerning the phenomenon to be investigated in order to arrange the program of observations in such a way that it is possible to prove or disprove these hypotheses. These remarks apply especially to the somewhat elusive meanders in the Gulf Stream. It is for this purpose that the following theoretical ideas about the Gulf Stream are presented here.

The idealized current profile--It is generally agreed among oceanographers that on the coastal side of the Gulf Stream the increase in velocity towards its maximum value is considerably stronger than the decrease on the other side of the current. The former zone will be referred to as the "shear zone," the latter as the "transition zone." Such a velocity distribution is indicated clearly by most of the salinity and temperature profiles taken across the current. Reference may be made for example to the cross sections published by ISELIN [1940], especially to the temperature section from Montauk Point toward Bermuda from October 5-9, 1939, which shows a very sharp temperature discontinuity about 180 mi from shore. Figure 1 shows the current profile which has been computed on the basis of this temperature section and of the corresponding salinity section for the Gulf Stream. Other temperature and density profiles show similar conditions, although the transitions are not so sharp, presumably because the oceanographic stations are not spaced as closely as for the cruise on which Figure 1 is based.

It is difficult to establish the exact width of the shear zone and the zone of transition, because for practical reasons the oceanographic stations during these cruises could not be spaced too closely. Moreover, in the shear zone the large speed of the water prevents the ship from crossing this zone at right angles. More closely spaced direct current measurements can be obtained with the geomagnetic electrokinetograph (GEK) of von Arx. Figure 2 summarizes some observations

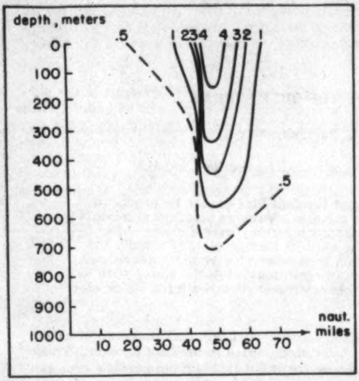

Fig. 1--Vertical cross-section through the Gulf Stream between Montauk Point and Bermuda, October 5-9, 1939, showing the geostrophic current in knots (no velocity observed at 1000 m)

obtained with this instrument. These records show the great variability of the Gulf Stream velocities and indicate that the profile in Figure 1 is apparently not found all the time, at least in the waters near the surface where all the observations of Figure 2 were taken. Nevertheless, in the later theoretical discussion attention will be paid mainly to the asymmetric profile suggested by Figure 1 because most observations indicate that it is the prevalent one, and sufficient data have not yet been accumulated to decide how frequently other profiles may occur.

The fact that the shear is strong at the left boundary and weak at the right boundary can be understood from a consideration of the dynamics of currents. The large shear is cyclonic, the weak shear anticyclonic. Just as in the atmosphere, a limit equal to the Coriolis parameter is placed on the magnitude of an anticyclonic shear, whereas there is no limit for a cyclonic shear. If an anticyclonic shear ever became greater than the Coriolis parameter, the current distribution would show inertia instability, with the result that the transition zone would soon become wider again. In particular, at latitude 43° an anticyclonic speed difference of two miles per second should not occur over a distance of less than 12.5 mi.

It is not possible to find the slope of the shear and transition zones with any great degree of accuracy from Figure 1 because the vertical scale is 185 times the horizontal scale. Nevertheless

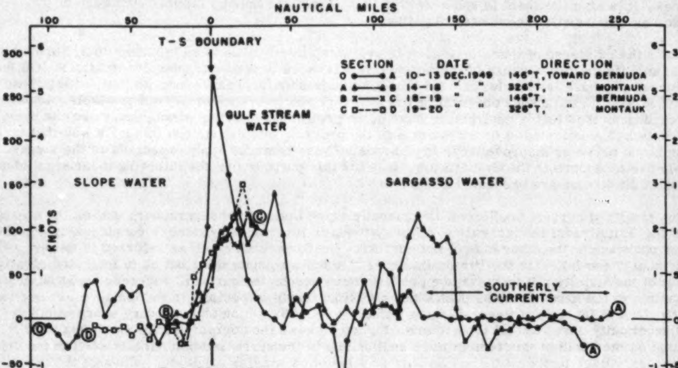

SURFACE VELOCITY SECTION, 355°T-175°T
FROM DATA COLLECTED ON ATLANTIS CRUISE 159 ALONG THE MONTAUK PT.-BERMUDA LINE.
T-S BOUNDARY DETERMINED BY S-T-D AT SURFACE.

Fig. 2--Surface current measurements obtained with the geomagnetic electrokinetograph (GEK) it appears that at least the shear zone is very steep, of the order 1/25 to 1/50, compared to other surfaces of discontinuity on the ocean. Margules' formula gives similarly high values, and the BT section also confirms in general the extreme steepness of the slope. Therefore it appears justified to make in the subsequent calculations the assumption that the boundaries between the different current zones are vertical.

Basic assumptions for the theoretical Gulf Stream models--As explained before it is the purpose of this investigation to develop an hypothesis for the origin of the Gulf Stream meanders whose consequences can be tested by field observations. With this aim in mind the hypothesis is put forth that the Gulf Stream system is stable for lateral oscillations when it flows close to the continental shelf, but becomes unstable when it leaves the shelf north of Cape Hatteras. If this hypothesis is correct, the meanders would begin as sinusoidal waves with exponentially increasing amplitudes. The theoretical basis of this hypothesis is tested by the study of several greatly simplified models of the Gulf Stream. All these models have a number of common characteristics. Since the shear zone is steep compared to other oceanic surfaces, and since the wave motions are essentially horizontal, simple models can be expected to have realistic properties if the shear zone is assumed to be vertical and parallel to the continental shelves at both shores of the ocean.

This means that the stabilizing effect of gravity, which should be very slight in this case, has been entirely neglected. In addition, the characteristics of the system were assumed to be independent of depth. As Figure 1 shows, this condition is not satisfied for the current speed, and NEUMANN [1948] has discussed how the combination of surface wind shear and stratification of the water may combine to give the observed vertical current distribution in the Gulf Stream. His analysis suggests that the vertical variation of the current is of considerable importance for the dynamics of the Gulf Stream. Therefore the assumption of a vertically homogeneous current may prove to be a serious limitation of the models. Nevertheless, the study of the simplified models at least shows whether or not the anticipated instability of the current and the stabilizing effect of the shore do exist. The effect of the Earth's rotation is included, but not its variation with latitude. This simplification is justified because the curvatures of the velocity profile across the Gulf Stream are large compared to the variation of the Coriolis parameter with latitude. Two additional assumptions are made which are almost completely satisfied by the actual ocean: the water is assumed to be incompressible, and its flow nondivergent. Also, the possibly important effect of friction was not taken into account, mainly because of the mathematical difficulties involved in including it.

In its undisturbed state, the current speed U varies in the cross-stream direction y only, but not along the current (in the x direction) or with time. Under these conditions, the undisturbed current is governed by

$$0 = -fU - (1/\rho)\partial P/\partial y \quad \ldots\ldots\ldots\ldots\ldots \quad (1)$$

$$\partial U/\partial x = 0 \quad \ldots\ldots\ldots\ldots\ldots \quad (2)$$

where f is the Coriolis parameter, P the undisturbed pressure, and ρ density. Now a small disturbance is superimposed on the original field of flow so that the total velocity components are U + u and v, and the pressure is P + p. The perturbation quantities u, v, and p are assumed to be so small that second order terms in these quantities are neglible compared to first order terms. Consequently the results can be applied only as long as the disturbance remains small. For example, if the amplitude of the meanders is greater than 1/60 of the wave length, terms are omitted in the equation which are of the order of ten per cent of the terms which are retained. The perturbation theory can determine whether small disturbances will decrease or increase in amplitude after formation, that is, whether the system is stable or unstable, because a disturbance developing in the undisturbed current must have an infinitely small amplitude at the start.

The disturbed motion satisfies the two horizontal equations of motion, and the equation of continuity. These equations become (after substitution of (1) and (2), and omission of second order terms)

$$\partial u \partial t + U\partial u/\partial x = (f - \partial U/\partial y)v - (1/\rho)\partial p/\partial x \quad \ldots\ldots\ldots\ldots \quad (3)$$

$$\partial v/\partial t + U\partial v/\partial x = -fu - (1/\rho)\partial p/\partial y \quad \ldots\ldots\ldots\ldots \quad (4)$$

$$\partial u/\partial x + \partial v/\partial y = 0 \quad \ldots\ldots\ldots\ldots\ldots \quad (5)$$

These three equations describe the variation of the three dependent variables u, v, and p as a function of the three independent variables, x, y, and t. The different models differ only in U and its variation with y.

In all the models treated here, the Gulf Stream system is made up of two or more distinct slabs, bounded by vertical planes. In each of these regions, U is assumed to be either constant or linearly varying with y. By composing the model of a large number of such slabs, the actual velocity distribution can be approximated to any desired degree of accuracy; however, this method leads to extraneous solutions [LIN, 1945]. Nevertheless, it is likely that the motion is really unstable when the approximate model indicates instability, and stable if all the solutions to the approximate model are stable.

The solutions of the equations must satisfy the following boundary conditions. At rigid boundaries $v = 0$. At internal boundaries where U is discontinuous

$$(\partial/\partial t + U\partial/\partial x)(p - p') + v\partial(P - P')/\partial y = 0$$

and an analogous equation in U' and v'. The primes indicate that the quantities are to be taken on the other side of the boundary. If, as in most of the subsequent models, U itself is continuous and only its variation with y changing abruptly the above conditions are simplified inasmuch as then v and p must be continuous across the boundary. In all examples considered here, the solutions are assumed to be of the form

$$u = Ae^{\pm 2\pi y/L}\, e^{2\pi i(x - ct)/L}$$

$$v = Be^{\pm 2\pi y/L}\, e^{2\pi i(x - ct)/L}$$

$$p/\rho = Ce^{\pm 2\pi y/L}\, e^{2\pi i(x - ct)/L}$$

where L is the wave length and c the wave velocity. The constants A, B, and C in the different zones are all interconnected by the differential equations and the boundary condition, so that if a single one of these is fixed all the others are determined. The equations and boundary conditions can be satisfied, provided that a relation exists between wave speed and wave length. These relations, which indicate whether or not the motion is stable, are discussed in detail below.

If the wave velocity is real, the wave is stable and will propagate with this velocity, provided it can start at all. Once started it will neither grow nor decay. If the wave velocity is complex, the real part gives the speed of propagation. The imaginary part, c_i, determines the rate of increase or decrease of the amplitude of the wave: if A_o is the amplitude at time t_o, the amplitude at time t will be

$$A = A_o \exp\left[2\pi c_i(t - t_o)/L\right]$$

Waves with positive c_i will grow exponentially; waves with negative c_i will be damped out.

Model 1: Zero order discontinuity of flow at the shear zone--The most significant property of the Gulf Stream is the velocity discontinuity on the shoreward side. Rather a crude model consists of two bounded zones, of infinite extent in the x-direction with current speeds U_1 and U_2 respectively, of thickness d_1 and d_2. The wave velocity is then given by

$$c = (U_1a_1 + U_2a_2)/(a_1 + a_2) \pm i(U_1 - U_2)/(\sqrt{a_2/a_1} + \sqrt{a_1/a_2}) \ldots\ldots\ldots\ldots (6)$$

Here, and in the following equation we have written a_n for coth $(2\ \ d_n/L)$ where n is an integer.

As is well known, a pure shearing wave such as this is always unstable. The imaginary part of the wave velocity is largest when the two hyperbolic cotangents are unity. This condition is satisfied within 0.5 per cent if the discontinuity occurs more than a half wave length from both boundaries. On the other hand, as the velocity discontinuity approaches either boundary, one or the other cotangent tends to infinity, and the imaginary part of the wave velocity to zero. Therefore the waves formed when the stream is close to shore are less unstable than if the stream is far from shore.

The real part of the wave velocity tends to the mean of U_1 and U_2 if the discontinuity occurs more than half a wave length from the boundary and approaches the speed in the narrower of the two zones as the jump approaches either continental shelf.

Model 2: Two currents separated by a finite shear zone--According to Figure 1, a more realistic model would show the two currents with speeds U_1 and U_2 separated by a shear zone of finite thickness, in which the current varies linearly with y. RAYLEIGH [1896, Chap. 2] first showed that in the absence of rotation a finite shear zone exerts a stabilizing influence on the waves so that only waves with wave length greater than 4.9 times the width of the shear zone are unstable. HAURWITZ [1943] proved the same result for a rotating fluid. Neither Rayleigh nor Haurwitz considered a bounded fluid. As was seen in Model 1, even waves at sharp discontinuities became less unstable when the discontinuity moves closer to either boundary. It can be suspected that waves developing in fluids with finite transition zones will become stable when the shear zone occurs close to the boundary. Figure 3 shows a schematic view of the model. The wave speed is given by

$$c = (U_1 + U_3)/2 + (U_3 - U_1)\,L\,(N - R)/4\pi d_2 M$$
$$\pm (U_3 - U_1)\sqrt{\{1 - (N + R)\,L/M\pi d_2 + L^2[(N - R)^2/M + 4]/4\pi^2 d_2^2 M\}}/2 \quad \ldots (7)$$

where $M = 1 + a_1 a_2 + a_1 a_3 + a_2 a_3$, $N = a_2 + a_3$, and $R = a_1 + a_2$. For long waves, the expression under the square root is negative everywhere (instability), excepting if the shear zone is close to either boundary. For example in the limit $d_3 = 0$, the expression under the square root becomes $[1 - L/2\pi d_2(a_2 + a_1)]^2$ which is, of course, positive, and hence the waves are stable. There must thus exist a critical value at which the stability changes sign. If the width of the ocean is greater than one wave length, this critical distance is given by

$$a_3 = [(L/2\pi d_2)(2\sqrt{(a_2^2 - 1)} + (1 + 2a_2)$$
$$- (a_2 + 1)]/(1 + a_2 - L/2\pi d_2) \quad \ldots\ldots\ldots (8)$$

For example, a wave of wave length 250 mi will become stable when the shear zone approaches within 0.2 mi of the continental slope. For steep gradients of the shear zone, d_2 is large and nearly equal to $L/2\pi d_2$. In that case, the distance at which the change from stability to unstability takes place is proportional to the square of the width of the shear zone and inversely proportional to the wave length.

The exact distance from the shelf at which the stability changes is probably not of great importance, as can be seen if the velocity distribution of Model 2 is replaced by a similar smooth distribution. Figure 4 shows (a) a

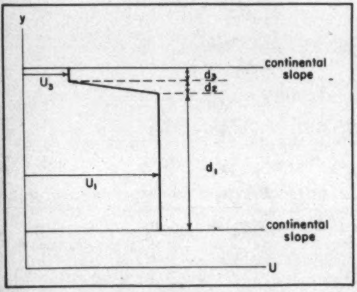

Fig. 3--Velocity distribution and definition of terms in Model 2

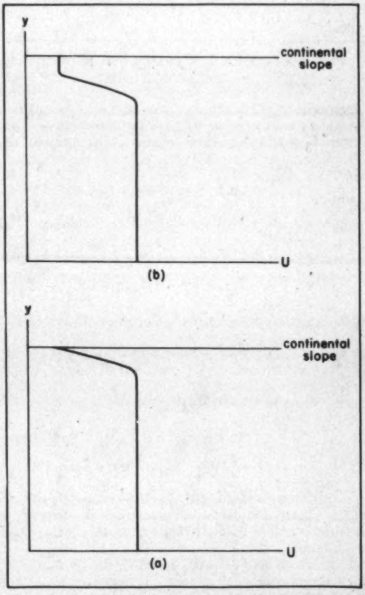

Fig. 4--Smooth distributions of currents corresponding to Model 2; (a) shear zone adjacent to shore, and (b) shear zone at some distance from shore smooth distribution when the shear zone is adjacent to shore, and (b) a distribution when the shear zone is far from shore. RAYLEIGH [1896, Chap. 21] proved that a distribution without points of inflection is stable. LIN [1945] showed that velocity distributions with points of inflection permit unstable oscillations, at least under certain conditions. It is clear then that the distribution in Figure 4a is stable, and in Figure 4b unstable, provided that the right boundary is sufficiently far away. Therefore, the distance from shore at which the stability changes to instability is smaller than any small distance that might be proposed arbitrarily. The existence of a small, but finite, distance from shore at which the stability changes in Model 2 is due to the probably unrealistic discontinuity in velocity gradient.

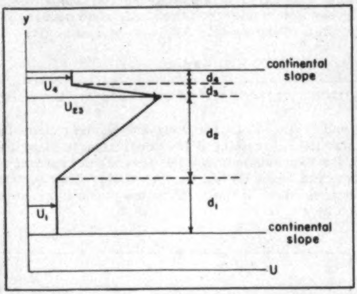

Fig. 5--Velocity distribution and definition of terms in Model 3

__Model 3: Four zones__--Figure 1 shows that the shear zone does not separate two currents of constant speed. A better approximation to the actual distribution could include four zones: In the two outer zones, the current speeds are constant; between these lie the shear zone in which the velocity gradient is large and constant, and the "transition" zone in which the gradient is smaller and also constant. Figure 5 shows schematically the four zones and the current distribution in each.

All quantities referring to the transition zone will be characterized by subscript 2, all quantities referring to the shear zone by subscript 3. Subscripts 1 and 4 will refer to characteristics of the outer zones. The thickness of the zones will again be denoted by d, and U_{23} will be the undisturbed velocity at the boundary between shear zone and transition zone. It is convenient to introduce the following auxiliary symbols $A = (a_1 + a_2)(1 + a_3 a_4) + (a_3 + a_4)(1 + a_1 a_2)$; $B = 1 + a_1 a_2 + a_1 a_3 + a_2 a_3$; $D = 1 + a_2 a_3 + a_2 a_4 + a_3 a_4$; $E = (a_1 + a_2)(a_3 + a_4)$; $J = a_1 + a_2$; $H = a_2 + a_3$; $I = a_3 + a_4$; $\zeta_2 = L/2\pi d_2$; and $\zeta_3 = L/2\pi d_3$. The frequency equation in this case is a cubic

$$Ac^3 + Kc^2 + Lc + M = 0$$

where

$$K = -A(U_1 + U_{23} + U_4) - \zeta_3(U_{23} - U_4)(B - E) - \zeta_2(U_{23} - U_1)(D - E),$$

$$\begin{aligned} L = {} & A(U_1U_4 + U_1U_{23} + U_{23}U_4) + \zeta_3 B(U_{23} - U_4)(U_1 + U_{23}) \\ & + \zeta_2 D(U_{23} - U_1)(U_{23} + U_4) - \zeta_3 E(U_{23} - U_4)(U_1 + U_4) \\ & - \zeta_2 E(U_{23} - U_1)(U_1 + U_4) - \zeta_3^2 J(U_{23} - U_4) - \zeta_2^2 I(U_{23} - U_1)^2 \\ & - \zeta_2 \zeta_3 (U_{23} - U_1)(U_{23} - U_4)(J + I - H) \end{aligned}$$

$$\begin{aligned} M = {} & -AU_1U_{23}U_4 - \zeta_3 B(U_{23} - U_4)U_1U_{23} - \zeta_2 D(U_{23} - U_1)U_{23}U_4 \\ & + \zeta_3 E(U_{23} - U_4)U_1U_4 + \zeta_2 E(U_{23} - U_1)U_1U_4 \\ & + \zeta_3^2 J(U_4 - U_{23})^2 U_1 + \zeta_2 \zeta_3 J(U_{23} - U_4)(U_{23} - U_1)U_1 \\ & + \zeta_2 \zeta_3 I(U_{23} - U_4)(U_{23} - U_1)U_4 + \zeta_2{}^2 I(U_{23} - U_1)^2 U_4 \\ & - \zeta_2 \zeta_3 H(U_{23} - U_4)(U_{23} - U_1)U_{23} + \zeta_3^2 \zeta_2 (U_{23} - U_4)^2 \cdot (U_{23} - U_1) \\ & + \zeta_2^2 \zeta_3 (U_{23} - U_1)^2 \cdot (U_{23} - U_4) \end{aligned}$$

A complete discussion of this frequency equation requires a study of the effect of the possible variation of eight parameters: the three current velocities, the widths of the four zones, and the wave length. Such a discussion would be beyond the scope of this study. Fortunately, the expression is symmetrical and variation of the parameters in the shear zone has the same effect as variation of the parameters in the transition zone. The same kind of symmetry holds for the two outer zones.

Actually the equation was solved only for the case that $U_1 = U_4$, a condition which seems to be well satisfied in the case of the Gulf Stream. If we then introduce the dependent variable c' $= (c - U_1)/(U_{23} - U_1)$ the frequency equation becomes

$$c'^3 A - c'^2[A + \zeta_3(B - E) + \zeta_2 (D - E)] + c'[\zeta_3 B + \zeta_2 D - \zeta_3^2 J - \zeta_2^2 I - \zeta_2 \zeta_3 (J + I - H)] + \zeta_2 \zeta_3[\zeta_2 + \zeta_3 - H] = 0 \ldots\ldots\ldots\ldots \text{(9)}$$

Evidently, c' depends on the geometry of the zones only, not on the numerical values of the current speeds. In all examples, the wave length was chosen so that the Gulf Stream is much more than half a wave length from Europe, so that the coefficients in (9) could be simplified by letting $d_1 = 1$. Further, if the widths of all zones are divided by the wave length, there remain only three parameters: the ratios of the widths of Zones 2, 3, and 4 to the wave length.

Table 1--Relationship of discriminant and $d_4 L$

$d_3/L = 1/44$ and $d_2/L = 1/44$		$d_3/L = 1/44$ and $d_2/L = 1/11.4$	
d_4/L	Discriminant	d_4/L	Discriminant
∞	2.60	∞	1.523
1/63	0.43	1/63	0.244
1/630	0.044	1/630	0.024
1/6300	0.0024	1/4400	0.0006
1/14000	-0.0002	1/6300	-0.0005
0	-0.0020	0	-0.0030

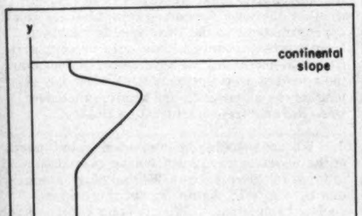

Fig. 6--Smooth distributions of currents corresponding to Model 3; (a) shear zone adjacent to shore; and (b) shear zone at some distance from shore

Of interest is the effect of varying distance between shear zone and American Continent on the stability of the motion. Unstable waves can develop only if the equation has a complex root with positive imaginary part. The above cubic equation has two complex roots, provided that the discriminant, given by $1/108\ A^4\ (-K^2L^2 + 4AL^3 + 4K^3M - 18AKLM + 27\ A^2M^2)$ is positive.

The two complex roots are complex conjugates so that one solution will have a positive imaginary part. Table 1 shows the variation of the discriminant with the ratio of distance d_4 of the shear zone from the continental shelf to wave length, for two combinations of d_2/L and d_3/L. The second of these was adjusted to fit the data represented in Figure 1. The table shows that, at least in these examples, Model 3 has similar stability properties to Model 2. The waves are unstable when the stream is far from shore, but become stable when it is close to shore. When the current distribution in Model 3 is approximated by a smooth distribution, a point of inflection remains even when the stream is close to shore (see Fig. 6a). This means that Model 3 must differ from Model 2 in an important respect; for some wave length the velocity distribution in Model 3 is unstable even when the stream flows close to shore. Therefore a special case of Model 3 was studied in detail, in which the width of Zone 4 is zero. This special case will be referred to as Model 3a.

Model 3a: Gulf Stream close to shore-- When the shear zone is adjacent to the continental shelf, which is assumed to act like a rigid wall, the frequency equation reduces to a quadratic, which can be discussed relatively easily. The discriminant of this quadratic is (for c' as dependent variable)

$$(1/4)\left\{1 - [\zeta_2(1 - a_3) + \zeta_3(1 + a_2)]/(1 + a_2)(1 + a_3)\right\}^2$$
$$+ \zeta_2(\zeta_2 - a_2 + \zeta_3 - a_3)/(1 + a_2)(1 + a_3)$$

It is interesting to note that the instability disappears entirely as the width of the shear zone goes to zero. This is in accordance with Rayleigh's stability criterion; for a profile with Zones 1 and 2 only would be approximated by a smooth curve with no point of inflection.

Model 3b: Shear zone and transition zone of equal width--The special case of Model 3 with equal values of d_2 and d_3 allows considerable simplifications in the algebra, but has little practical value for the Gulf Stream problem. This model again shows stability for long and short wave lengths and instability for intermediate wave lengths. When the stream is close to shore, instability occurs only in a small interval of d_2/L, and even then is quite weak. The waves of wave length greater than ten times the width of the transition zone are unstable only when the stream flows at a considerable distance from shore.

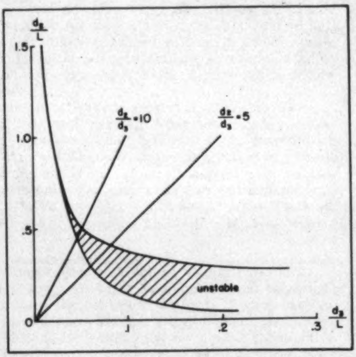

Fig. 7--Region of instability (hatched) as function of widths of shear and transition zones, for shear zone adjacent to continental shelf

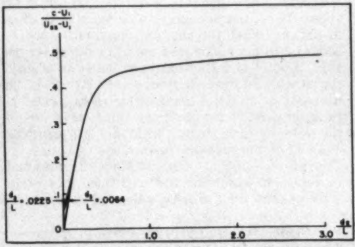

Fig. 8--The quantity $c' = (c - U_1)/(U_{23} - U_1)$ as function of the width of the transition zone, for two values of the ratio of the width of the shear zone to the wave length

The speed of Model 3 waves--There is little point in computing the speed of stable or neutral waves from the frequency equation of Model 3. Such waves will probably not develop amplitudes sufficiently large to be observed. In the case of unstable waves the real part of the velocity measures the actual speed of propagation of the individual waves. It is not certain whether the wave speeds so computed are good approximations to the wave speeds resulting from current models with smooth velocity profiles. In any case, the wave velocities measure the speed of propagation of the waves only as long as the amplitudes are small, since they were derived from perturbation theory.

We are principally interested in the speeds of the unstable waves which have been observed to form far from shore. We therefore assume that $a_1 = a_4 = 1$. Again, we put the current speeds in the first and fourth zone equal to each other. Figure 8 shows the variation of $(c - U_1)/(U_{23} - U_1)$ with d_2/L, for two values of d_3/L. It is seen that the influence of the variation d_3 (the width of the shear zone) is quite small, provided that the shear zone is much narrower than the transition zone. On the other hand, the width of the transition zone d_2 has a pronounced effect on the speed of propagation of these unstable waves. For extremely wide transition zones, the quantity $(c - U_1)/(U_{23} - U_1)$ approaches the value 0.500, that is, the wave speed itself tends to a value half way between U_1 and U_{23}. In this limit, Model 3 approaches Model 2, which would have led to the same result.

For narrower transition zones, the quantity $(c - U_1)/(U_{23} - U_1)$ may be considerably smaller than 0.500, but it always remains positive. For example if width of the transition zone is ten per cent of the wave length, the ratio $(c - U_1)/(U_{23} - U_1)$ is only 0.15. With realistic values for the currents $U_1 = 0$ and $U_{23} = 4$ knots, the wave speed would be 0.6 knots. If the wave length is 240 mi, the period is almost 17 days.

Wave speeds were also computed for the short and only slightly unstable waves which theoretically may form even when the stream is close to shore. With a wave length of 50 mi, a transition zone 25 mi wide, and the shear zone 2.5 mi wide $(c - U_1)/(U_{23} - U_1)$ comes out to be 0.18, almost the same as in the other example. With the same values of the current speeds, the waves propagate with 0.7 knots.

Conclusions--According to the hypothesis suggested here the eddies in the Gulf Stream which produce the meandering develop as unstable waves under certain conditions determined by the velocity profile across the Gulf Stream. One of the conditions favorable for the development of unstable waves is that the Gulf Stream is not too close to the continental shelf (Model 3). Even when the shear zone is directly adjacent to the shelf unstable waves are still possible, but the degree of instability is so slight that an appreciable growth of the amplitudes is unlikely to occur (Model 3a). In the case of Model 3, when the shear zone is at a finite distance from the continental shelf the degree of instability does vary with the wave length, with the width of the various zones, and with the current velocities. Computations of the influence of these parameters on the instability are now being carried out for various values of the relevant parameters. In order to check our hypothesis it will be necessary to know the velocity profile across the Gulf Stream, the width of the shear zone and the transition zone, and their distances from the continental shelf, as well as the size of the eddy. The theory gives also a certain value for the speed with which such unstable waves should move, and observations of this speed would therefore be very useful as an additional check on the theory. In this connection reference should be made in particular to one of the results in the preceding section, namely, that the width of the transition zone has a pronounced effect on the speed so that knowledge of this parameter is very important.

No reference has been made here to the possible effects of the bottom topography on the meandering of the Gulf Stream. It is quite likely that the bottom topography plays an important part in two ways. First, it may provide the initial trigger action which produces the unstable motion. Second, it may directly affect the stability conditions and the nature of the disturbed motion. If bottom topography sets off the disturbance one may expect to find certain preferred locations in which the Gulf Stream eddies originate. Evidently a large number of observations will be required in order to determine whether such locations exist, expecially since the eddies once started will not remain at their point of origin, but move along the current as indicated by the hypothesis. If more comprehensive observations show that the bottom topography has also an effect on the perturbation motions our hypothesis will have to be modified accordingly.

References

CHURCH, P. E., Temperatures of the western North Atlantic from thermograph records, International Union of Geodesy and Geophysics, Association of Physical Oceanography, Publ. Sci., v. 4, no. 4, 32 pp., 1937.

HAURWITZ, B., The effect of a gradual wind change on the stability of waves, Ann. New York Acad. Sci., v. 44, pp. 69-80, 1943.

ISELIN, C. O'D., Preliminary report on long period variations in the transport of the Gulf Stream, system, Papers Phys. Oceanogr. and Met., Mass. Inst. Techn., v. 8, no. 1, 40 pp., 1940.

ISELIN, C. O'D., and F. FUGLISTER, Some recent developments in the structure of the Gulf Stream, J. Mar. Res., v. 7, pp. 317-329, 1948.

LIN, C. C., On the stability of two-dimensional parallel flows, Q. Appl. Math., v. 3, pp. 117-142 and 218-234, 1945.

NEUMANN, G., Zum Problem des Golfstroms, Naturwiss. Runds., v. 1, pp. 22-28, 1948.

RAYLEIGH, LORD, Theory of sound, 2nd ed., v. 2, 504 pp., 1896.

UDA, M., On the correlated fluctuation of the Kuroshio current and the cold water mass, Oceanogr. Mag., v. 1, pp. 1-12, 1949.

Woods Hole Oceanograhhic Institution,
Woods Hole, Massachusetts

College of Engineering,
New York University,
New York 53, New York

(Manuscript received March 17, 1950; presented at the Thirty-First Annual Meeting, Washington, D. C., May 2, 1950; open for formal discussion until March 1, 1951.)

Transactions, American Geophysical Union   Volume 31, Number 5   October 1950

ACTIVITY OF PARICUTIN VOLCANO FROM JULY 1 TO DECEMBER 31, 1949

Carl Fries, Jr. and Celedonio Gutiérrez

(Published by permission of the Director, United States Geological Survey)

The activity of Parícutin Volcano, State of Michoacán, Mexico, during the second half of 1949 is represented diagrammatically in Figures 1, 2, and 3. An explanatory discussion of these diagrams of eruptive characteristics and a description of the lettered noise types shown on them appeared in an earlier report on this Volcano [WILCOX, 1947], to which the reader is referred. Photographs of two common types of eruptive activity are shown as Figures 4 and 5, and a map outlining the monthly advance of lava during the period covered is given as Figure 6. Altitudes of different points on Parícutin cone are listed in Table 1, and weather data are summarized in Table 3.

Data from which the eruptive diagrams, lava map, and weather table were constructed were gathered by the junior author, who continued as a constant observer at Parícutin. Measurements for the table of elevations and the arrangement of all the material for formal presentation were contributed by the senior author, who spent a total of 16 days at the volcano on three visits: July 3-8, October 16-20, and December 11-15. Presentation of the data follows the form of the previous report on Parícutin published in the Transactions [FRIES and GUTIERREZ, 1950].

Activity of the cone--Eruptions from the crater continued, as in other years, to be extremely variable from hour to hour and from day to day (see Fig. 1-3). Eruptive activity seemed, on the whole, to be slightly less intense than during the preceding half year. The eruptive column rose to heights of 3000 m or more above the cone on only eight days in July, one day in August, and three days in October, not reaching such heights during the rest of the period. Such strong eruptions were therefore less frequent than in former years, and periods of complete inactivity were moreover somewhat longer than usual. On November 28, for instance, eruptions ceased completely for one hour, and on December 23, the cone was inactive for two hours; periods of inactivity of less than 20 min were frequent. Emission of ash continued to decline, and only 1.8 mm fell at Cuezeño station, in contrast to 5.3 mm in the corresponding period of 1948. Heavily charged ash and bomb eruptions (see Fig. 4) were accompanied as usual by electric discharges within the column or from the column to the rim of the cone. Such discharges occurred on two days in July, three days in August, three days in September, one day in October, and three days in December, but they were less frequent than during the first half of 1949. At times the eruptive column was nearly invisible until it reached a height of 100 m or more above the cone, where it condensed into a thick whitish cloud of steam (see Fig. 5), a feature that has been noted at frequent times in former years. Eruptions seem to have issued from only one vent in the crater for the greater part of the period. Early in November, however, two distinct columns were visible, although when the junior author ascended the cone on the 14th of that month, the northeast vent was found to be stopped up. This vent was apparently blasted open again on the following day, for the two eruptive columns reappeared and remained visible for several days thereafter.

Unusually strong explosions that shook the Earth in a radius of several kilometers from the volcano and hurled large pyroclastic blocks out beyond the base of the cone occurred on August 5, November 21 and 28, and December 24. These tremendous explosions were usually preceded by short periods of almost complete inactivity, and some of them were so violent that fragments were blown nearly two kilometers from the volcano. The largest single block noted after the November 28 explosion was 5.6 m long by 1.6 m wide. It consisted of dense lava and was found near the northwest base of the cone. These eruptions seem to have come as a result of the crater vents being stopped up or the throat being reduced in size by pressure from the sides, and they were generally followed within 24 hr by a marked temporary increase in the flow of lava. The frequency of these explosions was much the same as in the preceding half year.

Form of the cone and crater--The outward form of the cone did not change greatly through the second half of 1949. The elevation of the east peak was unchanged (see Table 1), within the limits of accuracy of measurement, and it has in fact remained about the same since the end of October,

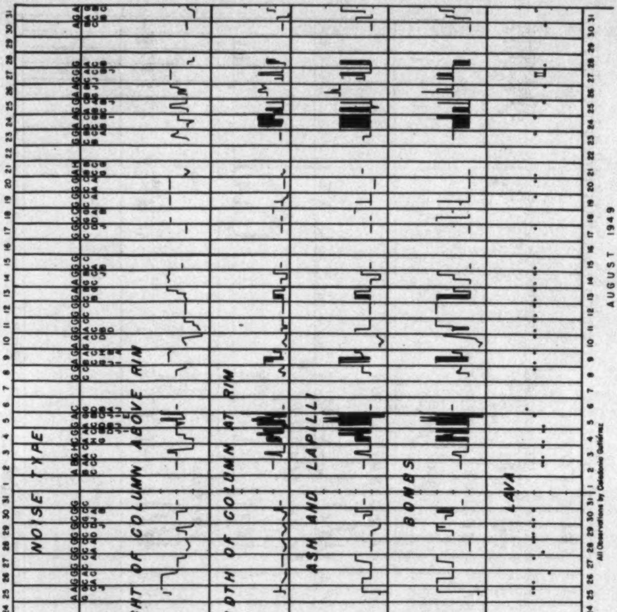

All Observations by Celedonio Gutiérrez

Fig. 1--Eruptive characteristics of Parícutin Volcano from July 1 to August 31, 1949

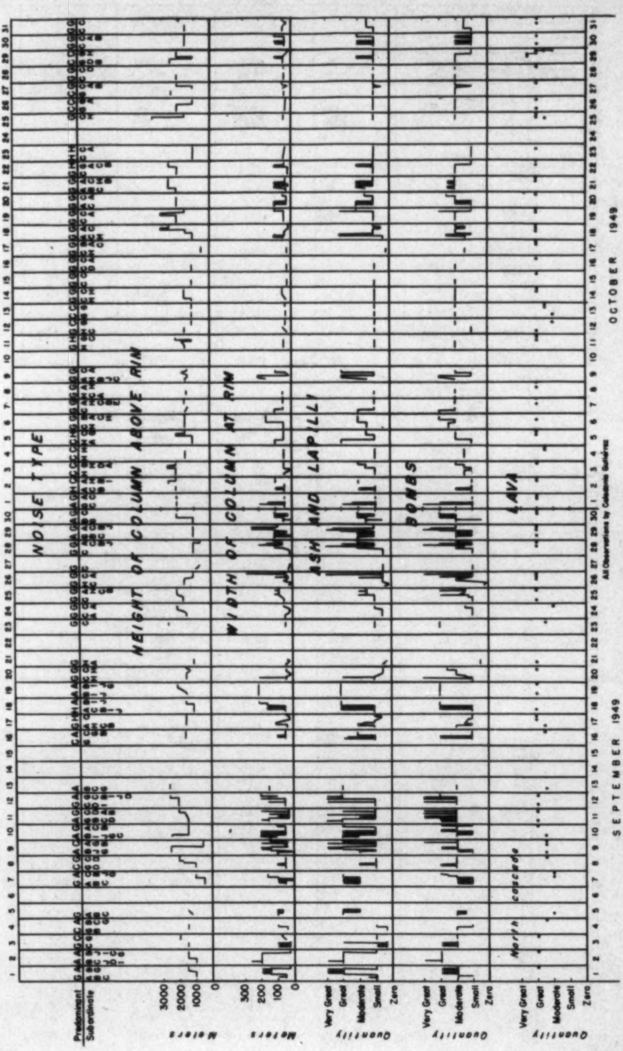

Fig. 2--Eruptive characteristics of Paricutin Volcano from September 1 to October 31, 1949

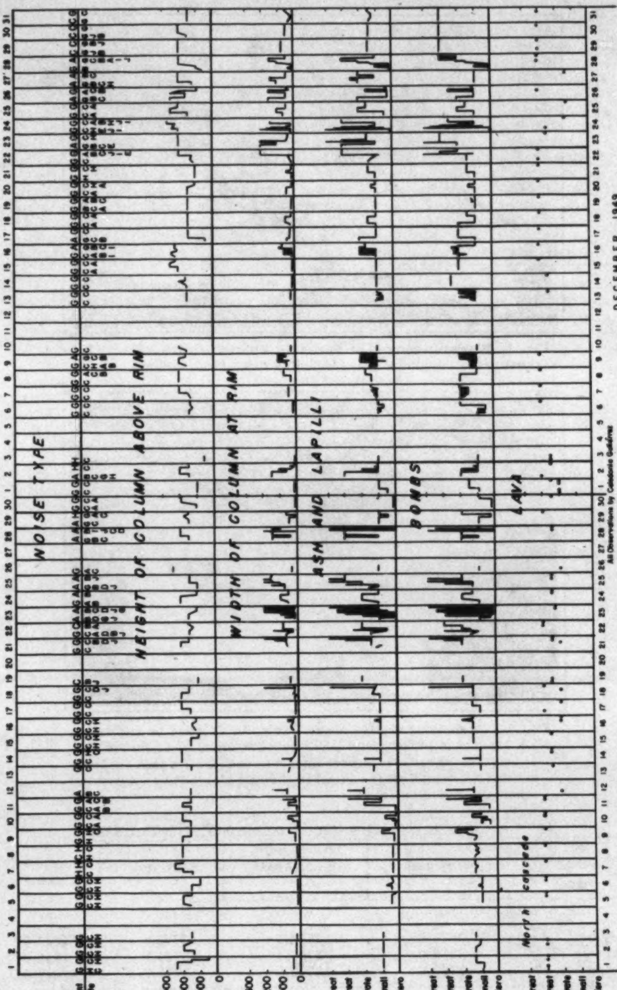

Fig. 3--Eruptive characteristics of Parícutin Volcano from November 1 to December 31, 1949

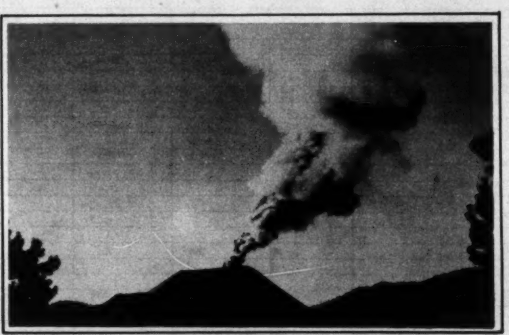

Fig. 4--Eruptive column of Parícutin Volcano on December 13, 1949; note curtain of ash streaming down from column

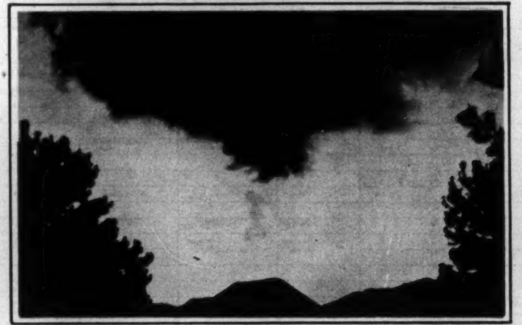

Fig. 5--Condensing vapors above Parícutin Volcano on December 13, 1949; this picture was taken several hours after that of Fig. 4; eruptive gases are almost invisible until they reach cooler air and condense; entire cloud is formed of eruptive vapors in otherwise cloudless sky

Table 1--Altitude above sea level of points on Parícutin Volcano[a]

Date 1949	West peak	Lowest point of northeast rim	East peak	Lava-vent mound
	m	m	m	m
July 5	2779.9	2755.6	2772.7	2643.6
October 17	2789.0	2761.7	2771.1	2645.0
December 12	2789.0	2770.8	2772.7	2647.9

[a] Determined by alidade from Cuezeño Station with estimated accuracy of ±1.5 m. Horizontal distances to points sighted were re-determined by triangulation from three known stations. These new distances and those formerly used are shown in Table 2. Re-determination of horizontal distances was necessary because the west peak had shifted craterward and the saddle had shifted northwestward and outward through accumulation of pyroclastic material.

1947, when it was 2774.2 m above sea level. The west peak, however, continued to be built up through accumulation of pyroclastic material. It reached a greater height by the end of December than at any former time, having risen nearly 17 m during the half year. The saddle, or low point of the northeast rim also continued to rise and reached nearly the same altitude as the east peak. This rise was possible because that flank of the cone did not slump during this six-month period as it had done in the previous year. The southwest saddle appeared on inspection on ascents to the crater to have remained about the same, probably because of repeated slumping of the southwest flank of the cone, which nullified the effect of filling by pyroclastic material.

Table 2--Re-determined distances from Cuezeño Station

Point sighted	Horizontal distances formerly used	New distances
	m	m
West peak	5100	5160
Low point of northeast rim	5230	5160
East peak	5260	5270
Lava-vent mound	4950	4950

In the first few days of July the southwest flank of the cone slumped actively between two bordering faults about 120 m apart (see map in Fig. 6). This movement was accompanied by the re-opening of the lava-vent on that side of the cone. On July 6, when the writers ascended the volcano from that side, the faults had vertical scarps more than one meter high, and gases and steam were issuing lazily from place to place along the fault lines. On October 18 the scarps had been covered by pyroclastic material erupted from the crater, although that segment of the flank was still appreciably depressed. In the middle of November a second, minor slump took place, principally at the saddle, but this had been healed when the crater was visited on December 14, at which time the flank of the cone had nearly regained its normally rounded form. In the last few days of December, however, the southwest rim and flank of the cone began to slump again, suggesting movement of lava concealed beneath that area. The depression that had formerly appeared at the southwest base of the cone and that had been nearly filled with pyroclastic material by the end of the previous six months, was eradicated completely early in July by lava pushing up into the area and forming, instead, a low mound. On December 14 the slope of the outer north, northwest, and west flanks of the cone was measured and was found to be uniformly 34°, which is 2° or 3° steeper than the slope of these flanks in the summer of 1943.

The cone was ascended in order to inspect the crater on July 7, October 18, November 14 and 17, and December 14. The form of the crater on July 6 was described and pictured in the previous report on Parícutin [FRIES and GUTIERREZ, 1950, Fig. 10]. The conical mound that occupied the center of the crater at that time was probably destroyed by the strong explosion of August 5, if not before; but at any rate, by October 18 the crater consisted of an oval-shaped bowl elongated in a northeast direction and about 25 m deep. The rounded bottom of the bowl, which was lined with scoria at dull-red heat, did not have any constant vents or openings. The eruptions, which at that time were so strong as to prevent more than a quick look and rapid retreat, rent through different parts of this pasty false bottom every few seconds, tearing off huge chunks of soft lava and hurling them as high as 100 m into the air, accompanied by deafening thunder. However, the bottom did not in any sense resemble a lava lake. The position of the bowl corresponded more or less to that of the southwest vent at those times when two vents have been present in the crater. A terrace with a maximum width of 100 m extended from the east peak to the lip of the central bowl, at about the same altitude; it narrowed at the northeast saddle and west peak and disappeared at the southwest saddle.

On November 14 the crater consisted of a double bowl with a very low divide. The bottom of the northeast part was stopped up, although it had a circular fissure in the center and appeared to be ready to blow open at any time; the southwest bowl was pierced by a vent about ten meters in diameter, through which the usual eruptions tore their way. On November 17 this double bowl was much the same, except that a vent two meters in diameter appeared 15 m or so to the northwest of the main southwest vent, and a circular slumped area had formed near the southwest saddle or rim of the crater. Gases and steam issued from cracks in this saddle during the entire period. On December 14 only one oval-shaped bowl was present, but, as the explosive activity was too intense to permit an appraoch to its lip, the bottom could not be seen. The eruptions appeared, however, to come from a single wide vent in the bottom of this bowl, which seemed to be no more than 20 m lower than the southwest saddle. The terrace from the rim of the cone to the central bowl was even wider than earlier in the six-month period.

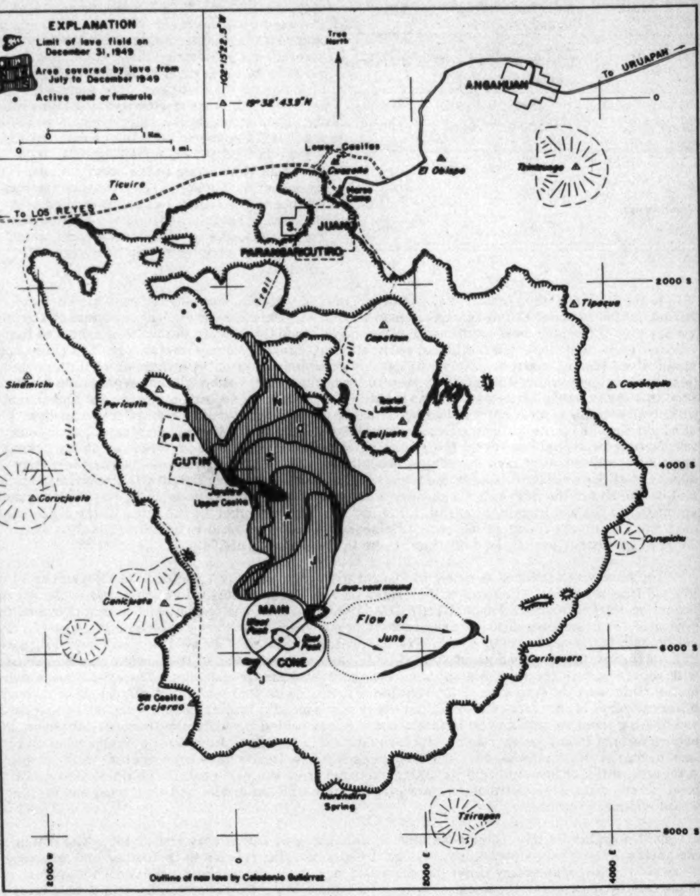
EXPLANATION
Limit of lava field on December 31, 1949
Area covered by lava from July to December 1949
Active vent or fumarole
0
1 Km.
0
1 mi.
102°15'22.5"W
19°32'43.9"N
True North
To URUAPAN
ANGAHUAN
0
Lower Casitas
El Cuarallo
Horno Camp
El Obispo
Tzintzungo
Ticuiro
To LOS REYES
S. JUAN
PARANGARICUTIRO
Trail
2000 S
Tipacua
Capatzun
Trail
Sinánichu
Paricutin
Capánguito
Tezitzi Lookout
Equijuata
PARI CUTIN
Trail
4000 S
Corucjuata
Jardines Upper Casita
Curupichu
J
Lava-vent mound
Canicjuata
MAIN
West Peak
East Peak
CONE
J
Flow of June
J
6000 S
Curíngüaro
Casita Cocjarao
Nurándiro Spring
Tzirapan
8000 S
2000 W
0
2000 E
4000 E
Outline of new lava by Celedonio Gutiérrez

Fig. 6--Areas covered by Parícutin lava flows from July 1 to December 31, 1949

Activity of the lava-vents--During the entire period, lava continued to issue without interruption from the vent at the northeast base of the cone, which has been named Nuevo Juatita by E. Ordóñez and will be so called by the writers, and for a few days early in July the old Puertecito vent at the southwest base of the cone was active (see Fig. 6). At the beginning of the period the northeast Nuevo Juatita vent supplied a sluggish flow of lava that cascaded toward the southeast, but on July 3 and 4 this lava became too stiff to move and came to a halt. On July 5 the pressure of the lava in the conduit forced up a large plug of solid material to a height of four or five meters above the lava-vent mound, and during the afternoon this plug gradually parted into several pieces [FRIES and GUTIERREZ, 1950, Fig. 2], permitting the fluid lava beneath to escape and, by evening, to flow in a cascade toward the north. In the following months this north cascade was constantly active and remained in the same position until the end of the six-month period.

On August 27 and 31 large gas bubbles pushed out through the lava conduit and tore off fragments of pasty lava, hurling them forcibly some tens of meters from the vent. Such gas eruptions occurred also on October 12 and 20 and on November 1 and 29. Some of these bubbles were accompanied by lava surges and slight flooding of the vent mound, but not all extra surges of lava were accompanied by gas eruptions. No ash eruptions were seen at the lava-vent during these six months. The unusually strong explosions in the crater, which were mentioned in a preceding paragraph, were generally followed within 24 hr by an increase in lava flow, although other increases in flow occurred without any apparent relation to strong crater eruptions. The volume of lava issuing from the Nuevo Juatita vent was more nearly uniform during this period than in the previous year. Because of intermittent floodings of the vent area, the lava-vent mound rose about seven meters in height during the six-months period (see Table 1).

While the Nuevo Juatita vent was stopped up early in July, the old southwest Puertecito vent was again forced open, probably on July 3 or 4. Lava apparently pushed through the side of the main cone, for the southwest flank slumped markedly while the vent was being reopened. A large plug of solid lava was shoved out ahead of the fluid material, into the area that had formerly been occupied by a depression [WILCOX and GUTIERREZ, 1948], the new lava then filling this depression and forming a low, roundish mound. The highest part of this mound consisted of two pyramids ten or 15 m high, composed of the older, solid lava that had been pushed out while the vent was being reopened. The duration of the activity is not known exactly, but it was probably less than two weeks, for on July 30 the flow was found to have come to a halt 150 m from the vent and the area was completely quiet, except for fumaroles and gas escape such as have characterized this area for the past year and a half. On visits to the crater in October, November, and December the Puertecito vent area was found almost unchanged, the only visible evidence of activity being a slight cracking of the ash cover and the issue at several places of burning-hot gases. Unless these gases should cool appreciably as time goes on, further lava activity can probably be expected in this area.

Activity of the lava flows--The lava flowing to the southeast and east from the Nuevo Juatita vent was cut off at its source in the first days of July and hence advanced only a few meters beyond its position at the end of June (see Fig. 6). The flow to the north and northwest advanced steadily through the period, until it had reached a maximum distance of 3100 m from the vent at the end of December, when it seemed to be advancing at about the same rate as in the preceding six months. One small island of original ground was covered by this flow, and four other islands were reduced in size. The island on which the upper casita was built and which formed the highest part of Cerro de Jarátiro was reduced in size but not entirely covered, although the lava now stands higher than the remaining old ground and hides the casita from view except from such high points as the top of Parícutin cone. The island to the north of the buried village of Parícutin was invaded by a tongue of lava late in December, as well as the large island between this village and San Juan Parangaricutiro, which was invaded by a second tongue. The lava fronts were generally from ten to 12 m high.

At a point just below the Nuevo Juatita vent on October 14, the lava stream was about ten meters wide by probably three meters deep and flowed at a rate of four meters a minute. This would amount to a flow of about 173,000 cu m a day or, assuming a constant rate, a total volume of about 32,000,000 cu m for the six months. This volume is some 15 per cent greater than the probable actual amount of lava extruded during this period, which may have been more nearly 25,000,000 cu m, indicating that the average rate of flow was somewhat less than four meters per minute, for the estimated width and thickness of the lava stream do not seem to be too great.

The southwest Puertecito lava flow was active probably less than two weeks. It divided into two tongues near the vent, one of which advanced about 150 m to the west and the other 150 m to the south before coming to a halt.

Weather data--Rainfall during the second half of 1949 (see Table 3) was about 230 mm less at Cuezeño Station than in the corresponding period of 1948, and daily temperature extremes were somewhat greater, probably reflecting a decrease in the ameliorating effect on temperature by rainstorms, which were less frequent in 1949. Precipitation at Equijuata Station was about 46 mm greater than at Cuezeño Station, thus continuing to exceed that at the latter station as in the preceding eleven months. Rain that fell at Cuezeño Station on October 7 mixed with the eruptive

Table 3--Monthly summaries of weather observations, rainfall, and ashfall near Parícutin Volcano

Month 1949	Cuezeño Station						Min humidity	Average direction of upper winds	Equijuata Station	
	Temp		Rainfall		Ashfall				Rainfall (total)	Ashfall (total)
	Max	Min	Total	Max	Total	Max				
	°C	°C	mm	mm	mm	mm	pct		mm	mm
July	24.7	8.1	277.5	66.6	tr	tr	48	ENE	359.7	0.3
August	25.0	7.5	248.2	29.4	0.0	0.0	52	ENE	290.9	0.2
September	22.8	8.3	333.3	93.3	0.5	0.5	57	E	274.0	1.8
October	23.9	6.4	164.9	24.2	1.2	1.0	57	ENE	138.5	1.5
November	25.3	0.0	0.0	0.0	0.0	0.0	13	ENE and WSW	0.0	0.0
December	26.1	0.6	7.0	4.5	0.1	0.1	25	SE	14.5	0.3

plume and fell as mud, although it did not seriously affect the vegetation as it had at other times. Pear and tejocote trees near the lava fronts over the northern part of the area covered by lava continued to bear fruit, and one type of grass not recognized in the region before the birth of Parícutin was rapidly catching hold in areas thickly covered by ash from the volcano. Dust began to be raised by surface winds in November, when no rain fell, and unless the spring months of 1950 should be wetter than usual, this season should be the dustiest so far experienced in the volcano region.

Acknowledgments--This report on the activity of Parícutin Volcano forms part of a cooperative project being carried on by the United States Geological Survey, the Geological Society of America, and the Comisión Impulsora y Coordinadora de la Investigación Científica of the Mexican Government. The latter organization, through Ing. Ezequiel Ordóñez, has carried the salary of Jesús Saldaña, who is assistant to the junior author and to whom the writers are indebted for some of the observations included in this paper. The Geological Society of America has continued to pay the salary of the junior author, while the Geological Survey has contributed the rest of the funds expended, from an allotment granted to it by the Interdepartmental Committee on Scientific and Cultural Cooperation of the Department of State.

References

FRIES, CARL, JR., and CELEDONIO GUTIERREZ, Activity of Parícutin Volcano from August 1, 1948, to June 30, 1949, Trans. Amer. Geophys. Union, v. 31, pp. 406-418, 1950.

WILCOX, RAY E., Activity of Parícutin Volcano from September 18 to November 30, 1946, Trans. Amer. Geophys. Union, v. 28, pp. 567-572, 1947.

WILCOX, RAY E., and CELEDONIO GUTIERREZ, Activity of Parícutin Volcano from April 1 to July 31, 1948, Trans. Amer. Geophys. Union, v. 29, pp. 877-881, 1948.

U. S. Geological Survey,
Paseo de la Reforma 64,
Mexico, D. F.

(Manuscript received April 18, 1950; open for formal discussion until March 1, 1951.)

Transactions, American Geophysical Union Volume 31, Number 5 October 1950

SOME SNOW-MELT RUNOFF CHARACTERISTICS

Stanley A. Miller

Abstract--This paper presents a method for evaluating maximum runoff from mountain snow melt in a large drainage basin and its application to studies for spillway design capacity of Garrison Dam on the Missouri River in North Dakota. The method involves consideration of degree-days and observed runoff for establishment of correlations between indicated heat supply, depth of snow pack, losses, and stream flow by double-mass curve plotting. The correlations thus obtained may be used to estimate floods from maximum probable hydrometeorologic conditions in the drainage basin.

Introduction--The Corps of Engineers, U. S. Army, in 1945 and 1946 conducted extensive hydrological studies of the effective drainage area above the authorized Garrison Dam on the main stem of the Missouri River in North Dakota (see Fig. 1), in order to determine the spillway requirements for that dam and other main-stem dams. As a part of these studies, detailed analyses were made of the mountain snow-melt runoff characteristics in the Big Horn River and the upper Yellowstone River drainage areas. The purpose of this analysis was to ascertain the maximum flood potentialities of the mountain snow-melt runoff, which, combined with storm runoff from the plains, produces the late spring floods on the Missouri River.

This paper presents the major problems encountered, and some of the more interesting mountain snow-melt runoff correlations obtained in the hydrological analysis of the mountainous regions.

Records available--Discharge records were available in U. S. Geological Survey Water Supply papers for some 100 stations in the Big Horn River and upper Yellowstone River drainage basins. The only discharge records used in the final analysis, however, were those for the Yellowstone River at Billings, Montana, and the Big Horn River near Hardin, Montana (used interchangeably with those near St. Xavier. Montana).

Presented on Figure 2 is a map of the Big Horn River drainage basin (the area chosen for illustrative purposes) upon which are shown the locations of the snow stakes and snow courses for which data were available. The snow stake data are published in Climatological Data, and the snow course data in Federal-State Cooperative Snow Surveys and Irrigation Water Forecasts for Missouri River

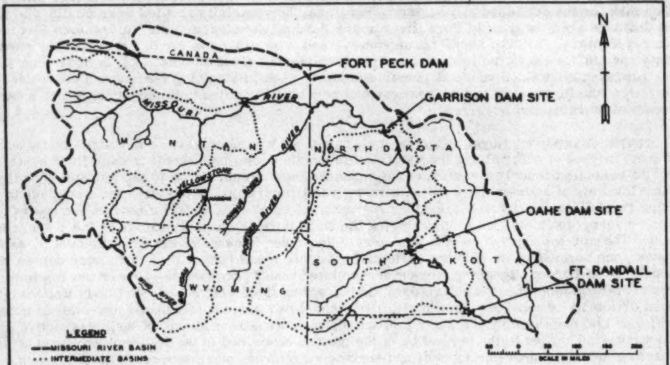

Fig. 1--Location map

and Arkansas Drainage Basins. Precipitation records were available in Climatological Data for approximately 45 stations now in operation in the upper Yellowstone River and Big Horn River basins.

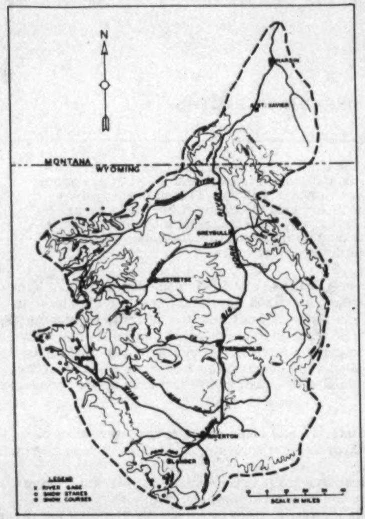

Fig. 2--Big Horn River drainage basin

Hydrometeorological report--The Hydrometeorological Section of the U. S. Weather Bureau prepared a detailed hydrometeorological report of the drainage area above the Garrison Dam Site. This report contained in part: (a) curves of the maximum possible snowfall accumulation from which it was possible to determine the maximum possible seasonal accumulation of snow on the ground; (b) the average date of disappearance of the snow on the ground for various elevations; (c) the maximum possible temperature departure from normal for 7- and 30-day periods; and (d) the variation of the mean monthly surface temperature with elevation.

Objective--Briefly, the objective of the studies was to obtain, from available hydrologic records, a snow-melt runoff-temperature relationship from which the maximum possible mountain snow-melt flood could be predicted. In this prediction, it was necessary to employ the limiting hydrometeorological factors prescribed in the Hydrometeorological Report by the U. S. Weather Bureau.

At the beginning of these hydrologic studies, attempts were made to obtain temperature-snow-melt runoff correlation in the headwater basins by many of the methods presented in the Transactions of the American Geophysical Union [see References]. The paucity of Weather Bureau stations in the headwater basins, and lack of information regarding irrigation diversions and channel losses precluded completion of the studies by these methods. The conclusions of these preliminary studies were, namely: (a) More accurate results would be assured if hydrological correlations were obtained for entire drainage basins, rather than for the combined sub-basins. Therefore, the remaining studies were confined to the total drainage areas of the Big Horn River above Hardin, Montana, and the Yellowstone River above Billings, Montana. (b) The snow course surveys and snow stakes of April 1 provided the most satisfactory indication of the ensuing late spring snow-melt flood volume. (c) In order that as many representative flood years as possible might be used in obtaining the snow-melt runoff characteristics, the flood years to be investigated should not be limited to those during which small amounts of storm runoff occurred.

Separation of storm runoff and snow-melt runoff--It was necessary to develop a fairly accurate and short method of determining the volume of mountain snow-melt runoff in each flood event, in order to evaluate properly the effect of the seasonal snow accumulation in the mountains on the volume and rate of snow-melt runoff with respect to temperature. Consideration was given to deducting rainfall excess from the flood hydrographs, by computing flood inflow into the rivers by the unit-hydrograph method, and then routing the flood through channel storage to the point of interest. The unit-hydrograph method was quickly discarded because of the great amount of work involved, and because of insufficient basic data. Double-mass curves of accumulated degree days above 32° F at Lander, Wyoming, versus accumulated runoff above a base flow of the Big Horn River at Hardin, Montana, were developed for the spring floods of record. In floods which were caused primarily by mountain snow melt, it was noted that periods of valley snow-melt and storm runoff could be identified by irregularities and sharp increases in slopes of their respective double-mass curves. This led to the derivation of the method described in the following paragraphs for separating mountain snow-melt runoff and surface runoff from other sources in a flood event.

Shown on Figure 3 are: (a) the degree days above 32° F, at the index weather station at Lander, Wyoming; (b) the recorded precipitation at Lander, Wyoming; and (c) the recorded flood hydrograph

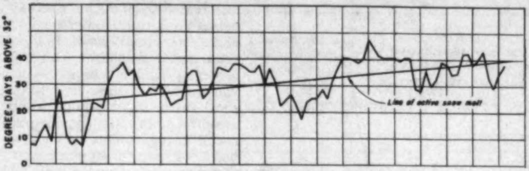

(a) DEGREE DAYS AT LANDER, WYOMING

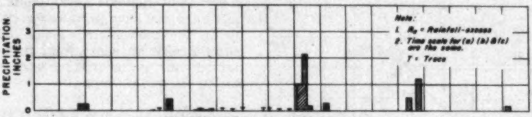

(b) PRECIPITATION AT LANDER, WYOMING

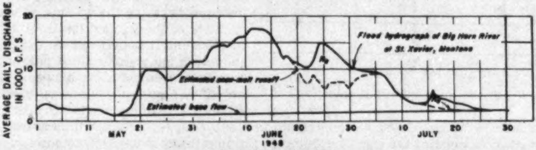

(c) FLOOD HYDROGRAPH

Fig. 3--Degree days and precipitation at Lander, Wyoming with Big Horn River hydrograph near St. Xavier, Montana

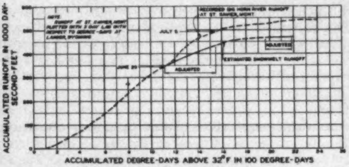

Fig. 4--Determination of snow-melt contribution in flood hydrograph of Big Horn River at St. Xavier, Montana

of the Big Horn River near St. Xavier, May to August, 1948. After the estimated base flow was deducted from the flood hydrograph at St. Xavier, the accumulated daily flow was plotted (with a three-day lag) against the accumulated degree days at Lander, Wyoming, as shown on Figure 4. This double-mass curve is smooth until June 20, which indicates that there was no appreciable surface runoff into the stream except from mountain snow melt. The increased rate of runoff per degree day for the period June 20 to July 5, indicates that there was inflow in addition to the snow-melt runoff. The slope of the double-mass curve to June 20 was extended to July 5, and is shown by the solid line marked "adjusted." The accumulated runoff values were then taken from the adjusted curve, and the daily discharge was computed from these values. The estimated snow-melt runoff thus derived for the period June 20 to July 5, is shown on Figure 3c.

Many trials are usually necessary before all hydrometeorological factors are satisfied in such a study, and often liberties must be taken in the construction of the computed snow-melt hydrograph to obtain a characteristic hydrograph. In order that the illustration might be simplified, no liberties have been taken with the example presented herein; however, further adjustments are indicated by the cold weather from June 17 to 28, Figure 3a. During this period, the only flow from the mountains was probably from a small amount of snow melt during the day and drainage from the snow blanket. Therefore, the snow-melt portion of the flood hydrograph (see Fig. 3c) for the period June 20 to July 1, should reflect the temperatures, and also reflect somewhat the normal recession of the stream. A secondary adjustment of the snow-melt hydrograph could be made by smoothing it between June 20 and July 1.

In many of the floods analyzed, the runoff at the beginning of the flood was from plains snow melt, followed by runoff from mountain snow melt. The plains snow-melt runoff can easily be

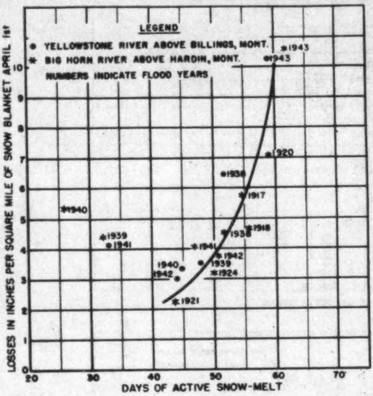

Fig. 5--Snow-melt runoff losses

eliminated from such a flood hydrograph by selection of the flood period. The end of the plains snow melt runoff is identifiable by a reduction in discharge with a constant or increasing temperature at the index station. When mountain snow melt is interrupted by a snow storm which produces appreciable depths over the plains, the ensuing plains snow-melt runoff is identifiable on the double-mass curve much the same as storm runoff. This method of separating mountain snow melt and storm runoff is not applicable to floods in which frequent storms have produced rainfall excess during the snow-melt period. It is necessary that there be at least two or three identifiable periods during the flood in which all runoff is due to snow melt alone.

Snow-melt runoff losses--The term "snow-melt runoff losses," as used herein, is the difference between the volume of water equivalent of snow of the ground on April 1, and the volume of snow-melt runoff during the corresponding mountain snow-melt flood period. It was used to obtain a correlation between the snow-melt runoff volumes of record on the Yellowstone River at Billings and the Big Horn River at Hardin, and the snow accumulated on the ground in these respective drainage basins. This correlation was then used to predict the runoff volume in the maximum possible mountain snow-melt flood. The snow-melt runoff losses are integrated values of irrigation diversions, transmission, evaporation and ground losses, all of which occur between April 1 and the end of the flood period. These losses also are affected by the precipitation accumulated in the snow blanket after April 1.

The volume of snow-melt runoff during each flood year considered was determined by the method described in the preceding paragraphs. The volume of water equivalent in the snow on the ground on April 1 in each basin, was obtained by plotting the snow stake and snow course measurements on topographical maps and then drawing isochions. The locations of the snow stakes and snow courses are shown on Figure 2. The total volume of water equivalent was then ascertained by planimetering the areas between isochions, and accumulating the computed volumes between isochions. Since the snow courses were scattered and not as representative as might be desired for this purpose, it was necessary to extrapolate the water-equivalent depths to higher elevations, and also to estimate the snow-line elevations. The total volumes of snow-melt runoff losses were computed for all important flood events by subtracting the estimated volume of snow-melt runoff

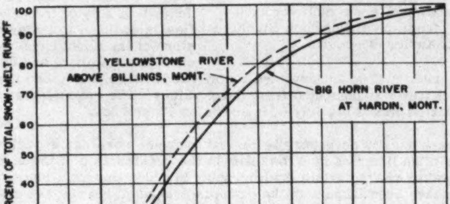

Fig. 6--Maximum snow-melt runoff

from the estimated volume of water equivalent of the April 1 snow blanket for each basin.

The factors included in the snow-melt runoff losses enumerated above are functions of time; the most important factors, irrigation diversion and ground losses, being functions of the length of time of the snow-melting period. A correlation was developed, therefore, between the snow-melt runoff losses and the length of the snow-melting period, by using the temperatures at index weather stations, Lander, Wyoming, and Livingston, Montana, respectively, for the Big Horn River and the Yellowstone River basins. Since the index weather stations are at fixed elevations, and the snow line in the mountains gradually ascends to higher elevations as melting continues, there is a gradually increasing difference in elevation between the index stations and the snow line. Consequently, the number of snow-melt days at the snow line must be determined from temperatures at the index station along a constantly increasing temperature line, the slope of which is indicative of the increasing temperature difference between the snow line and the index station. This constantly increasing temperature line at the index station, called the "active snow-melt line," is shown on Figure 3a, and the number of days producing snow melt is called "active snow-melt days." The active snow-melt line was determined for each of the snow-melt flood years used in these studies by comparing the flood hydrographs with the degree days at the index weather station, and locating the points on the degree-day curves (see Fig. 3a) where the sharp changes in temperature produced decided changes on the flood hydrographs (see Fig. 3c). A straight line was then drawn through the average of these points. It should be remembered that the degree-days at the index station are compared with the runoff three days later. The number of days on which the degree days at the index station exceeded those of the active snow-melt line, less the number of days on which the degree days dropped to within one or two degree days above the active snow-melt line, was considered as the number of active snow-melt days. There were usually a few days latitude in the number of active snow-melt days which could be obtained for each flood year, but, consistency in the choice of the days that did not produce runoff, made it possible to obtain a good correlation with the snow-melt runoff losses.

In order to give weight to the effect of areal distribution of the snow blanket on ground losses, the total volume of snow-melt runoff losses for each year considered was reduced to average depth in inches per square mile of area covered by the snow blanket on April 1. These values were plotted against their respective numbers of active snow-melt days as shown on Figure 5, and then an average curve was drawn. The losses per square mile in the Big Horn River and the Yellowstone River basins were of the same order of magnitude, and the curve on Figure 5 was used for determining the losses in both basins.

Maximum snow-melt runoff--It was necessary to convert the snow-melt runoff volume during the flood period to flood hydrographs at the Big Horn River and Yellowstone River gages. Snow-melt runoff volumes were computed for each consecutive 200 degree-day increment on the double-mass curves, similar to Figure 4, for nine flood events on each stream. The maximum runoff volume for each 200 degree day period was obtained, and the runoff volumes were the accumulated and reduced to a percentage of the total. The resulting values were plotted and smooth curves were drawn through the points. The resulting curves, presented on Figure 6, were used to obtain characteristic floods from their respective areas for various assumed temperature distributions, and predetermined volumes of runoff during the flood period.

References

CHURCH, J. E., Snow-study at Soda Springs near Donner Summit of Central Sierra, Nevada, pt. 3, pp. 77-90, 1943.

GARSTKA, WALTER U., Hydrology of small watersheds under winter conditions of snow-cover and frozen soil, Trans. Amer. Geophys. Union, pt. 4, pp. 838-871, 1944.

HORTON, ROBERT E., Infiltration and runoff during the snow-melting season, with forest cover, Trans. Amer. Geophys. Union, pt. 1, pp. 59-68, 1945.

LIGHT, PHILLIP, Analysis of high rates of snow-melting, Trans. Amer. Geophys. Union, pp. 195-205, 1941.

LINSLEY, RAY K., JR., A simple procedure for the day-to-day forecasting of runoff from snow-melt, Trans. Amer. Geophys. Union, pt. 3, pp. 62-67, 1943.

PAULSEN, JOSEPH B., JR., A method of calculating the effect of snow on runoff during rainstorms, Trans. Amer. Geophys. Union, pt. 1, pp. 15-20, 1944.

WILSON, W. T., An outline of the thermodynamics of snow-melt, Trans. Amer. Geophys. Union, pp. 182-195, 1941.

Corps of Engineers, U. S. Army,
Office of the District Engineer,
Denver District,
Denver, Colorado

(Manuscript received January 9, 1950; presented at the Twenty-Fourth Regional Meeting, Denver, Colorado, April 27, 1949; open for formal discussion until March 1, 1951.)

DISCUSSION

Bertram S. Barnes (7920 W. 9th Avenue, Lakewood 15, Colo.)--The determination of the daily discharge that would result from the melting of snow under design conditions is one of the more difficult problems in hydrology. The author has presented a logical and practical approach that should prove useful in routine design flood studies. It should also be an aid to further progress in this field.

In any study of the relation between temperature and snow melt it must be kept in mind that variations in humidity, wind velocity, and solar radiation will affect that relation. However, when practical problems are encountered, the only data that we can usually hope to obtain are temperatures at the nearest climatological station, runoff at some downstream gaging station, and a rough estimate of the water stored in the form of snow at the beginning of the melting season. There is a distinction between snow melt and effective snow melt, which is the part of the snow melt that reaches the stream. An equally sharp distinction, too often overlooked, must be drawn between the effective snow melt generated during a given period at the snow field and the volume of runoff observed in the stream during the corresponding period. The lag between temperature and river discharge can easily be determined by trial when plotting the double mass curve of temperature and runoff. It varies from a few hours to several days, in different basins. However, some of the water generated in a day's snow melt may not reach the river gage for many weeks. It is generally recognized that the apparent runoff per degree day increases as the season advances, and it is frequently assumed that the effective snow melt per degree day behaves in the same way. Data obtained from Fraser Snow Laboratory, however, indicate that the effective snow melt per degree day in St. Louis Creek basin is constant through the melt season until the snow is nearly gone, except as affected by other meteorological phenomena. Whether this is true in other basins is, as yet, undetermined.

The conventional procedures for determining snow-melt runoff from assumed temperatures consist, in general, of three main steps. They are stated crudely as follows: (1) determine the apparent runoff per degree day for various periods, from observed temperatures and stream discharge; (2) establish a relationship between the amount of snow on the ground and the apparent runoff per degree day; (3) adjust the maximum apparent runoff per degree day for the assumed, or design, amount of snow cover and apply it to the design temperature sequence.

The author's method employs the same underlying principles and can be expressed in a comparable way. Consider each observed sequence of melting temperatures as a series of increments or brackets representing 200 degree days each, the brackets being numbered consecutively from the start of the snow-melt season, each year. The basic procedure may then be outlined in the following steps: (1) For each numbered bracket of temperatures, find the greatest volume of corresponding apparent runoff that occurs in any of the years of record. Accumulate these values in the order of their bracket numbers, and express the subtotals as per cent of the total. Plot the percentages against the cumulative degree day values. Draw through the plotted points the curve of maximum snow melt runoff. (2) Determine the number of active snow-melt days in each year of record and relate it to the computed loss in inches from the snow available at the start of the melt season. Apply this relation to the assumed snow cover and temperature sequence of the season of the design flood, and compute the corresponding seasonal runoff. (3) Apply the curve of maximum snow-melt runoff to the cumulative degree day values computed from the design temperature sequence This will give cumulative daily runoff in per cent of the seasonal total. Determine the daily increments, in per cent, and apply them to the computed seasonal runoff in cfs-days to obtain the mean daily discharge in cfs.

Although this procedure embodies the three basic steps already in common use, it departs from the conventional methods in four important particulars. First, it makes use of the entire seasonal record instead of selected periods. Second, it provides for the application of lower values of the apparent runoff per degree day to those parts of the design season to which lower values are appropriate. Third, the total runoff of the design snow-melt season is obtained by direct computation and the daily discharge values are adjusted to produce that volume of runoff. Fourth, the adjustment of the heat-runoff relation for amount of available snow takes place automatically when per cent of runoff is being reduced to actual discharge.

Of the several assumptions implied in the author's procedure, two in particular are fundamental to the method. They may be stated as follows: (1) With a given total volume of snow-melt runoff for the season, the maximum apparent runoff per degree day at any time is solely a function of the number of degree days already accumulated at that time. (2) With a given number of degree days already accumulated, the maximum apparent runoff per degree day is a fixed percentage of the total volume of snow-melt runoff for that season. The first of the two assumptions just given has

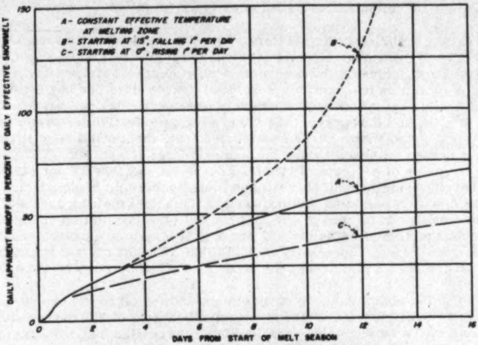

Fig. 7--Effects of rising and falling temperatures upon apparent runoff coefficient

been used extensively in other procedures, and little question regarding its accuracy seems to have been raised. Double-mass curves of temperature and runoff characteristically show a progressive increase in the apparent runoff per degree day as the season advances. This effect has been attributed variously to the gradual ripening of the snow, the increase in the effective width of the basin as the melting zone ascends, a widening of the melting zone as the temperature increases, and other causes. It has been the writer's belief that the progression of values is caused almost entirely by the gradual building up of the mass of residual flow from the whole series of daily events of snow melt. According to this assumption, the apparent heat-runoff factor should be considered a function, not of accumulated degree days alone, but of degree days and time.

An opportunity for a partial test of the writer's hypothesis was afforded by the discharge record of St. Louis Creek near Fraser, Colorado. This creek has a basin area of only 33 sq mi and the daily peaks of snow-melt runoff are well separated. Phyllis Peasley and W. U. Garstka have isolated the hydrographs of snow-melt runoff generated on 23 consecutive days. The writer combined several of the events into a composite unit graph of one day's snow-melt runoff and reduced it to a volume of 100 units of runoff. The ordinates at one-day intervals were then accumulated to obtain an S-curve hydrograph, or hydrograph of discharge continuously generated at a constant rate. This is the hydrograph that would be produced by a uniform temperature sequence of one degree day per day, assuming that runoff is generated at the fixed rate of 100 units per degree day. It has been expressed in terms of apparent runoff per degree day and plotted as Curve A of Figure 7. Note that 16 days are required to build the apparent runoff per degree day up to 71 per cent of the "true, or generated, amount.

The composite unit graph was applied to two other assumed temperature sequences. The first of these started at 15 degree days for the first day and diminished one degree per day. The second started at one degree day on the first day and increased one degree per day for 15 days. The two hydrographs were reduced to apparent runoff per degree day and plotted as Curves B and C, respectively, of Figure 7. Curve B shows the manner in which a falling temperature increases the apparent heat-runoff factor. In double mass curves of heat and runoff, this phenomenon produces a change in slope that can be mistaken for the effect of runoff from rainfall. Actually, small parts of the two irregularities adjusted by the author in his Figure 4 probably resulted from falling temperatures. The ordinates of Curve B Figure 7, will become infinitely great when the temperature falls below freezing, on the 16th day. If that condition continued for several days an extremely high value of the apparent runoff for the corresponding 200 degree-day bracket might be obtained. By the author's procedure, strictly followed, such a value would probably be selected as the maximum for that bracket and used in constructing the curve of maximum snow-melt runoff. However, since a drop in temperatures during the melt season will usually be followed by a corresponding rise before the snow is gone, a study of the temperature record may provide the means of adjusting the effects of rising and falling temperatures on the double-mass curve itself, before picking off the 200 degree day volume increments. The writer has found that a plotting, on the mass curve sheet, of daily temperatures against accumulated runoff volumes is useful for this purpose.

The 15-day falling and rising temperature sequences have been converted to the dimensions of the author's curve of maximum snow-melt runoff and plotted in Figure 8 as Curves B and C, respectively. A uniform temperature sequence of eight degree days per day for 15 days has been plotted as Curve A (8°), a uniform sequence of three degree days per day for 40 days has been plotted as Curve A (3°), and a uniform sequence of one degree day per day has been plotted as A (1°). Curves A (8°), B, and C represent the same average effective temperature, 8°. It is evident from the plotting that a composite curve constructed from them could be applied with comparatively little error to any design sequence having the same average temperature. Curve A (3°), however, gives much higher values of per cent of runoff. Therefore, any upward adjustment of the author's curve of maximum snow-melt runoff should make it applicable to a cooler design season instead of a warmer one, unless it be assumed that the area of the actual melting zone would be enough greater during the warmer season to offset the effect of the faster accumulation of degree days. The writer believes that the assumption of higher runoff per degree day in a warmer season is unwarranted, although the data from Fraser Laboratory indicate that an unusually warm single day may produce ripening over a larger area and increase the amount of effective snow melt on the following day.

The ordinates of the author's curve of maximum snow-melt runoff are accumulations of the maximum observed runoff increments for successive brackets of 200 degree days, expressed in per cent of the sum of the increments. It is important to realize that adjustment of the curve will not change the seasonal volume of runoff computed from it; it will only change its distribution in time. Therefore, the author's use of the maximum runoff increment observed in each bracket instead of the mean does not necessarily result in safer values for design purposes - it may fully as often have the opposite effect. The use of the minimum increments would be just as logical. If the mean increments provided reasonably consistent values, a curve obtained from them would be much more reliable because it would be based on several times as much data. The most likelv causes of deviation of the observed values of runoff for any given bracket may be stated as follows: (1) periods of rising or falling temperatures immediately preceding the bracket, or within it (the effect is illustrated in Figure 1); (2) different average temperatures for the various melting seasons (the effect is illustrated in Figure 2); (3) different amounts of snow available within the active melting zone (this affects the area of active melt because with a heavier snow cover the snow line will lag farther downhill from the 32° isotherm); (4) changing elevation of the active melting zone, the effective temperature having been computed for a fixed elevation; (5) possible variation of the area of active snow melt as the snow line recedes, on account of varying width or slope of the basin; (6) possible variation of the amount of water lost by retention.

The writer suggests that the deviations be studied and that various methods of correcting them be tried. If the spread of the observed apparent runoff values for each bracket can be reduced to a reasonable amount, the mean values should produce a consistent curve of maximum snow-melt runoff. A possible method of adjusting the double-mass curve for the effects of continued rise and fall of temperature has already been discussed. The effect of different average temperatures in different seasons can probably be eliminated by relating the amount of the increment to the average temperature from the start of the melt season to the end of the increment and extending the relation to the average temperature of the corresponding part of the design sequence. The effect of different amounts of snow cover might be eliminated in a similar way, at the same time, perhaps by the use of a double correlation of temperature and seasonal runoff with the runoff increment. A better method of correcting for the amount of snow cover might be to reduce each observed increment to per cent of its own seasonal runoff before the averages are determined. The determination of the actual effective temperature at the melting zone has always been a difficult problem. The author's line of active snow melt appears to be an excellen

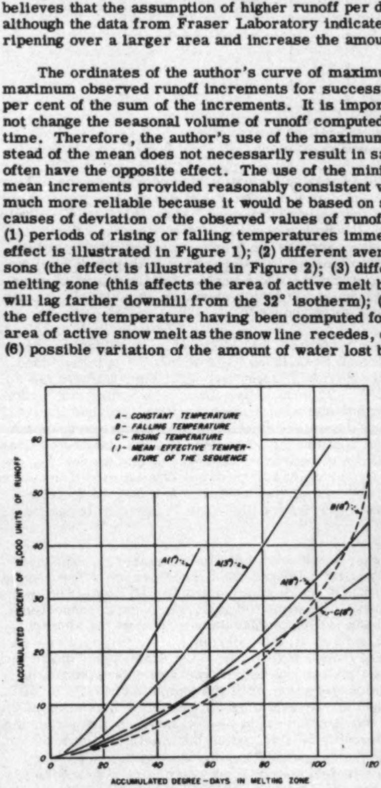

Fig 8--Effect of mean temperature upon curves of snow-melt runoff approach, although he uses it for a different purpose. The writer suggests that the position of the line for each year might be related to the total snow-melt runoff for the year and adjusted on the basis of that relation. It should then provide a variable correction for use in deriving the true effective temperatures from those observed at the climatological station. The position of the line for the design season should be predictable. The adjustment of temperatures even to a fixed elevation near the center of the general snow-melt area, will greatly increase the sensitivity of the double-mass curve to temperature fluctuations and permit more accurate adjustments of the curve. When the temperatures have been observed below the basin level and used without correction as the author has done, the smoothness of the mass curve may create a false sense of security. Also, by the author's procedure, degree days are computed for periods when no effective temperatures occurred at the elevation of the snow field.

The effects of the shape of the basin boundary and variations in the slope of the ground are difficult to determine. The writer believes that in most cases they can be disregarded. It seems likely that when these effects exist, they will be partly eliminated in the process of adjusting the runoff increments for the amount of seasonal runoff. The data from Fraser Laboratory indicate that in St. Louis Creek basin the amount of runoff generated per degree day is subject to a slow oscillation as air masses of different moisture content cross the basin, but there is clearly no seasonal progression of the value until the snow is nearly gone.

Variations in the amount of water lost by retention may be significant is some basins, or in some seasons. The limited data from St. Louis Creek do not indicate the presence of this effect. It is reasonable, however, to expect that if the first snow fell upon cold, dry soil and no material amount of thawing occurred during the winter, the average runoff per degree day would be noticeably reduced. This effect, again, would be partly eliminated in the adjustment of the runoff increment for variation of the amount of seasonal runoff. However, if the melting zone progressed from an area of porous material to one that was less pervious, or vice versa, there would be deviations of the runoff increments in certain brackets that might be difficult to adjust.

The writer believes that it is possible to eliminate enough of the causes of deviation so that the adjusted values of apparent runoff for each 200-degree-day bracket, expressed as per cent of the seasonal runoff, could be averaged with confidence. The resulting curve of maximum snow-melt runoff can be tested for plausibility by the consistency of the plotting and possibly by its shape. In Figures 7 and 8 of this discussion the amount of effective snow melt per degree day is assumed to be constant. Curve A of Figure 7 is essentially an S-curve hydrograph, constructed by accumulating the ordinates of the unit graph. Curves A of Figure 8 may be considered as accumulations of the ordinates of the S-curve hydrograph. They are therefore, curves of continuously increasing slope. The unit graph could be reconstructed from the second tabular differences obtained from either of these two curves or from the first tabular differences of the S-curve hydrograph. However, a unit graph cannot be constructed from the second tabular differences of the curve presented in Figure 6 of the author's paper, because of the presence of an inflection in the curve. This could be caused by an actual variation in the amount of effective snow-melt per degree day in Big Horn and Yellowstone basins or by the author's use of the maximum observed runoff increments, which presumably are more erratic and inconsistent with one another than the mean values.

A study of the curves of Figure 8 indicates that a curve of maximum snow-melt runoff similar to the author's can be applied with reasonable accuracy to any temperature sequence having the given mean temperature, but that it is not applicable to warmer or cooler sequences. When applied to warmer sequences, it will yield excessive discharge values. It seems important that before the curve is constructed an attempt should be made to adjust all of the observed runoff increments to the mean temperature of the design sequence. If it is necessary to make the curve applicable to sequences having different mean temperatures, its abscissae might be expressed in a function of both degree days and time.

In comparison with our limited understanding of the relation of runoff to rainfall, our knowledge of the laws of snow-melt runoff is meager, indeed. The author's novel approach to the problem of the design snow flood should provide a stimulus to further study.

Transactions, American Geophysical Union Volume 31, Number 5 October 1950

LAWS OF SOIL MOISTURE

L. A. Richards

Abstract--Observed regularities in the processes connected with the flow and distribution of water in soils may, if they are sufficiently general, be referred to as laws of soil moisture. The Darcy equation which expresses the proportionality between transmission velocity and the driving force for water in saturated soils is one such regularity that is commonly referred to as a law. Another regularity that applies without exception whenever outflow of free water occurs from soil, is of the nature of a boundary condition, but is here proposed as a law; namely, "Outflow of free water from soil will occur only if the pressure in the soil water exceeds atmospheric pressure." Examples for the application of the outflow law are cited and discussed.

Progress in science and engineering has been based largely on the discovery and use of regularities that occur in the processes of nature. The recognition, verification, and concise statement of these regularities constitute one of the prime objectives of organized experimentation and research. Sometimes we seem to get lost in our forest of experimental facts. When faced with the task of correlating and understanding a maze of seemingly unrelated observations it is comforting to consider the simplifications brought to chemistry by the laws of stoichiometry and the atomic table. It is helpful to think of the tremendous advances made possible in electrical engineering by the Maxwell equations and the brief and concise laws named after Coulomb, Ohm, Faraday, and Ampere.

The important relation of soil moisture to man's welfare has stimulated continuing investigations in agriculture, geology, soil mechanics, ceramics, and allied fields. As a result, a multiplicity of observations and facts have accumulated. Unfortunately these are not very well correlated or understood. Few regularities in soil-moisture processes have been discovered and clearly formulated. It is the purpose of this paper to promote and encourage this process by reference to two general principles. One of these is widely recognized and commonly referred to as a law, the other deserves wider recognition and use by students and investigators and perhaps deserves to be dignified by designating it as one of the laws of soil moisture.

Darcy's Law--DARCY [1856] reported that the rate of flow of water through sand filter beds was described by the equation

$$Q = ks\ (H + e)/e \quad \ldots\ldots \quad (1)$$

for the case where the pressure under the filter is equal to the weight of the atmosphere and where Q is the volume of water passed in unit time, s is the area of the bed, e is the thickness of the bed, H is the height of the water on the filter, and k is a coefficient depending on the nature of the sand. As stated, this equation applied to steady linear flow through saturated sand. Water motive forces arising from both gravity and the pressure gradient are taken into account. If we define the transmission velocity $v = Q/s$ and the hydraulic gradient $i = (e + H)/e$ we have

$$v = ki \quad \ldots\ldots \quad (2)$$

which is a vector equation applying to three-dimensional flow in isotropic media and is often taken as the general form of the Darcy flow law. The equation expresses the fact that the flow rate is proportional to the water motive force. MUSKAT [1937] has reviewed the conditions under which the law is valid and has given an excellent summary of methods and examples for the application of the law to the solution of practical flow problems. Numerous scientists and engineers throughout the world have used this law as a basis for a rational analytical attack on problems involving the flow of water in saturated soils.

Our definitions and methods for measuring permeability are based directly on the Darcy law. Numerous permeability units for soils have been considered [MUSKAT, 1937; RICHARDS, 1940]. The simple Darcy coefficient k in (1) and (2) is most commonly used in agricultural soils work. The large and rapidly changing effects produced by the interaction of colloidal and organic material and the quality of water make it impractical to take into account small effects such as are due to change in viscosity with temperature. It is seen that k, the permeability, is equal to the transmission velocity when the hydraulic gradient is unity, that is, when the driving force is equal to 980 dynes/gram.

It is surprising, in view of the long and useful history of the Darcy law, that some soil scientists and engineers are even yet reporting laboratory permeability data on the effect of various treatments on the water-transmitting properties of soils under conditions where the hydraulic gradient is unmeasured and unreported.

Practical applications of agricultural research are made in the field, and here the transmission velocity is a more useful, usable quantity than permeability. Permeability can be measured on samples which are transported to the laboratory. The hydraulic gradient which operates in the field, however, is determined by the characteristics and boundary conditions for the whole profile. Consequently, the hydraulic gradient is a soil moisture factor that generally must be measured in the field. Field methods for appraising both permeability and the hydraulic gradient are under active development at the present time and the Darcy law is a unifying and simplifying basis for progress with this work [PILLSBURY and CHRISTIANSEN, 1947; KIRKHAM and van BAVEL, 1948].

Outflow law--It has been recognized by some investigators that a special boundary condition for the pressure of water in soil must be met before water outflow will occur. A general statement of this principle which is here proposed as a law of soil moisture might be phrased as follows: "Outflow of free water from soil occurs only if the pressure in the soil water exceeds atmospheric pressure."

This relation is so simple and obvious as scarcely to need formulation and proof. Newton's first and third laws of motion also appear to be almost obvious, and yet these simple laws, when logically applied, can lead to conclusions which may not be obvious.

The outflow law may be simple demonstrated with a wick siphon as shown in Figure 1. Wet a piece of clean cotton cheese cloth with water and crumple it into a porous roll about three cm in diameter and 20 cm long. Hang the roll over a rod and mount a beaker with the water at the same level as the free end of the wick as shown at A. Surface tension action will cause water in the porous wick to come to pressure equilibrium with water in the beaker. Water at each level in the right hand side will have the same pressure as water in the left hand side of the wick at the same level. Thus water at the free end of the wick will be at atmospheric pressure and no outflow will occur. If the beaker is raised slightly as shown at B, pressure in the water throughout the wick will be raised and drops will begin to form and continue to fall from the free end of the wick.

The outflow law applies to the entry of water into underground tile drains and drainage of

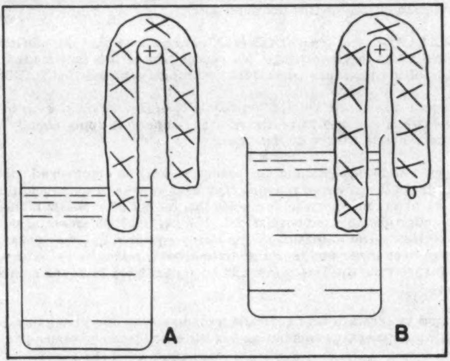

Fig. 1--Demonstration of the moisture outflow law with a wick siphon water from lysimeters and soil pots used for growing plants. The law applies to the anomalous field drainage case where a shallow soil layer of fine texture is underlain with coarse material. Instead of providing improved drainage, the abrupt transition zone from fine to coarse texture acts like a perched water table because the soil moisture at the lower boundary of the fine-textured layer must come practically to atmospheric pressure before it will move into the coarse material. ZUNKER [1930] has discussed this soil moisture phenomenon.

Applications of the outflow law--Lysimeters constitute an important case for the application of the outflow law. RICHARDS, NEAL and RUSSELL [1939] used tensiometers to study moisture relations in the lysimeters of the Soil Conservation Service Experiment Station at Clarinda, Iowa, and state, "Before free water will drain away from a lysimeter it is necessary that the pressure in the soil water at the base of the column shall approach atmospheric pressure." In the same volume, RICHARDS and JOFFE [1939] reported laboratory experiments with soil columns where drainage to a conventional lysimeter funnel and drainage to a tension plate that was used to simulate deep soil percolation were compared. They recognized and stated the zero pressure (zero tension) outflow boundary condition. Earlier statements of the outflow law as applied to lysimeters have undoubtedly been made and the writer would appreciate having these earlier statements called to his attention.

KOHNKE, DREIBELBIS, and DAVIDSON [1940] made a survey of the construction and use of lysimeters and state, "The greatest functional error in all three types of lysimeters probably occurs at the boundary of the lysimeter soil and the air beneath it. When the gravitational water reaches this point it will have to overcome the resistance set up by surface tension before it can leave the soil." These authors indicate that lysimeters have been used for experimental work for more than 260 yr and cite nearly 500 references to publications on lysimeter work. And yet it is only recently [COLMAN and HAMILTON, 1947] that this outflow boundary condition has been taken into account. Anomalous results obtained with different types and different depths of lysimeters in response to different cropping and rainfall conditions can often be explained if the outflow boundary condition and its effect on the moisture regime are clearly understood.

When the outflow law is more generally recognized it is expected that lysimeters designed for hydrological studies will embody porous structures such as proposed by RICHARDS and JOFFE [1939], WALLIHAN [1940], and COLMAN [1946], so as to simulate more closely moisture conditions in the natural profile.

Soil pots which are used in varying sizes for the experimental and commercial growing of plants are, like lysimeters, subject to the outflow law if sufficient water is applied so that drainage occurs. The moisture regime is quite different from field conditions and accounts for the fact that liberal admixtures of sand and peat are made to potting soil by commercial growers in order to increase the size of the soil pores. In view of the outflow law it is clear that special precautions with irrigation are required to avoid abnormal plant responses caused by water logging if tests are to be made with small lots of fine textured soils.

SHAFFER, WALLACE, and GARWOOD [1937] have shown that the outflow law applies at the periphery of porous media in a centrifuge and recognition of this fact made it possible to obtain a theoretical solution of the moisture equivalent centrifuge problem [RICHARDS and WEAVER, 1944].

While the present discussion relates primarily to soils, we must keep in mind the unity of all science. The two laws of soil moisture stated above appear to apply equally well to any liquid in any porous medium which is wetted by the liquid.

Additional laws--Additional laws of soil moisture will be discovered and formulated as our knowledge of soils increases. Some readers may wish now to propose additional laws. For example the movement of water in the root zone for soils that do not have water tables, permanent or temporary, takes place under unsaturated conditions. The original statement of the Darcy law did not include unsaturated flow. The extension of the Darcy equation to cover unsaturated flow for the isothermal case has been made and is in the state of what might be called a working hypothesis. Perhaps at some future time the Darcy law can be generalized to cover both saturated and unsaturated flow conditions.

The complicated interrelation of heat and moisture transfer in unsaturated soil can probably be expressed in simple general terms but as yet little progress has been made in this direction

Acknowledgment--This is a contribution from the U. S. Regional Salinity and Rubidoux Labotories, Bureau of Plant Industry, Soils and Agricultural Engineering, Agricultural Research Ad-

ministration, U. S. Department of Agriculture, Riverside, California, in cooperation with the eleven Western States and the Territory of Hawaii.

References

DARCY, HENRY, Les fontaines publique de la ville de Dijon, Paris, Dalmont, 1856.

COLMAN, E. A., A laboratory study of lysimeter drainage under controlled soil moisture tension, Soil Sci., v. 62, pp. 365-382, 1946.

COLMAN, E. A., and E. L. HAMILTON, The San Dimas lysimeters, U. S. Dept. of Agr., California Forest and Range Exp. Sta. Research Notes no. 47, pt. 1 and 2, pp. 1-33, 1947.

KIRKHAM, DON, and C. H. M. van BAVEL, Theory of seepage into auger holes penetrating below a water table, Soil Sci. Soc. Amer. Proc., v. 13, 1948.

KOHNKE, HELMUT, F. R. DREIBELBIS, and J. M. DAVIDSON, A survey and discussion of lysimeters and a bibliography of their construction and performance, U. S. Dept. of Agr. Misc. Pub. 372, pp. 1-68, 1940.

MUSKAT, MORRIS, The flow of homogeneous fluids through porous media, McGraw-Hill, New York, 1937.

PILLSBURY, A. F., and J. E. CHRISTIANSEN, Installing ground-water piezometers by jetting for drainage investigations in the Coachella Valley, California, Agr. Eng., v. 28, pp. 409-410, 1947.

RICHARDS, L. A., O. R. NEAL, and M. B. RUSSELL, Observations on moisture conditions in lysimeters, II, Soil Sci. Soc. Amer. Proc. v. 4, pp. 55-59, 1939.

RICHARDS, L. A., Concerning permeability units for soils, Soil Sci. Soc. Amer. Proc., v. 5, pp. 49-53, 1940.

RICHARDS, L. A., and L. R. WEAVER, Moisture retention by some irrigated soils as related to soil moisture tension, J. Agr. Res., v. 69, pp. 215-235, 1944.

RICHARDS, S. J., and J. S. JOFFE, Percolation and absorption of water as they relate to infiltration in Collington sandy loam, Soil Sci. Soc. Amer. Proc., v. 4, pp. 94-99, 1939.

SCHAFFER, R. V., J. WALLACE, and F. GARWOOD, The centrifuge method for investigating the variation of hydrostatic pressure with water content in porous materials, Trans. Faraday Soc., v. 33, pp. 723-734, 1937.

WALLIHAN, ELLIS F., An improvement in lysimeter design, J. Amer. Soc. Agron., v. 32, pp. 395-404, 1940.

ZUNKER, E., Das Verhalten des Bodens zum Wasser, Handbuch der Bodenlehre (E. Blank), v. 6, p. 125, 1930.

U. S. Regional Salinity and Rubidoux Laboratories,
Riverside, California

(Manuscript received March 20, 1950; presented at the Thirty-First Annual Meeting, Washington, D. C., May 1, 1950; open for formal discussion until March 1, 1951.)

DISCUSSION

E. C. Childs (University of Cambridge, Cambridge, England)--I am in general sympathy with Richards' thesis, and with him, deplore a current tendency to confuse permeability with an observed infiltration rate in unspecified and unreproducible conditions. I should, however, prefer to express Darcy's law in the three-dimensional form

$$v = -k \operatorname{grad} \phi$$

where ϕ is the hydraulic potential, grad ϕ reducing to Richards' i for one-dimensional flow. My preference is no doubt due to my greater concern with drainage problems which are rarely one-dimensional [CHILDS, 1943, 1945a, 1945b, 1946, 1947a, 1947b, 1948; CHILDS and GEORGE, 1948]. For the rest, I should like to discuss one section only of RICHARDS' paper, that dealing with unsaturated soil. I do not think that Darcy's law itself needs to be generalized; we just have to recognize that the permeability so defined is a function of moisture content (as indeed was demonstrated by Richards' own pioneering work) a function which has received a satisfactory formulation in my laboratory [CHILDS and GEORGE, 1948]. It may then be convenient and possible for some problems to express the rate of water movement in terms of moisture content gradient, that is, by a diffusion equation) since a given moisture profile implies both a known potential gradient and permeability at a given point [CHILDS and GEORGE, 1948]. The complete solution of the problem of water moving down a moisture profile then becomes a matter of solving the problem of non-linear diffusion, perhaps complicated by hysteresis. It seems to me that it is along these lines that progress appears most promising.

References

CHILDS, E. C., The water table, equipotentials and streamlines in drained land, I, Soil Sci., v. 56, pp. 317-330, 1943.

CHILDS, E. C., The water table, equipotentials and streamlines in drained land, II, Soil Sci., v. 59, pp. 313-327, 1945a.

CHILDS, E. C., The water table, equipotentials and streamlines in drained land, III, Soil Sci., v. 59, pp. 405-416, 1945b.

CHILDS, E. C., The water table, equipotentials and streamlines in drained land, IV, Soil Sci., v. 62, pp. 183-192, 1946.

CHILDS, E. C., The water table, equipotentials and streamlines in drained land, V, Soil Sci., v. 63, pp. 361-376, 1947a.

CHILDS, E. C., A note on Dr. Yngve Gustafsson's paper "Untersuchungen über die Strömungsverhältnisse in gedräntem Boden" Acta Agr. Suecana, v. 2, pp. 353-356, 1947b.

CHILDS, E. C., Discussion in Proc. 2nd. Int. Conf. on Soil Mechanics and Foundation Engineering, v. 6, pp. 150-153, 1948.

CHILDS, E. C., and N. C. GEORGE, Soil geometry and soil water equilibria, discussions of the Faraday Society, v. 3, pp. 78-85, 1948.

E. A. Colman (California Forest and Range Experiment Station, Berkeley, Calif.)--In order to emphasize the significance and implications of the outflow law which Richards has proposed, I should like to mention some of the information we have obtained from the San Dimas lysimeters [COLMAN and HAMILTON, 1947]. When the large lysimeters of this installation were built we did not cover the tank bottoms with a layer of gravel, recognizing that such a layer would not insure drainage of the soil above to field capacity. Instead the tanks were filled entirely with uniform soil. Later we placed tensiometers in the soil at the seepage outlets (the soil is six feet deep) and measured moisture tensions before, during, and after seepage periods. Over several years of observations we found, as was to be expected, that seepage did not start until moisture tension dropped to zero in these tensiometers, nor did the tension increase again until seepage had stopped.

During the period of these observations we also had tensiometers placed with their porous cups at various levels within the lysimeter soil. These tensiometers showed that during periods of seepage, zero moisture tension was maintained in the soil to a height of three feet above the seepage plane. This suggested that the lower half of the soil in these tanks was virtually saturated through a considerable part of the winter rainy season, a condition which is far from normal for this soil and the vegetation studied, in their natural state.

These and similar observations have led us to believe that lysimeters must be equipped with drainage control devices if results obtained from them are to have application beyond the lysimeters themselves.

Willard Gardner (Utah State Agricultural College, Logan, Utah)--It is to be expected that the curvature of the air-water interface at the bottom of the right-hand part of the tube represented in A of Figure 1, would be zero and the pressure throughout the tube would not be disturbed by placing this end of the tube also in water at the same level as that in the beaker. This should represent the same state of equilibrium as before, the force per unit volume due to the pressure gradient being balanced by the pull of gravity per unit volume.

The water at the end of the tube on the right of B would tend to develop a convex curvature with a slight increase in pressure sufficient to keep the water in the tube even though the interface at this end were slightly below the level of the water in the beaker. The interface, if curved, does therefore have a slight influence on the state of equilibrium. However, were this interface also removed by dipping the end into free water at a level lower than that in the beaker, the water would of course move out of the beaker through the tube however small the difference in elevation may be so long as it does not vanish completely. There exists also a small pressure gradient in the atmosphere that should not be overlooked but it would modify the problem very little to reduce the atmospheric pressure to zero.

Can we not infer all that this proposed outflow law implies? We may infer for example from Newton's second law that if a particle moves in the direction of a constant force that is applied to it the distance it travels is a quadratic function of the time, but we would not be inclined to regard this as a new law.

Don Kirkham (Iowa State College, Ames, Iowa)--In an article "Some tests of the diffusion theory, and laws of capillary flow in soils" [Soil Sci., v. 67, 1949], C. L. Feng and I report data which show that the horizontal capillary flow of water from a free water source into air-dry soil takes place in accordance with the laws $Q = At^{1/2} + a$ and $X = Bt^{1/2} + b$, where Q is the quantity of water absorbed in time t, X is the distance of advance of the wet front and A, B, a, and b are constants, the latter two for practical purposes zero. The equations were designated laws because of their simple nature and because Richards had pointed out, soil moisture laws, if we have them, should be announced. Whether or not the expressions should be called "laws," we are still aware that a more important expression, a law for capillary flow, remains to be discovered. It is hoped this law would relate simply the rate of water movement, moisture content, and driving gradient, all, over a wide range of moisture content. As Richards indicates this law must reduce to Darcy's law when the soil is water-saturated. The law will also have to conform to the laws given above.

Helmut Kohnke (Purdue University, Lafayette, Indiana)--I am glad to see the outflow law so clearly stated by Richards. It may be added that outflow begins at the threshold between tension and pressure. I believe the first time the outlfow law was taken into account in the design of lysimeters was 1936 at the North Appalachian Watershed Experiment Station near Coshocton. A depth of eight feet was chosen to provide adequate moisture tension in the main root zone. Shallow lysimeters with porous bottoms held at certain tensions have the disadvantage of removing water from the soil body that cannot climb up again in vapor or liquid form as it would under field conditions. It seems that a considerable depth is a prerequisite for future lysimeters, The wick experiment as demonstration of the outflow law is extremely clever and simple. I wonder why Darcy's law has not also been expressed in the form of a sentence in this paper as the outflow law has been.

M. R. Lewis (Bureau of Reclamation, Washington, D. C.)--The phenomenon discussed by Richards furnishes an excellent example of delay in formulating the laws governing soil moisture. WIDSTOE and MCLAUGHLIN [1912] found that after free drainage ceased, more moisture remained in a one-foot column of soil than in the upper foot of a three-foot column. VEIHMEYER, ISRAELSON, and CONRAD [1924] found that the deeper the soil column used in the determination of the moisture equivalent the less the average moisture content at the end of equal periods of exposure to the same centrifugal force. PIPER [1933] and others have noted that the field capacity or specific retention of soils cannot be determined by merely draining short columns of soil resting on coarse sands or screens. Undoubtedly such manifestations have been noted over a long period but the law was not clearly stated, so far as the writer knows, before the 1939 reports cited. About 1918, W. G. Sloan and the writer had occasion to make an interesting demonstration of the phenomenon. It was denied that a certain irrigation canal on high land was losing water by seepage and the denial was backed up by a showing that water did not drip from the roof of an unlined horizontal opening a few feet below the bed of the canal. To counteract this evidence a rectangular hole was cut in a strip of blotting paper and one end of this was placed in a tumbler of water while the other end, with the hole, was bent down on the outside. Soon water dripped from the end but none crossed the open space.

There is great need for a clearer understanding of the similarities and dissimilarities of flow in saturated and unsaturated soils and it is to be hoped that progress will be made in developing the applicable laws.

References

PIPER, A. M., Notes on the relation between the moisture equivalent and the specific retention of water-bearing materials, Trans. Amer. Geophys. Union, v. 14, pp. 481-487, 1933.

VEIHMEYER, F. J., O. W. ISRAELSON, and J. P. CONRAD, The moisture equivalent as influenced by the amount of soil used in its determination, Calif. Agr. Exp. Sta., Tech. Paper 16, pp. 1-16, 1924.

WIDSTOE, J. A., and W. W. McLAUGHLIN, The movement of water in irrigated soils, Utah Agr. Exp. Sta., Bull. 115, 268 pp., 1912.

A. F. Pillsbury (University of California, Los Angeles, California)--This paper serves the admirable purpose of pointing up simple, fundamental, soil-water relationships. Question might be raised as to whether or not the Darcy equation should be called a law because it holds only for laminar flow, and because of the problems related to unsaturation. Also, BUCKINGHAM [1907] appears to be the first to recognize the outflow law, and VEIHMEYER, ISRAELSON, and CONRAD [1924] recognize the saturated condition of the outer face of moisture equivalent samples.

References

BUCKINGHAM, EDGAR, Studies on the movement of soil moisture, USDA Bur. Soils, Bull. 38, p. 29, 1907.

VEIHMEYER, F. J., P. W. ISRAELSEN, and J. P. CONRAD, The moisture equivalent as influenced by the amount of soil used in its determination, Univ. Calif., Coll. Agr., Tech. Paper 16, 1924.

S. J. Richards (University of California, Riverside, Calif.)--By suggesting the use of the word laws to name the generalizations discussed in its report, the committee may be generating smoke which will hide the fire of the real purpose for writing the report. For example, many workers will prefer to call Equation (2) the Darcy Equation when applying it to unsaturated flow. However, the name used should be subordinated to the idea involved. The ideas suggested are fundamental and useful. They should be stated in terms that will give the greatest distribution among workers.

The outflow law as stated relates only to the moisture close to the horizontal plane at which the outflow boundary occurs. In the discussion of the application the suggestion is made that moisture in soil layers above the location of the outflow is influenced, which is certainly the case. Soil moisture above an outflow boundary may be under a tension, T, equal to the height of the soil, h, above the boundary. (T is here measured in length units of equivalent soil solution.) For the case when the soil moisture is draining downward to an outflow, then the tension at any elevation must be less than the vertical height measured to the outflow boundary.

L. A. Richards (U. S. Regional Salinity and Rubidoux Laboratories, Riverside, Calif.)--The reviewers' comments make distinct contributions toward the appraisal and interpretation of the contributed paper and scarcely need a summarizing statement. However, a few points brought out in the discussion will be briefly mentioned.

Equation (1) was developed by Darcy for a linear, one-dimensional flow case and Eq (2) was developed in the above paper by substituting new symbols in Eq (1). It was not the writer's intention, however, to imply, as Childs apparently does in his comments that Eq (2) does not apply to the three-dimensional case. CHRISTIANSEN [1943] and REEVE and JENSEN [1949] use a flow equation equivalent to Eq (2) for describing non-linear, ground-water, flow patterns under field conditions. The hydraulic gradient i in Eq (2) may be taken as identical with grad ϕ in Childs' equation. The negative sign signifies only a difference in an arbitrary convention of nomenclature between physics and engineering.

The points raised by Gardner are certainly pertinent. Back pressure from positive curvatures of the air water interface will usually exist and will influence outflow. The negative form used in the above statement of the outflow law, namely, "Outflow of free water from soil will occur only if the pressure in the soil water exceeds atmospheric pressure," takes the back pressure effect into account. The effect connected with the pressure gradient in the atmosphere as mentioned by Gardner does not appear to apply if atmospheric pressure mentioned in the above statement is considered at the point of outflow.

The last question raised by Gardner is quite appropriate. What criteria should be satisfied by an observed, formulated and verified regularity in the processes of nature before it may properly be designated as a law? If the relation $f = ma$ can be inferred from the principle of least action, should we cease to refer to this equation as a law? Are the empirical relations mentioned by Kirkham similar to the examples of the quadratic function mentioned by Gardner?

Because the Darcy equation does not hold for turbulent flow and has not been demonstrated to hold for unsaturated flow, Pillsbury and Richards question whether it should be referred to as a law. Following the same reasoning would these men say that since a relativity correction must be applied at high velocities, $f = ma$ should not be called a law?

Certainly these are questions for which there is no brief answer. Obviously it was the objective of the contributed paper to state the outflow boundary condition in clear, concise form for pedagogic purposes. This important relation which has many practical applications does not appear to be widely familiar to soils workers. Whether ultimately it will be referred to as a law or simply as a boundary condition will have little effect on its usefulness. Discussion on whether it constitutes a law might even promote the objective of the contributed paper.

References

CHRISTIANSEN, J. E., Ground-water studies in relation to drainage, Agr. Eng., v. 24, pp. 339-342, 1943.

REEVE, R. C., and M. C. JENSEN, Piezometers for ground-water flow studies and measurement of subsoil permeability, Agr. Eng., v. 50, pp. 435-438, 1949.

Transactions, American Geophysical Union Volume 31, Number 5 October 1950

MINIMUM EVAPORATION FROM WATER SURFACES

N. W. Cummings

(Contribution from the Scripps Institution of Oceanography, New Series, No. 484)

Editor's note: During editing of this paper, which is published posthumously, questions arose regarding notation and subscripts of some of the symbols. While it is hoped that they are now correct, it seems appropriate to inform readers that there may still be inconsistencies, particularly in making direct comparisons with Cummings' 1946 paper. George F. McEwen, one-time co-worker and long-time friend of the author, has agreed to prepare a closure on the author's behalf if discussion should make this appropriate.

Abstract--It is shown that if the water surfaces in a series are in the steady state, and subjected to the same incoming rate of energy supply, but differing wind, one of them will have a smaller evaporation rate than those under either greater or less wind. This fact is utilized to point out serious limitations on pans as indicators of lake evaporation. The conclusion so obtained is supported by available data.

Introduction--YOUNG [1947, 1948] and his associates have rendered an important and valuable service in compiling the large mass of evaporation data (including many pan records) recently published by the California Department of Public Works. But to say that the compilation has value is not equivalent, by any means, to saying that the pans themselves have value as indicators of true lake evaporation. Fortunately, Young included a number of records applying to actual lakes, and these undoubtedly have great value.

Recognition of the existence of a temperature at which evaporation during a given time interval is a minimum, was stimulated by an examination of Young's work.

There appears to be no historical evidence to show that when any of the commonly used pans, with the possible exception of the one bearing the name of the Bureau of Plant Industry, were introduced, anything in the nature of design was attempted, apart from obvious structural considerations. Nevertheless, some of the pans might conceivably turn out by good fortune alone, to have genuine indicator value, although the probabilities are against such an outcome.

In order to appraise any pan records completely, we must take account of the relation between the variability of pan-to-lake coefficients and that of lake evaporations. There are two ways in which this relation can be investigated. The first is by direct observations, and the second by inference from fundamental generalizations, but in view of the extreme scarcity of reliable direct observations, the more fundamental attack has obvious advantages. It will therefore be presented first, and available data bearing directly on the question will be briefly summarized later. The random components of turbulent motion are supposed to integrate to zero, so that only average velocities are considered.

Energy components--The fundamental generalizations reveal several energy components [CUMMINGS, 1946], all of which can, in general, vary, but the variations are not entirely free from constraints imposed by the first and second laws of thermodynamics and the properties of air and of water vapor. For examining those variations of the dissipative energy rates which are possible under the constraints, we may write the following equations for the discharge from unit area of a water surface in unit time,

$$Q_L = g_L\,(\theta_o - \theta_2) \qquad (1a)$$

$$Q_S = g_S\,(\phi_o - \phi_2) \qquad (1b)$$

$$B = \alpha(T_w^4 - T_a^4) \qquad (1c)$$

The left-hand members are the evaporative, convective, and radiative components, while the g's are functions of wind. Some writers have regarded each g as proportional to the wind velocity, but since in the Epstein solution of the basic differential equation, it does not come out exactly that way, the more general form is retained. The binomials $(\theta_o - \theta_2)$ and $(\phi_o - \phi_2)$ are measures of the differences in respect to vapor pressure and temperature between air and water, while T_w is the Kelvin temperature of the water surface, T_a a temperature representative of sky conditions, and α the Stefan constant.

It is an erroneous, but unfortunately a very common assumption, that since g_L is an increasing function of wind, if we increase wind, we necessarily increase Q_L, whereas in actual fact, we may do nothing of the kind. Some writers forget all about the decrease in $(\theta_o - \theta_2)$ that may accompany an increase in g_L. Without further information we have no means of knowing whether the overall effect will be an increase or a decrease in Q_L, and accordingly, as a step toward procuring the needed additional information, a hypothetical experiment will be described.

Simultaneous conditions at different water bodies--Let two similar water bodies, X and Y, warmer than wet bulb, be provided, and let conditions be so controlled that both are in a steady state, and subject to the same T_a conditions. Let the sum of the dissipative energy components be the same for both bodies, as also the wet and dry bulb, while the wind velocity is greater for X than for Y. That is, let

$$[Q_L + Q_S + B]_X = [Q_L + Q_S + B]_Y \qquad (2a)$$

and

$$[g_L]_X > [g_L]_Y \qquad (2b)$$

At any height greater than a few millimeters, $g_L = g_S$, and may accordingly be factored out of the sum of the right hand members of (1a) and (1b). If then, the wind velocity increases as we go from Y to X, at least one of the three binomials must decrease. But since the wet and dry bulb remain constant, each binomial decreases with water-surface temperature so that as the wind increases, the water-surface temperature decreases. This temperature relation in its proper quantitative aspect, is a necessary and sufficient condition for meeting the designated experimental requirements. Temperature can accordingly (under the constraints) be regarded as a measure of wind, so that if we take full account of the effect of changes in temperature, we do not in addition need to take explicit account of changes in wind. That is, wind is implicitly taken care of when we deal properly with temperature, or the curve between evaporation rate and temperature, is two-dimensional. While this conclusion may come as a surprise to persons unaccustomed to think in terms of any definite dissipation of energy, its truth can be easily seen by remembering that by division, the g's, which are the only terms containing wind, can be eliminated from (1a) and (1b) [CUMMINGS, 1946]. Although in doing so, we diminish by one, the number of equations at our disposal, the conservation of energy enables us to restore the loss. At the temperature of the wet bulb, it is easily shown in various ways that the relation between wind and temperature becomes indeterminate. From an observational standpoint, this relation becomes less and less definite, as the wet bulb is approached.

If now in (1a) and (1b), we decrease g by going from X to Y, and at the same time increase the binomials, what (under the constraints) do we do to Q? In particular, do we do the same thing to both Q's, or do we increase one and decrease the other?

Second law of thermodynamics--A well-known principle which helps provide the easy answer, is the second law of thermodynamics. Thus if X is slightly cooler than the air, while Y is slightly warmer, then according to the second law, Q_S is negative for X and positive for Y so that it increases as we go from X to Y. But B certainly increases as we pass from X to Y so that Q_L must decrease if the sum of all three is to remain constant. Thus, under these conditions, Q_L and Q_S vary oppositely. A commonly held view, on the contrary, implies that they vary in the same direction.

Condition under which evaporation is independent of surface temperature--Differentiating (1a) with respect to T_w, [see (6b)] and taking account of the relation between temperature on the one hand, and rate of change of pressure of saturated vapor with temperature, on the other, suggests that the curve between evaporation rate and temperature, may be convex toward the temperature axis, since the derivatives of g_L and θ_o have opposite signs. Does its slope ever pass through zero and change sign? To answer this we can replace our two experimental water surfaces by a whole series which may be called a reference series, and we can write the basic energy equation [CUMMINGS, 1946]

$$E \text{ cm} = [(I - B - S - C) \text{ cal/cm}^2]/[(L \text{ cal/gm})(1 \text{ gm/cm}^3)(1 + R)] \qquad (3)$$

where E is the evaporation during any specified time interval, I and B are the corresponding radiation terms, S the heat accumulated in the water during the time interval, C a general correction, and L the heat of vaporization. For convenience let $h = I - B_o$ since $S = 0$ in the steady state, and C is negligible for most lakes; and let $B = B_o + b$, with B_o independent of such changes in T_w as occur; $R = Q_S/Q_L$. Generalizing further to permit the arbitrary variation of h, gives the mathematical relation

$$DE = (dE/dT_w)DT_w + (dE/dh)Dh \quad \ldots\ldots\ldots\ldots\ldots\ldots (4)$$

It is a matter of considerable importance to keep the meanings of the symbols clear. The left member of (4) is the total differential when wind, temperature and radiation all change, while the first term on the right, is that part of the differential not due to changes in h; that is, it corresponds to those changes in E that would occur, if there were no changes in h, but were changes in wind and temperature. This means that, subject to the conditions for (1a), dE/dT_w is a total derivative, because in the steady state h is constant when the sum of the dissipative components does not vary. Consequently wind is not neglected in (4). The temperature referred to in connection with equations (4) through (8) is that of the water surface.

From (3) and (4), it is obvious that if $dE/dT_w = 0$,

$$DE = (dE/dh)DH = [Dh]/[L(1 + R)] \quad \ldots\ldots\ldots\ldots\ldots\ldots (5)$$

so that, under such conditions, evaporation may be expressed as a function of h and R alone. From (3) or (1a), we obtain, for the derivative dE/dT_w, either

$$dE/dT_w = (\partial E/\partial b)(db/dT_w) + (\partial E/\partial R)(dR/dT_w) = -[(db/dT_w)/(1 + R) + h(dR/dT_w)/(1 + R)^2]/L \quad (6a)$$

or

$$dE/dT_w = (\partial E/\partial T_w) + (\partial E/\partial g_L)(dg_L/dT_w)$$

$$= g_L(d\theta/dT_w) + (\theta)(dg_L/dT_w)/L\,, \qquad \theta = \theta_o - \theta_2 \quad \ldots\ldots\ldots\ldots\ldots\ldots (6b)$$

But (6a) is more convenient because it easily shows the derivative to be zero when

$$-(db/dT_w)(1 + R) = h(dR/dT_w) \quad \ldots\ldots\ldots\ldots\ldots\ldots (7)$$

Failure to distinguish between dE/dT_w and $\partial E/\partial T_w$, undoubtedly accounts for some of the erroneous comments that have been made regarding the application of the energy equations. If h is constant, R and the variable part of B in (3), could, under any particular conditions except T_w equals wet bulb, be replaced by functions of the single variable T_w, so that there is no inconsistency between the total derivative property of dE/dT_w, and the two dimensional character of the curve between evaporation and temperature.

The numerical value, (0.5 cal/cm^2) per hour per degree, of the derivative db/dT_w, is obtained by differentiating the Stefan fourth power equation for radiation, since $dT_a/dT_w = 0$, and a reasonable value for h is (14 cal/cm^2) per hour, giving from (7),

$$dR/dT_w = -0.05 \text{ deg}^{-1} \quad \ldots\ldots\ldots\ldots\ldots\ldots (8)$$

There can be no doubt as to the existence of a negative rate of change of R with water surface temperature under certain conditions. If (7) does not explain its relation to evaporation, what does? In the differentiating, time is, of course, not regarded as a variable. Instead, we are passing instantaneously from lake to lake or from pan to pan in a reference series.

No conflict with turbulence theory--It is obvious from (6a) that under the assumed experimental conditions, the evaporation rate may increase, decrease, or (over an infinitesimal range) remain constant while the wind increases, and this conclusion is in no way incompatible with turbulence theory. Thus, to say that Q_L remains constant, is merely to set $(\theta_o - \theta_2)$ proportional to the reciprocal of g_L, which is entirely permissible under turbulence theory, and merely provides an answer to a question with which turbulence theory has thus far not concerned itself.

Heat storage--In the theoretical treatment as thus far presented, perfect consistency with basic postulates takes us through (7), but we cannot proceed farther without making certain judgments as to magnitudes, and without mentioning the relation between incoming and outgoing energy, which involves the heat accumulated in the water as designated by S. But the aim which stimulated the writing of the paper in the first place, was to find some basis for judging the value of a pan as

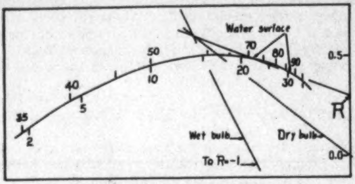

Fig. 1--Alignment diagram for R, the ratio of convection to evaporation; when the rate of change of R with water surface temperature is about -0.05 per degree, the evaporation is independent of water surface temperature, and therefore of wind

a lake indicator. How can the neglect of S as it has been done here, interfere with the attainment of that aim? Over an annual cycle S is known to be almost exactly zero for many lakes, and over any interval of time for which the commonly used pans could be imagined to have any usefulness, it is small by comparison with evaporation. Moreover, it is a time change, whereas the aim of the paper is to investigate the behavior of water bodies under differing average conditions, particularly with respect to air movement. There is no reason why (I - S) cannot be constant over any segment of a reference series and a bad pan cannot be made good by the removal of such restrictions.

Minimum evaporation--As any actual lake may be a member of a reference series, and as (6b) and the relation $(dE/dT_W)(dT_W/dg_L)$ jointly make dE/dg_L and dE/dT_W vanish together, (8) tells us the condition under which the particular lake in question would have a smaller evaporation than any other lake receiving the same energy from sun and sky, but subject to greater or less wind, and (6a) tells us the conditions under which a small change in wind produces a negligible change in evaporation rate.

An examination of the alignment diagram [CUMMINGS, 1930] of Figure 1, shows that the rate of change of R with surface temperature has the value required by (8) under conditions frequently met. This means that evaporation from a lake can, during an important part of the time, be regarded as independent of wind, and an earlier paper has pointed out that it is nearly independent of humidity [CUMMINGS, 1929]. For any given combination of wet and dry bulb and incoming radiation, the slightly negative rate of change of R with water surface temperature corresponds to that particular water surface temperature that yields a minimum evaporation and a near maximum discharge of sensible heat by convection. Above that temperature, the increasing driving tendency for water vapor prevails, and below, the decrease in the driving tendency for sensible heat prevails, reducing that tendency to zero when the water surface and dry bulb have the same temperature. To state the facts roughly but briefly, the wind does so much cooling, that it can do only a little evaporating at the temperature of minimum evaporation. In other words, the wind blows away sensible heat instead of water vapor, because R is so large, say 30 per cent.

Lakes different from pans--In this respect a lake is notably different from any of the commonly used pans, because none of these pan temperatures combines with wet and dry bulb temperatures in such a way as to give a slightly negative rate of change of R with water surface temperature. Nevertheless, it is reasonable to suppose that a pan can be so designed as to give these desired temperature combinations. We consequently have no reason to expect a pan to be a good indicator of lake evaporation unless it is specifically designed with this end in view, and with an understanding of the fact that wind and humidity exert only a minor influence on evaporation from a lake.

Examination of data--(The abbreviation, WB pan, will refer to the Weather Bureau pan that has long been in use.) No satisfactory observational check on the foregoing conclusion is at present possible, because there never have been adequate parallel series of pans and lakes. Nevertheless, some little work of this kind has been done, so that, by improvising, we can draw some inferences, albeit rather tenuous ones. The real question is not whether a pan can or cannot yield information, but rather how does the pan compare with other means in respect to the yielding of information about lakes?

This question has been investigated for several localities chiefly by the aid of two methods of calculation. The first is the simple proportion: the evaporation from lake X, is to the evaporation from Lake Elsinore in California, as the pyrheliometer reading near X, is to the pyrheliometer reading at Riverside, a short distance from Lake Elsinore. The second assumes that when reduced to the same units, the difference in evaporation at any two points is equal to the difference in radiation divided by (1 + R), according to (5). For lakes, R appears to be fairly close to 0.2, while for WB pans it fluctuates about zero. When the time intervals are the same, radiation in cal/cm^2 may be reduced to inches of evaporation by dividing by $2.54\ cm/in \times 585\ cal/cm^3 = 1480\ (cal/cm^2)/in$. The only case in which there seemed to be any reason for supposing that a pan-to-lake coefficient could yield a smaller error, was the Ft. Collins, Colorado data for which the Lincoln, Nebraska pyrheliometer had to be used. But by using the WB pans at Ft. Collins and Lincoln (not in the pan-to-lake coefficient manner, but merely for the purpose of reducing the Lincoln radiation to the substantially lower Ft. Collins value), a highly satisfactory result was obtained. If other records had been available, even this use of the WB pan could probably have been avoided [HAND, 1937; ROHWER, 1931].

If this supposition is correct, the absence of any need for the pan would have been more clearly demonstrated. Although the Lincoln and Ft. Collins pans appear to have acted in a mutually consistent manner, Young's compilation provides ample evidence that WB pans are frequently erratic, so that we cannot depend on the good fortune that existed in this particular case.

Over large areas, the lake evaporation may, with a remarkably small error, be treated as uniform. Thus for six non-desert lakes in California reported by YOUNG [1948], the average loss is 54.3 in/yr, and the average departure from this average is 2.75 inches or five per cent. For two desert lakes, the average is 72.0 in/yr and the departure is about the same. The difference between desert and non-desert lakes is $72.0 - 54.3 \approx 18$ inches or about 35 per cent, whereas some of the pans have a ratio of 2 to 1.

In view of these relations, it is difficult to imagine circumstances in which the WB pan can render any real assistance in estimating lake losses, when the person making the estimate has any choice whatever as to the kind of instrument that is to yield the basic information. The data are less complete for other commonly used pans, but we have no reason to suppose that any of them, with the possible exception of the one bearing the name of the Bureau of Plant Industry, have any indicator value when that term is interpreted in the comparative manner previously suggested.

Pan design--It is difficult to understand how the WB pan can be reconciled with scientific meteorology and hydrology. The design of this pan could be improved with ease. Thermal insulation might constitute a substantial improvement even when the pan is used in the ordinary way. It is quite possible that obstructing the opening would improve the design by raising the average temperature and throwing the high temperature toward early morning so as to yield more favorable combinations with wet and dry bulb thermometer readings. Screening devised by YOUNG [1937, p. 15] does something of this kind, although a continuous obstruction around the edge of the opening would probably have important advantages. The objective in designing a pan should be to make Eq. (3) when applied to the pan, correspond in magnitude, term by term, with the same equation when applied to a lake. Although this objective can probably never be exactly reached, commonly used pans can be improved with respect to it.

Of course, when estimates are quickly needed at places where no records of any kind are available except WB pan readings, it may sometimes be necessary to use those records, particularly when, as at Ft. Collins, there is reason to suspect some purely local condition which makes the radiation depart from the general trend. These emergencies cannot, however, be regarded as a reason for continuing the use of such pans.

San Diego County lakes-- It would be helpful if the engineer who made the evaporation computations for the SAN DIEGO COUNTY INVESTIGATION [1935], would explain how he found enough energy to account for the high losses reported. Table A-2 and page 165 show 72 inches for Cuyamaca, 63 inches for El Capitan and San Vicente, and 60 inches for Mission Gorge, notwithstanding only 56.2 inches for Lake Elsinore [YOUNG, 1948, p. 99]. Because of proximity to the coast, one might reasonably expect the radiation in San Diego County to be less than in Riverside County, the location of Lake Elsinore. This difference is shown by a pyrheliometer reading of 365 (cal/cm^2)/day at La Jolla in San Diego County, as compared to 424 (cal/cm^2)/day at Riverside [HAND, 1937, p. 436], near Lake Elsinore. The published evaporations appear to be based on floating pans.

Presumably, a more reliable figure would be obtained for Mission Gorge, San Vicente, and El Capitan, by assuming a radiation equal to the mean of Riverside and La Jolla, that is, 390 (cal/cm^2)/day. Subtracting this from Riverside, dividing by 1.2×1480 (cal/cm^2)/inch and multiplying by 365 to reduce to an annual basis, gives seven inches less for the San Diego lakes than for Elsinore, or 49 inches per year. This is most likely a lower limit, since the back radiation is probably less for the San Diego lakes than for Elsinore. But if instead of using the entire reduction of seven inches per year, we use half that figure, we shall obtain 53 inches per year, which is, without doubt, a very close approximation to the actual loss.

Until reliable measurements of radiation at Cuyamaca become available, there is no way of estimating the evaporation from that lake that would be any better than a rough guess as to what the radiation might be. Nevertheless, such a guess, if made intelligently, may not be as far wrong

as might at first appear, because the radiation data [HAND, 1937], show a degree of unformity that must be gratifying to anyone confronted by the practical need for some kind of an estimate of evaporation. This uniformity, in the light of the facts embodied in (5), and the fairly close approximations underlying (8), no doubt accounts for the samll variation among the lakes reported by Young.

References

CUMMINGS, N. W., Relation between evaporation and humidity as deduced quantitatively from rational equations based on thermodynamics and molecular theory, Trans. Amer. Geophys. Union, Bull. 68, Natl. Res. Coun., pp. 47-56, 1929.

CUMMINGS, N. W., Alignment diagram for R of the energy equations, Mon. Wea. Rev., v. 58, pp. 142-146, 1930.

CUMMINGS, N. W., Reliability and usefulness of the energy equations for evaporation, Trans. Amer. Geophys. Union, v. 27, pp. 81-94, 1946.

HAND, IRVING F., Review of United States Weather Bureau Solar Radiation Investigations, Mon. Wea. Rev., v. 65, pp. 415-441, 1937.

ROHWER, CARL, Evaporation from free water surfaces, U. S. Dept. Agri. Tech. Bull. 271, 96 pp., 1931.

SAN DIEGO COUNTY INVESTIGATION, Div. of Water Resources, Dept. of Public Works, State of California, Bull. 48, 1935.

YOUNG, ARTHUR A., Evaporation from water surfaces in California, Div. of Water Resources, Dept. of Public Works, State of California, Bull. 54, 1947 and 54-A, 1948.

768 Twenty-Sixth Street,
San Bernardino, California

(Manuscript received March 23, 1949, and, as modified, June 6, 1949; presented at the Thirtieth Annual Meeting, Washington, D. C., April 21, 1949; open for formal discussion until March 1, 1951.)

Transactions, American Geophysical Union Volume 31, Number 5 October 1950

HYDRAULIC INFLUENCE OF MODIFICATIONS TO THE SAN DIMAS CRITICAL-DEPTH MEASURING FLUME

K. J. Bermel

Abstract--An experimental determination of various factors which affect the rating of critical-depth measuring flumes is presented in this paper. Those factors investigated included entrance conditions, floor slope, wall and floor friction, length of flume, method of measuring the head, and the effect of an idealized obstruction in the entrance channel.

Introduction

Several critical-depth flumes, such as the Parshall and San Dimas Flumes, have been developed for the measurement of flow in open channels. The primary advantage of the latter type flume is that it is more or less self-cleaning where debris-laden flows are involved. To determine if modifications of the initial design of the San Dimas Flume were desirable, and to ascertain the general magnitude of factors that might influence the operation of such a flume, investigations were made in the Fluid Mechanics Laboratory of the University of California, Berkeley, in cooperation with the California Forest and Range Experiment Station of the U. S. Forest Service. The following summary, based on observations of flumes one-half foot in width, is submitted as the results are applicable in general to other critical-depth flumes of short length.

Experimental equipment

In these studies water was pumped from a storage sump through a supply line to a constant-head tank from which it was conducted by a six-inch line, containing a six-inch by four-inch venturi meter into a forebay. From there it passed through a baffling system into the approach channel, through the test flume, and then through an afterbay and into a return channel. For small flow rates, water was taken from the constant-head tank through a four-inch line and measured by a four-inch by two-inch venturi meter. Differential heads on the venturi meters were measured by means of carbon tetrachloride and mercury manometers. Both of the venturi meters were calibrated prior to the experiments and the six-inch by four-inch meter was checked at the conclusion of the experimental runs.

Four separate models were used in the course of experimental investigations. The first model made of brass plate, was adjustable in width and side slope and used as three different flumes, making a total of six models used. In the initial set of runs, which were made to study the characteristics of inlet transitions, the flume had vertical side walls with eight piezometer holes on each side, one-half inch up from the bottom and located as indicated in Figure 1. Thirteen feet below the forebay, the flume was sealed off at the transitions, and by adjustment of the legs, could be set for various floor slopes. Immediately upstream from the flume, a varnished wood section, five feet long, was provided for adjustment of approach channel conditions. The transitions were also of varnished wood. By adjustment of the flume sides to give a trapezoidal section, this same flume was used for one series of runs with 1:1 side slopes and for another series of runs with 1/2:1 side slopes.

For the fourth series of runs, the test flume was constructed of wood with a smooth varnish finish (Manning's n estimated as 0.010). The most desirable entrance transition as determined in the first series of tests was used and the approach channel, transition, and flume were of unit construction. The flume occupied the same relative position as the former flume, but the approach channel acted as a cutoff wall. A secondary floor within the flume, hinged at the upstream end allowed changes to be made in the slope of the floor. In this flume only four piezometer holes were inserted, corresponding to well positions 2, 3, and 5 in Figure 1.

This same flume was used for a later series of runs in which the surface roughness was increased by application of a sandcoat to the flume walls and floor up to and including the inlet transitions. In other runs of this series, the 50-60 sandcoating was removed and replaced with sand passing a No. 28 sieve (0.589 mm) and retained by a No. 30 sieve (0.0232 inches). To see if

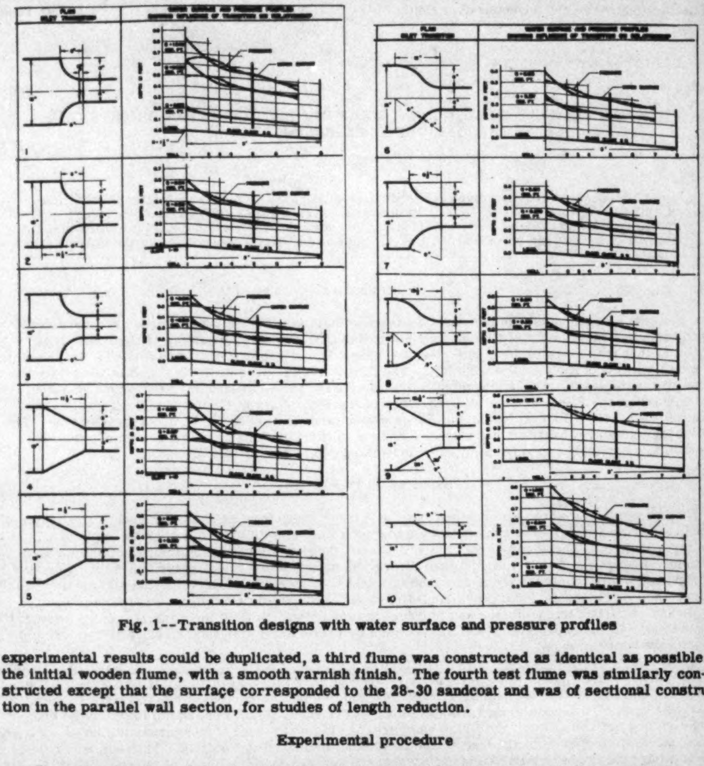

Fig. 1--Transition designs with water surface and pressure profiles

experimental results could be duplicated, a third flume was constructed as identical as possible to the initial wooden flume, with a smooth varnish finish. The fourth test flume was similarly constructed except that the surfaçe corresponded to the 28-30 sandcoat and was of sectional construction in the parallel wall section, for studies of length reduction.

Experimental procedure

Since the objective of this investigation was to determine the relationship between depth, pressure head, and discharge for all test conditions, a standard test procedure was established. The zero readings of all gages were made before and after each series of runs and measurement of discharge, water surface, and pressure head were made concurrently. For the first test flume, pressure measurements were made at eight points on each side, corresponding to well positions 1-8, as indicated in Figure 1. In the second test flume, pressure measurements were made at positions corresponding to well positions 2, 3, and 5, Figure 1. A detail of the piezometer openings used at these positions and the static tube used at position 5 is shown in Figure 2. In the third flume, static tubes and slots were used at position 5. A detail of these slot installations is also shown in Figure 2. In all cases the pressures were transmitted to wells and the water surfaces measured by traveling point gages. Water surface measurements within the flume were made along the centerline.

Experimental results

Flume of trapezoidal cross-section--Tests of a flume with a trapezoidal cross-section with 1:1 side slopes in one case and 1/2:1 in the other, with conical or wedge-shaped entrance transitions, did not give desirable flow conditions. The most objectionable feature was the relatively

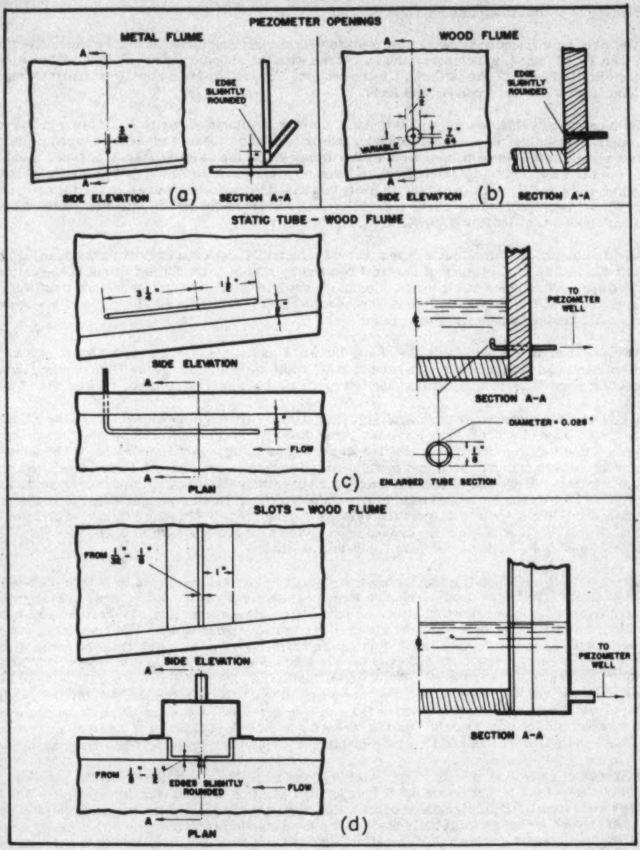
PIEZOMETER OPENINGS
METAL FLUME
A
3/32"
EDGE SLIGHTLY ROUNDED
SIDE ELEVATION
(a)
SECTION A-A
WOOD FLUME
1/2"
7/64"
VARIABLE
EDGE SLIGHTLY ROUNDED
(b)
STATIC TUBE - WOOD FLUME
3 1/4"
1 1/2"
TO PIEZOMETER WELL
FLOW
DIAMETER = 0.028"
1/8"
ENLARGED TUBE SECTION
PLAN
(c)
SLOTS - WOOD FLUME
FROM 1/32" - 1/8"
1"
FROM 1/8" - 1/2"
EDGES SLIGHTLY ROUNDED
(d)

Fig. 2--Methods of measuring water pressure in models of the San Dimas flume

low velocity through the flume, owing to insufficient entrance contraction at the higher rates of discharge. This produced depths of flow that were readily influenced by downstream obstructions or backwater. From the standpoint of debris transport this probably would necessitate increasing the floor slope beyond the five per cent slope tested.

Entrance transitions--Selection of a desirable entrance transition was based on a comparison in performance with the San Dimas flume as originally designed [WILM, COTTON, and STOREY, 1938] and eleven other arrangements. Desirability was based largely on two criteria: (1) the amount of turbulence caused by impact or by change in flow direction, as judged by flow appearance in the transition section and throughout the flume; and (2) agreement between depth and pressure measurements within the flume.

The first nine transitions tested were made with the approach channel three times the flume width (see Fig. 1, no. 1-9 inclusive), the last three with the approach channel reduced to twice the flume width. Only one of the latter is illustrated (see Fig. 1, no. 10). For all transitions tested, the slope of the approach channel was level.

With entrance velocities (up to 1.0 ft/sec), and flume velocities (up to 5.0 ft/sec) in the model, transitions 1-3, inclusive, produced considerable impact and caused a diamond-shaped pattern of standing waves in the flume proper which varied in position for varying stages of flow. Modification of the floor section in the transition produced no significant difference. The wedge shape transition, no. 4 and 5, while reducing impact, increased the standing waves in the flume caused by the abrupt angle. The reverse curve transition no. 6, while reducing the standing waves as compared with type no. 5, indicated further refinement desirable.

Modification of the three basic types tested (cylindrical, reverse curved, and wedge) by increasing the radius of curvature of the first two and by rounding the abrupt break in the latter, improved the performance of all three. Comparison of pressure and water-surface profiles (see Fig. 1, no. 7, 8, and 9) indicates little difference; however, transition no. 7 effected the greatest reduction of standing waves within the flume.

Tests of transitions with the same shape and radii as no. 7 and 8, but with higher entrance velocities due to reduction of the approach channel width to twice that of the flume width, indicated the need for a more gradual transition and led to the development of type no. 10 (see Fig. 1).

Effect of floor slope on head-discharge relationship--Although measurement of the effect of floor slope on head-discharge was made for three different roughness values, only the one having a Manning's n of 0.010 is presented. Figure 3a shows the influence of floor slope on the head-discharge relationship and indicates that pressure head varies inversely with floor slope. With an average maximum discharge of approximately 1.65 cfs, the velocity at the measuring section varies from 5.56 to 5.14 ft/sec for a variation in floor slope of from five to one per cent. For the minimum measured discharge of 0.210 cfs the velocity varies from 3.82 to 2.63 ft/sec. Selection of the most desirable floor slope must depend upon future experiments with debris-laden flows. Tentatively, a floor slope of three per cent has been selected.

Effect of wall and floor friction on head-discharge relationship--Tests to determine the influence of flume friction on head-discharge measurements were made using three gradations of surface roughness. Using Manning's n as an index of roughness these values were 0.010, 0.013, and 0.015. The first was an estimated value for smooth varnished wood. The remaining values were computed using the CHANG [1939] formula, $n = 0.043D^{0.167}$, in which D is the grain diameter in feet. For the two gradings of sand used for the surface coatings, grain diameters of 0.0092 and 0.00192 ft, respectively, were used. For a given discharge, depth of flow or pressure head increased directly with increase of surface roughness. Figure 3b is a comparison for the range of roughness and discharges tested, with the floor at five per cent. Decrease in floor slope, with its attendant reduction of flow velocity, while increasing the depth of flow for a given discharge tended to decrease the difference in head measurements due to the variations in flume roughness.

Influence of reduction of length downstream of the measuring section--With the length of the parallel section of the initial flume 3.0 ft long and the position of head measurement at 1.5 ft from the upper end, a reduction in length of 0.5 ft of the downstream section for the range of discharge measured showed no appreciable difference in the head-discharge relationship; however, a reduction by one foot caused considerable deviation for depths of flow or pressure heads exceeding 0.25 ft. This would indicate that the minimum length of flume, downstream from the measuring section, should not be less than twice the head of the maximum discharge in order to maintain the intial head-discharge relationship.

Reduction of length by removal of sections both up and downstream of the measuring section--Comparison of head-discharge relationship for reductions in length from 3.0 to 0.5 ft indicated that a decrease in length produced an increase in head (see Fig. 3c). For the shortest length tested (total length 0.5 ft) increase in head was obtained only for flows less than 0.42 cfs (see Fig. 3c). Comparison of measurements of depth of flow and pressure head indicate, in general, best agreement for the lowest rate of discharge in the flume one foot long and for the highest flow rate in the flume 2.5 ft long. For intermediate rates of flow best agreement was obtained for flumes between these two lengths. A total reduction of one foot in length appears to be the maximum possible for

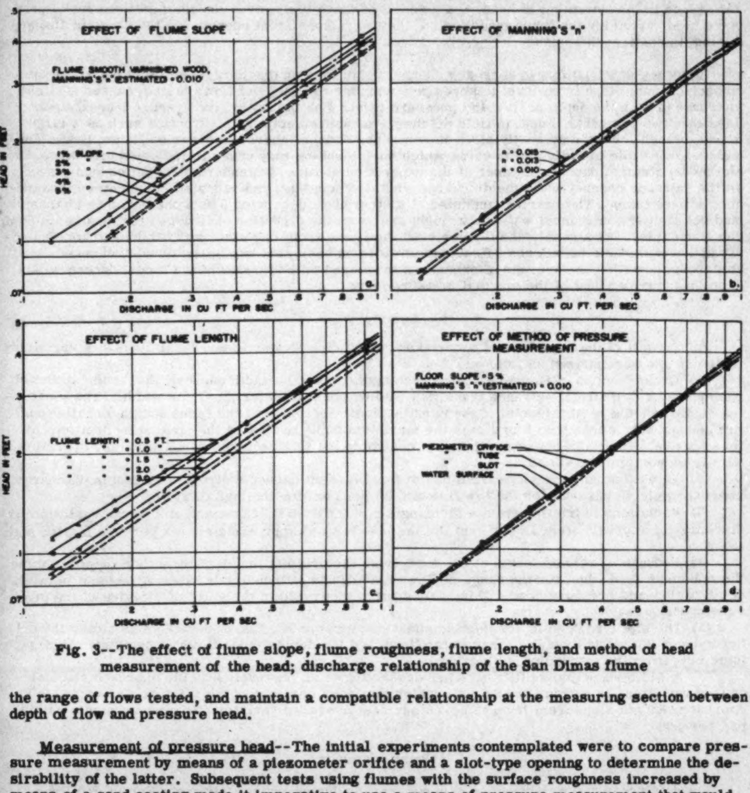

Fig. 3--The effect of flume slope, flume roughness, flume length, and method of head measurement of the head; discharge relationship of the San Dimas flume

the range of flows tested, and maintain a compatible relationship at the measuring section between depth of flow and pressure head.

Measurement of pressure head--The initial experiments contemplated were to compare pressure measurement by means of a piezometer orifice and a slot-type opening to determine the desirability of the latter. Subsequent tests using flumes with the surface roughness increased by means of a sand coating made it imperative to use a means of pressure measurement that would not be influenced by surface roughness adjacent to the piezometer opening. To circumvent this a static tube (see Fig. 2c) was used as the standard.

The slots studied in these tests were formed by placing brass angles in the flume wall, with one leg of each angle in a plane with the wall, and the two angles fixed at the desired distance apart so as to form a vertical slot with its center line at the desired measuring point. This width was varied from 1/32 to 1/8 inch. The slots led directly into a metal box, which communicated with piezometer wells by means of tubing. Thickness of the slot wall could also be varied from 1/8 to 1/2 inch (see Fig. 2d). These tests were made in wooden models with approximately three and five per cent floor slopes, and Manning's roughness factors of 0.013 and 0.015.

Measurement of pressure head by means of the piezometer openings shown in Figure 2a indicated greater heads than obtained with the static tube. Measurement by means of the slot type indicated values smaller than those obtained with the static tube. Figure 3d compares head measurement by these three methods for a flume with a five per cent floor slope. Variation in width of slot from 1/32 to 1/8 inch, or thickness of slot from 1/8 to 1/2 inch, produced no significant difference in measurement of head. As a result of these tests, even though measurement of pressure head varied for the three types tested, they were consistent enough, for the range of flows tested, to confirm their usage.

Influence of variations in approach channel conditions on discharge--An increase in the approach channel slope from level to seven per cent, for the range of flows tested, caused a slight increase in both the depth of flow and pressure head. For the latter, the average increase was less than two per cent. Since, in field discharge measurements, an obstruction such as a large stone, branch, or log may partly block the entrance channel above a measuring flume, it was considered desirable to evaluate the error which such blocking may cause in indicated discharge. In the model studies, during a number of the experimental runs, a standard obstruction was placed in the entrance channel while the discharge was held constant, and repeated piezometer measurements were taken. The barrier consisted of a steel plate occupying 5/9 of the entrance channel and set against one channel wall and at right angles to the direction of flow two feet upstream from the flume inlet. As a result, the flow entered the flume from one side, with a high entrance velocity and considerable turbulence. Readings in wells on each side were considerably changed; in all instances, however, the average of pressures measured on both sides of the model agreed within less than four per cent of the original measurements.

Summary

As a result of the experiments undertaken, using clear water flows, the influence of variations in design are summarized as follows:

(1) Cross-section of flume should be rectangular with the width one-half that of the approach channel and a cylindrical entrance transition (radius equal to twice the flume width). The measuring section should be at midpoint of the parallel flume section, and the flume length (parallel portion) should not be less than four times the maximum depth of flow at the measuring section. A three per cent floor slope appears the most desirable but this requires verification for operation with flows containing bedload.

(2) Variations in floor slope from one to five per cent caused a direct variation in discharge, approximately 43 per cent for the low flow and 21 per cent for the high flow.

(3) Variations in friction from a Manning's n of 0.010 to 0.013 caused an inverse variation in discharge of approximately 12 per cent for the low flows to approximately six per cent for the high flows.

(4) Reduction in flume length of one foot, from the original length of three feet, appears to be the maximum desirable, for the range of flows tested, and still maintain close agreement between depth of flow and pressure head. This agreement is desirable in the event of clogging of the pressure openings.

(5) The slot type opening for measurement of pressure head is as desirable as either the orifice type or the static tube, for clear water flows and for debris laden flows is certainly more satisfactory, from the standpoint of clogging.

(6) A width reduction by fifty-five per cent owing to an obstruction in the approach channel caused variations in measurements not greater than four per cent of the original. An increase in approach channel slope from level to seven per cent produced variations in measurements within two per cent.

Acknowledgments

The data presented was based on experiments conducted by the California Forest and Range Experiment Station in cooperation with the Division of Mechanical Engineering of the University of California. The experiments were planned and conducted by the Experiment Station under the supervision of C. J. Kraebel, H. G. Wilm and S. M. Munson, The facilities of the hydraulic laboratory were furnished by the University under the direction of M. P. O'Brien.

References

CHANG, Y. L., Laboratory investigation of flume traction and transportation, Trans. Amer. Soc. Civil Engrs., v. 104, pp. 1246-1284, 1939.

WILM, H. G., J. S. COTTON, and H. C. STOREY, Measurement of debris-laden stream flow with critical-depth flumes, Trans. Amer. Soc. Civil Engrs., v. 103, pp. 1237-1253, 1938.

University of California,
Berkeley, California

(Manuscript received March 17, 1950; presented by title at the Thirty-First Annual Meeting, Washington, D. C., May 1, 1950; open for formal discussion until March 1, 1951.)

DISCUSSION

H. G. Wilm (Pacific Northwest Forest and Range Experiment Station, 423 U. S. Court House, Portland 5, Oregon)--Bermel's paper gives an excellent portrayal of a series of studies conducted at the hydraulic laboratory of the University of California. As he says, the main purpose of these studies was to work out desirable modifications in the original design of the San Dimas measuring flume. He cites detailed discussions of the original investigations and of a preliminary design for this flume, presented by Wilm, Cotton, and Storey in 1938.

Because Bermel's paper is devoted to the factual results of his laboratory investigations, it may be desirable to add some discussion of the general design of this measuring flume, of its usefulness, and of developments which have occurred during and since the period in which Bermel made his investigations. The first work in developing the San Dimas flume was prompted by the need for a water-measuring device adapted to the conditions encountered in steeply sloping mountain streams. Such streams commonly contain sufficient bed-load and suspended material, so that the approach channels and stilling boxes of sharp-crested weirs and other conventional measuring devices become filled with sediment. Experience in measuring mountain streams for experimental purposes has shown that the following requirements must be met by any gaging station designed for this purpose: (1) Protracted ground-water flow should be measured within a range of five per cent above or below the true discharge. At the same time the station must be capable of handling with reasonable accuracy, peak discharges up to several hundred times the ordinary minimum. (2) The cross-section should be simple and regular, to facilitate calibration in field or laboratory. (3) Velocities in the measuring section must be high enough so that any debris or bed-load reaching the station is carried through rapidly and without deposition.

After a good deal of testing, a measuring device conforming to these general specifications was found in the San Dimas flume. In principle, this flume resembles a broad-crested weir, in which the measurements of depth or pressure are taken at the longitudinal midpoint of the weir. To obviate the removal of contractions by sediment, the bottom contraction of a conventional weir is replaced by cylindrical transitions. Approaching the flume proper, the stream enters a short channel section which is two times as wide as the flume itself. From this point it enters the cylindrical transition and then passes through a rectangular section, the floor of which is inclined to a slope greater than the critical. Pressure or depth measurements are taken in this rectangular section, where the stream is moving at super-critical velocities. At the downstream end of the flume, sufficient overfall is provided so that tail-water levels do not encroach upon the stream flow level in the flume itself, even at the highest stages to be measured.

Thus, for any discharge, the depth or pressure at the point of measurement is under almost complete control: by the zone of critical depths upstream; by the fixed slope, cross-section, and friction of the flume itself; and by the overfall downstream. Because of these controls, the depth-discharge relation is quite exact and relatively unaffected by variations in either upstream or downstream conditions. This fact is illustrated by Bermel's tests.

Bermel's investigations have resulted in a number of improvements on the original design. Even though these results had not been previously published, a number of flumes incorporating the general principle of the original flume and Bermel's improvements have been installed in various places in the United States, and are giving satisfactory service under difficult conditions. W. C. Ackermann of the Tennessee Valley Authority, for example, has told me that his organization has installed a number of these devices in streams containing sediment loads and is quite pleased with them, after having had poor results with other types of stream-flow measuring equipment.

Forest Service men have had similar experience with San Dimas flumes in a variety of sizes, located on steep mountain streams. One of these, a two-foot flume installed in the central Rocky Mountains, was described by this writer in Civil Engineering in 1942. During the period since records have been started in this flume, the upstream channel conditions have been completely changed by unusually high discharges which widened the channel, and swept out alders and other growth. These changes have had no effect on the rating formula for the flume, and the standard error of estimate for all rating points fitted to this equation was ± 2.0 per cent.

The San Dimas flume was designed particularly for the measurement of discharges containing a moderate amount of bed-load and suspended material. Because it does this job successfully, it has considerably extended the range within which open-channel discharges can be measured with reasonable accuracy. In common with other measuring flumes of rectangular cross-section, however, it has some limitations. It does not measure very low discharges with great accuracy, because of the relatively large bottom width. By the same token, it has a limited capacity for

measuring high discharges. As a secondary disadvantage, the flume is somewhat narrower than the natural channel section and generally not of the same shape; therefore it occasionally becomes clogged with unusually large rocks or other debris.

With these disadvantages in mind, B. C. Goodell of the Rocky Mountain Forest and Range Experiment Station made a series of hydraulic laboratory studies under my general supervision, to work out desirable characteristics for a trapezoidal flume embodying the main principles of the San Dimas flume. An earlv edition of this kind of station has been in operation at the Fraser Experimental Forest in Colorado since about 1942, and has operated quite satisfactorily. The results of the laboratory studies indicate that a flume of flat trapezoidal cross-section should provide suitable discharge characteristics. The best designs had long-radius entrance transitions, side walls on a slope of 25 to 35°, and a longitudinal floor slope of four to six per cent. A station paper covering these laboratory studies has been issued by the Rocky Mountain Station (Goodell, B. C., A trapezoidal flume for gaging mountain streams, Sta. Paper 2, Rocky Mountain Forest and Range Experiment Sta., Ft. Collins, Colo., 18 pp., 1950).

Transactions, American Geophysical Union Volume 31, Number 5 October 1950

RAINFALL, INFILTRATION, AND HYDRAULICS OF FLOW IN RUNOFF COMPUTATION

H. N. Holtan and M. H. Kirkpatrick, Jr.

(Joint contribution of Research Division, Soil Conservation Service, U. S. Department of Agriculture, and the Agricultural Engineering Department, Virginia Agricultural Experiment Station, Blacksburg, Virginia.)

Abstract--This study considers three broad phases of hydrology (rainfall, infiltration, and hydraulics of flow) as they affect the occurrence of surface runoff. These three phases are not conglomerated into one single computation of runoff but are kept separate and considered consecutively which is the manner of their occurrence in nature. Rainfall expectancy is founded on the relatively longer and stronger rainfall records. The expectancies used are those derived by Yarnell.

Infiltration capacities of the soils in the watershed area are estimated from infiltrometer data for various soil and vegetative cover complexes. Rainfall must satisfy infiltration capacities before excesses can be produced for runoff. The rate at which excess rainfall runs off is a function of the characteristics of the watershed drainage system. Excess rainfall must supply the volumes of runoff simultaneously with the volumes of surface detention needed in order to produce given rates of flow. By the analysis of watershed data, it was learned that a definite relationship exists between the amount of detention and the rate of runoff from a given watershed. Although considerable refinement is needed it is evident that this relationship is affected by size of watershed area, vegetative cover, land-tillage practices, and presumably slopes or terrain of the watershed.

Through the isolation of the three phases, a new avenue of application is opened. With research designed to associate infiltration and hydraulics of flow with measurable characteristics of the watershed, the science of runoff prognostication should be appreciably advanced. The consecutive application of these phenomena permits and encourages comprehension and logic rather than acceptance of results on faith alone.

Introduction--Determinations of infrequent peak rates of runoff are handicapped because records are not usually started until the need for results is already evident. Most of our watershed runoff records, which are relatively meager, are of ten to 15 years duration. In many areas the studies cover only one or two specific sets of conditions. The application of these data even to "similar" watersheds is hazardous without proper isolation of factors of runoff to aid in judging similarity.

Records of rainfall and runoff were obtained on three watersheds near Chatham, Virginia, during the period 1939-1948. These watersheds were terraced and planted to mixed crops, with tobacco predominating. They were very similar in size, terrain, and treatment. Size ranged from 13 to 17 acres and predominating slopes ranged from five to ten per cent. Soils were mostly mixtures of Madison, Louisa, Mayodan, Cecil, Granville, Durham, and Appling series. Three terraces on one of these watersheds were also equipped for recording runoff. The areas above the terrace outlets were all slightly less than one acre in area. Measurements were continued on these terraces from 1939 through 1944.

Projection of results from probability analysis of these runoff records to other areas appeared very hazardous and limited, owing to the similarity of the areas measured. As an alternative, an effort is made herein to isolate and comprehend the hydrologic principles involved in the process of runoff from rainfall.

Undoubtedly all of the detailed phases of hydrology have a bearing on the nature and amount of surface runoff of water falling as rain. Within the limits of the data available and within the limits of practicability, it is impossible to consider each of these numerous phenomena in detail. On the other hand, it is not feasible to predict runoff without recognizing at least some of them.

Enough data are available to permit the isolation and study of three broad hydrologic phenomena affecting the rate of runoff. Rainfall, infiltration, and hydraulics of flow are estimated in this

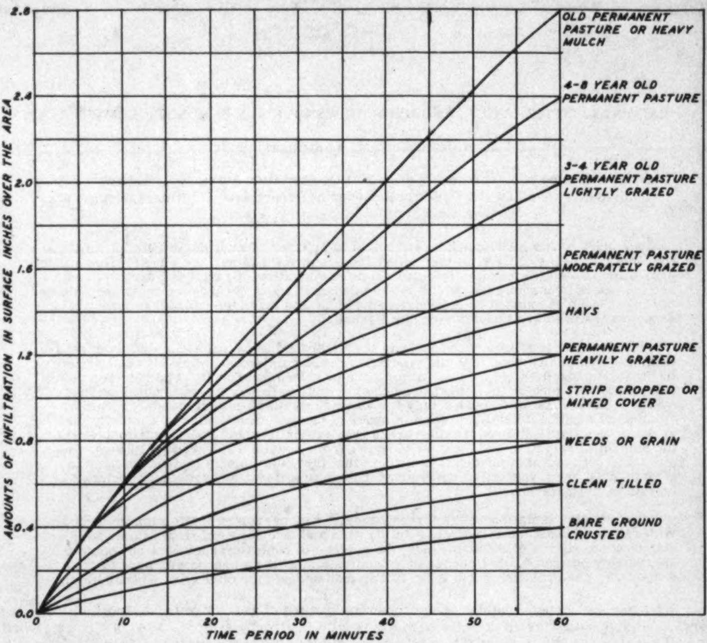

Fig. 1--Typical mass infiltration curves based on data from Clemson, S. C. on Cecil, Madison, and Durham soils; cropping estimates based on Clemson, S. C., Edwardsville, Ill., and Peoria, Ill. infiltrometer data

paper for watersheds of predominantly five to ten per cent mixed slopes, ranging in size from five to 50 acres, having a mixture of Cecil, Madison, and Durham soils or any mixture of soils known to have an infiltration capacity similar to these, under various tillage practices.

Rainfall--Rainfall expectancies up to 100 yr are provided by YARNELL [1935]. It is suggested that the amounts of rainfall for the frequency of interest be plotted on rectangular coordinates versus increasing time periods until a logical estimate of the time of concentration is definitely passed. Connect these points with a smooth curve since interpolations may be needed. The order of plotting does not imply a storm pattern but is used purely for expedience in later application.

Infiltration--Capacity to absorb rainfall varies for different soils. For the present, infiltration-capacity curves are on file for only the Cecil, Madison, and Durham soils of the Piedmont as determined with the Type-F infiltrometer [PARSONS, 1939] at Clemson, South Carolina [PEELE, BEALE, and LESESNE, 1947]. Vegetative cover is also a factor influencing infiltration capacity. Within a soil type, the infiltration-capacity curves as affected by vegetation are of one family; that is, they are very similar in shape but differ in amount of infiltration. The curves for Cecil, Madison, and Durham as obtained at Clemson are adjusted for vegetative cover effects as indicated by the infiltrometer studies at Edwardsville, Illinois [SHARP, HOLTAN, and MUSGRAVE, 1949]. The curves of Figure 1 for heavy mulch, hays, weeds, and clean tilled were quite definitely established. Curves to represent antecedent soil moisture of approximately 14 to 18 per cent (usual for growing season) were derived by adjustment of the dry-run and wet-run infiltrometer curves. The

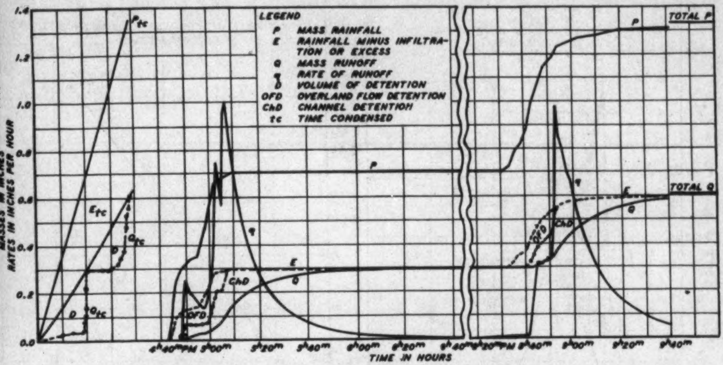

Fig. 2--Storm of June 13, 1939 on W-III watershed at Chatham, Va., analyzed by the time-condensation method to provide detention-rate of runoff relationships

other curves were interpolated logically with cognizance of soil differences and with the vegetative effects as found at Edwardsville. The curves of Figure 1 represent infiltration capacity of these soils as affected by cropping. They indicate the progress of water absorption during periods of rainfall. If the proper infiltration capacity curve is subtracted (coordinated time periods) from rainfall to be expected, the remainder is excess rainfall which is free to run off. The manner or rate at which this water runs off is the direct result of the hydraulic characteristics of the watershed drainage system.

Hydraulics--Obviously, whenever there is a flow of water past a given point in a channel there is also a quantity of water present in the channel above the point of observation. Further it is obvious that more water is detained in the upstream channel for high flows than is detained for low flows. It follows, therefore, that excess rainfall must supply water to satisfy this detention and at the same time provide water for the actual flow past the point of observation. If conditions in the channel cause great amounts of detention to accumulate, then a lesser rate of flow will occur. In other words, the more perfect the drainage efficiency of a watershed, the more nearly the reflection of rainfall minus infiltration by runoff.

Efficiency of drainage of a given watershed is expressed and utilized in the form of a graphical plotting of discharge in surface inches per hour versus volume of detention in surface inches. The derivation of such a relationship involves no new thinking, but purely the adoption of previously established concepts [HORTON, 1935; SHARP and HOLTAN, 1942; HOLTAN, 1945].

Two methods were used in analyzing watershed hydrographs for this report. Storms having intermittent runoff were analyzed by the time-condensation method [HOLTAN, 1945]. Figure 2 portrays this type of analysis graphically. Time is condensed in such a manner as to cause the mass rainfall to become a straight line. The same identical condensations of time when applied to runoff give a curve illustrated in Figure 2 (left) as Q_{tc}. The theory is that with rainfall constant (P_{tc} is a straight line), runoff (Q_{tc}) should also become constant after some small initial abstractions for storage. It does not do this because of detention of flow. Therefore, a curve fitted to all points where detention is zero (rate of runoff is zero) represents the curve of runoff had detention been negligible. This curve is labeled E_{tc}. By expanding the time scale again as dictated by rainfall, the E_{tc} curve becomes the E (excess rainfall) curve as it occurred during the storm. Differences between this excess curve and the observed runoff curve at given times are detentions of flow. Detentions are directly related to rate of runoff. Pertinent, and of special interest, is the discrepancy between the depth of detention for a given rate of runoff on the rising side of the runoff rate curve and the depth of detention for a corresponding rate on the drawdown side. Detention-discharge relationships as determined from the drawdown side only are plotted in Figure 3. The discrepancy is illustrated by plotting the drawdown detention to its related discharge rate on the

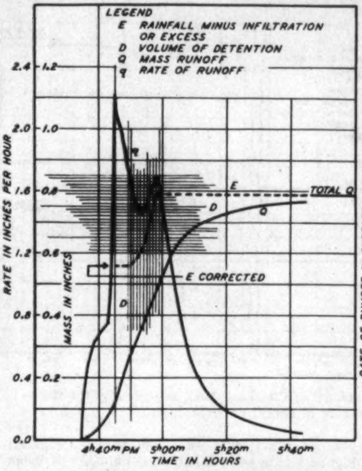

Fig. 3--Detention-discharge relationship for June storms on W-III watershed at Chatham, Va., as developed by two methods of hydrograph analysis

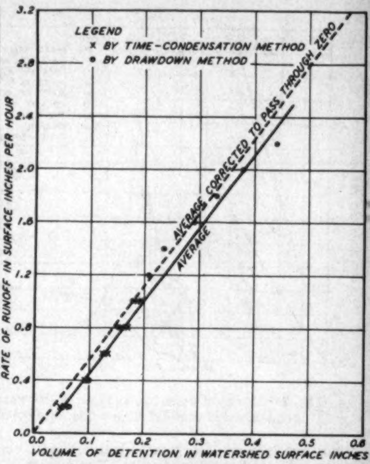

Fig. 4--Drawdown analysis for storm of June 2, 1941 on W-III watershed at Chatham, Va., showing correction in detention for accretions to runoff occurring later than the peak rate of runoff

rising side of the peak. Two things become evident: (1) The discrepancy is sensibly attributable to overland flow detentions. (2) The discrepancy (or overland flow detention) becomes negligible at the peak rate of runoff. Comparisons of overland flow and channel flow from a single storm on the watersheds at Edwardsville, Illinois [SHARP, HOLTAN, and MUSGRAVE, 1949; HOLTAN, 1945], illustrate this phenomenon very clearly.

Based on this premise, all the detention-discharge relationships were determined on the recession side of the hydrograph. Figure 4 illustrates a short-cut method applied to a storm, wherein secondary peaks of runoff occur during the recession. It also serves to explain the technique for those simpler cases wherein rainfall ends abruptly before the peak rate of runoff occurs.

Total runoff from the storm of June 2, 1941, on W-III watershed at Chatham, Virginia (see Fig. 4) was 0.79 inches. Practically no rain occurred after the peak rate of runoff at 16^h58^m; therefore, 0.79 inch of water had either run off or was free to run off thereafter.

The detention-discharge relationship is therefore determined for rates back to and including 1.69 in/hr, the rate at 16^h58^m. Changes in the rate of recession and the occurrence of the subpeak of runoff indicate an accretion to excess rainfall (water free to run off) between 16^h50^m and 16^h58^m. A direct estimate of this accretion would be difficult. However, the partial development of the detention-discharge curve has already related the two values 0.31 inch detention and 1.69 in/hr rate of runoff at 16^h58^m. The excess curve can then be corrected to provide 0.31 inch detention at 16^h49^m when the rate of runoff is again 1.69 in/hr. Without further accretions by rainfall the excess curve progresses at this level back to the maximum peak runoff at 16^h45^m.

Two detention-discharge curves are plotted in Figure 3. They both represent June storms on W-III watershed at Chatham, Virginia. On some watersheds and for some storms, it becomes impossible to separate return-flow seepage from apparent surface detention. In such cases the slope of the detention-discharge curve was maintained as the curve was shifted bodily to pass through zero detention at zero flow.

It was found during the analysis that the detention increased with season for those watersheds

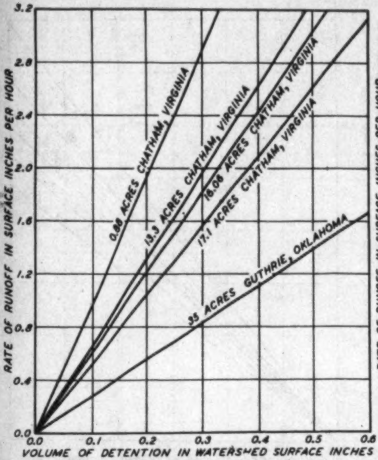

Fig. 5--Detention-discharge relationship for terraced, clean tilled, clipped channels, mixed slopes five to ten per cent predominating as indicated by June storms on various size watersheds

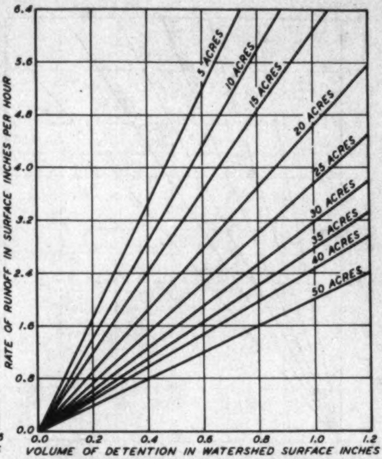

Fig. 6--Hydraulics of flow, volume of detention needed to produce various rates of runoff on terraced, clean tilled, clipped channels, mixed slopes five to ten per cent predominating

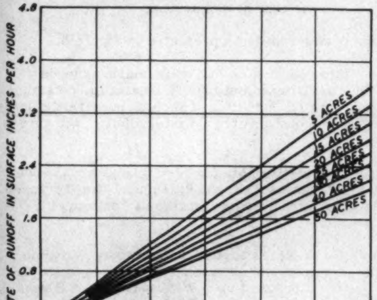

Fig. 7--Hydraulics of flow, volume of detention needed to produce various rates of runoff on terraced, weedy row crop, rank growth in channels and mixed slopes five to ten per cent predominating

on which weeds and litter were known to increase as the season progressed. June storms were analyzed to give detention-discharge relationships for clean-tilled, and the August storms for weedy crops with rank growth in channels.

Three watersheds equipped for runoff measurements at Chatham, Virginia, had detentions in the same order of magnitude as their respective sizes except that late in the season increased vegetation disrupted the efficiency in varying degrees.

Relative positions of the detention-discharge curves in Figure 5 show the effect of size of watershed. Three one-acre terraces at Chatham were also controlled but, owing to frequent overtopping of the upper two terraces, they had to be handled as an average of the three.

Hydraulic principles are the same regardless of geographic location, hence it should be feasible to use data from any location to develop detention-discharge relationships for a set of physical conditions. The curve for 35 acres (see Fig. 5) is an average of several June storms on terraced watershed Ravine A with five per cent slope while planted to cotton, at Guthrie, Oklahoma [HYDROLOGIC STUDIES, 1940]. Together with the Chatham, Va. data, it provides a basis for

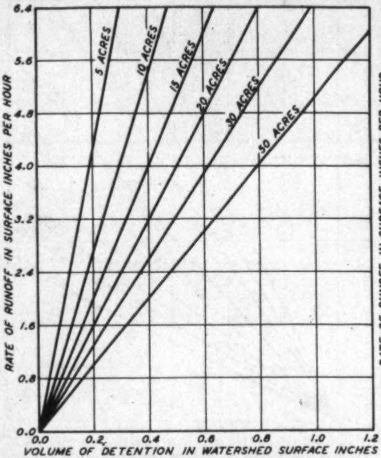

Fig. 8--Hydraulics of flow, volume of detention needed to produce various rates of runoff on clean tilled, straight row up and down hill, channels cultivated, mixed slopes five to ten per cent predominating

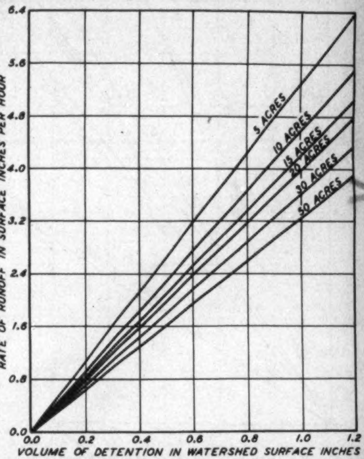

Fig. 9--Hydraulics of flow, volume of detention needed to produce various rates of runoff on contour strip cropping with minimum sodding in waterway and mixed slope five to ten per cent predominating

interpolation and extrapolation for increment sizes of watersheds as presented in Figure 6.

All curves may be extended as straight lines. It is conceivable that as detention exceeds a certain depth, grass obstructions in the channel may be flattened out thus disrupting the detention-discharge relationship. The data considered herein gave no indication of such an occurrence, however, and there is no present means of estimating such a probability. By interpolation, the curves of Figure 6 were prepared from Figure 5.

Through similar procedure the detention-discharge relationship for various size areas under other farm practices were developed and presented in Figures 7, 8, and 9. Figure 7 for Terraced weedy row crops, rank growth in channels was developed from August storms at Chatham, Virginia, and Guthrie, Oklahoma.

Figure 8 was developed from W-II (five acres) and W-III (19 acres) at Blacksburg, Virginia. These watersheds were in corn, exceptionally free of weeds, and showed no differences in the detention-discharge relationship over the season. Figure 8 is based upon W-II and W-III at Blacksburg, now in contoured strip crops together with a 1.73-acre watershed GS-5 at Tyler, Texas [HYDROLOGIC STUDIES, 1941].

Application--Consider a group of watersheds at Chatham, Virginia, having (1) mixed slopes predominantly from five to ten per cent; (2) ranging in size from five to 50 acres, unterraced; (3) planted to tobacco in straight rows running up and down hill; (4) cultivated channels; and (5) the soils a mixture of Madison, Cecil, and Durham.

Figure 10 is a graphical work sheet illustrating the derivation of peak rates of runoff to be expected once in ten years. Rainfall for this recurrence interval is taken from YARNELL [1935] and is plotted in order of time period. The infiltration curve labeled "clean tilled" in Figure 1 is subtracted (with time periods coordinated) from rainfall, thus giving a curve of the excess rainfall to be expected for various time periods. This is the supply to runoff which can be expected

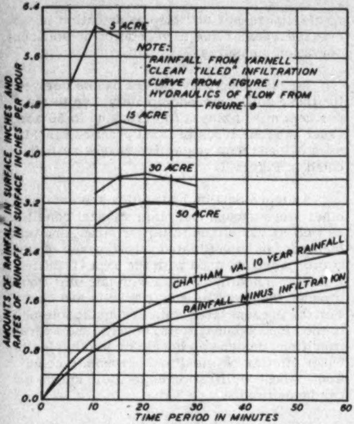

Fig. 10--Work sheet illustrating the application of infiltration and hydraulics of flow to the ten-year frequency rainfall expectancy on various size watersheds of predominately five to ten per cent slopes planted to corn in straight rows running up and down hill and with channels cultivated

once in ten years for each time period. It is the same for all size watersheds of this soil and cover complex since infiltration and rainfall are expressed in units of surface inches, and is not affected by size of area.

Hydraulics, however, is influenced by size. The detention-runoff curve to be used, therefore, must be chosen first to meet the tillage-practices conditions (see Fig. 8) and then to fit the size of watershed. As an example, the top curve is used to predict peak runoff from a five-acre watershed.

Since the time of concentration is not known for the watershed, it is necessary to try several and see which produces the highest rate. At five minutes (see Fig. 10) the excess rainfall to be expected is 0.45 inches. As a first trial assume that one-half of this excess goes to detention and one-half to supply five minutes of runoff. If 0.225 inches ran off in five minutes, the average rate would be 2.70 in/hr. This, however, is an average rate, and since the initial rate is zero the rate at the end of five minutes must be 2 × 2.70 or 5.40 in/hr to give the average. The rising side of the runoff rate curve for unit storms on small watersheds, with sensible corrections for depression storage, implies very nearly constant acceleration to the peak rate. Therefore, in consulting the detention-runoff curve (top dashed curve, Fig. 8) a rate of 5.40 in/hr must relate to 0.225 inches of detention if our initial guess is to be correct. This guess is wrong since 5.40 in/hr actually requires 0.26 inches of detention, we had only 0.225 under this assumption. Next, try a lesser rate of runoff and check again. Assume a final rate of 5.00 in/hr. Then the average rate 5.00/2 = 2.50 in/hr applied for five minutes would require 2.50 × 5/60 = 0.208 inches of the excess rainfall to satisfy runoff. Excess rainfall equals 0.45 inches thus 0.45 inch - 0.208 inch = 0.242 inch of detention. Referring to the top curve of Figure 8, 0.242 inch of detention is related to approximately 5.12 in/hr rate of runoff. Evidently this guess of 5.00 in/hr was a little too low.

In this case the only point of balance is at 5.10 in/hr and 0.24 inch detention. At this point the average rate was 5.10/2 or 2.55 in/hr. If applied for five minutes (2.55 inches × 5/60) the mass runoff in five minutes would be 0.212 inch. This plus the 0.24 inch detention needed to provide the peak rate of 5.10 in/hr gives a total of 0.45 inch which is the amount of excess rainfall available in five minutes. Plot this rate at five minutes in Figure 10.

The entire process of locating this point is facilitated by using a slide rule. The equation to be balanced is as follows: (time period in minutes/60) × (assumed rate in inches per hour/2) + related detention in inches = excess rainfall in inches for the time period. Returning to Figure 10, at ten minutes the excess rainfall is 0.80 inch. A balance of the equation occurs only at R = 6.10 in/hr. Figure 8 gives D = 0.29 inch at R = 6.10 in/hr, therefore 10/60 × 6.1/2 + 0.29 = 0.798 or 0.80.

The rate 6.10 in/hr is plotted on Figure 10 at ten minutes. Similar procedure yields maximum rates for other time periods. It is necessary to carry the calculation only until the maximum peak rate is evident. If the prognosticator is only interested in the five-acre area he can stop here. Figure 10 continues on and includes sufficient determinations to illustrate several interesting phenomena. Notice the change in time of concentration as size increases. Also notice the broadened time of concentration as size increases. These are characteristics which have been recognized for a number of years. They are of value in many applications of hydrology to field design.

Figure 11 presents the results of applying infiltration and hydraulics as influenced by vegetation and tillage. During their preparation, the work sheets clearly depicted a broadening of peaks as size increased and also as detention increased whether due to vegetation or soil conservation measures.

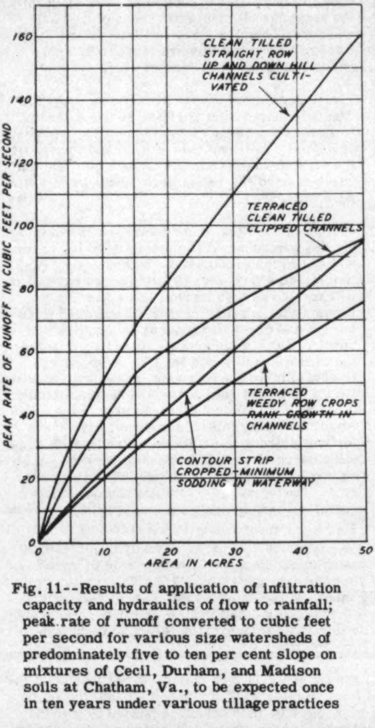

Fig. 11--Results of application of infiltration capacity and hydraulics of flow to rainfall; peak rate of runoff converted to cubic feet per second for various size watersheds of predominately five to ten per cent slope on mixtures of Cecil, Durham, and Madison soils at Chatham, Va., to be expected once in ten years under various tillage practices

Runoff expectancy curves can be derived for these soils on predominantly five to ten per cent mixed slopes for areas up to 50 acres under the four types of farm practices in Figures 6-9 and with vegetative covers as indicated in Figure 1.

As more data on hydraulics are obtained, other slope groups and other channel conditions as well as variations in larger sizes, and other factors, can be estimated. The curves of infiltration were obtained with the Type-F infiltrometer. Additional data with this unit would broaden the scope as regards soils and cover. For the present these data are applicable only to the slope groups, soils, covers, and hydraulic conditions designated herein or to other soils, under similar physical and agronomic conditions, whose infiltration capacity is known or can be estimated.

Discussion--Several advantages attend the hydrologic approach to runoff prognostication: (1) It borrows strength from the longer records of rainfall. (2) Complex interacting phenomena are separated and estimated individually rather than collectively. (3) Similarity of watersheds is much more easily judged on this integrated basis. (4) Universal principles of hydraulics expand the sources and applicability of data. (5) Infiltration capacity, although complex, is less difficult to study as a single criterion than it is in combination with rainfall and hydraulics. (6) Integration of the three phases of hydrology permits a rational application which should lead to increased knowledge and efficiency.

Acknowledgments--The data were obtained and compiled jointly by the staffs of the Agricultural Engineering Department of Virginia Agricultural Experiment Station and the Soil Conservation Service Research under the direction of J. H. Lillard and T. W. Edminster. Acknowledgment is due for review and constructive suggestions in the preparation of this report by Lillard, Edminster and also to R. C. Jones, Zone Conservationist, Soil Conservation Service, Operations, Region 2, who spent several days in conference with the authors.

References

HOLTAN, H. N., Time-condensation in hydrograph analysis, Trans. Amer. Geophys. Union, v. 26, pp. 407-413, 1945.

HORTON, R. E., Surface runoff phenomena, on file U. S. Dept. of Agric. Library. 1935 (processed)

HYDROLOGIC STUDIES, Rainfall and runoff from the watersheds of the Red Plains, U. S. Dept. of Agric., SCS-TP-32, Guthrie, Oklahoma, June 1940.

HYDROLOGIC STUDIES, Rainfall and runoff data from the watersheds of the Arkansas, Louisiana, and East Texas sandy lands, U. S. Dept. of Agric., SCS-TP-41, Tyler, Texas, June 1941.

PARSONS, D. A., Operation of the type-F artificial rainfall apparatus, U. S. Dept. of Agric., SCS research in-service report, 1939.

PEELE, T. C., O. W. BEALE, and F. F. LESESNE, Irrigation requirements of South Carolina soils, Clemson, South Carolina, U. S. Dept. of Agric., SCS research in-service report, 1947.

SHARP, A. L., and H. N. HOLTAN, Extension of graphic methods of analysis of sprinkled-plot hydrographs to the analysis of hydrographs of control-plots and small homogeneous watersheds

Trans. Amer. Geophys. Union, pp. 578-593, 1942.
SHARP, A. L., H. N. HOLTAN, and G. W. MUSGRAVE, Infiltration in relation to runoff on small watersheds, U. S. Dept. of Agric., SCS-TP-81, June 1949.
YARNELL, DAVID L., Rainfall intensity frequency data, USDA Misc. Publ. 204, 1935.

Soil Conservation Service,
Virginia Agricultural Research Station,
Blacksburg, Virginia

(Manuscript received December 27, 1949, and, as modified, June 27, 1950; presented at the Thirty-First Annual Meeting, Washington, D. C., May 1, 1950; open for formal discussion until March 1, 1951.)

Transactions, American Geophysical Union Volume 31, Number 5 October 1950

CLASSIFICATION OF GEOTECTONIC ELEMENTS

Wallace M. Cady

(Published by permission of the Director, U. S. Geological Survey)

Abstract--The basis for a genetic classification of geotectonic elements is provided by the works of several geologists. Bubnoff has presented a spatial classification: continental blocks, oceanic basins, geosynclines, and mobile and stable shelves. Stille has described an evolutionary development of the geotectonic elements through four stages here referred to as: (1) the primary geosynclinal stage, (2) the primary mountain building stage, (3) the secondary mountain building stage, and (4) the stage of final differential uplift and local subsidence. Characteristic magmatic and sedimentational features are associated with the elements developed in each of the stages. Kay, Kuenen, Umbgrove, and others have provided refinements to the interpretation of geotectonic elements. A nomenclature has arisen that is believed to be generally useful in the discussion of geotectonics.

Introduction

More than three-quarters of a century ago James Hall concluded that the rocks of the Appalachian Mountains had accumulated in a subsiding trough which was later uplifted and folded. He believed this pattern--subsidence followed by mountain building--to be true of other regions also, and since his time the most fundamental parts of the theory have been verified and generally adopted. In more recent years several workers, principally STILLE [1940, 1943, 1944], BUBNOFF [1931], KAY [1942, 1944, 1947], KUENEN [1935], and UMBGROVE [1947], have undertaken extensive regional tectonic investigations of large areas of the Earth's surface. These studies have shown that mountain belts, such as the Appalachians, form only a part of a much more extensive framework comprising a variety of geotectonic elements developed in a rather well defined evolutionary pattern.

It is the purpose of the present discussion to review the spatial relationships of these geotectonic elements and to describe their evolution. It is hoped that this will furnish the groundwork for a better understanding of the origin and distribution of various types of rocks and mineral deposits.

Geotectonic elements in space and time

BUBNOFF'S [1931, pp. 146-203] breakdown of geotectonic elements into continental blocks, oceanic basins, geosynclines, and mobile and stable shelves points up the space relationships with which most geologists are familiar. STILLE [1940, pp. 4-23] has presented an evolutionary development of geotectonic elements through four critical stages and thereby emphasizes the very great significance of time as well as space relationships in their classification. This process explains the growth of continents through accretion of rocks formed in geosynclinal belts and also takes into account the subsidence of continental areas beneath the sea. Stille's four stages are referred to in the following discussion as (1) the primary geosynclinal stage, (2) the primary mountain building stage, (3) the secondary mountain building stage, and (4) the stage of final differential uplift and local subsidence.

I have illustrated these four stages by generalized cross-sections of an hypothetical continent (see Fig. 1). The continent illustrated is in some respects like North America and in others it is not; a comparison should not be attempted, therefore, except in certain details. The continental block is located centrally and is bordered on each side by mobile shelves; stable shelves are developed locally on the continental block. Outside of the mobile shelves are the geosynclines. Stable nuclei may occur within the geosynclines. Oceanic basins lie beyond the geosynclines. Although these sections do not show the situation in which a geosyncline lies between two continental blocks the pattern of such a relationship is evident; intercontinental mobile belts are characterized by a central geosynclinal zone bordered by mobile shelves on the edges of the continental blocks.

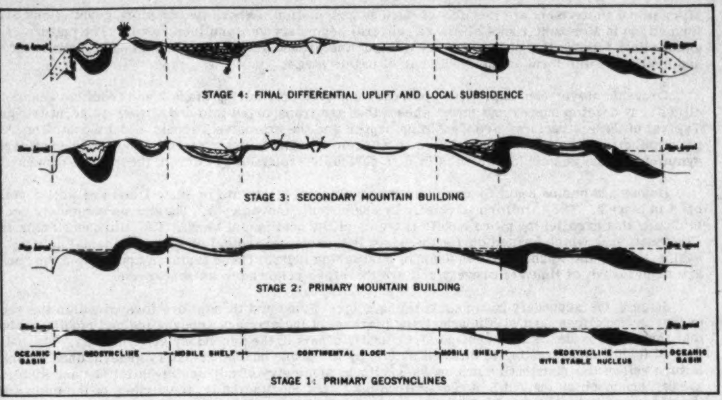

STAGE 4: FINAL DIFFERENTIAL UPLIFT AND LOCAL SUBSIDENCE

STAGE 3: SECONDARY MOUNTAIN BUILDING

STAGE 2: PRIMARY MOUNTAIN BUILDING

STAGE 1: PRIMARY GEOSYNCLINES

Fig. 1--Evolution of geotectonic elements of an hypothetical continent

Stage 1, the primary geosynclinal stage--Arcuate belts of subsidence form between the major stable elements; for example, between continental blocks and oceanic basins as in the belt that borders the Pacific Ocean, or between two continental blocks as in the Alpine-Himalayan belt. The subsidence of the primary geosynclines is not uniform and results in the formation of longitudinal ridges and troughs. The deepest of the troughs are commonly most remote from the continental blocks that adjoin the geosynclinal belt. Typical primary geosynclines in North America are those of the western part of the Cordilleran belt, formed during the Paleozoic and early Mesozoic, and of the New England-Piedmont belt of the East, formed during the early Paleozoic. The primary geosynclines may divide locally around more stable nuclei whose deficient mobility is more like that of the continental blocks. The Seward Peninsula of western Alaska and the Chukotski Peninsula on the Siberian side of Bering Strait are together the site of a stable nucleus developed in Paleozoic time.

The deposits of the primary geosynclines (Fig. 1, solid black) converge laterally into those of the mobile shelves at the margins of the continental blocks, where subsidence is less. The Paleozoic and early Mesozoic strata of the eastern Great Basin region and the early Paleozoic strata of the Champlain Valley and Folded Appalachians were deposited on mobile shelves. Stable shelves, characterized by relatively minor subsidence, are more centrally located on the continental blocks and were well developed particularly in early Paleozoic time in the Central States.

As Stage 1 progresses the longitudinal ridges of the primary geosynclinal belt may rise above sea level. Such epeirogenic movements may be associated with local folding and thrusting that are precursors of the extensive orogenic movement of Stage 2. Preliminary orogenic movements of this type are recorded in late Paleozoic and early Mesozoic rocks of the primary geosynclinal belt in the western Great Basin region.

Stage 2, the primary mountain building stage--The longitudinal ridges of Stage 1 continue to rise and form extensive geanticlines whose arcuate pattern reflects the arcuate pattern of the primary geosynclinal belt. An example familiar to all is the great Mesozoic Nevadan geanticline of the West. A similar geanticline was formed in the northeastern states at the time of the Taconic orogeny. UMBGROVE [1947, pp. 144-216] has shown how geanticlines form the single island arcs of the western Pacific Ocean and the inner arc of the double-arc chain of the East Indies.

The geanticlinal zone divides the primary geosyncline into marginal troughs. These troughs are the sites of secondary geosynclines whose subsidence may involve not only the outer portions of the primary geosyncline but commonly includes wide portions of the adjacent continental block; the mobile shelves are thus extended farther onto the continental block than in Stage 1. The Cretaceous strata of the Rocky Mountains and California, and the Silurian and Devonian rocks of the Folded Appalachian belt form typical secondary geosynclines. The deposits of the Gulf Coast and

Mississippi embayment are possibly of such an association. Where two or more geanticlines are formed, as in Mesozoic rocks of Alaska, several secondary geosynclines result. The pattern of the geanticlines follows that of the primary geosyncline around stable nuclei. Comparatively broad and shallow basins form on the stable nuclei in this stage.

Orogenic movements supersede epeirogenic movements during Stage 2 and from the geanticlines may develop nappes and thrust sheets that are transported into and across adjacent troughs. Typical of these structures are the Alpine nappes and the extensive Taconic allochthone. The principal direction of transport relative to adjacent troughs is determined by the cross-sectional symmetry of the geanticline which is in turn variously explained by current theories of orogeny.

Domes and basins begin to appear on the continental block late in Stage 1 and are well developed in Stage 2. They are formed chiefly by epeirogenic movements. The domes commonly occur in chains that parallel the more mobile margins of the continental block. The Adirondack axis and Cincinnati arch which formed during the early Paleozoic are typical of such continental uplifts; basins such as the Michigan basin form in intervening belts. These features appear to form, or are rejuvenated, at times of orogeny and are therefore referred to as synorogenic.

Stage 3, the secondary mountain building stage--Folds and thrusts are formed within the secondary geosynclines, and within underlying portions of the primary geosyncline and mobile shelves that through subsidence have become structurally a part of the secondary geosynclines. The pattern of folding and thrusting is dictated chiefly by the shape of the secondary geosynclines, which in turn reflect the distribution and cross-sectional symmetry of adjacent geanticlines and stable areas. Inasmuch as the width of geanticlines may vary longitudinally, the strikes of the folds and thrusts, commonly developed parallel to the borders of the geanticline in the adjacent secondary geosynclines, may be at considerable variance with the arcuate pattern of the geanticlinal axis that was inherited from an earlier stage. The average dip of thrust planes and of axial planes of folds formed in the secondary geosyncline is parallel to its plane of symmetry. Thus the movement pattern of secondary mountain building reflects in a general way that of primary mountain building, but local deviations are to be expected.

The Folded Appalachian belt, site of the classic geosyncline of Hall, and therefore possibly to be considered the type geosyncline of nomenclature, is one of the most familiar examples of secondary mountain building. The thrusts and folds of the Laramide orogeny of Idaho, Utah, and western Wyoming were also formed during secondary mountain building. UMBGROVE [1947, pp. 173-191, 200-205] ascribes the outer arc of the double island arc of the East Indies to such mountain building activity. He explains the absence of the outer arc in the single-arc chains of the western Pacific Ocean by the proposition that the marginal troughs outside of the geanticlinal single arcs never received appreciable sediments, being too remote from adequate sources.

The movements of Stage 3 are in part epeirogenic. Folding and thrusting diminish in the direction of the continental block and stable nuclei and to some extent toward the geanticlinal tracts. In these areas folding and thrusting are superseded by vertical movements. Broad arches may be formed on those portions of the mobile shelf that become extended onto the continental block during formation of the secondary geosynclines in Stage 2. These arches have some of the features characteristic of orogeny, such as their marginal thrusts, but vertical uplift is a prime requirement of their broad span. Typical of such arches are the uplifts of the Rocky Mountains, particularly in Wyoming, Utah, and Colorado. The areal patterns of these structures may diverge markedly from those of both the primary geosynclinal belt and adjacent portions of the mobile shelf, further witness to the proposition that they are not directly related to the orogenic-movement plan evolved in the primary geosynclinal belt. This is emphasized particularly by the eastward trend of the Uinta Mountains, nearly at right angles to the trend of the folds and thrusts farther west.

Domes and basins, such as those related to primary mountain building, continue to develop on the continental block during secondary mountain building.

Stage 4, final differential uplift and local subsidence--This might be considered a third stage of mountain building, though mainly epeirogenic. It is characterized by block faulting that takes place chiefly within the orogenic belts developed in Stages 2 and 3. Such movements, almost entirely epeirogenic, succeed the orogenic movements of earlier stages and their initiation marks the consolidation of the geosynclinal accumulations with the continental block, and consequent extension of the limits of the continental block into former geosynclinal belts. The areal pattern of the block faults is conditioned by their position with respect to geotectonic elements extant in the earlier stages. Thus block faults developed in and near the primary geosynclinal belt tend to perpetuate the arcuate pattern of the primary geosyncline, but as the continental block is approached the pattern of block faulting may become more diverse and may reflect a structural control unrelated to the geosynclinal belts. Block faulting accompanies rather general differential uplift of the newly extended continental block which is most extreme in the belts of both primary and secondary mountain building. This uplift accounts for the present mountain elevations.

The Triassic basins of the eastern United States and the mountains of the Great Basin are familiar examples of block faulting of belts of earlier orogenic movement. The Tertiary uplifts of the Sierra Nevada and Cascade Ranges and of the Alaska Range illustrate the extremes of upward movement in western North America in Stage 4.

Many block fault features, such as the Rhine Graben, the Ottawa Valley Graben, and the Rift Valleys of Africa that are diversely oriented with respect to orogenic belts, seem to be a rather obvious effect of stretching of the Earth's crust as opposed to the compressional effects of orogeny. Likewise the fault basins formed in orogenic belts suggest the effects of stretching with subsidence. Several regions of the Earth's surface, particularly the basins of the Indian Ocean, Mediterranean Sea, North Atlantic, and Arctic Ocean, include extensive areas in which portions of continental blocks, including consolidated geosynclinal belts, have subsided beneath the sea.

Magmatic and sedimentational associations

Characteristic magmatic and sedimentational features, some of whose processes of formation strongly affect the tectonic history, and most of which on the other hand are influenced by it, commonly are associated with the geotectonic elements developed in each of the four stages. Such associations are sufficiently common to assist in identification of the element and the stage in which it occurs.

The primary geosynclines of Stage 1 are characterized by submarine volcanic rocks, notably spilite interbedded with chert, argillite, and graywacke; these are intruded by ultramafic rocks. The Calaveras formation of Paleozoic age, the Mariposa slate and Franciscan group of Mesozoic age of California, the Cambrian and Ordovician rocks of central New England east of the Green Mountains, and many of the schists and gneisses of the Piedmont originated as primary geosynclinal accumulations.

The mobile shelves of Stage 1 are commonly amagmatic and characterized by shale and limestone that, in the direction of the continental block, pass laterally into first-cycle orthoquartzite, a little arkose, and dolomite. The Cambrian and Ordovician rocks of the Folded Appalachians and the Champlain Valley are typical.

Synorogenic plutons, typically extensive granodioritic batholiths, such as those of the Sierra Nevada and of western British Columbia, intrude the strata of the primary geosynclines in Stage 2. The secondary geosynclines of Stage 2, which rest chiefly on the rocks formed in the primary geosyncline, contain shale and graywacke and, locally, arkose, derived from the geanticlines, as in the Upper Cretaceous strata of southwestern Alaska. On the other hand the secondary geosynclines that rest primarily on the rocks of the mobile shelves and adjacent portions of the continental block commonly contain graywacke derived chiefly from the geanticline nearest the continental block, and second-cycle orthoquartzite produced by reworking of the orthoquartzites formed on the mobile shelves of Stage 1. The Silurian and Devonian strata of the Folded Appalachians contain a typical geosynclinal deposit of the latter sort, whose weight upon the continental block is believed to have contributed to subsidence and therewith to the encroachment of the mobile shelf upon the continental block. The secondary geosynclines, particularly in the vicinity of the geanticlines, generally contain volcanic rocks and hypabyssal intrusives, chiefly andesites,. rhyolites, dacites, and quartz porphyries; the hypabyssal rocks are commonly intruded near the time of secondary mountain building in Stage 3.

Alkalic intrusives, characteristically granitic and syenitic stocks, are emplaced after the stage of secondary mountain building and consolidation of the geosynclinal belt with the continental block. They intrude rocks formed both in the primary geosynclinal belt, as in New Hampshire, and on the continental block and extended mobile shelf, as in the eastern Rocky Mountains.

Plateau basalts are extruded in Stage 4 and in company with arkose and graywacke may be found in down-faulted basins. Such formations are a familiar feature of the Columbia River Plateau, the Great Basin, and the Triassic basins of the East.

The stable continental blocks and oceanic basins show less differentiation of rock types with

passage through the various stages. Thus red clay and organic ooze are formed in the oceanic basins rather continuously; and reef limestone and dolomite, black shales, and evaporites may continue to form on the continental blocks at least through Stage 3. After Stage 3, and consolidation of the geosynclinal belt with the continental block, deposits characteristic of the continental block may extend into the former geosynclinal belt. Alkalic intrusives and certain volcanics may show a closer relationship to deep crustal fractures, such as those of the rift patterns, which may be formed in the continental blocks, than to the geosynclinal belts. The alkalic intrusives of the Monteregian Hills, for example, form a west-northwest oriented linear pattern that extends onto the continental block and is normal to the geosynclinal belt of New England and southeastern Quebec; likewise the alkalic rocks of central Colorado trend nearly at right angles to the geosynclinal pattern. The curvilinear pattern of the basaltic volcanic accumulations of the Hawaiian Islands suggests a comparable relationship to a crustal fracture in the oceanic basin.

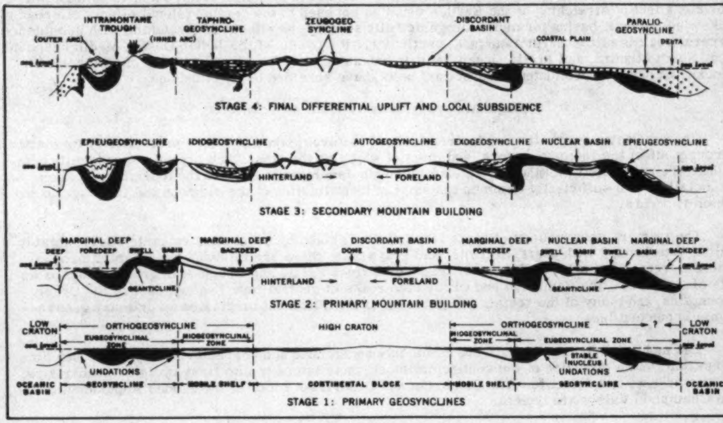
INTRAMONTANE TROUGH
(OUTER ARC)
(INNER ARC)
TAPHRO-GEOSYNCLINE
ZEUGOGEO-SYNCLINE
DISCORDANT BASIN
COASTAL PLAIN
PARALIO-GEOSYNCLINE
DELTA
sea level
STAGE 4: FINAL DIFFERENTIAL UPLIFT AND LOCAL SUBSIDENCE
EPIEUGEOSYNCLINE
IDIOGEOSYNCLINE
AUTOGEOSYNCLINE
EXOGEOSYNCLINE
NUCLEAR BASIN
EPIEUGEOSYNCLINE
HINTERLAND →
← FORELAND
STAGE 3: SECONDARY MOUNTAIN BUILDING
MARGINAL DEEP
DEEP
FOREDEEP
SWELL
BASIN
GEANTICLINE
MARGINAL DEEP
BACKDEEP
DISCORDANT BASIN
DOME
BASIN
DOME
MARGINAL DEEP
FOREDEEP
NUCLEAR BASIN
SWELL
BASIN
SWELL
MARGINAL DEEP
BASIN
BACKDEEP
GEANTICLINE
HINTERLAND →
← FORELAND
STAGE 2: PRIMARY MOUNTAIN BUILDING
LOW CRATON
ORTHOGEOSYNCLINE
EUGEOSYNCLINAL ZONE
MIOGEOSYNCLINAL ZONE
HIGH CRATON
ORTHOGEOSYNCLINE
?
LOW CRATON
MIOGEOSYNCLINAL ZONE
EUGEOSYNCLINAL ZONE
STABLE NUCLEUS
UNDATIONS
UNDATIONS
OCEANIC BASIN
GEOSYNCLINE
MOBILE SHELF
CONTINENTAL BLOCK
MOBILE SHELF
GEOSYNCLINE
OCEANIC BASIN
STAGE 1: PRIMARY GEOSYNCLINES

Fig. 2--Nomenclature of geotectonic elements

Nomenclature

The terminology applied to geotectonic elements has proved to be the most confusing aspect of the subject. In the foregoing discussion an attempt has been made to avoid unfamiliar terms in order to focus attention on the process and sequence of formation of the various elements. It seems worthwhile, however, to point out briefly some of the terms that have been proposed.

The nomenclature is illustrated in Figure 2 by addition to the diagram shown in Figure 1. The terms applied to geosynclinal successions illustrated in Stage 3, after secondary mountain building, are equally applicable to these successions in Stage 2 before secondary mountain building, but to simplify the diagram they are not shown in the cross-section for Stage 2. Many of the terms for geomorphic features illustrated in the cross-section for Stage 2 have been applied by various authors to more or less comparable features formed in later stages.

The North American continental block is commonly referred to as the foreland. This usage presents no difficulties inasmuch as thrusting and overturning of folds is predominantly in the direction of the continental block in all of the bordering mountain belts. Were this not so, however, part of the block would have to be called a hinterland. Use of the term "craton," or more specifically "high craton," relieves this difficulty; the term "low craton" may be used to refer to the stable oceanic basins.

STILLE'S [1940, pp. 653, 656] terms "eugeosynclinal zone" and "miogeosynclinal zone" are becoming familiar. Eugeosyncline refers to the primary geosyncline. Miogeosyncline refers to the mobile shelf that borders the primary geosyncline. WELLS [1949, p. 1927] has recently

employed the terms ensimatic and ensialic, respectively, in reference to a pure type of the eugeosyncline considered to have formed on a sima basement, and of the miogeosyncline considered to have formed on a sialic basement.

Terms such as "foredeep" and "backdeep" refer to the marginal troughs or deeps of the primary mountain-building stage, and, like the terms "foreland" and "hinterland," they relate to the cross-sectional symmetry of the orogenic belt. They are particularly useful in discussions of deep-sea troughs, such as those of the western Pacific Ocean, that have apparently not received appreciable quantities of sediments. HESS' [1938, pp. 77-81] geotectocline is essentially a secondary geosyncline formed by sedimentation of a trough or tectogene, so named because it becomes the site of later (secondary) mountain building, developed in the primary mountain building stage. KAY [1947, pp. 1292, 1293] has applied several terms to the geosynclines formed in the primary mountain-building stage. His term "epieugeosyncline" is self-explanatory. "Exogeosyncline" refers to the deposits of the marginal trough that extends onto the continental block. "Idiogeosynclines" [see also UMBGROVE, 1947, pp. 181, 194] suggest local persistence or renewal of the miogeosyncline. KAY [1947, pp. 1292, 1293] has also expanded the use of geosynclinal terminology to the fault troughs, and to delta and coastal plain deposits of the final stage (taphrogeosyncline and paraliogeosyncline) and to basins formed entirely on the continental block (autogeosyncline and zeugogeosyncline). The terms "marginal deep," "intramontane trough," "nuclear basin," and "discordant basin" are presented by UMBGROVE [1947, pp. 42-65] and refer to features also described by KUENEN [1935, pp. 37-47]. They are variously applicable to the geotectonic elements of Stages 2, 3, and 4.

STILLE [1940, p. 21] refers to Stage 1 as the "geosynclinal state," to Stage 2 as the state of "orogeny," to Stage 3 as the "quasi-cratonic state," and to Stage 4 as the "full-cratonic state." The orthogeosyncline of STILLE [1940, p. 656] includes the eugeosynclinal and miogeosynclinal zones of Stage 1. The term "undations" [STILLE, 1940, p. 659] refers to the longitudinal ridges in the orthogeosyncline that later may become geanticlines. STILLE'S [1940, p. 657] "parageosynclines" refer to the geosynclines and fault troughs of later stages that mark more advanced states of consolidation with the craton. He includes basins and swells [STILLE, 1943, pp. 4-5] among features formed in the later stages.

The question of the proper nomenclature to use in designating the geotectonic elements is manifestly difficult, and improvements have been and will be suggested. However, many of the terms cited above have been found meaningful, and it is believed that they have a place in the discussion of geotectonics.

Acknowledgments

The author is indebted to V. E. McKelvey, who proposed the preparation of this paper and contributed much helpful advice as to its proper content and emphasis. F. G. Wells and H. G. Ferguson have also made many useful suggestions. The reports of field investigations of numerous geologists, many of which are cited by Stille, form the factual basis of the synthesis presented here. The manuscript was read critically by Esther Aberdeen, A. H. Chidester, Ferguson, and McKelvey.

References

BUBNOFF, S. VON, Grundprobleme der Geologie, Borntraeger, Berlin, 237 pp., 1931.
HESS, H. H., Gravity anomalies and island arc structure with particular reference to the West Indies, Proc. Amer. Phil. Soc., v. 79, pp. 71-96, 1938.
KAY, MARSHALL, Development of the northern Allegheny synclinorium and adjoining regions, Bull. Geol. Soc. Amer., v. 53, pp. 1601-1657, 1942.
KAY, MARSHALL, Geosynclines in continental development, Science, v. 99, pp. 461-462, 1944.
KAY, MARSHALL, Geosynclinal nomenclature and the craton, Bull. Amer. Assoc. Petr. Geol., v. 31, pp. 1289-1293, 1947.
KUENEN, P. H., Geological interpretation of the bathymetric results, Snellius Expedition in the Eastern Parts of the Netherlands East Indies, pt. 1, Kemink en Zoon, Utrecht, 124 pp., 1935.
STILLE, HANS, Einführung in den Bau Amerikas, Borntraeger, Berlin, 717 pp., 1940.
STILLE, HANS, Malaiischer Archipel und Alpen, Abh. Preus. Akad. Wiss., Math.-natur. Kl. 1943, no. 1, 16 pp., 1943.
STILLE, HANS, Geotektonische Gliederung der Erdgeschichte, Abh. Preus. Akad. Wiss., Math.-natur. Kl. 1944, no. 3, 80 pp., 1944.
UMBGROVE, J. H. F., The pulse of the Earth (2d ed.), Martinus Nyhoff, The Hague, 358 pp., 1947.
WELLS, F. G., Ensimatic and ensialic geosynclines (abstract), Bull. Geol. Soc. Amer., v. 60, p. 1927, 1949.

160 1/2 Main Street,
Montpelier, Vermont

(Communicated manuscript received May 15, 1950;
open for formal discussion until March 1, 1951.)

Transactions, American Geophysical Union Volume 31, Number 5 October 1950

OCEANOGRAPHIC ACTIVITIES OF THE U. S. COAST AND GEODETIC SURVEY

Robert F. A. Studds

As part of its work of surveying and charting the coastal waters of the United States and possessions, the Coast and Geodetic Survey is accumulating oceanographic and geophysical data pertaining to depths of water, character of the sea bottom, rise and fall of the tide, and the study of currents and physical properties of sea water.

The methods and techniques employed in the collection of such data are continually being improved. This is especially true with respect to position determination in hydrographic surveying, which is constantly undergoing study and modification in our electronic instrument laboratory. These modifications are undertaken not only to obtain greater accuracy in distance measurements but to adapt the equipment to the varied conditions under which our surveys are conducted.

Improvements made during the year in the Bureau's Electronic Position Indicator and associated equipment have materially increased the accuracy of distance measurements. Circuits have been redesigned to reduce to a minimum the variation in operation caused by aging of vacuum tubes and other components. The phase errors caused by the ship's superstructure have been reduced to a minimum by the installation of a special type of antenna. The latest information indicates that the error in a single distance measurement will not be more than 75 yd for 80 per cent of the time at distances as great as 285 mi. These errors were checked by visual fixes on shore objects.

Modification of Shoran equipment consisted chiefly of converting the standard ship equipment to serve as ground-control equipment. With this modification, a lighter weight equipment for difficult shore installation was produced, which can be so calibrated that the error within the equipment can be reduced to a negligible quantity so far as control for hydrographic surveys is concerned.

During the past year, 17 of the Bureau's ships and two shore-based parties were engaged in hydrographic surveys along the coasts of continental United States and in Alaskan waters. Over 52,000 mi of sounding lines were surveyed comprising an area of 12,000 mi.

Along the Atlantic coast, surveys were accomplished in the vicinities of Mount Desert, Maine; Hempstead Bay, Long Island; and in Chesapeake Bay. Wire-drag surveys for locating sunken wrecks off the Maryland and Delaware coasts were continued.

In the Gulf of Mexico, inshore surveys were begun on the west coast of Florida and offshore surveys were continued between the 10- and 50-fm curves in the east-central portion of the Gulf. On the Pacific coast, hydrographic operations were continued in the vicinities of San Francisco Bay and the Columbia River as part of a program of modernizing the surveys of inshore areas.

Hydrographic surveys in Alaska continued to receive emphasis. Work was accomplished in southeast Alaska, Prince William Sound, the western Aleutians, Bristol Bay, and along the Arctic Coast. A survey of Kukuk Bay, on the south coast of the Alaska Peninsula, has been completed. In the Aleutian Islands standard Shoran equipment was used for all offshore hydrography to distances as great as 145 mi. In the Bristol Bay area and in the Arctic region, modified Shoran equipment was used with success. The maximum distances obtained in Bristol Bay were approximately 50 mi, due, in the main, to low elevations obtainable for the control-station antennas.

Our hydrographic surveys are bringing to light additional interesting submarine features along the continental margins and in our inland waters. In the Gulf of Mexico, between Florida and the Mississippi Delta, the first of a new series of offshore surveys revealed 150 mi of escarpment where the continental slope abruptly drops 4000 ft on a 35° slope to depths of 9600 ft. The escarpment terminates in De Soto Canyon, about 65 mi south of Pensacola. Echo sounder profiles in one area of San Francisco Bay have revealed in detail a pattern of sand waves.

The surveys completed west of Amchitka Island in the Aleutians provide an opportunity for further studies of the Aleutian Ridge. With the exception of Petrel and Bowers Banks, the trend of the north side of the Ridge is generally uniform, whereas two prominent canyons or valleys indent the south slope. In the vicinity of the canyons west of Buldir Island, the surveys revealed several truncated knolls, the tops of which stand at about the same depth of 350 to 500 ft.

Three deep-sea sounding lines, totaling approximately 7800 mi, were run across the North Pacific Ocean by the ships Pioneer, Explorer, and Pathfinder while en route from their Alaska working grounds to Pacific Coast bases. Two of the lines were begun in the vicinity of Adak Island in the Aleutians and crossed the intervening ocean area by great-circle courses to the vicinities of San Francisco Bay and Yaquina Head, respectively. A similar sounding line was run from the vicinity of Unimak Pass along a great-circle course to the Oregon coast. In general, all depths were in excess of 2000 fm except when passing over several seamounts. In the vicinity of the Aleutian Trench, depths as great as 4070 fm were obtained. Three new seamounts rising 500 to 1500 fm above the ocean floor were found on these great-circle profiles. One of these, rising to a depth of 665 fm from surrounding depths of 2100 fm, is located about 800 mi northwest of Seattle. The westward continuity of the submarine scarp off Cape Mendocino, California, was substantiated at a distance of 200 mi off the coast.

As another aspect of our oceanographic work, our collection of tidal data has been augmented by an expanded tide and current program. Long-period tide observations for the determination of tidal characteristics and sea-level variations were continued at key points along the coasts of the United States and its possessions and on a number of islands in the Pacific. Valuable data are also being received through participation in the programs of the Department of State and the Inter-American Geodetic Survey in Latin-American countries. These projects are supplying records from 150 tide stations, and will furnish basic data for the prediction of tides and for the study of tidal action in these areas.

The comprehensive current survey of Tampa Bay, Florida, will be completed in the near future. Data from this survey have already been utilized to calculate daily predictions of the current for Tampa Bay entrance. A current survey of the entrance to Grays Harbor, Washington, was begun early in March. Projected programs call for current surveys of Rosario Strait, Washington; the Aleutian Island passes; and Bering Sea and Strait.

The program of securing long series of hourly current observations at selected lightship stations along our coasts has been continued through the cooperation of the United States Coast Guard. Observations were continued at Five Fathom Bank Lightship off Delaware Bay and Frying Pan Shoals Lightship off Cape Fear, North Carolina. The results of these observations, besides furnishing information for navigation, are an important addition to our fund of oceanographic data.

As part of its tide and current program, the Bureau observes the temperature and density of sea water at selected tide stations. Observations were obtained at 118 stations in the United States and foreign countries. Seven thermograph installations distributed along our coasts provide continuous temperature records. Studies of sea-water temperatures along our North Atlantic coast indicate that the average temperatures during the past five years have been 1° or 2° F warmer than the long-period means.

Several tidal and related publications, of interest to oceanographers, have been published during the year in revised editions. These include Special Publication No. 196, Manual of Tide Observations; Special Publication No. 228, Tide and Current Glossary; and Publication DW-1, Density of Sea Water, Atlantic and Gulf Coasts.

To facilitate future expansion of the tide tables, several important changes will be made, beginning with the 1951 edition. The Tide Tables, Atlantic Ocean, and the Tide Tables, Pacific Ocean and Indian Ocean, will be discontinued. World coverage will be obtained through the publication of four volumes representing the following general areas: (1) Europe and west coast of Africa; (2) east coast, North and South America; (3) west coast, North and South America; and (4) central and western Pacific Ocean and Indian Ocean.

Under the Philippine Rehabilitation Program, the survey work in the Islands was continued. Hydrographic surveys were made in the vicinity of Cebu and wire-drag investigations were made of wrecks in the Manila Bay area. This program will terminate on June 30, 1950.

The system for warning the Hawaiian Islands of an impending seismic sea wave has been considerably advanced. There are now 18 stations in the network of wave-reporting stations. The

Army, Navy, Air Force, and CAA have cooperated in setting up an improved system of rapid communication between these stations and Honolulu. Seismic sea wave travel time charts to wave-reporting stations at Midway, Attu, Adak, Dutch Harbor, Kodiak, and Sitka have recently been printed.

In the development and issue of nautical charts, a program has been initiated for adding Loran lines of position to all sailing and general charts of the Bureau. On the Atlantic coast, offshore charts covering the coast from Nova Scotia to Key West have been published in this manner. On the Pacific coast the curves are being added to a small-scale sailing chart which covers the Pacific coast from Mexico to the Aleutians. These curves are to be added to the 1100 series charts on the Atlantic coast and other charts on the Pacific coast as soon as the Loran stations now under construction have been completed. Reports indicate that the combined use of Loran with the charted courses in the Gulf Stream has lessened considerably the sailing time northbound along the Atlantic coast. In the revision of the Bureau's existing charts, surveys are being applied as rapidly as seasonal field results can be reviewed and compiled.

Another development that is in progress is the application of hydrographic data to topographic quadrangle maps of coastal areas. These data provide a graphic correlation of land topography with the submarine configuration and should be of interest to students of the geophysical sciences.

The Coast and Geodetic Survey is primarily concerned with increasing safety in marine navigation. This is being accomplished through improvements in methods and equipment for obtaining data which go into the production of the nautical chart. As a by-product of these activities we are accumulating a vast amount of precise data, relating to the bottom configuration and the movements and physical properties of water masses along our continental shelves and slopes, useful not only to the mariner but to many branches of science, particularly the field of oceanographic research. We are constantly adding to this storehouse of knowledge, both quantitatively and qualitatively. The Coast and Geodetic Survey has an important interest in the work of the American Geophysical Union and is pleased to make available to its members and others the published results and original records of the Bureau.

**U. S. Coast and Geodetic Survey,
Washington 25, D. C.**

(Manuscript received May 18, 1950; presented at the Thirty-First Annual Meeting, Washington, D. C., May 3, 1950; open for formal discussion until March 1, 1951.)

Transactions, American Geophysical Union Volume 31, Number 5 October 1950

THE ESTABLISHMENT OF THE DEPARTMENT OF OCEANOGRAPHY IN THE AGRICULTURAL AND MECHANICAL COLLEGE OF TEXAS

Dale F. Leipper

(Contribution No. 1 of the Department of Oceanography of the Agricultural and Mechanical College of Texas)

The need for a central agency to teach oceanography and to undertake studies of the Gulf of Mexico has been recognized for many years. Texas herself has 600 mi of tidewater coastline. Eight of the principal rivers of the United States empty into the Gulf of Mexico across her shores, creating changing environments which affect marine life and sedimentation processes. Thirteen man-made deep-water ports between Brownsville and Orange handle a large amount of sea traffic, having moved approximately 130,000,000 tons of freight during the 12-month period ending June 30, 1949. Shipping on the intra-coastal canal extends the length of the coast. On the continental shelf along the Gulf Coast, which averages 70 mi in width, it has been estimated that crude oil recovery per square mile of area will exceed that of the oil-rich coastal land belt. A huge chemical industry along the Texas coast makes extensive use of raw materials from the sea. There is a grand total annual catch of fish and shellfish in Texas which exceeds 21,000,000 lb. Weather from the Gulf receives particular attention because of its daily importance in activities along the coast and because of disasters which have occurred, such as the Galveston flood of 1900. Because of these and other similar facts, it was only a matter of time until one of the state universities would embark upon the study and teaching of oceanography.

There are many oceanographic problems which face the local fishing industry. In addition, there are others arising in the production of the offshore oil [BATES and GLENN, 1948]; in the operation of the industrial plants along the coastline; in the forecasting of hurricanes, squalls, and fogs of marine origin; in the reduction of beach contamination; in the prevention of beach erosion; in the reduction of dredging costs in marine channels; in the development of recreational facilities on the beaches; in construction along shore and offshore; in aiding marine transportation; in providing information of value to national defense; and in unifying local oceanographic knowledge. An academic organization is needed which can offer the secure and promising positions required to attract outstanding scientists into this field and can provide facilities for the gradual accumulation and dissemination of the large body of oceanographic information.

The interest in a department of oceanography at the A. and M. College developed naturally out of an extensive marine program, at times involving the services of as many as 90 individuals, conducted largely by the staff of the College through the Texas A. and M. Research Foundation. During this program the Departments of Chemistry, Biology, and Geology, and the School of Engineering, in particular, recognized the need for the Department of Oceanography and were instrumental in its establishment in the School of Arts and Sciences.

The curriculum in oceanography, which has been approved by the Academic Council, includes courses at the senior and graduate levels only. Three types of training are available. The first is an introductory or survey course for seniors in the biological or physical sciences or in engineering. The second is a group of courses which graduate students working toward degrees in other fields may use as a minor. Finally, there is a full curriculum leading toward a graduate degree in oceanography. The basic textbook used is SVERDRUP, JOHNSON, and FLEMING [1942], but emphasis is also placed upon publications describing recent developments. A graduate student in his first semester registers for a course in each major aspect of the field. In succeeding semesters he concentrates upon research and advanced course work related to his basic field and to his chosen aspect of oceanography.

In the present semester two courses are being offered with an enrollment of 54 students. Next year the full curriculum begins.

Prerequisites for the graduate study of oceanography are a bachelor's degree or its equivalent from a recognized college or university, with a major in biology, chemistry, engineering, geology, meteorology, mathematics, or physics. Also required are at least eight semester hours in each of mathematics, physics, and biology or chemistry.

To qualify for a graduate degree in oceanography the student must be thoroughly trained in one of the pertinent basic sciences, must know how to apply this training in the marine environment, (which requires a combination of principles and methods unique to oceanography), and must have an interest in the other marine sciences as well as at least an elementary knowledge of them.

Although the subject matter of oceanography has been divided into five major aspects, an essential feature of the program is the integration of these various parts into a unified whole within a single department. The aspects are: (1) biological oceanography, which is the study of life in the sea including both plants and animals; (2) physical oceanography, which is the physics of the sea and includes the study of ocean waves and water movements, of transformations of energy, and of the physical characteristics of sea water; (3) geological oceanography, which deals with the relationships between the land and the oceans and includes studies of beach erosion and sedimentation, determination of bottom topography, and the interpretation of marine deposits; (4) chemical oceanography, which is the study of the chemical constituents of the sea and of chemical reactions which take place within it, and which includes determinations of the amount of various constituents present, development of methods of extraction, and studies of corrosive effects; (5) marine meteorology, which deals with the winds and weather over the sea, with the manner in which winds set up ocean waves and currents, and with the climate as determined by evaporation and conduction from the sea surface.

The initial academic staff of the department has been selected with one specialist in each of these fields. J. G. Mackin is Professor of Biological Oceanography. W. Armstrong Price is Professor of Geological Oceanography. The writer is Associate Professor of Physical Oceanography and Marine Meteorology. Donald W. Hood, who is completing work for his doctor's degree in Biochemistry and Nutrition, will become Assistant Professor of Chemical Oceanography on August 1, 1950. A position is open for an additional physical oceanographer and marine meteorologist.

Work at sea will be conducted by cooperative arrangement from the Alaska, oceanographic vessel of the U. S. Fish and Wildlife Service, which is to be based in Galveston. A completely equipped shore laboratory is available through the Texas A. and M. Research Foundation at Grand Isle, Louisiana. Also, a reserve fund of $50,000 has been set aside for laboratory equipment.

One of the great advantages of the oceanographic program as set up at A. and M. College is the opportunity for close coordination of this program with the work of the other schools and departments of the college. Undergraduate students may take the survey course in oceanography as an elective and, on the basis of information gathered in this course, may plan further work as desired. Students taking oceanography as a major may also register for any of the courses offered in other departments. Thus, they may continually improve and augment their basic training. In case of the candidates for the Ph. D. degree, double majors - one major being in the basic field and one in oceanography - are encouraged.

Financial assistance is provided for worthy students. A $2000 research fellowship in chemical oceanography is sponsored by the Dow Chemical Company. A graduate assistantship paying $100 per month is available and it is expected that four half-time assistantships in physical oceanography paying $125 per month will be offered.

As has been mentioned, the oceanographic program is conducted at the graduate level. A graduate course is defined in the College catalog as one "requiring an attitude of critical analysis or of research on the part of instructors and students." Also, since only preliminary oceanographic studies have been completed in the Gulf of Mexico, further information is needed for the development of material to be used in teaching. For these reasons, research comprises a large part of the academic program. According to F. C. Bolton, President of the College, "This department should serve as a nucleus around which to develop fundamental research into the varied scientific problems of marine life and should provide a group of men with the technical training to assume the leadership both in the basic research and in its industrial application."

Through the Texas A. and M. Research Foundation, which is legally and financially independent of the College but is dedicated to its welfare, the staff and facilities of the Department of Oceanography may be made available for sponsored research when the research is of such nature that it can be conducted more efficiently through an independent corporation than through a state organization such as the College itself. The objectives of the Research Foundation are partially expressed in the following excerpt from the Articles of Incorporation:

> "The objects for which this corporation is organized are to promote educational purposes by encouraging, fostering, and conducting scientific investigations and research; by training and developing persons for the conduct of such investigations and research; and by acquiring and disseminating knowledge in relation thereto; and further, both in connection with the Agricultural and Mechanical College of Texas and independently thereof in case it is found necessary, to foster and encourage education and learning in all fields and to promote the liberal and practical education of all classes in the several pursuits and professions of life."

The Foundation is administered by a body of counselors representing equally agriculture, industry, the Texas A. and M. College System, the alumni of A. and M. College, and the public at large. Research undertaken through the Foundation may use the services of the personnel and the facilities of any or all of the departments of the College, as well as those of other institutions or organizations when needed.

For both research and teaching purposes, oceanographic problems are defined as being those marine problems requiring the use of two or more of the basic sciences for their proper solution. Marine problems and subject matter not falling into this category are referred to the appropriate basic department.

The administration of the A. and M. College of Texas feels that, by the establishment of an academic department and the encouragement of a program of teaching and research in oceanography, it will be contributing to the conservation and proper utilization of one of our greatest natural resources, the Gulf of Mexico. This should lead to an improvement in the general welfare and to the further cultural and economic development of the people of Texas and adjoining states.

References

BATES, C. C., and A. H. GLENN, Oceanography in the offshore drilling campaign, World Oil, v. 127, pp. 114-126, April 1948.

SVERDRUP, H. U., M. W. JOHNSON, and R. H. FLEMING, The oceans, Prentice-Hall, New York, N. Y., 1942.

Department of Oceanography,
College Station, Texas

(Manuscript received May 15, 1950; presented at the Thirty-First Annual Meeting, Washington, D. C., May 3, 1950; open for formal discussion until March 1, 1951.)

REPORT OF THE COMMITTEE ON PHYSICS OF SOIL MOISTURE, 1947-1949

L. A. Richards, Chairman

Don Kirkham	W. O. Smith	V. C. Jamison
J. F. Lutz	J. R. McHenry	R. M. Hagen

In continuance of a custom, the chief effort of the Committee during this period has been the preparation of a symposium on an aspect of the physics of soil moisture. A paper was prepared by the Chairman of the Committee on the subject, Laws of soil moisture. This paper was sent to members of the Committee and other reviewers for comment and discussion. The paper, with the discussions, is published on pages 750-756 of this issue as a contribution of this Committee.

REPORT OF THE COMMITTEE ON EVAPORATION AND TRANSPIRATION, 1949-1950

H. G. Wilm, Chairman

1950	1951	1952
B. G. Holzman	E. G. Dunford	C. Warren Thornthwaite
Luna B. Leopold	A. H. Hendrickson	Henry W. Anderson
Harold C. Troxell	Adolph F. Meyer	Robert W. Gerdel

Largely because of the pressure of other activities during the last half of the year, most of the members did not have results to report in this Committee's field of work. Two interesting reports were received, however, discussing the disposal of soil moisture in the Colorado Rocky Mountains and in two mountain areas of California.

E. G. Dunford (Rocky Mountain Forest and Range Experiment Station, Fort Collins, Colorado)- At Manitou Experimental Forest the relative depletion of soil moisture was obtained in the fall of 1949 on six one-acre watersheds undergoing a type-conversion treatment. A second-growth cover of ponderosa pine was removed in 1948 from four watersheds; the remaining two were left uncut to provide control. Slash was broadcasted on two of the treated watersheds and piled on the other two. In February 1949 the slash was burned.

All six watersheds are formed by a recent dissection of a mature alluvial bench. The soil is a coarse mixture of Pikes Peak granite and various sedimentaries. A well-defined clay zone is found only on the ridges between drainages. Profile studies indicate that the present channels have cut through a once-uniform clay zone and have now reached an undeveloped C horizon. Channel flow occurs only for brief periods during spring snow-melt and intense summer rains.

Soil-moisture samples taken in the fall of 1949 indicate the effect of evaporation and transpiration for the first growing season following cutting and burning. The primary object was a treatment test but, because of the general westerly aspect of the watersheds, it was also possible to measure the separate effects of north and south exposures. A preliminary analysis of the results shows consistently less fall moisture remaining in the soil on south exposures, regardless of the cover or burning treatment. For both exposures, cutting and broadcast burning left the greatest amounts of soil moisture at the end of the growing season whereas the least amounts were found on the control watersheds. Considering both aspect and treatment, the results showed that the greatest consumption of soil moisture occurred in south exposures of the uncut watersheds and the least on north exposures of watersheds on which timber was cut and slash broadcast and burned.

P. B. Rowe and E. A. Colman (Submitted by H. W. Anderson, California Forest and Range Experiment Station, Berkeley, California)-- A manuscript, "Disposition of rainfall in two mountain areas of California," has been prepared for publication as a Department of Agriculture bulletin. The study reported had two phases: one phase employed small hillside runoff and soil moisture sampling plots to determine water losses and water yield from natural tree and brush vegetation, and effects of annual burning and denudation upon these losses and yield. The second phase employed soil moisture plots established so as to sample an 875-acre brush-covered watershed for which stream-flow measurements were available, thus permitting interpretation of results on a watershed basis.

Annual burning of the vegetation in both tree and brush types sampled did not appreciably affect total evapotranspiration losses. It did reduce the infiltration capacity of the soil, thereby greatly increasing surface runoff. Reduced interception loss in the brush type resulted in increased water yield (surface runoff plus seepage), but this increase was achieved at the expense of greatly increased storm flows of surface runoff, and correspondingly reduced underground yields.

Denudation and maintenance of a vegetation-free soil eliminated all interception and transpiration losses. Total evaporation losses were reduced, but surface runoff and erosion were greatly increased. During each summer the bare soils lost appreciable quantities of water from all depths (zero to six feet), but drying was slower and less complete in deep than in shallow soils. Total water yield was greatest from plots with bare soil, but underground yield was greatest from the plots covered with natural vegetation.

In the Monroe Canyon Watershed of the San Dimas Experimental Forest, where the second phase of the study was carried on, annual rainfall during the two years of study averaged 31.1 in/yr. Interception loss averaged 2.5 inches, evapotranspiration 10.8 inches, and water yield (underground plus stream flow) 17.8 in/yr. of the total yield only about four inches, or less than one-quarter, left the watershed as measured stream flow. The disposition of the remaining 13.8 inches could not be directly determined, but it was assumed that most, if not all, of this water passed into the highly fractured underlying rock and eventually drained from the watershed as underground flow.

The fiberglas electrical soil moisture instrument developed by the Experiment Station has been subjected to continued testing in field and laboratory. Results of laboratory studies were presented by COLMAN and HENDRIX [1949]. In field tests on the San Dimas Experimental Forest the soil units have maintained a constant calibration (moisture content versus resistance) through four wetting-and-drying cycles spread over a period of nearly a year. The field calibration was not the same as that determined in the laboratory for the same soils packed to field density. The soils tested were clay loams, and it appeared likely that field structure was not duplicated in the laboratory tests. Soil units are now being calibrated in the laboratory in cores of undisturbed soil in order to learn whether this method will yield calibrations that duplicate those determined in the field.

Reference

COLMAN, E. A., and T. M. HENDRIX, The fiberglas electrical soil-moisture instrument, Soil Sci., v. 67, pp. 425-438, 1949.

Pacific Northwest Forest and Range Experiment Station,
423 U. S. Court House,
Portland 5, Oregon

(Manuscript received April 28, 1950; presented at the Thirty-First Annual Meeting, Washington, D. C., May 1, 1950; open for formal discussion until March 1, 1951.)

Transactions, American Geophysical Union Volume 31, Number 5 October 1950

BIBLIOGRAPHY

BIBLIOGRAPHY: GENERAL

COOPER, R. I. B., Internal constitution of the Earth, Nature, London, v. 165, pp. 216-219, 1950 [abstr. in Phys. Abstr., v. 53, no. 630, p. 524, 1950].

POLKANOV, A. A., and E. K. HERLING, The absolute age scale of the Earth's geological history, Izvest. Akad. Nauk S. S. S. R., Ser. Geol., pp. 29-38, 1946 (summary in English) [abstr. in Chem. Abstr., v. 44, no. 15, p. 6788, 1950].

ROTHÉ, EDMOND, and J. P. ROTHÉ, Prospection Géophysique, Paris, v. 1, 438 pp., 1950.

VERCELLI, FRANCESCO, Il superamento delle altezze e delle profondita nelle esplorazioni geofisiche, Istituto Talassografico, Trieste, Pub. 244, 17 pp., 1950.

BIBLIOGRAPHY: GEODESY

CALVO, LOZANO, Determinación de una fórmula para la gravedad normal a partir del elipsoide terrestre de Struve, adecuada especialmente para España, Inst. Nac. Geofís., Madrid, v. 9, no. 33, pp. 1-41, 1950.

CARRIER, A., Appareil autoréducteur pour la mésure des bases, Bull. Géod., no. 16, pp. 146-153, June 1950.

CHUDOBA, VRATISLAV, L'édification du réseau gravimétrique en Tchécoslovaquie, Zeměměřický Obzor, v. 38, pp. 81-90, 1950 (in Czechish).

CORON, SUZANNE, Valeur de la pesanteur à Paris déterminée à l'aide des liaisons internationales européennes, Bull. Géod., no. 16, pp. 118-139, June 1950.

CUNIETTI, M., Collegamento gravimetrico delle stazioni di Padova, Bologna e Milano per mezzo di un gravimetro Western G. 4 A., Riv. Geofis. Applicata, v. 11, pp. 27-34, 1950.

ERRULAT, FRITZ, Zur Frage der lokalen und regionalen Anomalien der erdmagnetischen Säkularvariation, Deutsche Hydrographische Zs., v. 3, pp. 153-161 + 1 pl., 1950 (summary in English).

FRANCE, L'INSTITUT GÉOGRAPHIQUE NATIONAL, Rapport sur l'activité, in two parts, 122 pp. of text and a folder of 22 charts, 1949.

FREIESLEBEN, HANS CHRISTIAN, Genaue astronomische Positionen bei Vermessungs- und Forschungsfahrten, Deutsche Hydrographische Zs., v. 3, pp. 144-152, 1950 (summary in English).

GIGAS, ERWIN, Theodolites with photographic registration, Bull. Géod., no. 16, pp. 140-145, June 1950.

IMMLER, WERNER, Die sphärische Hyperbel, Deuts. Hydr. Zs., v. 2, no. 6, pp. 233-242, 1949 (in German with summary in English).

JELEN, MIR, Remarques sur la précision des mésures pendulaires effectuées par R. Sterneck, Zeměměřický Obzor, v. 38, pp. 102-103, 1950 (in Czechish).

KOEMAN, C., The effect of change of focus in astrolabe observations, Bull. Géod., no. 16, pp. 176-181, June 1950.

KITSCH, WILLI, Behandlung von Richtungssätzen ohne gemeinsame Richtung in der Netzausgleichung nach bedingten Beobachtungen, Veröffentlichungen 8, Inst. Erdmessung, Bamberg, pp. 21-29, 1949 (abstract in English).

KITSCH, WILLI, Elimination von Bedingungs- bzw. Normalgleichungen aus einer Korrelatenentwicklung bei der Anwendung des Boltzschen Entwicklungs-Verfahrens, Veröffentlichungen 8, Inst. Erdmessung, pp. 71-84, 1949 (abstract in English).

KITSCH, WILLI, Über die Verbesserung von Korrelaten bei der Anwendung des Boltzschen Entwicklungs-Verfahrens, Veröffentlichungen 8, Inst. Erdmessung, pp. 45-69, 1949 (abstract in English).

KITSCH, WILLI, Zur Aufstellung der Diagonalbedingungen in der Netzausgleichung nach bedingten Beobachtungen, Veröffentlichungen 8, Inst. Erdmessung, Bamberg, pp. 7-10, 1949 (abstract in English).

LEJAY, R. P., Exploration gravimétrique de l'extrême-orient, Comité Nat. Français de Géod. Géophys. 75 pp. + 4 maps, 1936.

LEJAY, R. P., Exploration gravimétrique des états du Levant sous Mandat Français, Comité Nat. Français, Géod. Géophys., 54 pp. + 1 map, 1938.

LEJAY, R. P., Étude gravimétrique des Iles Philippines, T'ou-sè-wè, Shanghai, 129 pp. + 1 map, 1939.

LEVALLOIS, J. J., and M. DUPUY, Sur le calcul des grandes géodésiques, Bull. Géod., no. 16, pp. 105-117, June 1950.

MEYER, OTTO, Ergebnisse der erdmagnetischen Messungen im nordwestdeutschen Raum zur Erfassung der Säkularvariation, Deutsche Hydrographische Zs., v. 3, pp. 161-162 + 1 pl., 1950 (summary in English).

PERRIER, GEORGES, Kurze Geschichte der Geodäsie, wie der Mensch die Erde gemessen und gewogen hat, Veröffentlichungen 2, Inst. Erdmessung, Bamberg, 192 pp., 1950 (translation from the French by ERWIN GIGAS).

PICHA, JAN, La comparaison de quelques stations gravimétriques en Tchécoslovaquie à l'aide de l'appareil Noergaard, Zeměměřický Obzor, v. 38, pp. 90-95, 1959 (in Czechish).

RANTZ, J., Mésure des longueurs avec un fil métallique suspendu muni d'un niveau pour la réduction à l'horizon, Bull. Géod., no. 16, pp. 154-175, June 1950.

SIEBER, ADOLF, Das Vermessungs- und Forschungsschiff Gauss des Deutschen Hydrographischen Instituts., Deutsche Hydrographische Zs., v. 3, p. 163 + 1 pl., 1950 (summaryin English).

STANEK, VACLAV B., La détermination de la densité du Sous-Sol pour la réduction des mésures de la pesanteur, Zeměměřický Obzor, v. 38, pp. 95-101, 1950 (in Czechish).

TSUBOI, CHUJI, On seismic activities, Geophys. Notes, Tokyo, v. 3, no. 4, 22 pp., 1949.

TSUBOI, CHUJI, Dependence of the isostatic depth on the horizontal scale of the topographies to be compensated, Geophys. Notes, Tokyo, v. 3, no. 6, 4 pp., 1950.

TSUBOI, CHUJI, Is the condition Σ(isostatic anomaly)^2 = a minimum a good criterion for determining the thickness of the isostatic Earth's crust?, Geophys. Notes, Tokyo, v. 3, no. 7, 9 pp., 1950.

TSUBOI, CHUJI, Thickness of the isostatic Earth's crust in various parts of the United States of America, Geophys. Notes, Tokyo, v. 3, no. 5, 37 pp., 1950.

VAN DER STRAETEN, J., Triangulation du Katanga; les bases géodésiques; mésure de la base de Gandajika, Bull. Séances, Inst. R. Col. Belge, pp. 945-997, 1949.

WOLF, HELMUT, Rechenproben bei der Anwendung des Boltzschen Entwicklungs-Verfahrens, Veröffentlichungen 8, Inst. Erdmessung, Bamberg, pp. 31-43, 1949 (abstract in English).

WOLF, HELMUT, Über die zweckmässige Behandlung einseitig beobachteter Richtungen in der Netzausgleichung nach bedingten Beobachtungen, Veröffentlichungen 8, Inst. Erdmessung, Bamberg, pp. 11-19, 1949 (abstract in English).

WOLF, HELMUT, Triangulation adjustment, general discussion and new procedure, Bull. Géod., no. 16, pp. 87-104, June 1950.

BIBLIOGRAPHY: SEISMOLOGY

ALIVERTI, G., and L. LOLAINI, Sulla velocità di propagazione delle onde sismiche su brevi percorsi superficiali, Riv. Geofis. Applicata, v. 11, pp. 3-13, 1950.

ASADA, TOSHI, and ZIRO SUZUKI, On microearthquakes having accompanied aftershocks of the Hukui earthquake of June 28, 1948, Geophys. Notes, Tokyo, v. 2, no. 16, 14 pp., 1949.

CALOI, P., and F. PERONACI, The earthquake of 28th August, 1946, and the depth of the Earth's core, Ann. Geofis., v. 2, pp. 493-502, 1949 (in Italian) [abstr. in Phys. Abstr., v. 53, no. 630, p. 522, 1950].

HUGHES, D. S., E. B. BLANKENSHIP, and R. MIMS, Variation of elastic moduli and wave velocity with pressure and temperature in plastics, J. Appl. Phys., v. 21, pp. 294-297, 1950.

SUZUKI, ZIRO, and TOSHI ASAKA, Observations of microearthquakes in Sikoku District, Geophys. Notes, Tokyo, v. 2, no. 17, 4 pp., 1949.

TREUSEIN, EDGAR, Der Zeitsignalgeber des Deutschen Hydrographischen Instituts, Deuts. Hydr. Zs., v. 2, no. 6, pp. 245-251, 1949 (in German with summary in English).

TSUYA, H., (Ed), The Fukui earthquake of June 28, 1948, Report of the Special Committee for the Study of the Fukui Earthquake, Earthquake Res. Inst., Tokyo, 197 pp. + 6 pl. + 1 map, 1950.

VALLE, P. E., On the measurement of the group velocity of seismic surface waves, Ann. Geofis., v. 2, pp. 370-376, 1949 (in Italian) [abstr. in Phys. Abstr., v. 53, no. 630, p. 522, 1950].

BIBLIOGRAPHY: METEOROLOGY

ABILD, BRUNO, Zum täglichen Temperaturgang in der freien Atmosphäre, Ann. Met., Hamburg, v. 3, pp. 38-41, 1950 (summary in English).

ANDERSON, CHARLES E., Evaluation of results of joint Air Force Weather Bureau cloud seeding trials conducted during winter and spring, 1949, Geophys. Res. Papers, no. 4, Base Directorate for Geophys. Res., 30 pp., 1950.

ASP, M. O., Tornadoes in Oklahoma, 1875-1949, Mon. Wea. Rev., U. S. Wea. Bur., v. 78, no. 2, pp. 23-26, 1950.

BATCHELOR, G. K., The application of the similarity theory of turbulence to atmospheric diffusion, Q. J. R. Met. Soc., v. 76, no. 328, pp. 133-146, 1950.

BAUR, FRANZ, Introduction to global meteorology, Wiesbaden, Dieterich'sche Verlagsbuchhandlung, 168 pp. + 1 chart, 1948 [abstr. in Appl. Mech. Rev., v. 3, no. 8, p. 255, 1950].

BAUR, FRANZ, Über falsche und richtige Statistik in der Meteorologie, Ann. Met., Hamburg, v. 3, no. 3-4, pp. 74-83, 1950 (summary in English).

BEEBE, ROBERT G., Forecasting winter precipitation for Atlanta, Georgia, Mon. Wea. Rev., v. 78, pp. 59-68, 1950.

BERKES, Z., A nehézségi erőtér szerepe a hőmérséklet függélyes csökkenésében (Le rôle du champs de gravitation terrestre au point de vue de la dimunition verticale de la température atmosphérique), Időjárás, Budapest, v. 54, no. 3-4, pp. 80-87, 1950 (in Hungarian with abstract in French).

BEST, A. C., Empirical formula for the terminal velocity of water-drops falling through the atmosphere, Q. J. R. Met. Soc., v. 76, no. 329, pp. 302-311, 1950.

ČADEŽ, M., Vpliv turbulence na nastanek in razvoj inverzij ter na razvoj ničstopinjskih izotermij. S tremi slikami v tekstu, Razprave, Ljubljana, Jugoslavia, v. 21, pp. 481-501, 1942 (summary in Italian).

COLLMANN, WOLFGANG, Troposphärische Mitteltemperaturen der Hauptluftmassen über Nordwestdeutschland, Ann. Met., Hamburg, v. 3, pp. 20-25, 1950 (summary in English).

COURVOISIER, P., Über Luftdruckvariographen und Luftdruckschwankungen, Archiv für Met., Geophysik und Bioklimatologie, Ser. A, v. 1, no. 1, pp. 1-38, 1948 (summary in English and French).

COURVOISIER, P., and H. WIERZEJEWSKI, Beiträge zur Strahlungsmessmethodik, I: Die

physikalischen Grundlagen der kalorischen Strahlungsmessmethoden; II: Die Berechnung der Wirkungsweise kalorischer Strahlungsmess-Instrumente, Archiv für Met., Geophysik und Bioklimatologie, Ser. B, v. 1, pp. 45-53 and 156-198, 1948 (summary in English).

CRARY, A. P., Investigation of stratosphere winds and temperatures from acoustical propagation studies, Geophys. Res. Papers, no. 5, Base Directorate for Geophys. Res., 32 pp., June 1950.

CROSSLEY, A. F., Relation between the standard deviations of temperature at constant pressure and at constant height, Q. J. R. Met. Soc., v. 76, no. 329, pp. 337-340, 1950.

DAS, P. K., The growth of cloud droplets by coalescence, Indian J. Met. Geophys., v. 1, no. 2, pp. 137-144, 1950.

DEUTSCHER WETTERDIENST, Die Vorträge anlässlich der 1. Tagung der Meteorologischen Gesellschaft Bad Kissingen, Berichte des Deutschen Wetterdienstes, Bad Kissingen no. 12, 271 pp., 1950 (collection of about 65 short papers bearing on various aspects of meteorology).

DUFOUR, L., Sur quelques résultats obtenus dans le domaine de la prévision à longue échéance, Inst. R. Met. Belgique, Misc. 39, 28 pp., 1950.

EL-FANDY, M. G., Troughs in the upper westerlies and cyclonic developments in the Nile Valley, Q. J. R. Met. Soc., v. 76, no. 328, pp. 166-172, 1950.

ERTEL, HANS, A method of approximate prediction of the displacements of air masses, S.-B. Deutsch. Akad. Wiss. Berlin, Math.-Nat. Kl., no. 3, 23 pp., 1948 (in German) [abstr. in Appl. Mech. Rev., v. 3, no. 5, p. 159, 1950].

FLORIDA STATE BOARD OF CONSERVATION, Observed rainfall in Georgia, Monthly totals from beginning of records to 31 December, 1949, Div. of Water Surv. Res., Florida, 226 pp. + 18 maps, 1950.

FORREST, J. S., Variations in thunderstorm severity in Great Britain, Q. J. R. Met. Soc., v. 76, no. 329, pp. 277-286, 1950.

FRANCE, METEOROLOGICAL SOCIETY, Bibliographie Météorologique Internationale, Mét. Nat. E. C. M., Soc. Mét. France, Paris, 174 pp., 1948.

FUKUDA, K., On the periodical appearance of abnormally low air temperature in Tohuku District and some particular paths of typhoon, and the sea water temperature, Geophys. Mag., v. 21, no. 2, pp. 125-127, 1950.

GENTRY, ROBERT C., Forecasting local showers in Florida during the summer, Mon. Wea. Rev., U. S. Wea. Bur., v. 78, pp. 41-49, 1950.

GEORGI, JOHANNES, Hochstürme über der Dänemarkstrabe, Deutsche Hydrographische Zs. v. 3, pp. 136-143, 1950 (summary in English).

GÖDECKE, KARL, Die "vollständige" Temperaturkorrektion an Stations-Barometern mit nicht einstellbarem Teilungsnullpunkt, Ann. Met., Hamburg, v. 3, pp. 103-105, 1950 (summary in English).

GORDON, A. H., The ratio between observed velocities of the wind at 50 feet and 2000 feet over the North Atlantic Ocean, Q. J. R. Met. Soc., v. 76, no. 329, pp. 344-348, 1950.

HARTMANN, WILHELM, Die Genauigkeit der Ermittlung des Höhenwindes aus den Kartin der absoluten Topographie, Ann. Met., Hamburg, v. 3, pp. 27-34, 1950 (summary in English).

HINKELMANN, KARL, Neuberechnung des thermodynamischen Diagrammes nach Stüve., Mitteilungen, Deuts. Wetter. US-Zone, Bad Kissingen, no. 6, 19 pp. + 1 pl., 1950.

HINZPETER, MAX, Grundlagen der Temperaturkorrektion bei Aneroidbarometern in Radiosonden, Ann. Met., Hamburg, v. 3, pp. 49-53, 1950 (summary in English).

HOINKES, H., Die interdiurnen Änderungen von Druck und Temperatur in der unteren Troposphäre bis 5 km Höhe und ihre gegenseitigen Beziehungen in statistischsynoptischer Betrachtungsweise, Archiv. für Met., Geophys. und Bioklim., Serie A: Met. Geophys., v. 2, pp. 239-304, 1950.

HOLLMANN, GÜNTHER, Zur Dynamik der Druck- und Drucktendenzfelder, Ann. Met., Hamburg, v. 3, pp. 65-73, 1950 (summary in English).

HOOPER, J. E. N., and A. A. KIPPAX, The bright band--a phenomenon associated with radar echoes from falling rain, Q. J. R. Met. Soc., v. 76, no. 328, pp. 125-132, 1950.

HOOVER, ROBERT A., Forecasting radiation fog at Elkins, West Virginia, Mon. Wea. Rev., v. 78, no. 5, pp. 75-80, May 1950.

HOUNAM, C. E., Climate of the western district of Victoria, Studies in Appl. Climatology, no. 3, 20 pp. + 30 maps, 1949.

IMAI, I., On the velocity of falling raindrops, Geophys. Mag., Tokyo, v. 21, no. 3, pp. 244-249, 1950.

ISONO, K., and Y. HUZIWARA, An improved radiosonde, Geophys. Mag., v. 21, no. 2, pp. 127-134, 1950.

JAMES, R. W., On the theory of large-scale vortex motion in the atmosphere, Q. J. R. Met. Soc., v. 76, no. 329, pp. 255-276, 1950.

JONES, R. F., The temperatures at the tops of radar echoes associated with various cloud systems, with discussion, Q. J. R. Met. Soc., v. 76, no. 329, pp. 312-336, 1950.

JORDAN, C. L., North-south profiles of the average zonal wind component at the surface, Q. J. R. Met. Soc., v. 76, no. 329, pp. 343-344, 1950.

KANO, K., On the Richardson's criterion concerning the increase or decrease of turbulent energy in the free atmosphere, Geophys. Mag., Tokyo, v. 21, pp. 220-226, 1950.

KNIGHTING, E., A note on nocturnal cooling, Q. J. R. Met. Soc., v. 76, no. 328, pp. 173-181, 1950.

KÖHLER, HILDING, On the problem of condensation in the atmosphere, Nova Acta Regiae Soc. Scien. Upsaliensis, Uppsala, ser. 4, v. 14, no. 9, 75 pp., 1950.

KREUTZ, W., Merkblatt zur Mietenbehandlung, Verminderung von Mietenschäden durch Steuerung des Mietenklimas, Mitteilungen, Deuts. Wetter., Bad Kissingen, no. 7, 6 pp., 1950.

KUHLBRODT, ERICH, Jahreszeitlicher Gang des Nordatlantischen Kernpassates, Deuts. Hydrograph. Zs., v. 3, pp. 127-136, 1950 (summary in English).

LÁZLÓ, AUJESZKY, An attempt to a more complete formulation of the concept of climate, Idöjárás, v. 55, pp. 140-145, 1950 (summary in English p. 191).

LETTAU, HEINZ, Maxima of wind velocity as function of the Earth's rotation, Met. Rdsch., v. 1, pp. 451-453, Sept.-Oct. 1948 (in German) [abstr. in Appl. Mech. Rev., v. 3, no. 6, p. 190, 1950].

LETTAU, HEINZ, On weather-producing motions and their determination from the pressure field, Met. Rdsch., v. 1, pp. 257-260, Mar.-Apr. 1948 (in German) [abstr. in Appl. Mech. Rev., v. 3, no. 6, p. 190, 1950].

LOEWE, F., "Difficult days" at Melbourne, Commonwealth (Australia) Met. Bur., Wea. Dev. Res. Bull., no. 15, pp. 12-27, 1950 (processed).

LÖNNQVIST, O., A general method and a simplified formula for calculating effective radiation, Arkiv för Geofysik, Stockholm, v. 1, no. 1, pp. 79-115, 1950.

LUNSON, E. A., Sandstorms on the northern coasts of Libya and Egypt, Met. Office, London, Prof. Notes 102, 12 pp., 1950.

MANIG, MARIANNE, Monatsmittel der Lufttemperatur in Deutschland für die Periode 1881-1940, Mitteilungen, Deuts. Wetter., Bad Kissingen, no. 4, 30 pp. + 12 maps, 1950.

MEURERS, JOSEPH, Sichtuntersuchungen am Aeronautischen Observatorium Lindenberg, Berichte, Deuts. Wetter., no. 13, Bad Kissingen, 19 pp., 1950.

MIDDLETON, W. E. KNOWLES, The colors of distant objects, J. Optical Soc. Amer., v. 40, pp. 373-376, 1950.

MITCHELL, L. R., Arctic or Antarctic and polar fronts, Commonwealth (Australia) Met. Bur., Wea. Dev. Res. Bull., no. 15, pp. 40-50, 1950 (processed).

MIYAKE, Y., and K. SARUHASHI, A photochemical theory on the ozone layer in the atmosphere, Geophys. Mag., v. 21, no. 2, pp. 99-107, 1950.

MIYAKE, Y., and K. SARUHASHI, The estimation of the height of fog by observing the ultra-violet solar radiation, Geophys. Mag., v. 21, no. 2, pp. 122-125, 1950.

MÖRIKOFER, W., Zur Terminologie in der Strahlungsforschung, Archiv für Met., Geophys. Bioklim. Ser. B, v. 1, no. 1, pp. 32-44, 1948 (summary in English).

MULL, S., and Y. P. RAO, Dynamics of thunderstorms, Pt. 1, Indian J. Met. Geophys., v. 1, pp. 116-136, 1950.

MÜLLER-ANNEN, HANS, Über den statistischen Hintergrund der Singularitäten, Ann. Met., Hamburg, v. 3, pp. 107-115, 1950 (summary in English).

NICOLET, M., On the measurement of temperatures in the neighborhood of the ground, Inst. R. Met. Belg. Mem., v. 32, no. 38, pp. 3-8, 1949 (in French) [abstr. in Phys. Abstr., v. 53, no. 629, p. 434, 1950].

NICOLET, M., and L. BOSSY, Ensoleillement et orientation en Belgique, II, Inst. R. Met. Belgique, v. 36, 49 pp. + 7 pl., 1950.

NISHIMURA, D., On the structure of typhoon, pt. 1, Geophys. Mag., v. 21, no. 2, pp. 107-122, 1950.

OGAWARA, M., On the form of turbulent vortex near the Earth's surface, Geophys. Mag., Tokyo, v. 21, pp. 226-244, 1950.

OHTA, S., Investigations on condensation nuclei (abstract) I-IV, Geophys. Mag., Tokyo, v. 21, pp. 208-214, 1950.

PASQUILL, F., Some further considerations of the measurement and indirect evaluation of natural evaporation, Q. J. R. Soc., v. 76, no. 329, pp. 287-301, 1950.

PERL, GERTRUD, Die relative Feuchtigkeit an Tagen mit Hochnebeldecke über dem schweizerischen Alpenvorland, Archiv für Met., Geophys. Bioklim., Ser. B, v. 1, pp. 207-210, 1948 (summary in English).

PERL, GERTRUD, Über die Beziehung zwischen Tagesmitteln der Bewölkung und relativer Sonnenscheindauer in drei verschiedenen Klimagebieten der Schweiz, Archiv für Met., Geophys. Bioklim., Ser. B, v. 1, pp. 75-92, 1948 (summary in English).

POLLI, SILVIO, Il ciclo climatico di 8 anni e sua realta' fisica, Ann. Geofis., v. 3, pp. 63-76, 1950.

POLLI, SILVIO, Valori medi ed estremi del clima di Trieste, Istituto Talassografico, Trieste, Pub. 257, 15 pp., 1950.

PRAGER, ERWIN, Zur Frage der Erwärmung kalter Festlandsluft nach ihrem Übertritt auf See, Ann. Met., Hamburg, v. 3, pp. 10-19, 1950 (summary in English).

RAAB, L., and N. RODSKJER, A study of the accuracy of measurements of the Väisälä radiosonde, Arkiv för Geofysik, Stockholm, v. 1, pp. 33-44, 1950.

RADOK, U., Report of flight investigation of lee wave disturbances near Melbourne, Commonwealth (Australia) Met. Bur., Wea. Dev. Res. Bull., no. 15, pp. 28-39, 1950 (processed).

RAO, D. V., V. VITTAL SARMA, and S. S. LAL, Studies on forecasting local rainfall in India with the help of precipitation Index, Indian J. Met. Geophys., v. 1, no. 2, pp. 105-115, 1950.

RIEHL, H., and T. C. YEH, The intensity of the net meridional circulation, Q. J. R. Met. Soc., v. 76, no. 328, pp. 182-188, 1950.

RIEHL, H., and T. C. YEH, Some comments of the trade-wind cell, Q. J. R. Met. Soc., v. 76, no. 329, pp. 340-342, 1950.

ROLL, HANS-ULRICH, Gedanken über Zusammenhang der vertikalen Profile von Windgeschwindigeit und Temperatur in der wassernahen Luftschicht, Ann. Met., Hamburg, v. 3, pp. 1-9, 1950 (summary in English).

ROSSBY, C.-G., On the dispersion of planetary waves in a barotropic atmosphere, Tellus v. 1, pp. 54-58, Feb. 1949 [abstr. in Appl. Mech. Rev., v. 3, no. 7, p. 222, 1950].

SAWADA, R., Temperature difference between mountain top and free air, Geophys. Mag., Tokyo, v. 21, no. 2, pp. 190-198, March, 1950.

SCHERHAG, RICHARD, Betrachtungen zur allgemeinen atmosphärischen Zirkulation: Bestehen Zusammenhänge zwischen der elfjährigen Sonnenfleckenperiode und der allgemeinen Zirkulation?, Deuts. Hydrogr. Zs., v. 3, pp. 108-111 + 2 pl., 1950 (summary in English).

SCHOVE, D. J., The climatic fluctuation since A. D. 1850 in Europe and the Atlantic, Q. J. R. Met. Soc., v. 76, no. 328, pp. 147-165, 1950.

SCHÜEPP, WALTER, Die Bestimmung der Komponenten der atmosphärischen Trübung aus Aktinometermessungen, Archiv für Met., Geophys. Bioklim., Ser. B, v. 1, pp. 257-346, 1949 (summary in English).

SCHULZE, RUDOLF, Zum Einsatz der Radiosonde in der Meteorologie, I: Mitteilung, Ann. Met., Hamburg, 29 pp., 1950.

SCHULZE, WERNER, Platzhöhen von Radiosondenballonen und Ozongehalt der freien Atmosphäre, Ann. Met., Hamburg, v. 3, pp. 42-48, 1950 (summary in English).

SEKERZH-ZEN'KOVICH, YA. I., On the influence of the form of the shore line on the strength of the monsoon field, Izv. Akad. Nauk S. S. S. R., Ser. Geog. Geophys., v. 13, pp. 194-211, 1949 (in Russian) [abstr. in Appl. Mech. Rev., v. 3, no. 7, p. 222, 1950].

SEKIGUCHI, T., Climatological water balance problem in Japan, Geophys. Mag., Tokyo, v. 21, no. 2, pp. 177-189, 1950.

SHIOTANI, M., and G. YAMAMOTO, Atmospheric turbulence over the large city - turbulence in the free atmosphere (2nd report), Geophys. Mag., Tokyo, v. 21, pp. 134-147, 1950.

SIEBER, PETER, Vertical motions and atmospheric pressure variations, Met. Rdsch., v. 1, pp. 322-329, May-June, 1948 (in German) [abstr. in Appl. Mech. Rev., v. 3, no. 6, p. 190, 1950].

SMITH, E. J., Experiments in seeding cumuliform cloud layers with dry ice, Aust. J. Sci. Res., Ser. A, v. 2, pp. 78-91, March 1949 [abstr. in Phys. Abstr., v. 53, no. 629, p. 434, 1950].

SMITH, R., The release of radiosonde balloons, Commonwealth (Australia) Met. Bur., Wea. Dev. Res. Bull., no. 15, pp. 51-57, 1950 (processed).

STAUDE, RUDOLF, Über Formveränderungen und Achsenbewegung von 24-stündigen Bodendruckänderungsgebieten und deren Lage zum Frontenverlauf, erläutert an einigen besonders markanaten synoptischen Entwicklungen, Ann. Met., Hamburg, v. 3, pp. 84-91, 1950 (summary in English).

STRANZ, DIETRICH, Die D-Schicht, Berichte deuts. Wetter. no. 14, Bad Kissingen, 31 pp., 1950.

SUTCLIFFE, R. C., and A. G. FORSDYKE, The theory and use of upper air thickness patterns in forecasting, Q. J. R. Met. Soc., v. 76, no. 328, pp. 189-217, 1950.

THAMS, J. C., La radiazione del sole cielo a Locarno-Monti, Geof. Pura Appl., Milano, v. 14, no. 1-2, 16 pp., 1949 (summary in English).

THAMS, J. C., La radiazione globale relativa secondo le diverse specie di nebulosità, Geof. Pura Appl., Milano, v. 14, no. 3-4, 12 pp., 1949 (summary in English).

TOJO, S., On the thermal structure of troposphere over Japan, in 1947, Geophys. Mag., Tokyo, v. 21, pp. 166-177, 1950.

TYLER, A. G., and E. B. KELL, Upper air analysis and prognosis at 2000Z, Commonwealth (Australia) Met. Bur., Wea. Dev. Res. Bull., no. 15, pp. 5-11, 1950 (processed).

UWAI, K., Analysis of the typhoon "Kathleen," (1) Mechanism of heavy rainfall and front in Kwanto, Chubu and Tohoku Districts, Geophys. Mag., Tokyo., v. 21, no. 2, pp. 147-166, 1950.

WAHL, EBERHARD, Strahlungseinflüsse bei der Wassertemperaturmessung an Bord von Schiffen, Ann. Met., Hamburg, v. 3, no. 3-4, pp. 92-102, 1950 (summary in Englsih).

WATSON-WATT, ROBERT, The evolution of meteorological institutions in the United Kingdom, Q. J. R. Met. Soc., v. 76, no. 328, pp. 115-124, 1950.

WEXLER, A., Low-temperature performance of radiosonde electric hygrometer elements, J. Res. Nat. Bur. Stand., Washington, v. 43, pp. 49-56, July 1949 [abstr. in Phys. Abstr., v. 53, no. 628, p. 352, 1950].

WILKES, M. V., Oscillations of the Earth's atmosphere, Cambridge, Univ. Press, 74 pp. + 23 fig., 1949 [abstr. in Appl. Mech. Rev., v. 3, no. 5, p. 159, 1950].

WÜST, GEORG, Wasserdampf und Niederschlag auf dem Meere als Glieder des Wasserkreislaufs, Deuts. Hydrogr. Zs., v. 3, pp. 111-127, 1950 (summary in English).

YAMAMOTO, Y., The secular change of the climate in Japan, Geophys. Mag., Tokyo, v. 21, no. 3, pp. 249-268, 1950.

YOLDI, MIGUEL AZPIROZ, La afinidad en procesos termodinámicos de interés meteorológico, Inst. Nac. Geofis., Madrid, v. 9, no. 33, pp. 42-72, 1950.

ZWART, JACOB, On the relationships between the advection theories, Met. Rdsch. v. 2, pp. 1-5, 1949 (in German) [abstr. in Appl. Mech. Rev., v. 3, no. 7, p. 222, 1950].

BIBLIOGRAPHY: TERRESTRIAL MAGNETISM AND ELECTRICITY

BELLUIGI, A., Su alcuni orientamenti teorici per le misure elettromagnetische (e. m.) in galleria di miniera, Riv. Geofis. Applicata, v. 11, pp. 15-25, 1950.

EYFRIG, R., The height of the F_2 layer and sunspot numbers, Rev. Sci., Paris, v. 86, pp. 673-674, 1948 [abstr. in Phys. Abstr., v. 53, no. 630, p. 525, 1950].

EYRIES, M., Observations de déclinaison magnétique sur la côte NW du Cotentin, Com. Central Oceanogr., Etude Côtes, Bull. Inf., v. 2, no. 5, pp. 195-199, June 1950 (processed).

FEINSTEIN, J., Higher-order approximations in ionospheric wave-propagation, J. Geophys. Res., v. 55, pp. 161-170, 1950.

HATAKEYAMA, H., On the distrubance of the atmospheric potential gradient caused by the smoke-cloud of the Volcano Yake-yama, J. Geomag. Geoelec., Kyoto, v. 1, pp. 48-51, 1949.

MATSUSHITA, SADAMI, Circulatory motions in the ionospheric atmosphere and their relations to the S-field of the terrestrial magnetism, I and II, J. Geomag. Geoelec., Kyoto, v. 1, pp. 35-47, 1949.

NAGATA, TAKESI, KUNIO HIRAO, and HARUO YOSHIKAWA, Remanent magnetization of "Pleistocene" deposits - Palaeomagnetism in Japan, J. Geomag. Geoelec., Kyoto, v. 1, pp. 52-58, 1949.

NORINDER, H., and O. SALKA, The effect of geological discontinuities on artificial lightning discharges as studied in a model test arrangement, Arkiv för Geofysik, Stockholm, v. 1, no. 1, pp. 45-78, 1950.

NORINDER, HARALD, and REINHARDS SIKSNA, The measurements of the variation characteristics of the density of small-ions, Arkiv för Geofykik, Stockholm, v. 1, no. 1, pp. 1-32, 1950.

PFISTER, W., Effect of the D-ionospheric layer on very low frequency radio waves, J. Geophys. Res., v. 54, pp. 315-337, 1949.

UTASHIRO, SHINKICHI, On the character of the micorpulsation in the magnetic storm, J. Geomag. Geoelec., v. 1, pp. 59-66, 1949.

YRIBERRY, A. J., Gradiente de potencial atmosférico negativo con cielo despejado, Acta Scientifica, Inst. Inv., San Miguel, Argentina, 6 pp., 1950.

BIBLIOGRAPHY: OCEANOGRAPHY

CARRUTHERS, J. N., and A. L. LAWFORD, Water movements and winds at the Mouse Light-vessel, Thames Estuary, Weather, v. 5, pp. 278-283, 1950.

ECKEL, O., Ueber die Mischungsarbeit von stabil geschichteten Wassermassen, Arch. Meteorol. Geophys. Bioklimatol., v. 1, pp. 264-269, 1948.

FRANCE ASSOCIATION D'OCEANOGRAPHIE PHYSIQUE, Monthly and annual mean heights of sea-level 1937 to 1946 and unpublished data for earlier years, Pub. Sci., v. 10, IUGG, 82 pp., 1950.

GERMANY, Meteor Festschrift, 21 papers mostly based on Meteor's work collected in Deutsche Hydrographische Zeitschrift, v. 3, no. 1 and 2, 168 pp., 1950. (In commemoration of the 25th anniversary of the first sailing of the former German research vessel Meteor on an oceanographic survey of the Atlantic Ocean, and of the 90th birthday of Friedrich Schmidt-Ott, who, as president of an emergency committee for German science after the inflation, was largely responsible for initiation of the work of the Meteor.)

GOLDSBROUGH, G. R., The tides in oceans on a rotating globe, Proc. R. Soc., A., v. 200, pp. 191-200, 1950.

GOUGENHEIM, ANDRE, Les canyons sous-marins de la côte sud de France, Bull. d'Inf., COEC, v. 2, pp. 93-95 + 1 pl., 1950.

GRANQVIST, G., Vattnets salthalt utmed Finlands kust under 1940-talet, Geophysica, v. 3, pp. 127-137, 1948.

HELA, I., On the stress of the wind on the water surface, Geophysica, v. 3, pp. 146-161, 1948.

HESS, H. H., Drowned ancient islands of the Pacific Basin, Smithsonian Rep. 1947, pp. 281-300, 1948.

HIDAKA, K., Water transport on convection currents and the lateral mixing, Geophys. Notes, v. 3, no. 2, 11 pp., 1950.

HIDAKA, K., and M. KOIZUMI, Vertical circulation of water due to winds as inferred from the buckling experiments of elastic plates, Geophys. Notes, v. 3, no. 3, 9 pp., 1950.

HIDAKA, K., and T. SUZUKI, On the secular variation of Tsushima current, Oceanogr. Mag., v. 1, pp. 39-42, 1949.

HIDAKA, K., and T. YAMAGAWA, On the absolute velocity of the subarctic intermediate current to the south of Japan, Oceanogr. Mag., v. 1, pp. 99-102, 1949.

HOMMA, S., On the behavior of seismic sea waves around a circular island, Geophys. Mag., v. 21, pp. 199-207, 1950.

ICHIE, T., On the diffusion in the field of Coriolis' force, Oceanogr. Mag., v. 1, pp. 121-127, 1949.

ICHIE, T., On the theory of the drift current in an enclosed sea, Oceanogr. Mag., v. 1, pp. 128-132, 1949.

JERLOV, N. G., Ultra-violet radiation in the sea, Nature, v. 166, pp. 111-112, 1950.

KASUMOVIC, MARIJAN, Niveau moyen de la mer Adriatique et le Niveau Zéro Trieste, Rad. Geofiz. Zavoda u Zagreb, ser. 2, no. 3, pp. 1-33, 1950 (in Croatian with summary in French).

LACOMBE, H., Aperçu de la circulation océanique dans la partie Sud-Est de l'Atlantique Nord, Bull. d'Inf., COEC, Paris, v. 2, pp. 44-53, 1950.

LA FOND, E. C., R. S. DIETZ, and J. A. KNAUSS, A sonic device for underwater sediment surveys, J. Sed. Petr., v. 20, pp. 107-110, 1950.

MENARD, HENRY W., Transportation of sediment by bubbles, J. Sed. Petr., v. 20, pp. 98-106, 1950.

MIYAZAKI, M., On the directivity of the current rips, Oceanogr. Mag., v. 1, pp. 133-134, 1949.

NAKAMIYA, T., and K. SUDA, On the variation of "Kuroshio," Hydrogr. Div., Maritime Safety Agency, Tokyo, 4 pp. + 14 fig., 1950.

NAKANO, M., On the secondary undulations of tides caused by cyclonic storms, Oceanogr. Mag., v. 1, pp. 13-32, 1949.

NEUMANN, GERHARD, Die Meeresoberfläche als hydrodynamische Grenzfläche und das Windfeld über den Wellen, Ann. Met., v. 2, pp. 156-164, 1949 (summary in English).

NICHOLS, HAVEN, New seamount in the North Pacific Ocean, Geogr. Rev., v. 40, pp. 457-461, 1950.

OVEY, C. D., Preliminary results from the study of an ocean core obtained by the Swedish deep-sea expedition 1947-48, J. Glaciol., v. 1, pp. 370-373, 1950.

PETTERSSON, HANS, Exploring the ocean floor, Sci. Am., v. 183, pp. 42-45, August 1950.

PETTERSSON, HANS, and H. ROTSCHI, Nickel content of deep-sea deposits, Nature, v. 166, p. 308, 1950.

PRESS, FRANK, and MAURICE EWING, Propagation of explosive sound in a liquid layer overlying a semi-infinite elastic solid, Geophysics, v. 15, pp. 426-446, 1950.

SAINSBURY, G. L., and I. C. CHEESEMAN, Effect of rain in calming the sea, Nature, v. 166, p. 79, 1950.

SAITO, Y., On the vertical stability of the sea, Oceanogr. Mag., v. 1, pp. 112-120, 1949.

SAUR, J. F. T., JR., Oceanographic features of Nodales Channel (British Columbia) with application to underwater sound, U. S. Navy Electronics Laboratory, San Diego, Report 188, iv, 21 pp., 1950.

SOULE, FLOYD M., Arctic ice drift and the Humboldt Current, Science, v. 112, pp. 61-62, 1950.

STOMMEL, HENRY, Note on the deep circulation of the Atlantic Ocean, J. Met., v. 7, pp. 245-246, 1950.

TAKENOUTI, Y., On the diffusion-ratio of underwater illuminations, Oceanogr. Mag., v. 1, pp. 43-48, 1949.

UDA, MICHITAKA, On the correlated fluctuation of the Kuroshio current and the cold water mass, Oceanogr. Mag., v. 1, pp. 1-12, 1949.

URSELL, F., On the theoretical form of ocean swell on a rotating Earth, Mon. Not. R. Astr. Soc., Geophys. Suppl., v. 6, no. 1, pp. 1-8, 1950.

WAHL, E., Temperaturmessungen in der Nordsee im Sommer 1948, Annal. Met., Hamburg, v. 2, pp. 65-71, 1941 (summary in English).

WISEMAN, J. D. H., and C. D. OVEY, Recent investigations on the deep-sea floor, Proc. Geol. Assn., v. 61, pp. 28-84, 1950.

BIBLIOGRAPHY: VOLCANOLOGY

BASTIAN, LEOPOLDO, Ocorrências de minerais de chumbo em Lageado, O I. G. G., São Paulo, Brazil, v. 4, pp. 406-426, 1946.

CALZOLARI, CLAUDIO, Analisi chimica e chimicofisica della sorgente solfurea di Lusnizza, (Bagni di Lusnizza in Valcanale, Tarvisio), Boll. Soc. Adriatica, Scienze Naturali, Trieste, v. 44, pp. 147-172, 1948.

CROOKSHANK, H., Minerals of the Rajputana pegmatites, Trans. Min. Geol. Metal. Inst. India, v. 42, pp. 105-189, 1948.

CUCUZZA-SILVESTRI, SALVATORE, L'eruzione dell' Etna del 1947, Bull. Volcanologique, v. 9, pp. 81-111 + 45 pl., 1949.

de MAGNÉE, M. I., Quelques aspects de l'emploi du compteur de Geiger-Müller en prospection minière, Bull. Séances, Inst. R. Col. Belge, pp. 900-928, 1949.

DOZY, J. J., Some notes on the volcanoes of Guatemala, Bull. Volcanologique, v. 8, pp. 47-67 + 11 pl., 1949.

EINARSSON, TRAUSTI, The eruption of Hekla, 1947-1948, no. 4, Chemical analysis and differentiation of Hekla's magma, 34 pp., and no. 5, The basic mechanism of volcanic eruptions and the ultimate causes of volcanism, 30 pp., Soc. Sci. Islandica, 1950.

ESCHER, B. G., Sur l'origine de la forme asymétrique de la surface de la terre et ses conséquences sur le volcanisme de la terre et de la lune, Bull. Volcanologique, v. 8, pp. 23-39, 1949.

GEORGALAS, G. C., Contribution à la connaissance des roches éruptives de l'île de Mételin, Bull. Volcanologique, v. 9, pp. 32-64 + 1 fig., 1949.

HAROLD, HERBERT, A contemplation of time in plutonism, Q. J. Geol. Soc. London, v. 105, pp. 101 156, 1949 [abstr. in Chem. Abstr., v. 44, no. 14, p. 6360, 1950].

JAMES, C. C., Parícutin eruption, Trans. R. Geol. Soc. Cornwall, v. 17, pp. 368-379, 1947 [abstr. in Chem. Abstr., v. 44, no. 16, p. 7197, 1950].

KOCZY, F. F., The thorium content of the Cambrian alum shales of Sweden, Sveriges Geol. Undersökning, v. 43, 12 pp., 1949.

LUNDEGÅRDH, P. H., Aspects to the geochemistry of chromium, cobalt, nickel and zinc, Sveriges Geol. Undersökning, v. 43, 56 pp., 1949.

MACGREGOR, A. G., Prediction in relation to seismo-volcanic phenomena in the Caribbean volcani arc, Bull. Volcanologique, v. 8, pp. 69-86, 1949.

MARMO, VLADI, Ein vulkanischer Komplex der Früh-Jotnischen Zeit bei Suoju in Ost-Karelien, Ann. Acad. Sci. Fenn., III, Geol.-Geog., no. 19, 77 pp., 1949.

PONTE, GAETONO, Riassunto delle principali osservazioni e ricerche fatte sull' Etna, Bull. Volcanologique, v. 9, pp. 65-80 + 26 pl., 1949.

RANKAMA, KALERVO, Geochemistry of columbium, Ann. Acad. Sci. Fenn., Ser. A, no. III, Geol.-Geog., no. 13, 57 pp., 1948 (in English) [abstr. in Chem. Abstr., v. 44, no. 9, p. 3855, 1950].

SCHENK, ERWIN, Ein miozäner Vulkanbau bei Beuern nordöstlich von Giessen, Notizbl. Hess. Landesanst. Bodenforsch. Weis, VI Folge, H-1, pp. 244-259, 1950.

SLAVIN, V. I., Some ancient volcanoes of the Little Caucasus, Izvest. Akad. Nauk U. S. S. R., Ser. Geol., pp. 148-152, 1947 [abstr. in Chem. Abstr., v. 44, no. 16, p. 7197, 1950].

TOMASI, LUIGI, Studi petrografici dei filoni e contatti del Passo della Bottiglia, Acta Geologica Alpina, Contr. Mineralogia, Petrografia e Geologia, Bologna, no. 2, 52 pp., 1950 (summary in English).

TOMBA, ANNA MARIA, Studio petrografico sopra alcune porfiriti del versante sinistro della media Val d'Ultimo (Alto Adige), Periodico Mineralogia, v. 16, no. 3, pp. 215-269, 1947 (summary in English).

TOMKEIEFF, S. I., The volcanoes of Kamchatka, Bull. Volcanologique, v. 8, pp. 87-113 + 9 pl., 194

VAN BEMMELEN, R. W., Report of the volcanic activity and volcanological research in Indonesia during the period 1936-1948, Bull. Volcanologique, v. 9, pp. 3-29 + 2 maps + 14 pl., 1949.

BIBLIOGRAPHY: HYDROLOGY

ALEMÁN, OSCAR SUCRE, Pluviógrafos, Revista, Col. Ing., Venezuela, no. 171, pp. 29-35 + 2 pl., 1950.

BRASIL, SECÇÃO DE HIDROLOGIA, Atlas pluviométrico do Brasil, 1914-1938, Departamento Nacional da Producção Mineral, Bol. no. 5, 48 pp. + 25 maps, 1948.

CHILDS, E. C., The Ghyben-Herzberg Lens, Proc. 2nd Intern. Conf. Soil Mech., v. 6, pp. 150-153, 1948.

DEVROEY, E.-J., Note sur le captage des eaux, Bull. Séances, Inst. R. Col. Belge, pp. 1007-1027, 1949.

DEVROEY, E.-J., Les sources du Nil au Congo Belge et au Ruanda-Urundi, Bull. Inst. R. Col. Belge, v. 21, no. 1, pp. 248-279 + 2 maps, 1950.

IWAI, S., A hydrostatistical study on duration curves, Japan Sci. Rev., v. 1, no. 1, pp. 3-8, 1949.

KURODA, M., Dynamics of snow cover, Japan Sci. Rev., Tokyo, v. 1, no. 1, pp. 45-52, 1949.

NICHOLSON, H. H., Field drainage and increased production, J. R. Agric. Soc., v. 109, pp. 212-221, 1948.

PASQUILL, F., Some estimates of the amount and diurnal variation of evaporation from a clayland pasture in fair spring weather, Q. J. R. Met. Soc., v. 75, pp. 249-256, 1949.

PÉREAU, AIMÉE, La phase de la composante annuelle des niveaux des rivières de la plaine de l'est Européen, Geofis. Pura e Appl., Milano, v. 16, 11 pp., 1950 (summary in English).

RAY, K. B., The section and armour of a guide bank for the training and control of the great alluvial rivers, Tech. Paper 309, Railway Board, Calcutta, 23 pp. + 2 pl., 1941.

SCHNACKENBERG, E. C., Extreme flood discharges, N. Zealand Inst. Engr., pp. 376-427, 1949.

SCHROEDER, G., Die Korrelationsrechnung und ihre Anwendung in der Wasserwirtschaft, Bundesanstalt für Gewässerkunde, Bielefeld, 115 pp. + tables and figures, 1950.

BIBLIOGRAPHY: TECTONOPHYSICS

BULLEN, K. E., Compressibility-pressure hypothesis and the Earth's interior, Mon. Not. R. Astr. Soc., Geophys. Suppl., v. 5, pp. 355-368, Oct. 1949 [abstr. in Phys. Abstr., v. 53, no. 628, p. 351, 1950].

BULLEN, K. E., An Earth model based on a compressibility-pressure hypothesis, Mon. Not. Astr. Soc., Geophys. Suppl., v. 6, no. 1, pp. 50-59, 1949.

DE SITTU, L. U., Le style structural Nord-Pyrénéen dans les Alpes bergamasques, Bull. Soc. Géol. France, v. 19, pp. 617-622, 1949.

FOURMARIER, P., L'étirement des roches et la schistrosité, Bull. Soc. Géol. France, v. 19(5), pp. 509-576, 1949.

FRICKE, K., Beispiele blockierter Faltung im nördlichen Ruhrkarbon, Geol. Jb. 1943-48, Geol. Landesanst. Bund. Deutschl., v. 64, pp. 589-593, 1950.

GARCIA SIÑERIZ, JOSÉ, Investigación geofísica en Larache, Rev. Geofís., Madrid, v 8, no 29, pp. 1-13 + 2 fig., 1949 (summary in English).

GIDON, P., Sur les relations de la zone du Flysch des Arguilles d'Arves et du massif du Pelvoux, Bull. Soc. Géol. France. v. 19, pp. 545-552, 1949.

JÁKY, JÓZSEF, State of stress at great depth, Proc. Sec. Inst. Conf. Soil Mech. Found. Eng. 1, pp. 90-93, 1948 (in English) [abstr. in Appl. Mech. Rev., v. 3, no. 5, p. 158, 1950].

KANITANI, JOYO, On a property of the conjugate net in connexion with generalized projective deformation, Mem. Coll. Sci., Univ. Kyoto, Ser. A, v. 25, pp. 41-43, 1949.

KONTOROVA, T. A., and O. A. TIMOSHENKO, Generalization of the statistical theory of strength for nonuniformly stressed bodies, Zh. teckh. Fiz. 19, pp. 355-370, 1949 (in Russian) [abstr. in Appl. Mech. Rev., v. 3, no. 3, p. 78, 1950].

LAHN, E., Contribution à l'étude tectonique de l'Anatolie Centrale, Bull. Soc. Géol. France, v. 19 pp. 577-584, 1949.

MAKIYAMA, JIRO, The bellows structure of Japan, Mem. Coll. Sci., Univ. Kyoto, Ser. B, v. 19, pp. 53-55, 1948.

NISKANEN, E., On the viscosity of the Earth's interior and crust, Ann. Acad. Sci. Fenn., III, Geol.-Geogr., no. 15, 22 pp., 1948.

OSBORNE, G. D., and P. B. ANDREWS, Structural data for the northern end of the Stroud-Gloucester Trough, J. Proc. R. Soc. N. W. S., v. 82, pp. 202-210, 1949.

PLÖCHINGER, B., Ein Beitrag zur Geologie des Salzkammergutes im Bereich von Strobl am Wolfgangsee bis zum Hang der Zwieselalm, Jb. Geol. Bundesanst. Wien, v. 93, pp. 1-35, 1949.

QUIRING, HEINRICH, Shell structure of the Earth and the origin of ores from deep-lying shells, Forschungen u. Fortschr., Tech. Univ., Berlin, v. 24, no. 3-4, pp. 36-38, 1948 [abstr. in Chem. Abstr., v. 44, no. 5, p. 1858, 1950].

RAMSEY, W. H., On the compressibility of the Earth, Mon. Not., R. Astr. Soc., Geophys. Suppl., v. 6, no. 1, pp. 42-49, 1950.

SCHULZE, G. A., and O. FÖRTSCH, Die seismichen Beobachtungen bei der Sprengung auf Helgoland am 18 April, 1947, zur Erforschung des tieferen Untergrundes, Geol. Jb. 1943-48, Geol. Landesanst. Bund. Deutschl., v. 64, pp. 205-241, 1950.

SHIMAZU, YASUO, and HITOSHI TAKEUCHI, Effect of tension upon the elastic parameters of isotropic solids, Geophys. Notes, Tokyo Univ., v. 2, no. 23, 6 pp., 1949.

SOKPATOV, G. I., Permian deposits of the Crimea and their relation to the geological structure of the Crimea, Dokl. Akad. Nauk. S. S. S. R., v. 71, pp. 733-736, 1950 (in Russian).

TANNI, L., On the continental undulations of the geoid as determined from the present gravity material, Ann. Acad. Sci. Fenn., III, Geol.-Geog., no. 16, 78 pp., 1948.

TYRRELL, G. W., Metamorphism and metamorphic rocks, a review of recent progress in geology, Sci. Prog., v. 38, pp. 509-519, 1950.

VAN DEN BERG, J. J., Petrofabric analysis of the Bushveld gabbro from Bon Accord, Trans. Proc. Geol. Soc. S. Africa, v. 491, pp. 155-208, 1946 [abstr. in Chem. Abstr., v. 44, no. 8, p. 3413, 1950].

VENING MEINESZ, F. A., Earth's crust deformations in geosynclines, Kon. Ned., Akad. Weten., Proc., v. 53, no. 1, pp. 27-46, 1950.

WAGNER, W., Diluviale Tektonik im Senkungsbereich des nördlichen Rheintalgrabens und an seinen Rändern, Notizbl. Hess. Landesanst. Bodenforsch. Weis., VI Folge, H-1, pp. 177-192, 1950.

WIEBOLS, JOHN, Zur Tektonik des hinteren Gross-Arl-Tales, Jb. Geol. Bundesanst. Wien, v. 93, pp. 37-81, 1949.

NOTES AND PERSONALIA

NOTES

The great earthquake of August 15, 1950--This ranks among the largest known shocks. Independent determinations of magnitude made at Pasadena, Wellington, and Praha agree on a value near 8 1/2; data now in hand suggest 8.6. Precise instrumental magnitudes can be assigned beginning with the year 1904. Since then the shocks of magnitude over 8.3 have been: 1906, Colombia, 8.6; 1906, Chile, 8.4; 1911, Tien Shan, 8.4; 1920, China, 8.5; 1933, Japan, 8.5.

The preliminary determination of the U. S. Coast and Geodetic Survey locates the epicenter at 28 1/2 N, 97 E, and origin time 14:09:30 GCT. This is north of the Assam-Burma boundary, in the district of Sikang or Chwanben, between China and Tibet. Incomplete and distorted press reports indicate damage in Assam exceeding that caused by the great earthquake of 1897. Interrupted communications, now being resumed, bring information of heavy loss of life, and of the destruction of thousands of houses. Much of the damage is due to flooding, probably caused by disturbance of ground water and changes in stream gradients in the alluviated valley of the Brahmaputra. The district reported as suffering most is that of Lakhimpur. Press accounts of "mountains" having disappeared presumably reflect the occurrence of great landslides.

New Swedish journal on geophysics--A new Swedish journal Arkiv för Geofysik is being published six times a year in Stockholm by the Library of the Royal Swedish Academy of Sciences (Kungl. Vetenskapsakademiens Bibliotek). The first number, dated June 1950, includes four scientific papers, three of which relate to terrestrial magnetism and electricity, and one to meteorology (see Bibliography in this issue).

Conference on Ionospheric Physics held at Pennsylvania State College--A conference on ionospheric physics was held at Pennsylvania State College, July 24-27, 1950, under the joint sponsorship of the School of Engineering of the College, and the Geophysical Research Directorate of the Air Force Research Laboratories. More than 20 papers and symposia were presented. There were 236 registered in attendance. It is the plan to publish the Proceedings of the Conference as a separate volume. Orders should be sent to Clinton H. Grace, Research Assistant, Department of Electrical Engineering, Pennsylvania State College, State College, Pennsylvania.

Civil Service examinations for physicists, meteorologists, and chemists--The Civil Service Commission announces unassembled examinations in the fields cited in various grades with salaries ranging from $3825 to $10,000 per annum. The vacancies to be filled are in connection with the work of the Geophysical Research Directorate of the Air Force Research Laboratories in Cambridge, Massachusetts. Persons interested should write to the Board of Civil Service Examiners, Air Force Research Laboratories, Cambridge, Mass.

Imperial Valley earthquakes, July-August, 1950--A swarm of moderate earthquakes at the close of July originated in the northern part of Imperial Valley, California. There was minor damage in Calipatria and neighboring communities, mostly to weak structures, some of which had been imperfectly repaired after earthquake damage in earlier years. The shocks shown in the following table exceeded magnitude 4.7. Over 130 smaller shocks of the group were registered.

Date	GCT		Magnitude
1950	h	m	
July 27	11	29	4.8
28	17	51	5.4
28	17	58	4.8
29	14	36	5.5
Aug 1	08	37	4.9

Petroleum industry announces ample facilities to meet the Nation's needs--The American Petroleum Institute announces that the petroleum industry's capacity to produce and refine petroleum, and the proved reserves, have increased approximately 1/4 since the peak demand for petroleum products in 1945. More than eight billion dollars have been plowed back into the industry for exploration and development, and to provide new facilities.

New journal of general science in Japan--Volume 1, number 1 of The Japan Science Review, Series I, Engineering Sciences, is dated March 1949 and contains 31 papers in English by various Japanese authors, with subjects bearing chiefly on the engineering aspects of science, such as "Dynamics of snow cover" and "A new method of tuning intermediate frequency transformer." In the foreword to this first number, it is noted that the issue contains papers of three types: (1) translations of papers already published in Japanese; (2) condensations of longer papers; and (3) newly published papers. The journal is published by the Association for Scientific Documents Information, Tokyo Institute of Technology, Meguro-ku, Tokyo.

New publication on speleology--Volume 1, number 1 of a new publication, Speleon, devoted to the scientific exploration and study of caves, dated June 1, 1950, has been received in the United States. It is published by the Instituto de Geología, University of Oviedo, Cviedo, Spain under the direction of N. Llopis Lladó. Number 1 contains three papers on caves and one on a newly discovered species, Viallia Alfanoi, and a section on news of expeditions. The papers are in Spanish, with French and English summaries.

Third annual summer camp in geology, University of Utah--The third annual summer camp-mapping expedition of the Department of Geology at the University of Utah was held this year from June 19 to September 6 in the 2500 square-mile rectangle chosen three years ago as the mapping project for summer students. This takes in the heart of the silver mining area of the state, which is rich in special geological structures which have been checked and re-checked by students and instructors for insertion on a base map of the area to be completed in six or seven years. The enrollment hit a new high of forty students with another forty applications turned down because of limited facilities. Students attended from all parts of the country and Canada. Camp was supervised by Norman C. Williams, Assistant Professor of Geology at the University.

Annual Meeting of Rocky Mountain Hydraulic Laboratory--The Fifth Annual Meeting of the Rocky Mountain Hydraulic Laboratory was held at Allenspark, Colorado, August 19, 1950. A business session and two technical sessions were held, with five papers and reports. About 40 persons were in attendance.

Meeting of the American Meteorological Society--The 108th National Meeting of the American Meteorological Society is to be held at Florida State University, December 5-7, 1950. Chairman of the Program Committee is Seymour L. Hess at the University in Tallahassee.

PERSONALIA

Harvey O. Banks, formerly associated with Harold Conkling, Consulting Engineer, has taken up duties with the California Division of Water Resources as Supervising Hydraulic Engineer in charge of a state-wide survey of water pollution, and the formulation of plans for the mitigation of pollution.

Morton L. Barad has entered upon duties as group head in experimental meteorology, Health Instruments Divisions, Nucleonics Department, General Electric Co., with headquarters in Richland, Washington.

Henry B. Bigelow, Alexander Agassiz Professor of Zoology at Harvard University and AGU William Bowie Medalist in 1944, has become Professor Emeritus.

L. D. Bonham recently received the degree of Doctor of Philosophy in geology from the University of Chicago and has taken up duties with the U. S. Geological Survey in Washington, D. C.

Robert S. Dahlberg, Jr., formerly a group leader with the Creole Petroleum Corp. of Venezuela, has taken up work as a project engineer on microwave communication with the Philco Corp.

Gilbert H. Dunstan has returned to the University of Alabama as Professor of Sanitary Engineering. Until recently, he was Sanitary Engineer with the Arctic Health Research Center of the Public Health Service at Fairbanks, Alaska.

Walter M. Elsasser of the Randal Morgan Laboratory of Physics, University of Pennsylvania, has accepted a professorship in physics at the University of Utah. He will have charge of the work in theoretical physics, and will continue his studies in the geophysical sciences.

R. W. Gerdel, formerly engaged in work with the U. S. Weather Bureau and the Cooperative Snow Investigations, is now engaged in research with the Snow, Ice, and Permafrost Research Establishment, with headquarters in St. Paul, Minn.

Geoffrey E. Greene, of the Southeastern Forest Experiment Station of the U. S. Forest Service has been granted an educational furlough to undertake graduate work towards a degree of Master of Science in forest influences. He will study at the University of California at Berkeley.

Dan K. Hamilton of the Department of Geology, University of Kentucky, has accepted a two-year mission with the ECA, with headquarters at Nairobi, Kenya.

Gail A. Hathaway, Special Assistant to the Chief of Engineers, Department of the Army, has been elected President of the American Society of Civil Engineers for the year 1951.

Norman Herz has recently received the degree of Doctor of Philosophy from Johns Hopkins University with a major in geology, He has taken up duties as instructor at Wesleyan University in Connecticut and will teach mineralogy and structural geology.

William Glenn Hoyt, Director of the Division of Water and Power, Department of the Interior, has retired after 43 years of service in the Department. He will make his home at Leatherhill Under, Wingdale, N. Y.

Hal J. Jones recently received the degree of Doctor of Philosophy in geology and physics from the University of Texas, and has accepted a position in the Exploration Department of the Shell Oil Co., with headquarters at Lake Charles, La.

C. E. Kindsvater has returned to his duties as Professor of Civil Engineering at Georgia Institute of Technology after a year's sabbatical leave which he devoted to advanced study in fluid mechanics at the University of Iowa.

Claud C. Lomax, Jr. has accepted an appointment as Assistant Professor of Civil Engineering at the University of Idaho.

John S. McNown of the Iowa Institute of Hydraulic Research has won a Fulbright Fellowship for a year of study and research in France.

Don Kirkham, Professor of Soils at Iowa State College, recently won the $50 cash award of the Iowa Academy of Sciences for his paper "Seepage into ditches in the case of a plane water table and an impervious stratum" which appeared in the June 1950 issue of the Transactions.

Douglas Whitaker, Dean of Graduate Studies at Stanford University, has been named Chairman of the National Research Council for the next year.

Kirk Bryan, Professor of Geology at Harvard University, died at Cody, Wyo., on August 22, 1950 at the age of 62. He was born at Albuquerque, N. Mex., and received his baccalaureate degree from the University of New Mexico in 1909. He received another baccalaureate degree in 1910, and his Doctor of Philosophy degree in 1920 from Yale University. From 1912 to 1927, he served as a geologist with the U. S. Geological Survey, instructing at Yale while working toward his doctorate. In 1926, he began his work at Harvard, becoming Professor in 1943. He served in France during World War I as a second lieutenant. In his professional scientific work he was frequently called upon in a consulting capacity, and was an especial authority on the geology of arid areas. He had been a member of AGU since 1930.

Charles J. Hubbard, Chief of the Arctic Section of the U. S. Weather Bureau, was killed July 31, 1950 in an airplane crash on Ellesmere Island which killed the eight others aboard, also. He was born in Kansas City, Mo. in 1902, received a baccalaureate degree in arts in 1924, and in science in 1925 from Harvard University. From 1925-1928 he was on the staff of Stone and Webster, Consulting Engineers, and from 1928-1931 was Vice President of George B. N. Macomber Co. His Arctic work began with aerial surveys of northern Canadian areas between 1931 and 1935, followed by independent exploration work in the North between 1935 and 1940. During the War, he served first in the Navy, later with the Army Air Force as a lieutenant colonel, and devoted much of his energies to the development of air routes over Greenland and the North. Since the War, he has been with the Weather Bureau, engaged chiefly in the establishment and operation of meteorological stations in the north. He had been a member of AGU since 1945.

Perley G. Nutting, Geophysicist with the U. S. Geological Survey, retired, died August 8, 1949, just a few days before his 76th birthday. He was born at Randolph, Wisconsin, received his baccalaureate degree from Stanford University in 1897, and his Master of Science degree from the University of California in 1899. He attended the University of Göttingen in 1901-02, and received the degree of Doctor of Philosophy from Cornell University in 1903. From 1903 to 1912 he was a physicist with the National Bureau of Standards, teaching part of this time at George Washington University. From 1912 to 1916, he was engaged in optical research work with the Eastman Kodak Co; from 1916-1920, he was in charge of scientific research for the Westinghouse Electric and Manufacturing Co. From 1920-1925, he engaged in consulting work, and from that later date until 1943, when he retired, he was Geophysicist with the U. S. Geological Survey. He had been a member of AGU since 1931.

William A. Orr, Officer in Charge, Snow, Ice, and Permafrost Research Establishment, and Lieutenant Colonel in the Corps of Engineers, U. S. Army, was drowned in the Mississippi River following a practice parachute jump on August 23, 1950. He was born at Heardmont, Georgia in 1915, and was appointed to the U. S. Military Academy while attending South Carolina A and M College. He received his baccalaureate degree from the Military Academy in 1938, advancing steadily in rank. His service in the Research Establishment began with its establishment in 1949, and he was the one largely responsible for its progress and development to date. He had only recently become a member of AGU.

Herbert H. Swasey, Jr., Chief Meteorologist of Eastern Airlines at Miami died October 18, 1949. He was born in New York City March 8, 1919 and received his baccalaureate degree from Davidson College in 1940. He took advanced work in meteorology in 1940-41, and served in the Air Force as a major, acting as Weather Officer. He entered the service of the Airlines in 1946. He became a member of AGU in 1949.

UNION, SECTION, AND COMMITTEE ACTIVITIES

American Standards Association--Fred Anderegg, AGU representative on the Committee on Photography Z38 of the ASA advises that the new American Standard Photographic Exposure Computer, Z38.2.2-1949 is now available. With this handy 3 1/2 × 5 1/4 booklet one can calculate exposures for any latitude zone and for all weather conditions. The new American Standard Dimensions for Amateur Roll Film, Backing Paper, and Film Spools, Z38.1.7-1950 has just been published.

Word has recently been received from the American Standards Association that the extremely large Committee Z38 is to be replaced by four smaller committees, believing that the work may be carried on more effectively by groups having a more direct interest in particular aspects of photography. The AGU has been invited to accept membership on the Committee on Photographic Sensitometry.

SPECIAL ANNOUNCEMENTS

The New Directory of Members--Part 2 of this issue of the Transactions is devoted to a directory of members and the committees of AGU. This replaces the last list, published as Part 2 of the Transactions of August 1948. Many names have been added to the membership, the net growth continuing at a steady rate.

For the first time since 1943, the directory also gives the geographical listing - by cities in the United States and Canada, and by countries, otherwise. We believe that this listing will be valuable to members, and thus of service in the development of the broad field of Geophysics. In addition, it is hoped that the direct organizational interests of AGU may be served in at least two ways: (1) Members will now be aided in suggesting qualified non-members for membership; and (2) Members interested in the development of a regional program in AGU will have opportunity to get into touch with other like-minded members to further that purpose. Regionalization of AGU activities must start with the desire and interest of the members. Members having such interest will be aided in organational and planning work by the National officers of the Sections and the Union [see December 1949 Transactions, pp. 931, 936-939, and 942; and August 1950 Transactions, p. 749].

Twenty-Sixth Regional Meeting to be held in Fresno, California, February 9-10, 1951--This meeting has been initiated by the Section of Hydrology, and though plans are as yet quite incomplete, it is anticipated that some other Sections will join in this. Arch R. Addington, Fresno State College, Fresno, California has been designated as Chairman of the Committee for the meeting. Those having interest in the meeting should write to the Office of AGU or to Professor Addington.

Ninth General Assembly of the International Union of Geodesy and Geophysics--Details of the program in connection with this meeting to be held in Brussels, August 21-September 1, 1951, are being worked out, and names of citizens of the United States who expect to be in attendance are being received in the office of the AGU. If you plan to attend, advise the AGU in order that we may keep you supplied with information regarding the meeting as it becomes available. Arrange for your passage as soon as possible. This is especially pertinent for those who will go by boat. Word of papers to be presented should be forwarded to the office of AGU without further delay in order that it may be coordinated with the program.

Scientific and technological manpower and mobilization--Federal agencies and other organizations such as the National Research Council are at work shaping a policy to avoid wasteful use of scientific and technological manpower. The Selective Service Act of 1948 states that "adequate provision for National security requires maximum effect in the fields of scientific research and development, and the fullest possible utilization of the Nation's technological, scientific, and other critical manpower resources." The President is authorized to provide for deferment of persons whose activity in study, research, or medical, scientific, or other endeavors is necessary to the maintenance of national health, safety, or interest.

Thus there is intent to utilize scientists, engineers, and technologists to the best National interests. How these policies will be carried into practice remains to be seen, but individual scientists and technologists, and organizations interested in the best use of such manpower, must do their part to see that these policies are translated effectively. There are three primary problems.

The first problem, which concerns scientists and technologists in the Organized Reserve, is perplexing. The Department of Defense has announced interim procedures for delay of call to active duty based on the "List of Critical Occupations" of the Department of Labor, and the "Tentative List of Essential Activities" of the Department of Commerce. A reserve officer may be deferred if engaged in work of the categories listed. Practically all fields of science and engineering, and teachers in these fields are included. The Department of Defense states that students who are in the Organized Reserve may be deferred until the completion of the school term for which they are registered. Graduate students in a field of primary interest to the Department of Defense may also be granted delay. Application for delay can be made only after the call to active duty is received. The press release states that for the Army, Marine Corps, and the Air Force, requests for delay must be made through the chain of command, although it is inconsistent in adding that in the case of the Air Force, the request is to be made to the Headquarters of the Area in which one resides. For the Navy, requests are generally to be made to the Bureau of Naval Personnel through the Naval District Commandant. The non-conformities likely to develop indicate that an effective appeals procedure should be established. At present, appeals may be made only to the Secretaries of the respective services.

The second problem relates to deferment from Selective Service. Operations Bulletin No. 1, issued by Selective Service on August 8, 1950, relates specifically to college students. It provides that students who have completed one academic year of full-time work, are in the upper half of their class, and had made arrangements prior to August 1, 1950, warrant consideration for occupational deferment. Full-time graduate students may be deferred, if, in their last undergraduate year, they were in the upper half of their class. Indications are that part-time graduate students who hold part-time assistantships may also be deferred, but the phrasing of the Bulletin is not clear. Those not in a student classification will be deferred or not depending upon their work in relation to critical manpower needs.

The third problem relates to scientists and technologists who enlist or are inducted under Selective Service. In the Army, a Technical Detachment has been established, in which technically trained men are assigned after basic training to activity where their special skills may be utilized. Such assignments probably will not lead to Officers Candidate Schools, but should afford some use of technical competence. Minimum requirements are three full years of college, an AGCT score of 130, and a college major in a scientific field, or two full years in an accredited school of engineering and an AGCT score of 110. Persons having such qualifications or other special training should inform appropriate authorities upon enlistment or induction. If no action results, their name, rank, serial number, and organization should be sent to Office of Scientific Personnel, National Academy of Sciences, National Research Council, 2101 Constitution Avenue, Washington 25, D. C.

Thirty-Second Annual Meeting, Washington, D. C., April 30-May 2, 1951--As stated in the preliminary notice in Special Announcements, the Thirty-Second Annual Meeting will be held in Washington, D. C., April 30 to May 2, 1951 (Monday to Wednesday). Plans are in their preliminary stages, and are progressing well, with all Sections and the Union arranging for sessions. Place this meeting on your calender, and make plans to come.

This announcement serves also as an invitation for members and others to send word of plans for papers to be presented. Titles of papers with three copies of the abstract should be sent as soon as possible, and not later than March 5, 1951, with advice concerning the time required (most papers are allowed from ten to twenty minutes) and the projection equipment needed. Send this word to the office of AGU at 1530 P Street, N. W., Washington 5, D. C., or to the Secretary of the appropriate Sections, as follows:

Geodesy	Frank L. Culley	U. S. Coast and Geodetic Survey Washington 25, D. C.
Seismology	James T. Wilson	Department of Geology University of Michigan Ann Arbor, Michigan
Meteorology	Woodrow C. Jacobs	4302 Kentbury Drive Bethesda, 14, Md.
Terrestrial Magnetism and Electricity	L. R. Alldredge	3133 Jennings Rd. Kensington, Md.
Oceanography	Richard H. Fleming	Divison of Oceanography, Hydrographic Office, Navy Department Washington 25, D. C.
Volcanology	Felix Chayes	Geophysical Laboratory 2801 Upton Street, N. W. Washington 8, D. C.
Hydrology	Ray K. Linsley or	Dept. of Civil Engineering Stanford University Stanford, California
	Ralph N. Wilson (Program Chairman)	3900 Hamilton Street, Apt. E-101 Hyattsville, Md.
Tectonophysics	Wilbur S. Burbank	3346 Runnymede Place, N. W. Washington 15, D. C.

As the Section Secretaries reserve the right to close a filled program in advance of the date indicated, it is desirable that word concerning papers be sent in early.

Complete manuscripts of papers should be forwarded in triplicate by April 10, 1951 in order that news releases may be prepared. Indicate whether the paper is being submitted for the program only or also for consideration for publication in the *Transactions*. (Papers for publication only are also welcome for consideration for the *Transactions*.)

If a paper is written in collaboration, please indicate by whom it will be presented. Arrangements can usually be made for presentation of papers by authors who are unable to attend.

The Chairman of the Committee on Meetings (J. P. Marble, 321 U. S. National Museum, Washington 25, D. C.) invites suggestions and comments that will be helpful in planning this meeting. Especially invited are comments relating to papers and symposia bearing on more than one Section.

Make hotel or room reservations directly with the hotel of your choice at an early date. Failing on the first attempt, bear in mind that advance bookings not taken up are cancelled two weeks in advance, so a follow-up request in mid-April may bring the desired response. It is anticipated that we will make block booking at two or three hotels again, an announcement concerning which will appear in the Special Announcements of the February 1951 issue of the *Transactions*.

John Putnam Marble, Chairman
Committee on Meetings

FRIEZ INSTRUMENT DIVISION
BENDIX AVIATION CORPORATION

Manufacturer of Meteorological Instruments

Taylor Avenue near Loch Raven Boulevard
Baltimore 4, Maryland

GEOPHYSICAL RESEARCH CORPORATION

Geophysical Prospecting
Application of Geophysical Methods in the Petroleum Industry

2607 North Boston Place
Tulsa 6, Oklahoma

INSTITUTE OF GEOPHYSICS

UNIVERSITY OF CALIFORNIA

Los Angeles 24, California

KEUFFEL AND ESSER COMPANY

Drafting, Reproduction, and Surveying Equipment and Materials
Slide Rules Measuring Tapes

300 Adams Street
Hoboken, New Jersey

RANNEY METHOD WATER SUPPLIES, INC.

Ground Water Exploration and Development

841 Alton Avenue
Columbus 3, Ohio

RUSKA INSTRUMENT CORPORATION

Developers, Designers, and Manufacturers of Instruments for Field and Observatory Use
Magnetic, Geodetic, Seismic, and Meteorological Work

4607 Montrose Boulevard
Houston 6, Texas

SEISMOGRAPH SERVICE CORPORATION

Seismic Exploration Service for
Oil and Gas Structures throughout the World

P. O. Box 1590
Kennedy Building
Tulsa 1, Oklahoma

SPRENGNETHER INSTRUMENT COMPANY

Manufacturer of Seismological and Geophysical Instruments
Instrumental Development and Research

4567 Swan Avenue
St. Louis 10, Missouri